Christian Leypold, BSc MSc

Functional Organic Materials for High Energy Batteries: Soft Mixed Electron and Ion Conductors and Organics in Singlet Oxygen Electrochemistry

DISSERTATION

zur Erlangung des akademischen Grades

Doktor der Naturwissenschaften

eingereicht an der

Technischen Universität Graz

Betreuer

Assoc. Prof. Christian Slugovc
Institut für Chemische Technologie von Materialien

Betreuer und Projektleiter

Dipl.-Ing. Dr. sc. ETH Stefan A. Freunberger
Institut für Chemische Technologie von Materialien

Graz, September 2018

EIDESSTATTLICHE ERKLÄRUNG

Ich erkläre an Eides statt, dass ich die vorliegende Arbeit selbstständig verfasst, andere als die angegebenen Quellen/Hilfsmittel nicht benutzt, und die den benutzten Quellen wörtlich und inhaltlich entnommenen Stellen als solche kenntlich gemacht habe. Das in TUGRAZonline hochgeladene Textdokument ist mit der vorliegenden Dissertation identisch.

Datum

Unterschrift

“Hey, kid, you did quite well…

It looks like you may be gaining some (…) skill…”

– Great King of Evil – Ganondorf

Danksagung

Während meiner Tätigkeit als Doktoratsstudent wurde ich stets mit Rat und Tat unterstützt. In diesem Kapitel meiner Doktorarbeit möchte ich mich diesbezüglich revanchieren. In erster Linie möchte ich mich bei meinen beiden Betreuern STEFAN FREUNBERGER und CHRISTIAN SLUGOVC bedanken, dass sie mir die Möglichkeit einräumten, eine Arbeit über ein innovatives Themengebiet, neue Batteriesysteme, zu verfassen. Sie haben sich nicht nur bereit erklärt, mich unter ihre Fittiche zu nehmen, sondern mir wurde auch bei etwaigen Problemstellungen mit hilfreichen Hinweisen und Ideen geholfen. Weiters möchte ich meinen Arbeits(gruppen)-kollegen NIKA MAHNE (FRDA), BETTINA SCHAFZAHL (BTTI), LUKAS SCHAFZAHL (LUKI), ALEKSEJ SAMOJLOV (DA RUSS), PETRA HOFSTADLER, ANITA LEITGEB, CHRISTIAN PREHAL, ANJANA RAJU, YANN PETIT und ELEONORE MOURAD für das gute Arbeitsklima danken. Besonderer Dank gilt hierbei FRDA, BTTI, LUKI, PETRA und N RUSSN, die mir nicht nur bei meinen Problemen im Laboralltag halfen, sondern auch mit tiefsinnigen Gesprächen und Zeitvertreibsaktivitäten wie dem STOASCHEIßA KOARL-Spiel meine Arbeitszeit versüßten und sich somit einen Platz in meinem Freundeskreis erwirkten. Des Weiteren möchte ich meiner Bacchelorstudentin MELINA MUCH (BLELINA) danken. BLELINA verrichtet ihre Arbeit sehr engagiert, aber dennoch mit einer aufmunternden Tollpatschigkeit und erleichterte/erheiterte meine Arbeit aufgrund dessen.

Weiters möchte ich mich bei den Angestellten des ICTM der TU Graz bedanken. Hierbei möchte ich mich bei unsere Institutssekretärin RENATE TREBIZAN für ihr Durchhaltevermögen in Bezug auf meiner bürokratischen Unwissenheit/Nachlässigkeit und für ihre Hilfe bei den organisatorischen Dingen bedanken. Zudem möchte ich mich auch bei den Laborantinnen

unserer Fakultät BIRGIT EHMANN und ELISABETH SEITLER für ihre Tätigkeiten und ihre auflockernden Gesprächen danken.

Des Weiteren wurden unzählige Probenmessungen für mich durchgeführt. Hierfür möchte ich mich recht herzlich bei JOSEFINE HOBISCH, PETRA KASCHNITZ, KARIN BARTL und ANA TORVISCO GOMEZ bedanken. Zusammenfassend möchte ich der Hilfsbereitschaft des gesamten Institutes, aber auch anderer Institute wie dem Institut für Anorganischer Chemie, Organischer Chemie als auch Analytischer Chemie und Lebensmittelchemie danken.

Weitere Unterstützung habe ich auch von meinen Freunden des Blasmusikvereins erfahren. Im Besonderen danke ich hierfür den Musikern der STADTKAPELLE LEIBNITZ und der GARTENMUSI LEIBNITZ für die zahlreichen unterhaltsamen Stunden bei Trank und Musik, Wind und Wetter, Tag und Nacht.

Abschließend gilt der wohl größte Dank meiner Familie, die mich tatkräftig moralisch als auch finanziell unterstützt hat. Zum einen gilt dieser Danke meinen Eltern, die mich in jeder Lebenslage unterstützen, meinem Bruder MARIO, der mir zusätzlich zur moralischen Unterstützung auch mit hilfreichen Ratschlägen in Bezug auf meine Arbeit zur Seite steht und nicht zuletzt meiner Freundin MELANIE, _@ll, die mich mit viel Geduld durch die gesamte Zeit des Studiums begleitet.

Abstract

The limitations of current battery technology motivate tremendous ongoing research to find better electrode materials in the area of ‘beyond intercalation’ chemistries. Replacement of current technologies include; carbon intercalation anodes with silicon alloying or conversion reactions, and intercalation cathodes with Li-oxygen or Li-sulfur cathodes. These new classes of electrode materials promise a leap in energy storage, improved material sustainability, recyclability and lower cost. However, ‘beyond intercalation’ materials have disadvantages, including an expansion of participating particle volume during cycling, as well as poor charge carrier mobility. Moreover, the new active materials pose several challenges with respect to interface reactivity and electrolyte stability. This PhD thesis focused on organic mixed conductors to provide intimate electronic and ionic contact of the conversion materials at all stages of cycling. Results demonstrate electronic and ionic conductivity within one material and cyclability for conversion-type materials. Experiments with metal-oxygen cells give rise to highly reactive intermediates, particularly singlet oxygen, which we discovered as part of this work. Interactions of organic materials with singlet oxygen were further investigated by applying traps to detect and quenchers to fight the singlet oxygen, along with mediators to alter reaction pathways sustaining mixed conductivity in the electrode.

Kurzfassung

Gegenwärtige Limitierungen in Batterien erfordern die Entwicklung neuartiger Technologien im Bereich der Batterienforschung. „Interkalationschemie und darüber hinaus“ wird durch diese Tatsache enorm motiviert und hat sich zum Ziel gesetzt, aktuelle Materialien zu ersetzen. Die Chemie dahinter umfasst den Austausch von Kohlenstoff-Interkalationsanoden durch Siliziumlegierungen oder Umwandlungsreaktionen und Interkalationskathoden mit Lithium-Sauerstoff oder Lithium-Schwefel-Kathoden. Diese neuen Klassen an Elektrodenmaterialien versprechen nicht nur einen Schritt vorwärts hinsichtlich Energiespeicherung, sondern erweisen sich als vorteilhaft in Verbindung mit Nachhaltigkeit, Kosten und Rezyklierbarkeit. Die neuen Materialien haben allerdings nicht nur Vorteile: Große Volumsänderungen und schlechte Ladungsträgermobilität zählen zu den negativen Nebeneffekten. Darüber hinaus bringen diese Aktivmaterialien Herausforderungen in Bezug auf Oberflächenreaktivität und Elektrolytstabilität mit sich. Die vorliegende Arbeit beschäftigt sich mit gemischten organischen Leitern. Ziel ist es, einen engen elektronischen und ionischen Kontakt zwischen den aktiven Materialien auf allen Stufen der Zyklisierung zu schaffen. Gemischte Leiter weisen gute elektronische und ionische Leitfähigkeit innerhalb eines Materials auf und zeichnen sich durch gute Zyklisierbarkeit aus. Ein Teil dieser Arbeit behandelt die Erforschung von hochreaktiven Intermediaten, insbesondere Singulett-Sauerstoff, welcher durch die Anwendung der Gemischtleiter in Metall-Sauerstoff Zellen entsteht. Dazu wurde die Wechselwirkung von organischen Materialien mit Singulett-Sauerstoff erforscht: Organische Verbindungen dienten hierbei als Fallen oder Quencher für die Detektion, oder wurden als Mediatoren genutzt, um alternative Reaktionswege zu beschreiten und so den Einsatz von Gemischtleitern in Elektroden zu ermöglichen.

Directory

1. Introduction

For millennia, humankind has been simultaneously afraid and fascinated by thunderstorms and their accompanying strokes of lightning. Once the titanic power of those weather phenomena were recognized, humans learned to indirectly take advantage with the created fires. Untapping this energy allowed for better food utilization, larger brain development and habitation of cold climates. However, only for a minute fraction of history have people understood the direct correlation between lightning bolts and charges. In the 18th century, FRANKLIN and VOLTA independently investigated the topic of electricity, and approximately 50 years later TESLA was able to create a lightning strike with the aid of science for the first time. Discoveries by these scientists became the foundation for numerous other inventions, which are now part of daily life.

Although the generation of electric charge plays a significant role in the existence of humans, the storage of electricity continues to gain attention. Various types of batteries for different applications were invented to store and supply energy at proper circumstances. While current use of Li-ion battery technology is now powering the electrification of vehicles, disadvantages include; decreased material sustainability and recyclability as well as increased overall ecological footprint and cost. The major drawbacks are rooted in active materials that rely on the redox chemistry of relatively scarce transition metals processed at high temperatures. Overcoming these limitations require utilizing main group elements, which are; more abundant, cheaper and promise higher energy storage. Making such new types of batteries practical would allow for widespread electrification and thus boost the next quantum leap in locomotion of humans. For technical, economical and ecological purposes, combustion engines should be

replaced with electric engines to harness renewable energy and prevent further negative impacts on the environment.

This work seeks to understand and solve fundamental material challenges of batteries based on main group elements. We based our investigations on previous knowledge to invent new battery systems. The goal of this work is to synthesize novel molecules with special physical and electrochemical properties to assemble new battery systems.

2. Aim of the Scientific Research

One main goal of this work is to synthesize organic mixed conductors (MIEC) suitable for various conversion-type electrode materials to combine electronic and ionic conductivities within the same material. Mixed conductors would be highly applicable in battery systems.[1] This thesis focuses on pyrene (Pyr) (**1**) as a side chain conductor and poly(paraphenylene) (PPP) (**2**) as a back bone conductor for electronic conducting units. Tetraethylene glycol methyl ether (TEG) (**3**) units should provide the ionic conductivity to our systems (Scheme 2.1).

Although battery systems using a conversion material as energy storage suffer from several problems[2] including rigid carbon frameworks, the advantage of mixed conducting polymers is that loading of electrochemical active material could be significantly improved.

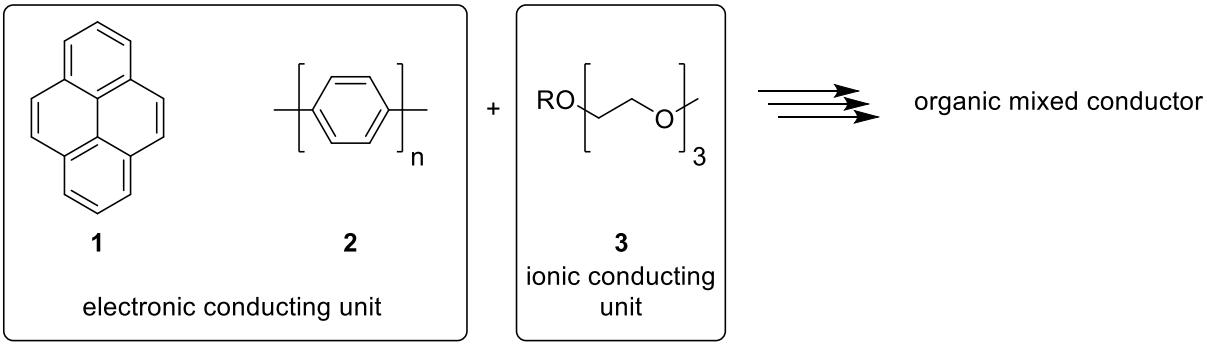

Scheme 2.1: Generation of mixed conduction substances using pyrene (**1**), poly(paraphenylene) (**2**) and tetraethylene glycol methyl ether (**3**) units as building blocks.

The second goal of the thesis was to investigate the electrochemical reaction of oxygen, as well as the generation mechanism and suppression of single oxygen $^1O_2$. *In situ* generated high reactive oxygen species force parasitic side product formation during oxygen cell cycling (Scheme 2.2).[3] Detection of $^1O_2$ is challenging due to its high energy and instability; understanding of high reactive oxygen species will help overcome these obstacles. Implementation of these oxygen batteries would contribute to enhanced cyclability and the potential for commercially available high energy storage.

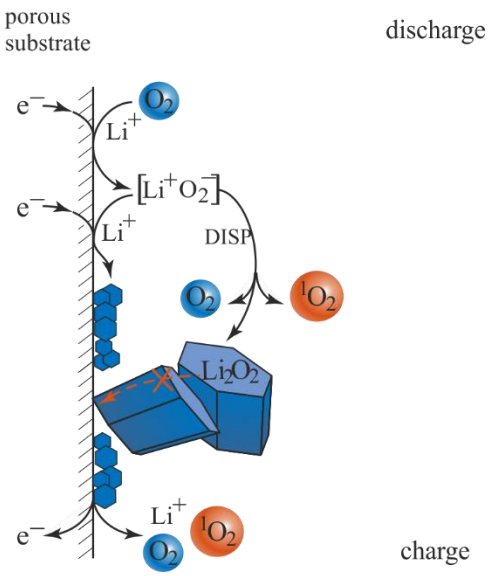

Scheme 2.2: Schematic of the reactions taking place in a Li-O_2 cathode: ($O_2 + 2Li^+ + 2e^- \rightleftarrows Li_2O_2$) with $^1O_2$ formation during discharge/charge in conventional electrolyte. The insoluble and insulating discharge product Li_2O_2 forms on the surface of the conducting porous substrate and passivates it.

3. Theory

3.1 History of Batteries

A battery is a chemical device which stores electrical energy. However, direct storage of electricity is not easily manageable and is usually converted into potential, kinetic, thermal, or chemical energy. *Vice versa*, chemical energy may be converted into electronic energy, which is the principle of batteries and fuel cells. In said devices the conversion of hydrogen produces electricity, therefore fuel cells belong to the category of energy-conversion devices, such as batteries.[4]

Conventionally, batteries are differentiated between two types: primary batteries and secondary batteries. Primary batteries are only able to supply their energy once, as the active materials cannot be reformed by electrochemical ways. Their components thus need to be recycled in chemical ways to produce new devices. On the other hand, secondary batteries have the ability to be recharged. During the charging process, chemical products generated during discharge are converted back using electrical energy. Unfortunately, the processes are accompanied by side reactions which cause degradation. After a certain amount of recharge processes, the capacity to store charge falls below a practical level.[4]

In 1800, VOLTA was the first scientist who produced electricity from chemical energy and developed a primary battery. In his experiment, he assembled a pile of alternate silver and zinc discs. Each pair of unequal metal discs was separated by a cloth, which was soaked with brine. One end of the disc stack was terminated with a silver disc, the other end with a zinc disc and continuous current was generated once the ends of the stack were connected by a wire conductor. This galvanic cell is known as ‘Volta’s pile’.[4-5]

Some decades later, in 1836, DANIELL created the first galvanic cell. A copper vessel was filled with a copper sulfate solution. A zinc rod was placed into a sulfuric acid solution and both solutions were isolated by a membrane (gullet of an ox). During discharge of the cell, the zinc electrode dissolved into the electrolyte, copper was plated at the positive electrode and a potential of 1.1 V was created (Figure 3.1).[4]

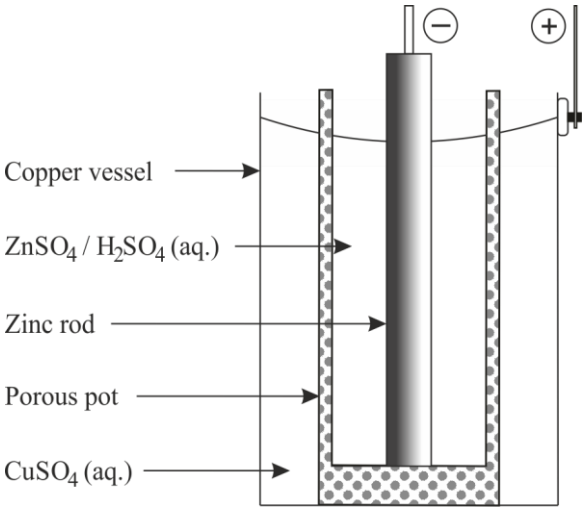

Figure 3.1: Construction of a DANIELL cell: Copper sulfate solution filled in a copper vessel separated by a membrane from a zinc rod in a sulfuric acid solution.[4]

In 1859, PLANTÉ demonstrated for the first time an effectively working secondary battery. In this electrochemical cell, two spirals of lead sheets immersed in diluted sulfuric acid were separated by porous cloth within a glass vessel. The so called 'lead acid battery' generates a potential of 2.0 volts. One year later PLANTÉ presented a battery consisting of ten lead acid cells, which gave an output of 20 volts (Figure 3.2).[4]

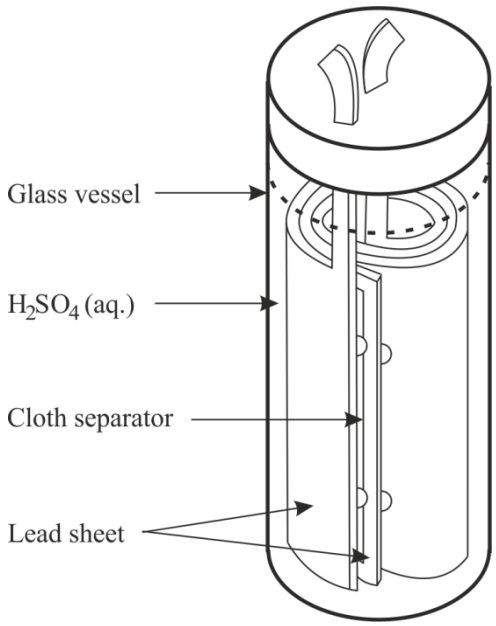

Figure 3.2: Illustration of PLANTÉ'S lead acid cell: two spirals of lead sheets immersed in diluted sulfuric acid were separated by porous cloth within a glass vessel.[4]

Around the turn of the 19th century, JUNGNER changed the constituents of the electrolyte solution inside the battery; an alkaline potassium hydroxide solution was introduced into the battery environment. Hence, it was not strictly necessary to use an acidic electrolyte for battery systems. Nickel hydroxide acted as material for the positive electrode and the negative electrode consisted of a mixture of cadmium and iron.[4]

3.2 Lithium Ion Batteries

LEWIS began to research on the topic of lithium batteries in 1912. Lithium exhibits beneficial properties including; light weight, low density, high theoretical specific capacity of 3,861 mAh/g and low electrode potential of −3.04 V *versus* standard hydrogen electrode (H^+/H_2).[6] Several decades later HARRIS observed the stability of lithium metal in nonaqueous electrolytes consisting of lithium salts dissolved in organic solvents. Those studies were crucial for production of primary lithium cells. In the years between 1960 and 1980, several primary lithium systems were invented: e.g. lithium-sulfur dioxide ($Li//SO_2$), lithium-manganese oxide ($Li//MnO_2$), or lithium-copper oxide (Li//CuO). All lithium battery systems provided a potential of approximately 3 V.[6a]

In the early 1970s, ARMAND discovered the phenomenon of reversible insertion/reinsertion of a guest species (ions, organic molecules or organometallic compounds) into a host lattice. During this insertion/reinsertion process the host maintained its structure but exhibited special physical properties.[6a,7] Later GOODENOUGH investigated the host behavior of lithiated transition-metal oxides e.g. lithium iron oxide ($LiFeO_2$). Delithiation/lithiation of most transition metal oxides occurs somewhat above the SHE potentials, which makes them appropriate as cathode material in combination with low voltage anodes such as Li metal. All additionally gained knowledge of secondary lithium ion batteries (LIBs) was built on GOODENOUGH'S research.[8]

The idea of ARMAND and SCROSATI was to use intercalation materials at both electrodes rather than Li metal, which proved hazardous; lithium ions move between intercalated states of the positive and negative electrode with different potentials. This model is often called rocking chair. Finding an anode material suitable for LIBs than cathode materials deemed more difficult.[8a] Early works of BASU and YAZAMI based on graphite electrodes failed because of intercalation and further reduction of solvent molecules.[9] However, YOSHINO described the use of lower temperature carbons (petroleum coke) and improved the performance of the negative electrode material due to almost no solvent intercalation/reduction.[10] Work by

TARASCON and DAHN introduced mixtures of EC and linear carbonates instead of the commonly used PC, and thus allowed for reversible cycling of graphite electrodes.

Some years later, in 1991, the company SONY introduced the commercially available secondary lithium ion battery into the worldwide market. The battery consisted of lithium cobaltate ($LiCoO_2$) as cathode material, a non-graphite carbon (lithiated coke LiC_6) as anode material and lithium hexafluorophosphate ($LiPF_6$) in propylene carbonate/diethyl carbonate as the electrolyte (Figure 3.3).[6a, 11]

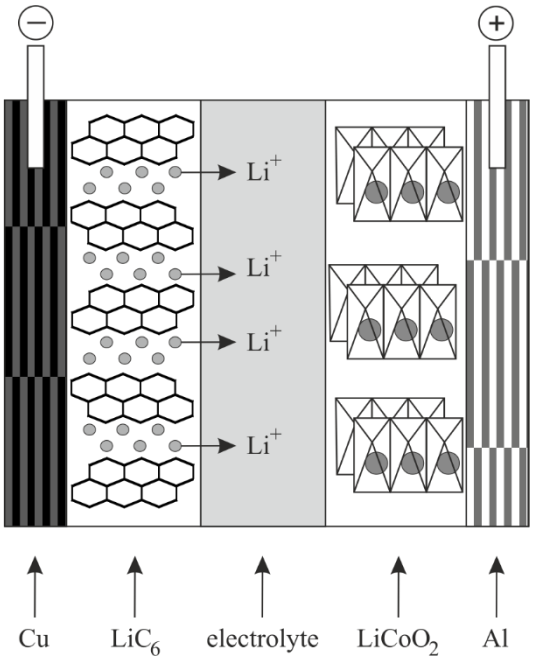

Figure 3.3: Schematic representation of secondary LIB: both electrode materials are able to intercalate/deintercalate lithium ions.[6a]

Today, tools, computers, automotive vehicles and more require portable energy sources. One major disadvantage of the present electric powered cars is the limited driving range compared to combustion engines. The crux of the matter is the low ratio of energy per weight (specific energy) of the intercalation type LIBs. Even if the performance is enhanced to the theoretical maximum and the specific energy is doubled, the obtained driving range may continue to be a barrier for the use of electrically powered cars.[2f] For that reason an ongoing topic in research is to find better electrode materials in the area of 'beyond intercalation chemistries' with the goal to replace the current materials.[2a-g] These chemistries include replacing carbon intercalation anodes with silicon alloying[2a-c] or with conversion reactions,[2d] and intercalation cathodes with Li-oxygen or Li-sulfur cathodes.[2e-g] Those new types of electrode material class deliver a leap in energy density (Figure 3.4).[2h]

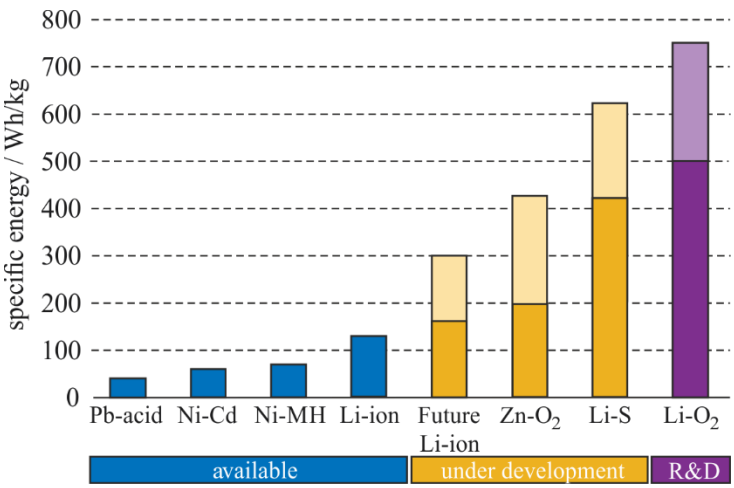

Figure 3.4: Practical specific energies of several existing batteries (blue), batteries under development (yellow) and future type batteries (violet).[2f]

Due to high availability and low cost, there is growing interest in sodium battery chemistries on the basis of similar avenues, e.g. alloying, conversion or Na-oxygen.[12] However, 'beyond intercalation' type materials possess disadvantages. Negative side effects include increased participating particle volume during cycling and high electronic resistance.[13] For instance, full alloying of silicon to $Li_{3.75}Si$ on charge implies a volume change of ~260%. In the case of fully alloying of tin relating to sodium ion chemistries to $Na_{3.75}Sn$, the volume change is even more distinct (~420%). In the case of oxygen cathode materials, lithium peroxide (Li_2O_2) and sodium superoxide (NaO_2) are generated during discharge (Figure 3.5).[2h]

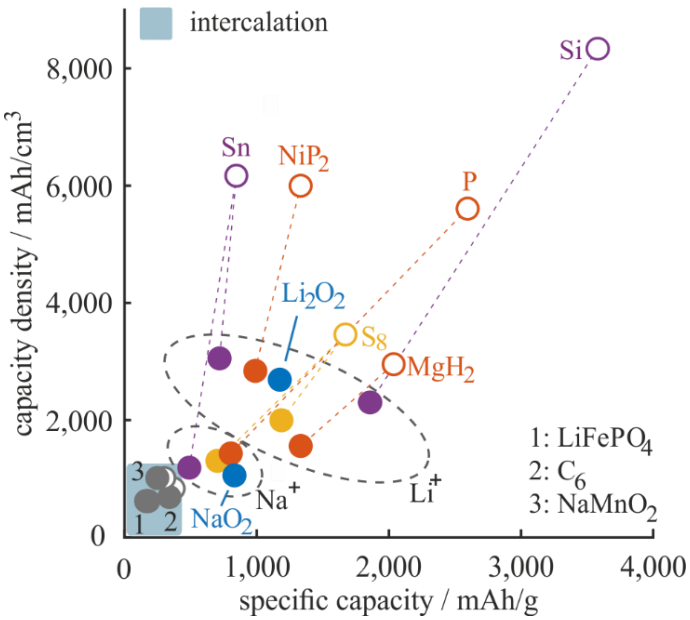

Figure 3.5: Formal capacity per weight *versus* volume of metalated (filled symbols) and demetalated (open symbols) phases of a selection of storage materials. Colors distinguish intercalation materials (grey), alloying (violet), sulfides (yellow), oxides (blue), and conversion materials (red).[2h]

To ensure the functionality of a battery, permanent ionic conductivity to the electrolyte and electronic conductivity to the current collector must be fulfilled. Generally, this process is achieved by imbedding the active material into an electronic conducting carbon network (carbon black or carbon fibers), which is cohered by a binder and soaked with liquid electrolyte for ionic conductivity. This method is optimal when intercalation type materials are used in batteries, as they are not affected by large volume changes during cycling. However, when the electrochemically active material is replaced by conversion materials, the battery host must provide enough space for the particles to expand. Otherwise, pressure is generated inside the battery, which ends with the destruction of the cell body. To overcome this problem, an engineered dead space is introduced into the battery, which diminishes the volumetric and gravimetric energy density (Figure 3.6).

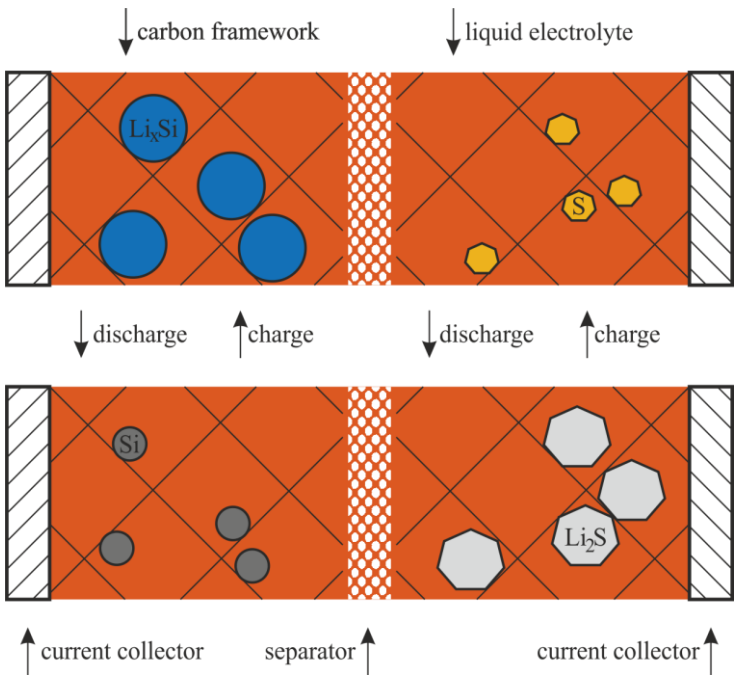

Figure 3.6: Embedding of electrochemically active material into a rigid carbon network, cohered by a binder and soaked with a liquid electrolyte.

3.3 Ionic Conducting Polymers (ICPs)

The first polymers have been used as insulating materials, such as metal wires coated with polymers. However, current research demonstrates that different types of polymers have special properties, e.g. conjugated conducting polymers, or ionically conducting polymers.[14] WRIGHT reported in 1975 the temperature dependence of direct current ion conductivity in a polymer.[15] Since then, a wide scope of ionically conducting polymers or polymer electrolytes has been developed for various applications. Dissociated salt ions in motion are required for ionic

conductivity. For this purpose, salts (e.g. $LiPF_6$) are dissolved into the polymer and complexed by suitable coordination sites at the polymer chain. Table 3.1 shows a selection of polymer functions that enable cation complexation by donating lonepairs. Typical for non-aqueous electrolytes, salt dissociation is dominated by the solvation of the cation since acceptor properties of organics are weaker[16] and the ions can be dissolved at different concentrations. Due to the large molecular weight of polymers and many coordination sites, a meaningful measure for the salt concentration is the number of salt molecules per repeating unit. Ion mobility is enabled by polymer motion. A basic requirement of ionical conducting polymers is the permanent presence of solvent molecule inside the polymer chains. Upon drying ionic conductors become insulators.[14, 17]

Table 3.1: Ionically conducting polymers: poly(ethylene oxide) (PEO), poly(ethylene imine) (PEI), poly(propylene oxide) (PPO) with corresponding repeating unit.[17]

Name	Repeating unit
Poly(ethylene oxide) (PEO)	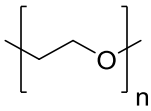
Poly(ethylene imine) (PEI)	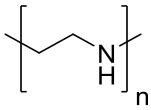
Poly(propylene oxide) (PPO)	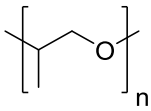

Generally, the ionic current density (j_i) is calculated the following way,

$$j_i = -\frac{\sigma_i}{q} \nabla \tilde{\mu}_i \tag{2.1}$$

where σ_i is the ionic conductivity, q is the elementary charge and μ_i the electrochemical potential of the ions. The temperature dependence of the conductivity σ_i includes the special nature of the ionic conduction mechanism, based on segmental motion. Additionally, the conductivity reflects the nature of the polymer/salt mixture. Albeit the conduction mechanism including solvent molecules is different. Small molecules act like solvating agents and thereby enhance the ionic mobility. Ionically conducting polymers such as PEO or PPO have a high stability towards chemical influences and furthermore show a large electrochemical stability window over several eV. Besides that, the electronic conductivity is negligible.[17a]

3.4 Electronic Conducting Polymers (ECPs)

Research on the topic of π-conjugated molecular semiconductors started around 1940. Due to the lack of proper capabilities of controlling the structure-property relationship, the organic material studies fell behind inorganic semiconductors. Between the 1970s and 1980s, two superior discoveries influenced the field of organic semiconductors. For this reason, SHIRAKAWA, MCDIARMID and HEEGER were awarded the NOBEL Prize for chemistry in 2000. In 1971 SHIRAKAWA produced partly crystalline polyacetylene (PA) films under well-defined conditions.[18] Six years later the NOBEL laureates showed unambiguous evidence, that after doping the PA films with iodine vapor, the electronic conductivity was increased by several orders of magnitude. The modified PA films then had the electronic behavior, a characteristic only typical for metals.[19]

After these pioneering developments, many other organic semiconductors were synthesized; the electronic conductivity was drastically enhanced by the process of doping (Table 3.2). The similarity of all structures is the consistent alternation between single (σ) and double (π) bonds within the carbon chain. This π-conjugation provides special optical, electrochemical and electronic properties. The addition of heteroatoms (e.g. N, S) into the conjugated π-system also influences the material properties by sharing their *p*-orbitals to the π-system. Research demonstrates that the length of the π-system is responsible for different physical properties: e.g. degree of crystallinity and intra- and inter- chain interactions. Compared to conventional inorganic semiconductors, the organic materials have several advantages such as; chemical diversity, low density, flexibility, corrosion resistance, easy controllable shape and morphology, and tunable conductivity.[14, 20]

Table 3.2: Electronically conducting polymers: *trans*-polyacetylene (PA), polypyrrole (PPy), polythiophene (PT), poly(paraphenylene) (PPP) and polyaniline (PANI) with corresponding repeating unit structure and conductivities in S/cm in their undoped and doped state.[19a, 20a, 21]

Name	Repeating unit	Conductivity undoped (S/cm)	Conductivity doped (S/cm) (Dopant)
trans-Polyacetylene (PA)	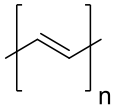	10^{-5}	80 (Na^+)
Polypyrrole (PPy)	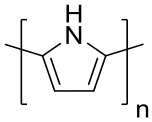	2.6×10^{-2}	10 (Cl^-)
Polythiophene (PT)	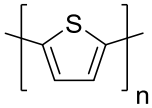	2×10^{-8}	20 (Cl^-)
Poly(paraphenylene) (PPP)	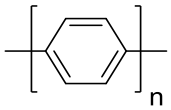	10^{-12}	1.5×10^4 (AsF_5)
Polyaniline (PANI)	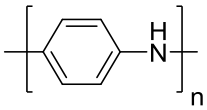	3.6×10^{-9}	8.3 (ASPB)

There are other types of electronically conducting, organic π-conjugated polymers, which do not belong to the group of linear homopolymers such as PA or PPy. For example, fused-ring and ladder-type polymers, blends and self-doped polymers, and conducting polymers based on bridged macrocyclic *d*-metal complexes are components of that class (Table 3.3).[19b, 20a]

Table 3.3: Examples for fused-ring and ladder-type polymers, blends and self-doped polymers, and conducting polymers based on bridged macrocyclic *d*-metal complexes are component of that class.[19b, 20a]

Fused-ring and ladder-type polymers	**Blends and self-doped polymers**	**Conducting polymers based on bridged macrocyclic *d*-metal complexes**
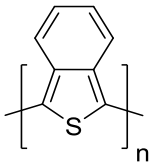	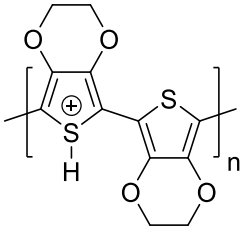	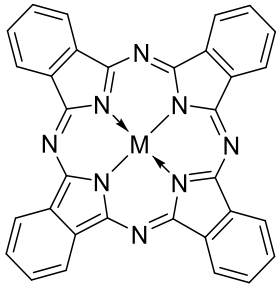
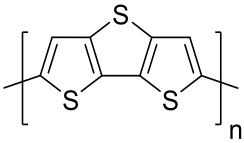	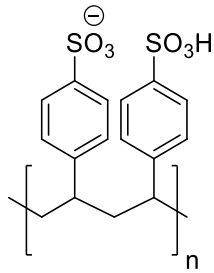	
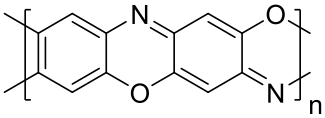	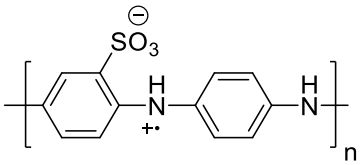	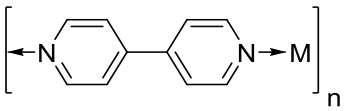

3.5 Doping

Typically, polymeric structures have an insulating behavior. Certain materials – for example electronically conducting polymers (ECPs) – can show metallic conductivity properties upon doping. Due to the unique chemical structures, ECPs posses a completely different doping mechanism compared to their inorganic counterparts. When a dopant reacts with an ECP, a redox reaction occurs and charges are transferred to the polymer. Simultaneously charge carriers are formed.[22] The dopant can either provide electrons to the polymer, or extract electrons from it. A simple declaration of the doping effect is the following: electrons are transferred to the lowest unoccupied molecular orbital (LUMO) of the conduction band (reduction) or electrons are extracted from the highest occupied molecular orbital (HOMO) of the valence band (oxidation). This redox reaction generates charge carriers in the form of polarons (radical ions), bipolarons (dianions or dications), or solitons in the polymer chain. Based on the structures of the ECP in the ground state, the ECPs can be classified into two categories: degenerated and non-degenerated systems. Degenerated polymers own two

geometric identical structures in the ground state, whereas non-degenerated ones possess two different structures with different energies in the ground state. In solitons, the charge carriers are located in degenerated systems, e.g. PA. However, in polarons and bipolarons the charge carriers can be provided in degenerated as well as in non-degenerated systems such as PPy and PT.[23] The movement of those charge carriers along the polymer chain are responsible for the electronic conductivity. According to solid-state physics terminology, *p*-type doping belongs to oxidation processes, whereas reduction processes correspond to *n*-type doping.[24] With *n*-type doping, electrons are transferred from the dopant to the LUMO of the polymer, which increases the electron density of the polymer. Conversely, in *p*-type doping, electrons located in the HOMO of the polymer move to dopant species. Thereby electron holes are generated in the polymer backbone. Consequently, doping processes can tune the density and mobility of the charge carriers.[20a, 25]

ECPs can undergo either *p*-type doping, or *n*-type doping, as shown in Figure 3.7 by the example of PT. Either positive or negative polarons/bipolarons are generated during doping processes. The delocalization of the charge carriers over the polymer chains enables the electronic conductivity. Generally, positively charged carriers in *p*-doping are more stable than negatively charged forms, which makes *p*-doping more popular for practical applications.[20a]

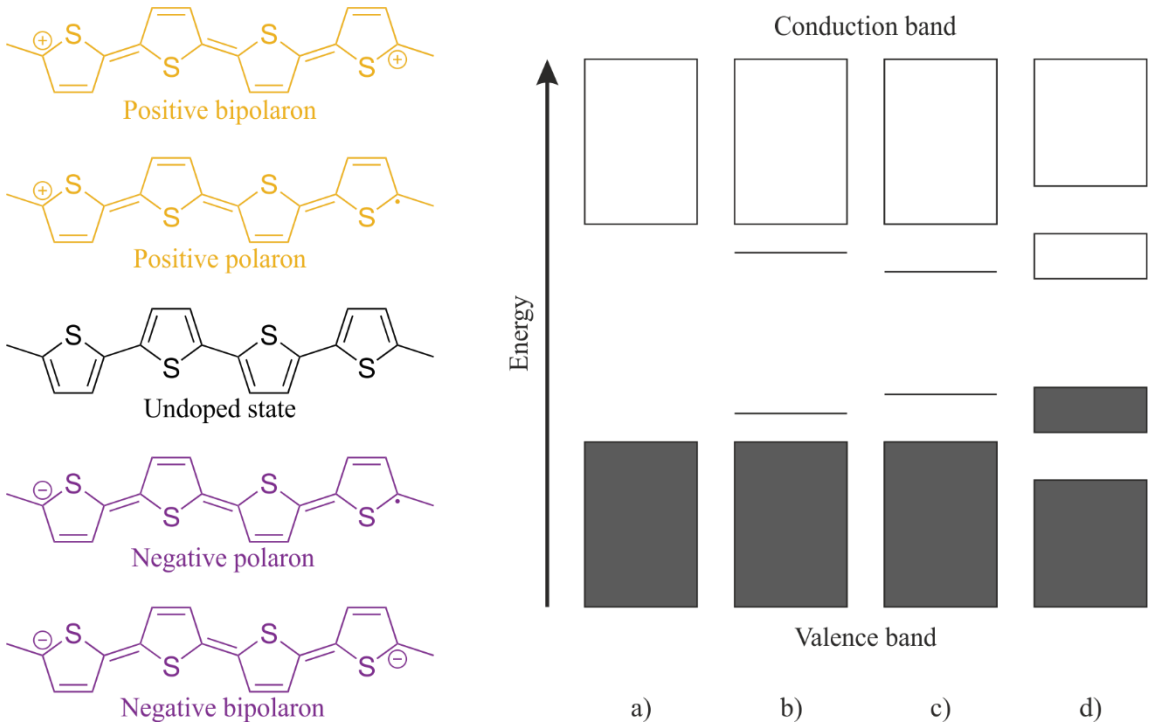

Figure 3.7: Chemical structures of polythiophene (PT) with *p*-type doping and *n*-type doping (left); electronic bands of electronically conducting polymers (ECPs) illustrating (a) undoped; (b) polaron; (c) bipolaron; and (d) fully doped states (right).[20a]

PA is a member of the category of ECPs with a degenerated ground state. When the polymer chain contains an odd number of carbon atoms, the single and double bond can exchange electrons. This leads to two geometrical structures (A and B phases), which have the same energy. A radical form located between the two phases contains an unpaired π-electron. Such a defect is usually called neutral soliton. Due to delocalization along the polymer chain, the soliton has a definite motion. A soliton can undergo a redox reaction with a dopant to a positive or negative soliton, which raises the stability of the species. Furthermore, charged solitons do not possess a spin. Interaction between charged solitons creates a band-like feature, which is called soliton band.[26] The energy level of the formed soliton band is located between the HOMO and the LUMO of the polymer. The wide of the soliton band depends on the doping level (Figure 3.8).[20a]

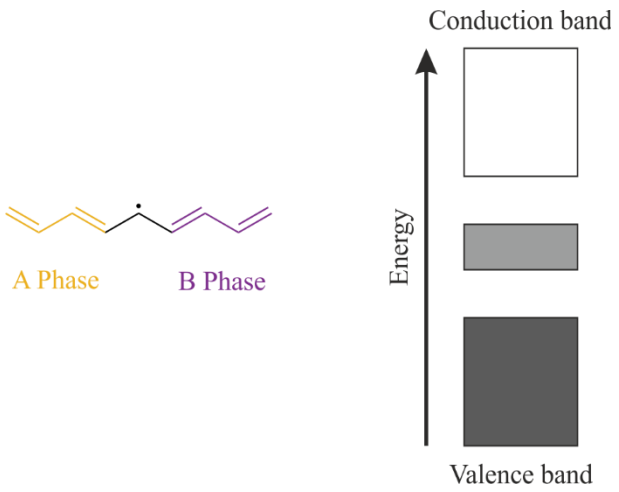

Figure 3.8: Schematic illustration of the geometric structure of a neutral soliton on a *trans*-PA chain (left); electronic bands of PA including the soliton band between the HOMO and LUMO (right).[20a]

3.6 Mixed Ionic and Electronic Conducting Polymers (MIECP)

Mixed conducting behavior is more common in organic semiconductors than in inorganic ones, because ECPs always show some ionic conductivity. Doping processes could tune the electronic conductivity to a higher extend, but the polymer may not reveal the ionic conductivity, which is needed for practical applications. In contrast, ICPs possess no electronic conductivity. The easiest way to produce a polymer with both – electronic and ionic – properties is to mix an ICP and an ECP to a blend. Unfortunately this may be experimentally difficult to achieve because of phase separation in the equilibrium.[17a] In 1995 ARMAND was one of the first, who attempted to synthesize a 'solid solution' MIECP – a co-polymer, which consisted of electronically and ionically conduction parts. However, the polymer exhibited low electronic conductivity. In this attempt, unsaturated carbocycles of various ring sizes were used as electronical conductors and PEO-units as ionical ones.[27] In the course of time the components

of the electronically conducting segments varied from PPy over PT, polycarbazoles and polyfluorenes to pyrene units, but in most of the cases PEO was used as ionically conducting part inside the MIECP.[1a, 1c, 1e, 1f, 28] The impedance range of different MIECPs varies from 10^{-5} to 10^{4} S/cm, which is in the field of undoped and doped ECPs.[27, 28b, 28d, 28e, 29] The impedance behavior relayed on different morphologies or oxidation states were also investigated.[30] In the last decade different working groups were able to assemble half-cells containing MIECPs. The results of the cycling experiments were quite promising and in near future the common battery systems could be changed to systems containing MIECPs.[1]

The huge advantage of battery systems containing MIECP is that in those systems the loading of the electrochemical active material could be significantly higher than in systems using rigid carbon framework compared Figure 3.6. Consequently, the capacity and the specific energy of the battery systems will noticeably increase. In an ideal case, the MIECP completely covers the storage material and ensures the permanent electronic and ionic conductivity. Furthermore, the polymer should accommodate the volume changes during charge/discharge and thus increase the cyclability of battery systems, in which beyond intercalation type materials are used (Figure 3.9).

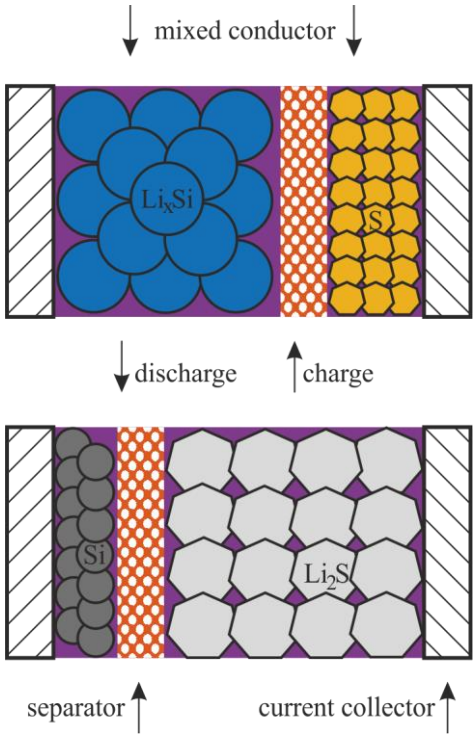

Figure 3.9: Imbedding of electrochemical active material into a MIECP, which is swollen with a liquid electrolyte.

3.7 Oxygen in Electrochemistry

Changing the current battery technology to metal-air (including Li-O_2) systems exhibits a tremendous increase of the theoretical capacity (e.g. 1,168 mAh/g for Li_2O_2). The reversible ongoing electrochemistry for Li-O_2 batteries during charge/discharge is following: $O_2 + 2e^- + 2Li^+ \rightleftarrows Li_2O_2$. However, a simultaneous two-electron reduction is unusual and therefore molecular oxygen (O_2) is reduced stepwise *via* two processes to form lithium peroxide (Li_2O_2).[3] During discharge, the first reduction step in aprotic Li^+-electrolytes involves a $1e^-$ reduction of O_2 to generate lithium superoxide (LiO_2).[31] In the second step, LiO_2 can either undergo a second $1e^-$ reduction or it disproportionates to form Li_2O_2.[32] The direct reduction mechanism implies that the process takes place on the surface of the electrode. Whereas, the disproportionation mechanism involves a solution-based process, in which LiO_2 dissolves in the electrolyte (Scheme 3.1). Following equation describes the division between surface-bound LiO_2 and the solubilization of it in the equilibrium:[33]

$$LiO_2^* \rightleftharpoons Li^+_{(sol)} + O_2^-{}_{(sol)} + \text{ion pairs} + \text{higher aggregates} \tag{2.2}$$

where * stands for surfaces bound species. The ability of solvents to dissolve cations is defined by the GUTMANN donor number (DN).[3] Standard solvents of electrolytes have DN from 14-30 depending on their functional groups. High DN solvents favor the solution mechanism, albeit they also enhance parasitic reactions and side product formation. However, the standard potential for O_2/O_2^- is ~2.65 V, 2.96 V for O_2/Li_2O_2 and ~3.3 V for O_2^-/Li_2O_2. Obviously, the second reduction has a stronger driving force and is therefore at higher discharge potentials.[3, 33]

Disproportionation requires low overpotentials and supports solution growth. The solution mechanism preserves the surface of the electrode from insulating Li_2O_2, but with shrinking surface and growing overpotential, the electrochemical process shifts towards the surface mechanism. Due to little mobility for reduced O_2 species, the surface mechanism leads to coherent coverage of the surface yielding low capacity.[3, 33-34] During charging, Li_2O_2 is oxidized to form LiO_2^* or $Li_{2-x}O_2$ *via* topotactic delithiation.[34-35] Afterwards, $Li_{2-x}O_2$ could disproportionate *via* $2LiO_2 \rightleftarrows O_2 + Li_2O_2$ or it could be further oxidized by $1e^-$.[3]

3.7.1 Solution based Li-O_2 Cell Chemistry

Different to other Li^+ storage systems, inside Li_2O_2 particle it is not required to transport Li^+ and e^- for the growth/dissolution. It could happen in any case of the surface. Bypassing Li^+ and

e^- transport trough another phase would create unprecedented opportunities for Li-O_2 batteries. For example, redox mediators – electronic conductive molecules, which are able to reduce/oxidize – move though the electrolyte and act in distant position to reduce O_2 to Li_2O_2. During electron transfer, they are regenerated and could enter the catalytic cycle again.[3] Reduced mediators M^- transfer $1e^-$ to dissolved O_2 in the electrolyte and reduce it to O_2^- within a so called outer sphere reaction. Afterwards O_2^- could undergo a further reduction by another M^- or it disproportionates.[3, 36] A different mechanism where reduction mediators are involved is the so called inner sphere process. Reduction of the mediator in the presence of Li^+ and O_2 would form a LiM and further a $LiMO_2$ complex, which is more stable than LiO_2. Ongoing reaction of $LiMO_2$ with another molecule of LiM or $LiMO_2$ produce Li_2O_2 and M, which is ready for next catalytic cycle (Scheme 3.1).[3, 37]

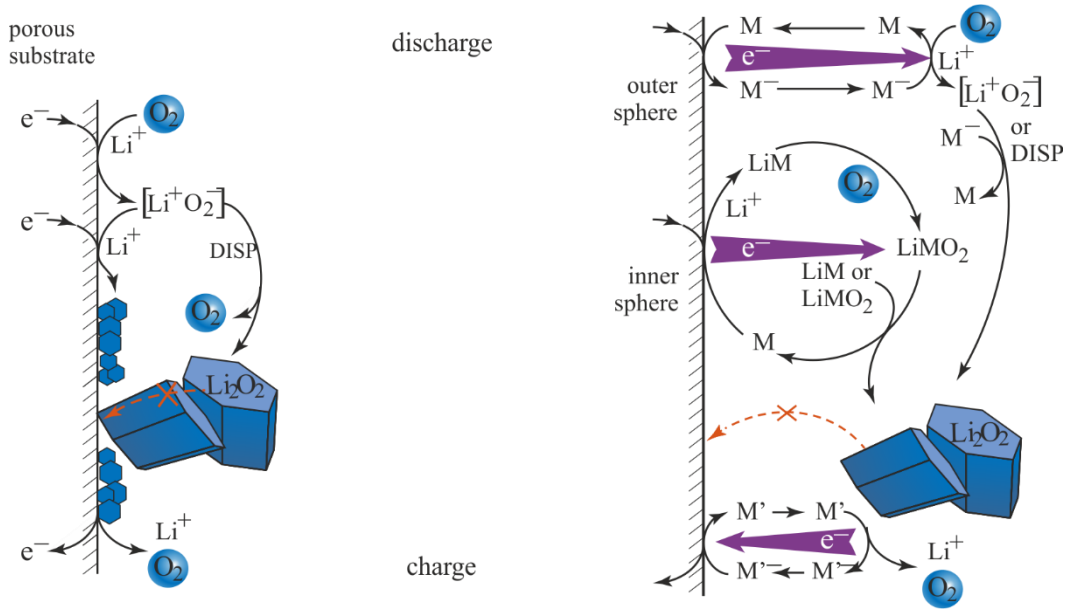

Scheme 3.1: *left:* Schematic of the reactions taking place in a Li-O_2 cathode: ($O_2 + 2Li^+ + 2e^- \rightleftarrows Li_2O_2$) during discharge/charge in conventional electrolyte. The insoluble and insulating discharge product Li_2O_2 forms on the surface of the conducting porous substrate and passivates it. *right:* Mediated electron/hole transport by mediators M and M'. The reduction mediator M may transfer electrons to O_2 either in an outer sphere process or via an O_2-binding transition state in an inner sphere process.[3]

3.7.2 Singlet Oxygen ($^1O_2$)

Oxygen is one of the most abundant elements on earth. It occurs in various chemical compounds as well as pure substance in the atmosphere. Elementary oxygen has two allotropically stable modifications: triplet oxygen ($^3O_2$; $^3\Sigma_g^-$) and ozone (O_3) and two instable modifications: singlet oxygen ($^1O_2$; $^1\Delta_g$ and $^1\Sigma_g^+$) and tetraoxygen (O_4). Singlet oxygen differs in the electronic configuration from triplet oxygen and could be seen as its excited state (Figure 3.10).[38]

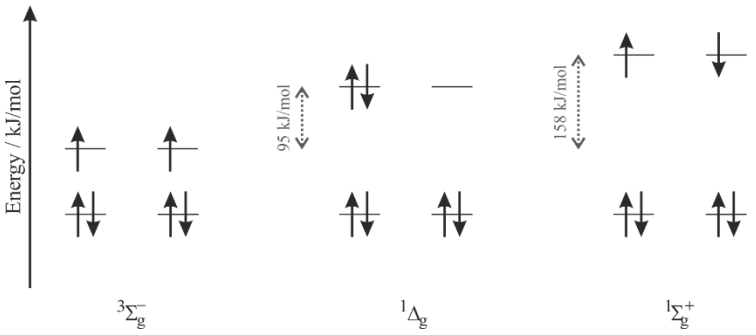

Figure 3.10: Occupied π-orbitals of triplet oxygen ($^3\Sigma_g^-$) and singlet oxygen ($^1\Delta_g$, $^1\Sigma_g^+$) in their lowest states.

The lifetime of $^1O_2$ in solution is extremely short ($^1\Delta_g$: 10^{-3} s; $^1\Sigma_g^+$: 10^{-9} s) for both configurations. Due to spin-forbidden transition from $^3\Sigma_g^-$ to $^1\Delta_g$ and *vice versa*, the lifetime of $^1\Delta_g$-configuration is many magnitudes higher.[38b, 39]

3.7.3 Singlet Oxygen Quenchers

Due to its high energy and reactivity, singlet oxygen causes trouble in diverse habitats. Nature developed mechanisms to protect the organism from serious damages.[40] Also in electrochemistry, $^1O_2$ is involved and leads to parasitic side-product formation and to inefficient cycling behavior.[41] Various amines exhibit the ability to quench $^1O_2$. Especially 1,4-diazabicyclo[2.2.2]octane (DABCO) owns a good $^1O_2$ quenching ability. and it was used to suppress $^1O_2$-formation during cycling of an electrochemical cell. Regrettably, DABCO possesses a relatively small potential window and is oxidized at ~3.6 V *vs* Li/Li^+. Therefore, in $Li\text{-}O_2$ cells it can only be used in certain with restrictions.[41b, 42]

4. Organic Mixed Conductors

As exemplified in Chapter 3.4 the range of units, which enhance the electronic conductivity is diverse. However, in this work the focus was on pyrene (Pyr) (**1**) and poly(paraphenylene) (PPP) (**2**) based structures. Tetraethylene glycol methyl ether (TEG) (**3**) units should provide the ionic conductivity to our systems. Those structures combined should yield mixed conducting substances (Figure 4.1). Subsequently the electrochemical behavior of these substances should be examined and batteries with containing organic mixed conductor should be assembled.

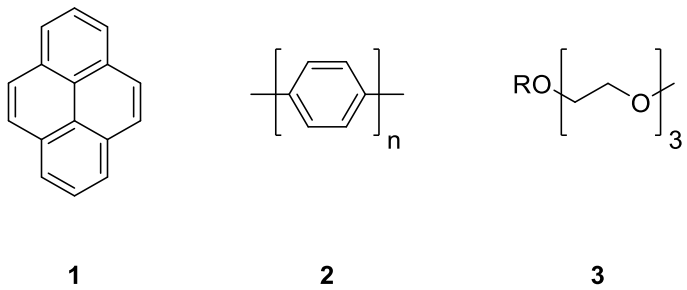

Figure 4.1: Electronical conducting units: pyrene (Pyr) (**1**), poly(paraphenylene) (PPP) (**2**) and ionical conducting unit: tetraethylene glycol methyl ether (TEG) (**3**).

In the course producing mixed conducting substances several pre-experiments were performed to combine electronic and ionic conducting units.

4.1. Physically Mixing of Electronical and Ionical Conducting Units

The simplest way to create a mixed conducting composite is to blend two substances. One big advantage of this method is that the ratio of the different substances can be adapted easily. The amount of functional units is also an important factor, which has to be considered. For that

reason, symmetric molecules were synthesized, which carry two functional units respectively. The in the following discussed molecules were synthesized based on the literature of STRASSER *et al.*.[43] The ulterior motive of this synthesis route was to create many functional units with low effort. The sulfone unit in both molecules may additionally enhance the ionic conductivity. In fact, molecules (**4**, **5**) consist of units, which exclusively provide mixed conductivity (Figure 4.2). Unfortunately, due to different polarities, phase separation occurred, which is already known for other blended systems.[17a]

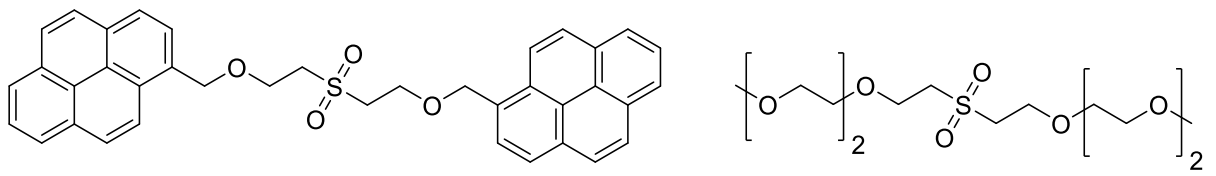

4 **5**

Figure 4.2: Composite with mixed conductive properties: 1,1'-(((sulfonylbis(ethane-2,1-diyl))bis(oxy))bis(methylene))dipyrene (**4**), 1-methoxy-2-(2-((2-(2-methoxyethoxy)ethyl)sulfonyl)ethoxy)-ethane (**5**).

4.1.1. Preparation of 1,1'-(((sulfonylbis(ethane-2,1-diyl))bis(oxy))bis(methylene))-dipyrene (**4**)

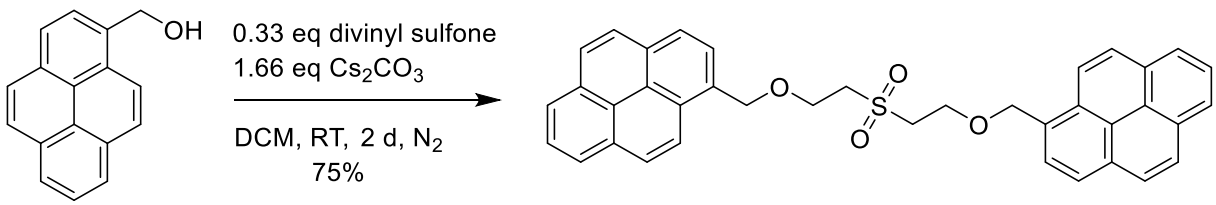

6 **4**

Scheme 4.1: Preparation of 1,1'-(((sulfonylbis(ethane-2,1-diyl))bis(oxy)bis(methylene)dipyrene (**4**) *via* an oxa-MICHAEL addition.

The MICHAEL addition reaction is frequently used in organic chemistry. Usually the electrophile is an α,β-unsaturated carbonyl compound. In this case, the carbonyl was exchanged to a sulfon moiety. Using optimized conditions, the product formation could be driven up to 99%. In this particular case, an excess of 1 equivalent alcohol (pyren-1-ylmethanol (**6**)) and 5 equivalents of an inorganic base (Cs_2CO_3) was used regarding a difunctional MICHAEL acceptor (divinyl sulfone). The advantage of an inorganic base is that it can be removed easily after the reaction. Furthermore, the product had a great crystallization ability. Therefore, the purification was done by recrystallization and fortunately, a crystal structure of the product was obtained. Surprisingly, the pyrene cores were ordered in a T-shaped style, which was not expected. The total obtained yield of this synthesis was 75% (Figure 4.3, Scheme 4.1).

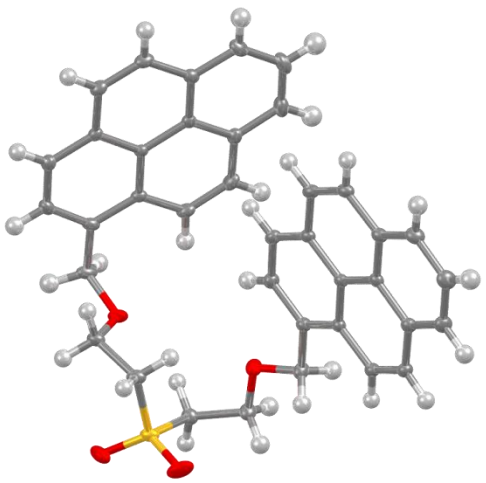

Figure 4.3: Crystal structure of 1,1'-(((sulfonylbis(ethane-2,1-diyl))bis(oxy)bis(methylene)dipyrene (**4**).

4.1.2 Preparation of 1-methoxy-2-(2-((2-(2-methoxyethoxy)ethyl)sulfonyl)ethoxy)-ethane (**5**)

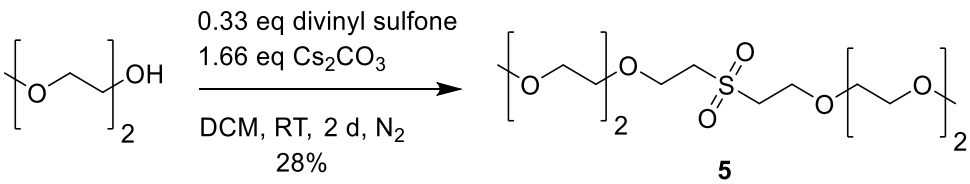

Scheme 4.2: Preparation of 1-methoxy-2-(2-((2-(2-(2-methoxyethoxy)ethyl)ethyl)sulfonyl)ethoxy)ethoxy)-ethane (**5**) *via* an oxa-MICHAEL addition.

Using the same conditions as before, the product formation was quantitative. Nevertheless, this time, the purification was more challenging, because the educt as well as the product are very polar molecules and therefore hard to separate. However, the product was purified using flash chromatography, albeit the consequences in the form of low yield were serious (28%) (Scheme 4.2).

4.2. Liquid Mixed Conductors

Because of the phase separation of the electronic and ionic conducting units in the blend, the next attempt to synthesize mixed conductors was to connect the units within a single molecule. Therefore, the TEG unit **3** was directly attached to the pyrene core **1** with the goal that the product exhibit mixed conduction. Both reactions follow the mechanism of a S_N2 reaction. The corresponding alcohol with the attached pyrene core reacted as a nucleophile with the TEG electrophile according to the WILLIAMSON ether synthesis (Figure 4.4).[44]

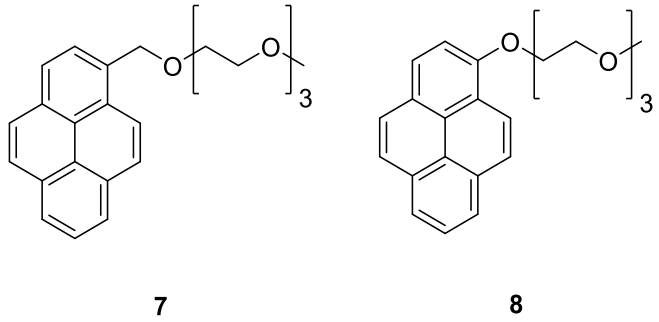

Figure 4.4: Liquid mixed conducting molecules: 1-(pyren-1-yl)-2,5,8,11-tetraoxadodecane (PenzOTEG) (**7**) and 1-(2-(2-(2-methoxyethoxy) ethoxy)ethoxy)pyrene (PyrOTEG) (**8**).

4.2.1. Preparation of 1-(pyren-1-yl)-2,5,8,11-tetraoxadodecane (PenzOTEG) (**7**)

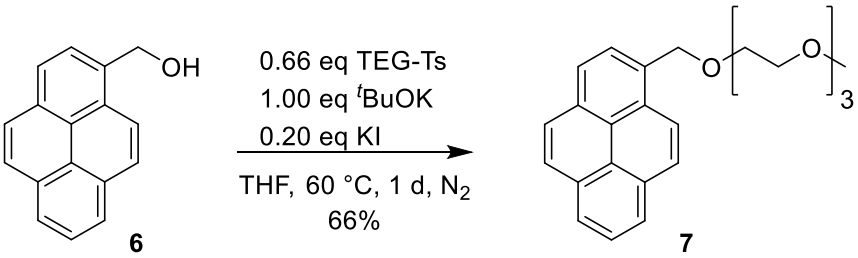

Scheme 4.3: Preparation of 1-(pyren-1-yl)-2,5,8,11-tetraoxadodecane (**6**) *via* a WILLIAMSON ether synthesis.

The ether synthesis itself is a straightforward reaction, but the purification of the product afterwards was tricky in this particular case. Using an equimolar ratio of the nucleophile and the electrophile, the product formation stopped slightly before full conversion. Afterwards three substances had to be separated *via* flash chromatography. Using an excess of 0.5 equivalents of the pyren-1-ylmethanol (**6**) instead, the product formation was quantitative and the following flash chromatography was easier to perform. Potassium iodide acted as a nucleophilic catalyst inside the reaction. Despite the versatile TEG-moiety, crystal growth occurred. The total obtained yield of this synthesis was 66% (Figure 4.5, Scheme 4.3).

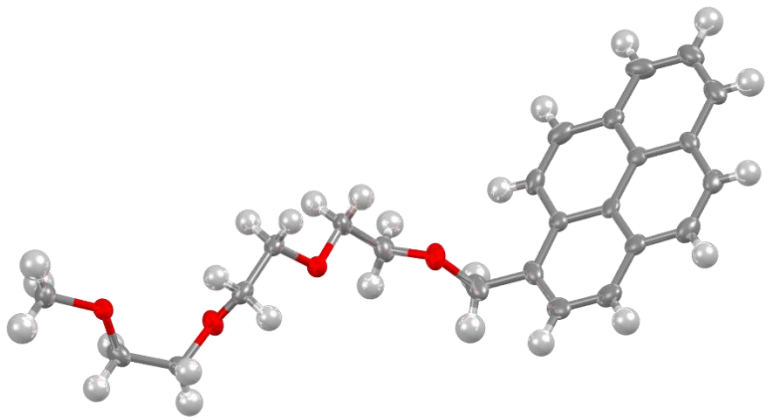

Figure 4.5: Crystal structure of 1-(pyren-1-yl)-2,5,8,11-tetra-oxadodecane (**7**).

4.2.2. Preparation of 1-(2-(2-(2-methoxyethoxy)ethoxy)ethoxy)pyrene (PyrOTEG) (**8**)

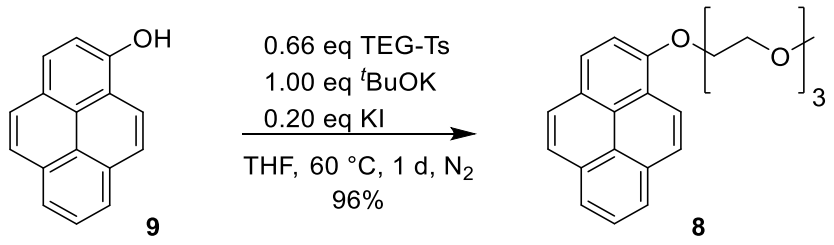

Scheme 4.4: Preparation of 1-(2-(2-(2-methoxyethoxy)ethoxy)ethoxy)pyrene (**8**) *via* a WILLIAMSON ether synthesis.

Using the same conditions as before, the product formation was quantitatively. The missing methylene group between the pyrene core and the alcohol moiety made the difference. Obviously, the purification turned out to be easier to handle compared to PenzOTEG (**7**). Therefore, the product yield was increased to 96% in total, which is impressive. In fact, during flash chromatography no fraction, in which educt and product were mixed, was obtained. Nevertheless, this time no crystallization of the product occurred (Scheme 4.4).

4.2.3. PenzOTEG (**7**)/PyrOTEG (**8**) and Modified PyrOTEG (**8**) as Liquid Mixed Conductors

Surprisingly, the aggregation state of both molecules was liquid. Furthermore, the substances are dark brown, which is uncommon for small organic molecules (Figure 4.6). Provided that both ionic and electronic conductivity of PenzOTEG (**7**)/PyrOTEG (**8**) are in suitable ranges, a new and unique class of mixed conducting substances was created – liquid organic mixed conductors.

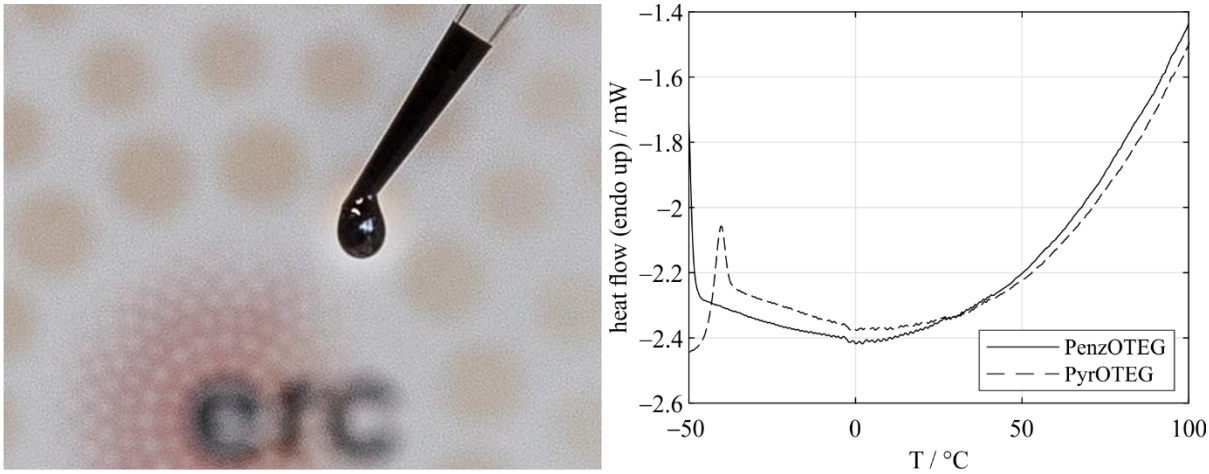

Figure 4.6: *left*: image of PyrOTEG (**7**) in substance inside a sampler tip; *right*: 3rd heat-run of a DSC analysis of PenzOTEG (**7**)PyrOTEG (**8**) using a heating rate of 10 °C/min.

For that reason, both molecules were investigated regarding their electrochemical response using cyclic voltammetry. For this purpose, the substances were diluted to a 3 mM concentration using a 0.1 M TBAP in MeCN electrolyte. CVs were then recorded on Au disc electrodes. The Pyr unit in PyrOTEG shows reversible oxidation and reduction waves at ~4.1 V and ~1.0 V *vs* Li/Li^+. PenzOTEG shows quasi-reversible waves at ~4.3 and 1.2 V *vs* Li/Li^+. Both substances show a nearly featureless range in between 1.2 and 4.0 V. (Figure 4.7).

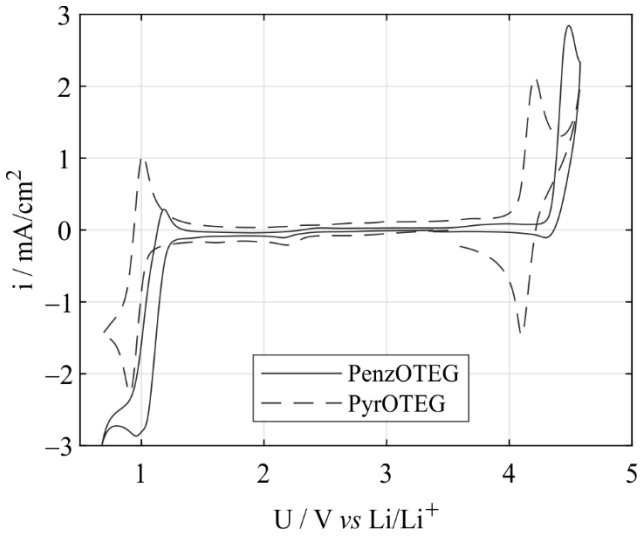

Figure 4.7: Cyclic voltammogram of 3 mM PenzOTEG (**7**; solid line), and PyrOTEG (**8**, dashed line) in 0.1 M TBAP/MeCN; working electrode material: Au, counter electrode material: Pt, pseudo reference electrode material: Ag which was calibrated *vs* Fc/Fc^+.

Furthermore, the electronic and total conductivities were measured using impedance spectroscopy and DC polarization experiments. The ionic conductivity could be calculated by subtracting the electronic from the total conductivity (Figure 4.8). The values of the electronic conductivities of PenzOTEG/PyrOTEG do not differ from other undoped electronical conductors such as PPP or PT. With ~10^{-4} S/cm at 50 °C the ionic conductivity is in a well suitable range to support electrochemistry.[20a] Performing electrochemical reactions in oxidized or reduced states of the molecules can be helpful, because the electronic conductivity would stay enhanced for reactions taking place at proper potentials. For that reason, the molecules were partly chemically or electrochemically oxidized/reduced by applying positive/negative currents, or using oxidation/reduction agents to see how the impedances changed after those processes. Unfortunately, the viscosity also increased with the impedance during the modification. According to STOKES-EINSTEIN equation the diffusion coefficient and charge transport are equally affected by viscosity. Excessive increase of viscosity must therefore be avoided. As compensation of the increasing viscosity, 0.5 equivalents of diethylene glycol dimethyl ether were added after (electro)chemical oxidation/reduction. Unfortunately, the electronic conductivity decreased. In fact, the system with the highest electronic conductivity and lowest viscosity was 0.1 M LiTFSI dissolved in PyrOTEG.

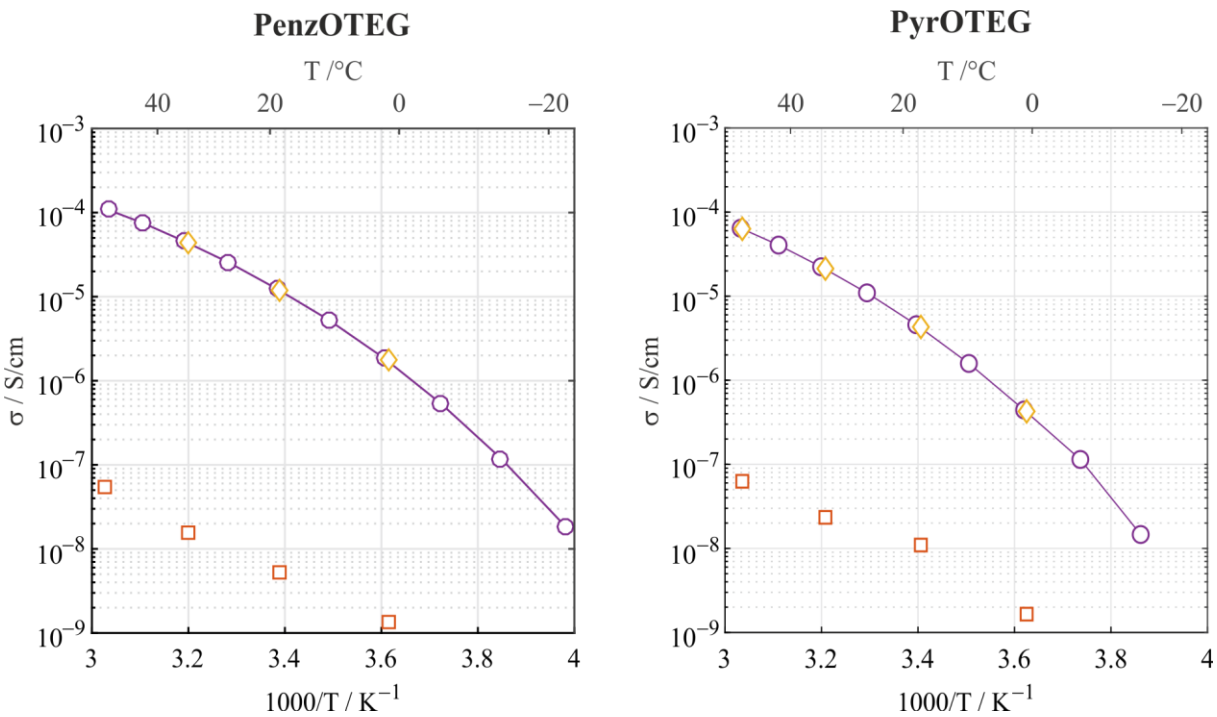

Figure 4.8: Electrochemical characterization of PenzOTEG (**7**, left) and PyrOTEG (**8**, right): combined impedance (violet), ionic impedance (yellow), electronic impedance (red).

Given that in some cases, electronic and ionic conductivities that can be expected to support electrochemical reactions were obtained, investigations towards the stability of the mixed conducting molecules and superoxide (O_2^-) were established whether they could be used to do O_2 electrochemistry therein. Therefore, the mixed conducting molecules were exposed to an excess of potassium superoxide (KO_2) and possible reactivity monitored by ^{1}H-NMR spectroscopy at times up to 96 h (Figure 4.9). PenzOTEG showed appreciable reactivity with KO_2 since already after 5 h reaction none of the initial molecule remained in the reaction mixture, whereas PyrOTEG was stable for several days. The likely reason was that the methylene group between the pyrene core and the next oxygen atom in the benzylic PenzOTEG appears too acidic and was abstracted by strongly basic superoxide. Both electrochemical characterization and stability testing against O_2^- suggest PyrOTEG to be a good candidate for further electrochemical tests with O_2 electrochemistry.

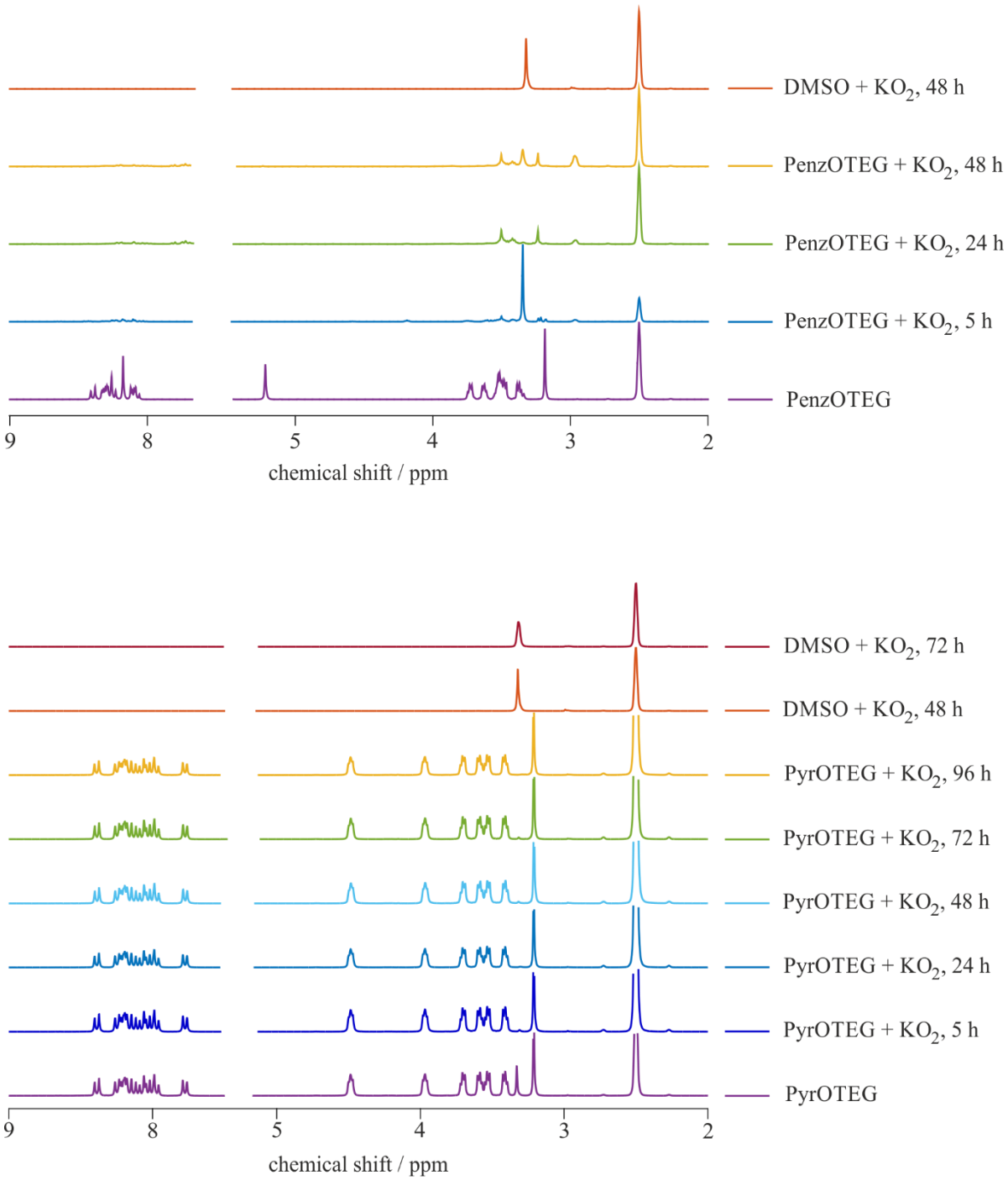

Figure 4.9: Stability screening of PenzOTEG (**7**, top) and PyrOTEG (**8**, bottom) against KO_2 using ^{1}H-NMR spectroscopy in DMSO-d_6.

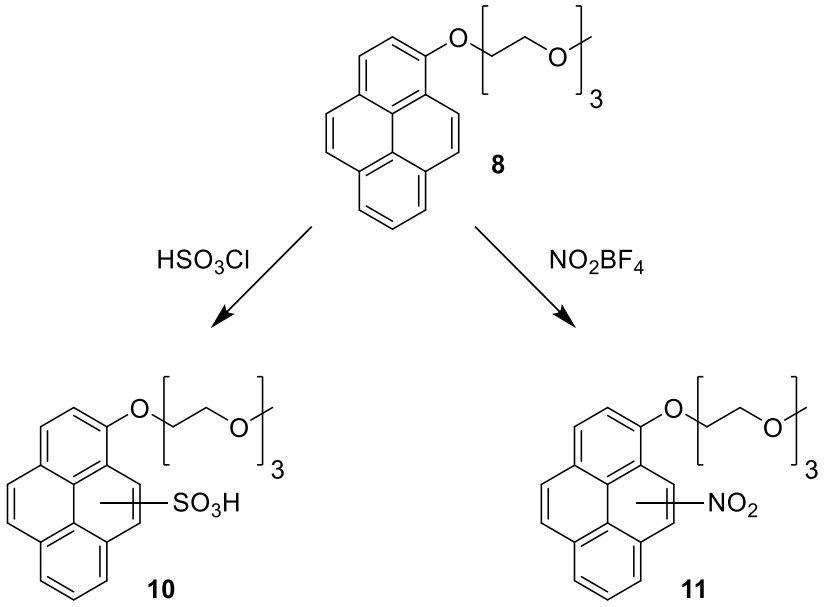

Scheme 4.5: Modification of PyrOTEG (**8**) to 3-(2-(2-(2-methoxyethoxy)ethoxy)ethoxy)pyrene-1-sulfonic acid (isomeric mixture) (**10**) or 1-(2-(2-(2-methoxyethoxy)ethoxy)ethoxy)-3-nitropyrene (isomeric mixture) (**11**).

Given that the conductivity of organic electron conductors is generally boosted by doping, changing the potentials where the Pyr unit is oxidized or reduced to influence the potential range where the substances exist in the doped state was aimed. To modify the redox potentials of PyrOTEG (**8**), electron withdrawing groups were attached to the pyrene core. For that reason, either a sulfonic acid (**10**) or a nitro (**11**) moiety was attached to the aromatic core of the PyrOTEG to shift the reduction potential to higher values (Scheme 4.5).

The sulfonic acid moiety was added by a reaction with sulfonyl chloride. After full conversion, the product was purified by extraction into aqueous phase. The drawback of this modification reaction was that undefined regio-isomers were generated. Nevertheless, all of them were mono substituted according to the ^{1}H-NMR spectrum and therefore they could be expected to affect the redox potential of the product more or less the same extent. Investigations towards the change in redox potential using cyclic voltammetry of 2 mM product dissolved in 0.1 M LiTFSI in TEGDME as the electrolyte were performed. It appeared that it was poorly soluble which we ascribed to the relatively weak basicity of the sulfonic acid group, which is typically not sufficient to be overcome by the solvating power of organic solvents. The CV shown in Figure 4.10 shows that the onset of reduction was positively shifted by ~200 mV. The oxidation shows a new plateau-like feature ~200 mV negative of the PyrOTEG followed by a further oxidation process ~100 mV positive the original Pyr oxidation. The later appear irreversible

while the first may to some extent be reversible. Given these electrochemical characteristics the substance was not further investigated.

The nitro moiety was added using nitronium tetrafluoroborate as reagent. This reagent provided the necessary NO_2^+ unit, which had to be generated *in situ*. After purification by flash chromatography, the product also consisted of a regio-isomeric mixture. Again, all the PyrOTEG molecules had one attached nitro moiety according to ^{1}H-NMR spectroscopy. The reduction potential was shifted over 250 mV, but the synthesis gave with ~30% only poor yield Given that the nitro group is not expected to be stable with superoxide the further investigation was given lower priority.

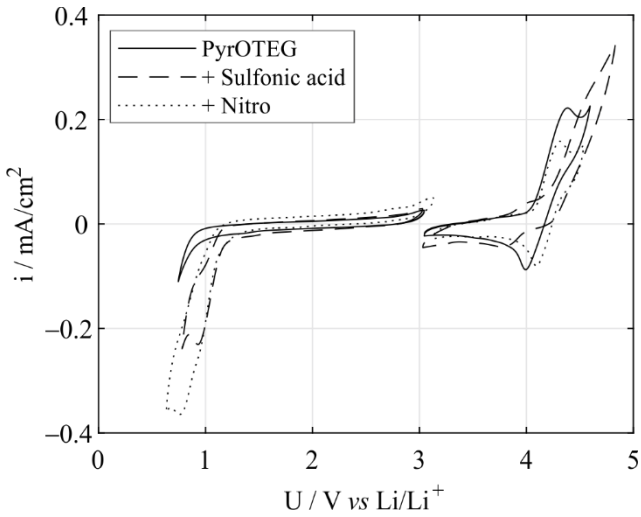

Figure 4.10: Cyclic voltammograms of 2 mM PyrOTEG (**8**; solid line), 3-(2-(2-(2-methoxyethoxy)ethoxy)-ethoxy)pyrene-1-sulfonic acid (isomeric mixture) (**10**, dashed line) and 1-(2-(2-(2-methoxyethoxy)-ethoxy)ethoxy)-3-nitropyrene (iso-meric mixture) (**11**, dotted line) in 0.1 M LiTFSI/TEGDME: working electrode material: Au, counter electrode material: Pt, pseudo reference electrode material: Ag which was calibrated *vs* Fc/Fc$^+$.

Finally, investigations whether the liquid mixed conductor enables electrochemical reactions to take place in the volume of the liquid mixed conductor were undertaken. To find out whether homogeneous electrochemistry as opposed to typical heterogeneous electrochemistry at the interface between pure electron and pure ion conductor takes place at a glass carbon electrode with and without the liquid mixed conductor, cyclic voltammetry with the ferrocene/ferrrocenium (Fc/Fc$^+$) redox couple were performed. Therefore, the obtained peak current density is used to calculate an effective reaction surface area, using STOKE-EINSTEIN and RANDLES-SEVCIK equation. A significantly higher current density in the mixed conductor than expected at the surface only would suggest that part of the current is generated by a homogeneous electrochemical reaction in the mixed conductor. To do so, the diffusivity of ferrocene in the mixed conductor needs to be determined by other means than electrochemically using the RANDLES-SEVCIK Equation (4.2). This equation relates the peak current density with the diffusivity of the redox species and the scan rate and is thus conveniently used to measure

diffusivities. To bypass this the STOKE-EINSTEIN equation was used that relates diffusivity with viscosity:[45]

$$D = \frac{kT}{6\pi\eta r} \tag{4.1}$$

where D is the diffusion coefficient, k the Boltzmann constant, T the temperature, η the dynamic viscosity and r the particle radius. But for that purpose η and r had to determined before.

First, the viscosity of PyrOTEG containing 0.1 M LiTFSI was measured, which was further used as the electrochemical medium. The obtained results are shown in Figure 4.11.

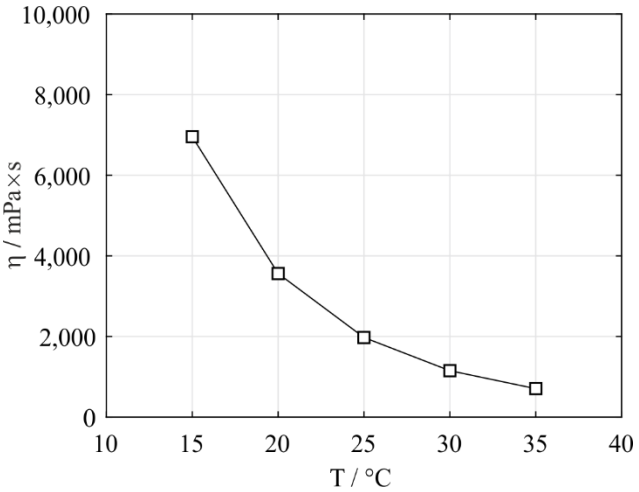

Figure 4.11: Viscosity of PyrOTEG (**8**) containing 0.1 M LiTFSI.

The solvate radius had to be assumed, because it was unknown for this particular system. Using crystallographic data for ferrocene,[46] crystallographic data from PenzOTEG (**7**) and geometrical calculations a molecule radius of 25 Å was estimated. Since all efforts crystallizing PyrOTEG (**8**) were unsuccessful, the crystallographic data of PenzOTEG was used here as an approximation. Size differences are expected to be minor since they differ only in one CH_2 group. After inserting the values into Equation (4.1), a diffusion coefficient D of 2.41×10^{-10} cm^2/s at 20 °C was obtained.

Afterwards CV measurements at different scan rates were performed with a 5 mM Fc and 0.1 M LiTFSI in PyrOTEG solution. The results are shown in Figure 4.12.

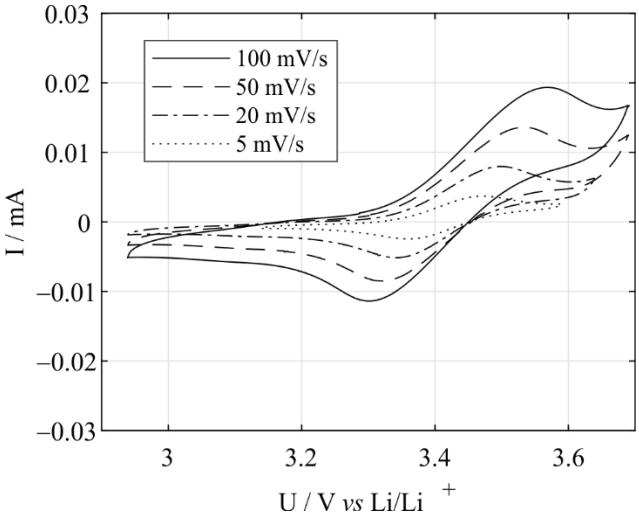

Figure 4.12: Cyclic voltammograms at different scan rates using 5 mM ferrocene and 0.1 M LiTFSI dissolved in PyrOTEG (**8**): working electrode material: GC, counter electrode material: Pt, pseudo reference electrode material: Ag.

Thereby the relationship between the maximum current, the scan rate and the surface area of the electrode, expressed by the RANDLES-SEVCIK equation, was used to calculate the electrode area:[45]

$$I_p = 0.4463nFAc\left(\frac{nF\upsilon D}{RT}\right)^{\frac{1}{2}} \tag{4.2}$$

Where I_p is the peak current, n the number of transferred electrons, F the FARADAY constant, c the concentration, D the diffusion coefficient, υ the scan rate, R the gas constant and T the absolute temperature.

Assuming a temperature of 20 °C at a resulting scan rate of 100 mV/s the surface area increased by the factor of ~400, compared to the flat glassy carbon electrode.

For comparison, a 5 mM ferrocene and 0.1 M LiTFSI in TEGDME solution was investigated (Figure 4.13).

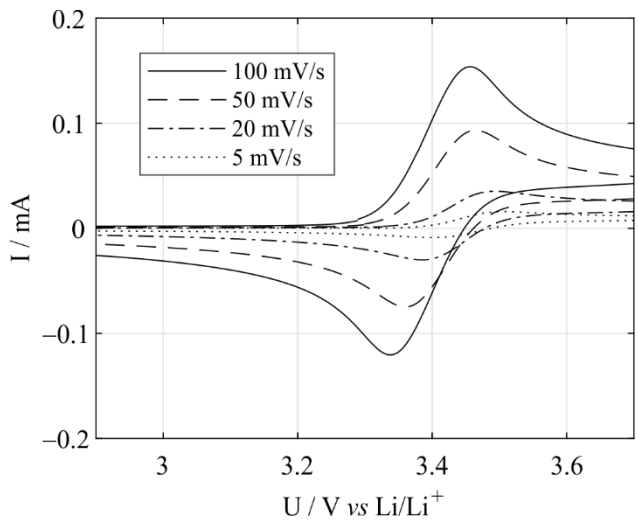

Figure 4.13: Cyclic voltammograms at different scan rates using 5 mM ferrocene and 0.1 M LiTFSI dissolved in TEGDME: working electrode material: GC, counter electrode material: Pt, pseudo reference electrode material: Ag.

As mentioned before, the comparison of the areas gives a hint, if electrochemical reactions inside the total volume of the liquid mixed conductor are plausible. However, due to the rough estimation of the molecule radius for the STOKES-EINSTEIN equation, comparing these values is delicate. Moreover, the definition of an atomically rough surface area caused by molecules within the liquid mixed conductor is somewhat arbitrary. If the maximum currents of the measurement with included PyrOTEG are compared with the blank one (Figure 4.12 and Figure 4.13), a significant difference is recognizable. The peak current of the measured CV containing PyrOTEG is roughly by a factor of 8 smaller. Also a bigger peak separation in the system containing PyrOTEG is visible, which refers either to slow electrochemical reaction, uncompensated resistance of the mixed conductor or bigger viscosity inside the system. If the higher viscosity and the impedance cp. Figure 4.7 are incorporated, the visual angle has to be adopted. The area increase of 400 times is rather low if the entire volume of the liquid mixed conductor is transferred into a surface area. However, in reality, the examined system is much more complicated to understand and more parameters have to be considered, but nevertheless those experiments give a push into the direction of making electrochemistry in the bulk of a liquid material.

In summary, this chapter describes the synthesis of likely the simplest possible organic mixed conductor, consisting merely of a Pyr as electron conducting moiety and an oligoglyme as ionomer. It presents thus a simplified monomeric version of the polymers (poly(PySOTEG); poly(PyrOTEG) compared Figure 4.28) that covalently links the same moieties to polymeric backbones. We made two types varying by either a phenolic or benzylic link. Curiously, both were black rather viscous liquids at room temperature that only solidified <–40 °C. The liquids readily dissolved Li salts and showed appreciable electronic conductivity and an ionic conductivity in the range expected for liquid electrolytes with similar viscosities. We had thus obtained an entirely new class of organic liquids with electronic and ionic conduction. These liquids appear to open unprecedented possibilities in fundamental electrochemistry (e.g. homogeneous electrochemistry in the bulk liquid as opposed to the classical electrochemistry at the interface of electron and ion conductor) as well as in energy storage. Within this work, we could only start first humble steps in the exploitation of the possibilities that such materials allow for. These included first experiments to establish whether the electronic conductivity suffices to support homogeneous electrochemistry in the bulk of the liquid. The results clearly point at a positive answer. Much further work including new experimental techniques and theory will be needed to better understand the processes. Exploitation only has started.

4.3. Electrochemically Polymerized Mixed Conductors

When used for metal-O_2 chemistry, the chemical stability of any organic material towards the reactive O_2 species as discussed before is a distinguishing feature, which requires special attention. Heteroatoms as found in most types of ECPs tend to induce polarity into the molecules, which make them more vulnerable to attack by the ROS. Pure hydrocarbons would thus likely have an advantage in stability. Poly(paraphenylene) (PPP) is a polymer with electronical conducting properties in the doped state and one of the few without heteroatoms.[20a] Earlier, PPP was synthesized *via* oxidative cationic polymerization of benzene.[47] Nowadays, PPP derivatives are synthesized *via* cross coupling reactions in lab scale due to higher tolerance to functional groups.[48] An additional potential method to couple phenylene units is *via* the electroreduction of diazonium salt reduction. This method is generally applicable to couple phenylene units to solid surfaces like metals or carbon. It has been used in the context of batteries to form an electronically conductive layer on the highly insulating intercalation material $LiFePO_4$ using by taking advantage of the reducing power of the lithiated phase.[49] A general limitation noted so far with most substituted phenyldiazonium salts was the limited layer thickness achievable, which in many cases was limited to a few monolayers.

Whether electrochemical polymerization of PEO substituted phenyldiazonium salts would be suitable to form thick layers (beyond µm) of mixed conducting polymer onto carbon structures was investigated. These should be suitable for O_2 electrochemistry and soft enough to accommodate the formation/decomposition of alkaline oxides. During the ECP process the monomers (aryldiazonium salts **12**) are reduced by an electron of the electrode, producing an aryl radical. In turn, the generated arylradical forms a covalent bond with the carbon electrode. Due to the electronic conducting property of the coated layer, the electrochemical reduction can be repeated and a polymeric layer can be formed. During the reduction one molecule of nitrogen gas is released (Scheme 4.6).[50]

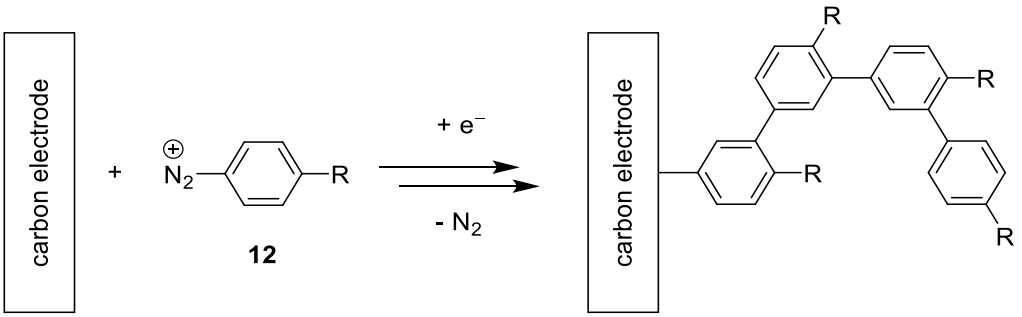

Scheme 4.6: Electrochemical polymerization of aryldiazonium salts on carbon surfaces.

Based on the literature of BAHR *et. al.* aryldiazonium salts with attached TEG moieties (**13**) were synthesized.[51] Due to the unexpected effect of the TEG substituent during polymerization, two synthesis routes were performed starting with *m*-nitrophenol (**14a**) and *p*-nitrophenol (**14b**) respectively. In the first step the phenol reacted as nucleophile with the TEG electrophile according to the WILLIAMSON ether synthesis (**15a**, **15b**, see Scheme 4.7).[44] Afterwards the nitro moiety was reduced to the corresponding amine (**16a**, **16b**) by hydrogen gas, which is generated *in situ* according to the BÉCHAMP reduction reaction.[52] Finally a functional group transformation was performed, where the amine moiety was exchanged into the diazonium moiety (**13a**, **13b**) using nitrosyl tetrafluoroborate as reagent.

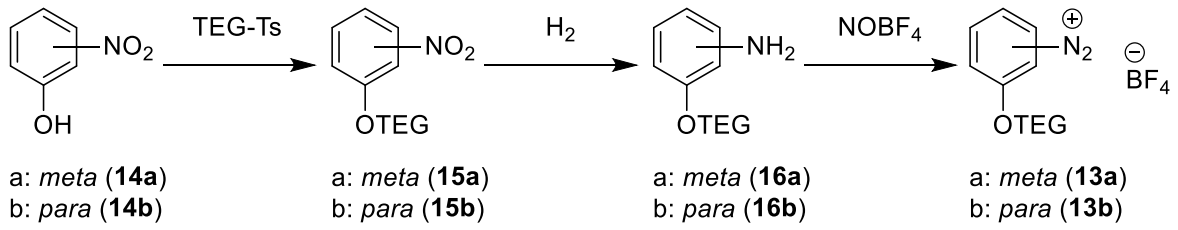

Scheme 4.7: Synthesis route for aryldiazonium salts (**13a**, **13b**) generation.

4.3.1. Preparation of 1-(2-(2-(2-Methoxyethoxy)ethoxy)ethoxy)-3/4-nitrobenzene (**15a**, **15b**)

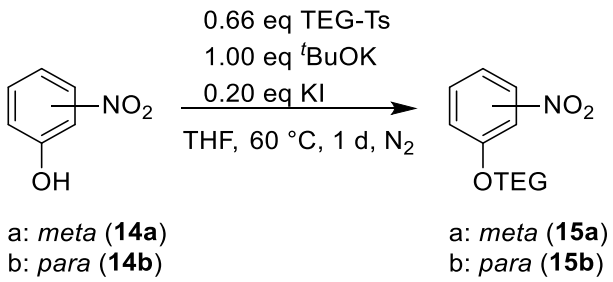

Scheme 4.8: Preparation of 1-(2-(2-(2-methoxyethoxy)ethoxy)ethoxy)-3/4-nitrobenzene (**13a**, **13b**) *via* a WILLIAMSON ether synthesis.

Using the experience of the PenzOTEG/PyrOTEG synthesis, the alkylation agent was the limiting substrate in the reaction mixture, because substances with attached TEG moieties were hard to separate. For that reason, an excess of nitrophenol (**14a, 14b**) was used. The importance of the base strength (^{t}BuOK) was minimally overestimated. Because of the electron withdrawing property of the nitro group the proton of the phenol was more acidic and a weaker base would also have been sufficient. Potassium iodide was used as nucleophilic catalyst. Purification was done by flash chromatography, because the nitrophenol could not be washed completely into alkaline water. Despite full conversion for both isomers, a big loss of the *para*-isomer was observed during flash chromatography (~40%; Scheme 4.8, Table 4.1).

4.3.2. Preparation of 1-(2-(2-(2-Methoxyethoxy)ethoxy)ethoxy)-3/4-aniline (**16a**, **16b**)

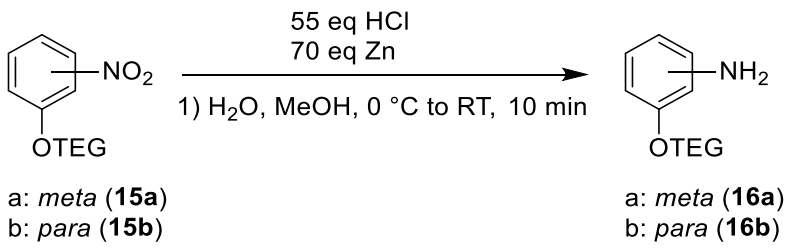

Scheme 4.9: Preparation of 1-(2-(2-(2-methoxyethoxy)ethoxy)ethoxy)-3/4-aniline (**16a**, **16b**) *via* a BÉCHAMP ether synthesis.

Due to solubility issues of the educt in water, a mixture of MeOH/water = 1:2 (v/v) was chosen. Therefore, the educt was dissolved in methanol and 6 M HCl was added afterwards. To compensate the heat production of the redox reaction, the reaction mixture was cooled to 0 °C during the addition of zinc. Afterwards the reaction mixture was allowed to warm to RT. Subsequent to full conversion a pH of 10 was adjusted, because the product could be easily purified by extraction into the organic phase although the amine moiety of the product had to be deprotonated. Before the product was extracted, the resulting solids were filtered off. Tiny losses of the product occurred during extraction and filtration (Scheme 4.9, Table 4.1).

Table 4.1: Isolated yield (%) of the etherification and reduction reaction for *meta*-, and *para*-isomers respectively.

	***meta*-Isomer**	***para*-Isomer**
Yield of etherification (%)	94 (**15a**)	55 (**15b**)
Yield of reduction (%)	99 (**16a**)	94 (**16b**)

4.3.3. Preparation of 3/4-(2-(2-(2-methoxyethoxy)ethoxy)ethoxy)benzenediazonium tetra-fluoroborate (**13a**, **13b**)

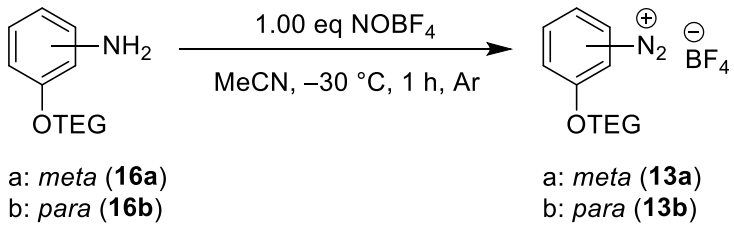

Scheme 4.10: Preparation of 3/4-(2-(2-(2-methoxyethoxy)ethoxy)ethoxy)benzenediazonium tetrafluoroborate (**15a**, **15b**).

The functional group transformation reaction of an arylamine into an aryldiazonium compound is a well-known reaction in organic chemistry.[53] However, in this reaction a rarely used reagent – nitrosyl tetrabluorobarte ($NOBF_4$) – was added.[51] Usually the nitrosyl cation is generated *in situ* during that transformation reaction. By using the $NOBF_4$-reagent instead, a well-defined molar ratio of reactant to reagent could be applied within the mixture. In this particular case, the reaction was performed at –30 °C, because $NOBF_4$ is a harsh reagent. Furthermore, exactly 1.00 equivalent of the reagent was used to suppress side product formation. According to the conversion process, which was monitored by ^{1}H-NMR spectroscopy, full conversion occurred after 1 h. During the reaction, several intermediates were formed until the product was generated and one molecule of water was cleaved off. To force the equilibrium to the product side, molecular sieves (MS) were added after 1 h. ^{1}H-NMR spectroscopy was continued until one month after reaction start to investigate the long term stability of the product solution. The aryldiazonium compound was stable in the generated solution. For illustration, ^{1}H-NMR spectra are presented for the *meta*-isomer (**13a**) (Figure 4.14, Scheme 4.10).

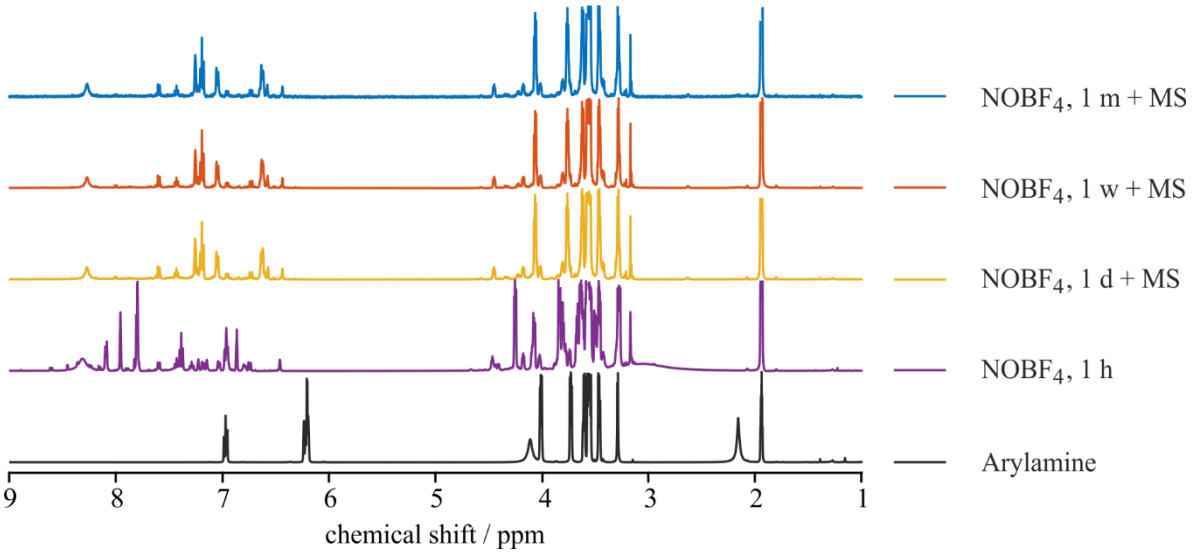

Figure 4.14: Reaction control of the preparation of 3-(2-(2-(2-methoxyethoxy)ethoxy)ethoxy)benzenediazonium tetrafluoroborate (**13a**) by ^{1}H-NMR spectroscopy and further long-term stability investigation in MeCN-d_3.

4.3.4 Preparation of poly((2-(2-(2-methoxyethoxy)ethoxy)ethoxy)phenylene) (**17**)

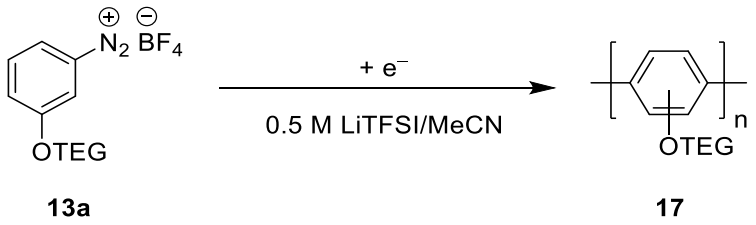

Scheme 4.11: Preparation of poly((2-(2-(2-methoxyethoxy)ethoxy)ethoxy)phenylene) (**17**) by electrochemical polymerization.

The electrochemical polymerization reaction, based on literature of BAHR *et. al.*, was performed on a glassy carbon working electrode.[51] For the reaction a concentration of 30 mM monomer and 0.5 M LiTFSI (conducting salt) in MeCN was used. Completely lithiated lithium iron phosphate (LFP) acted as counter electrode. Partly delithiated LFP was used as reference electrode. The advantage of this synthesis route was that the monomer synthesis and the polymerization were performed in the same vessel. After generation of the monomer, the conducting salt and the electrodes were added. The polymerization was performed for screening reasons with the *meta*-isomer using cyclic voltammetry (Scheme 4.11). If a galvanostatic discharge experiment was performed instead, no polymer formation was observed. By using cyclic voltammetry, the formed surface was permeable for electrons on the condition that the potential was forced to a certain point (3.8 V *vs* Li/Li^+), where oxidation was possible. Without using that certain precondition, no polymerization reaction occurred either as shown in Figure 4.15. Electrochemical polymerization was performed on flat carbon electrodes as well as on carbon paper fibers. Performing the reactions on well-defined surface areas help to understand the ongoing reactions and gives a hint on the reaction mechanism. Nevertheless, it was hard to make chemical characterizations, because only a tiny amount of substance is formed at the surface. For several reasons, polymerization was also done on carbon fibers. One of them was to subsequently perform detailed characterizations and the other was to see, if electrochemical reactions could be performed in the bulk of the formed polymer. Unfortunately, <30% of the passed electrons were engaged in polymer formation and therefore the carbon fibers were covered with a thin layer (Figure 4.16). Mass spectrometry of the used electrolyte gave a hint on the side products, which were formed during electrochemical polymerization. One of the identified side products was a diazo compound **18** (Scheme 4.12). Polymerization in the carbon fibers were followed by IR spectroscopy. In the region between 1,000 and 1,100 wavenumbers, there is a typical signal for ether bonds. After polymerization and washing of the fiber, the IR spectrum of the coated fiber showed a signal in the mentioned region, which indicated that the coating of the fibers was successful (Figure 4.17).

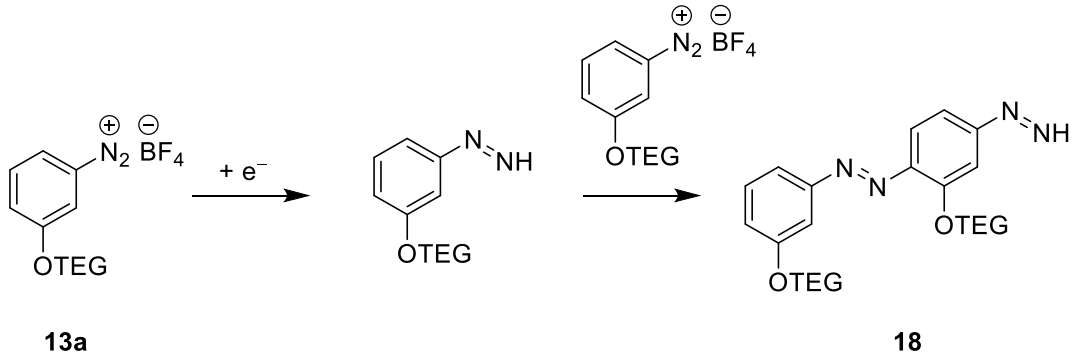

Scheme 4.12: Side product formation during electrochemical polymerization reaction generating diazo compound **18**.

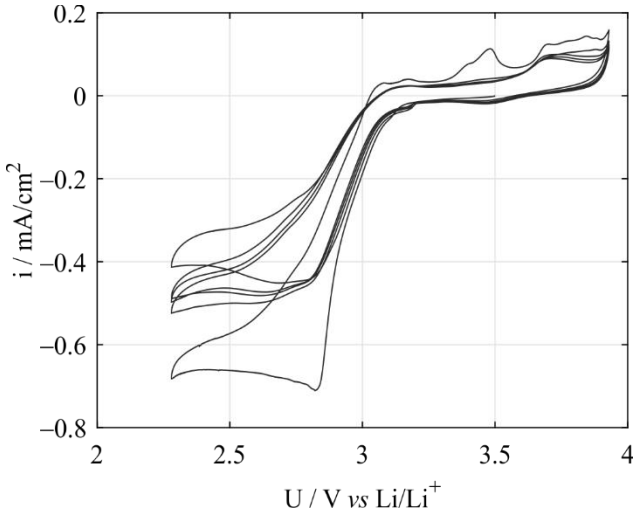

Figure 4.15: Electrochemical polymerization reaction of 3-(2-(2-(2-methoxyethoxy)ethoxy)ethoxy)benzenediazonium tetrafluoroborate (**13a**) in 0.5 M LiTFSI/MeCN using cyclic voltammetry (5 cycles) working electrode material: GC, counter electrode material: LFP, pseudo reference electrode material: LFP.

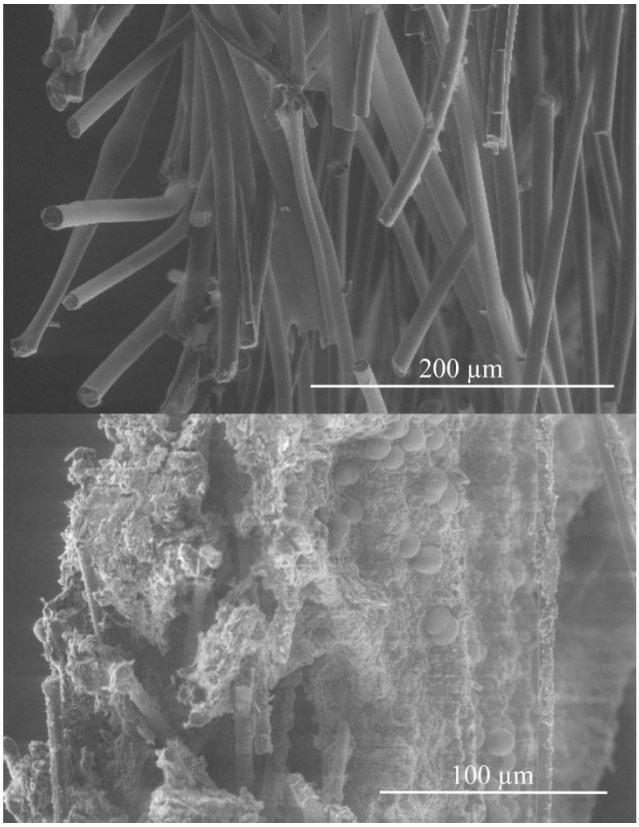

Figure 4.16: SEM image of the uncoated carbon fiber (top) and fiber coated with the mixed conducting polymer (bottom).

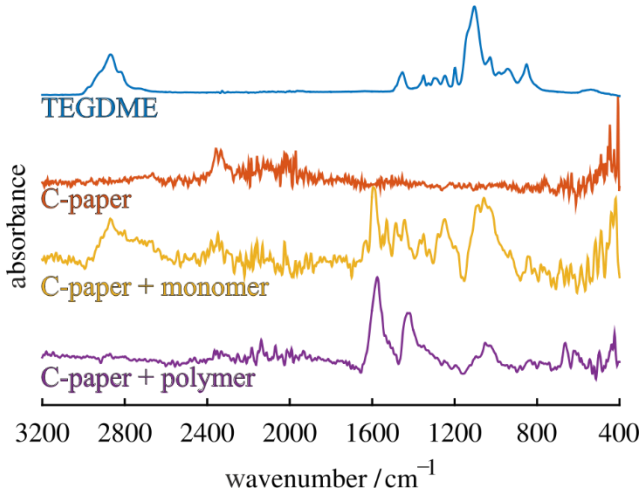

Figure 4.17: Characterization of the polymer and reference spectra using IR-spectroscopy.

4.3.5. Electrochemical Oxygen Reduction Reaction Inside the Electro Polymerized Polymer on a Neat Electrode

The mechanism of oxygen reduction in aprotic Li^+ electrolytes to form Li_2O_2 was investigated by JOHNSON *et. al.* and led to the current understanding of solution or surface mechanisms, respectively, as discussed in Chapter 3.7.[33] Depending on the solubility of the LiO_2 intermediate, rather thin layers of Li_2O_2 up to ~10 nm can be formed if the reduction follows a surface mechanism and somewhat thicker layers if the mechanism follows the solution mechanism. The consequence are discharge capacities of a few µAh/cm^2 active are in the first case and several 10 µAh/cm^2 in the latter case. Nevertheless, also the solution mechanisms typically does not allow for high volume filling of the electrode with Li_2O_2 and electronic contact is poor, which requires redox mediators to recharge the cell. We thus targeted Li_2O_2 in the bulk of the soft mixed conducting polyphenylene polymer. A basic test to demonstrate this is to compare capacities obtained on bare flat GC electrodes with those obtained after forming a polymer layer on them. Figure 4.18 and Figure 4.19 show the result for galvanostatic discharge on bare and polymer coated electrodes in MeCN and DME electrolytes. The massively increased capacity unequivocally demonstrates that O_2 reduction to Li_2O_2 occurs in the bulk of the formed polymer layer. The bare layer allows for ~5 µAh/cm^2 while the polymer achieved a discharge capacity of 23 and 250 µAh/cm^2 compared to 5 µAh/cm^2. When MeCN was used, the capacity with the mixed conducting polymer is 5 times the capacity without the polymer; by using DME it was increased by 50 fold. These experiments are the first to demonstrate O_2 electrochemistry in the bulk of a mixed conductor rather than at the interface between an electron conductor (such as metals or carbon) and an ion conductor. The large capacity also demonstrates that the polymer is flexible enough to follow the shape changes of the formed Li_2O_2.

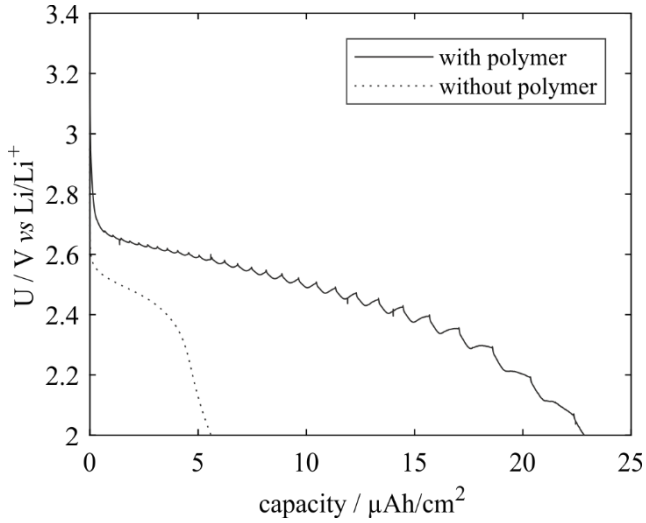

Figure 4.18: Discharge curves of oxygen in 0.1 M $LiClO_4$ in MeCN with a discharge current density of 10 µA/cm^2 at the surface of a flat electrode (dotted line) and inside the bulk of the mixed conducting polymer (full line).

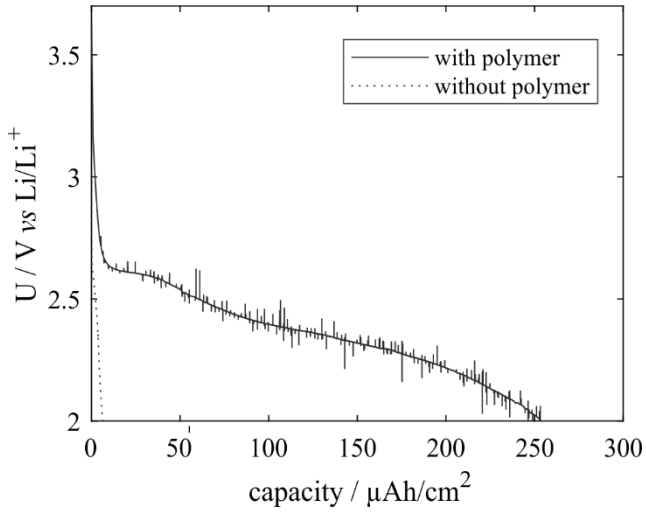

Figure 4.19: Discharge curves of oxygen in 0.1 M $LiClO_4$ in DME with a discharge current density of 10 µA/cm^2 at the surface of a flat electrode (dotted line) and inside the bulk of the mixed conducting polymer (full line).

4.3.6. Electrochemical Oxygen Reduction Reaction Inside the Electro Polymerized Polymer on Carbon Fibers

To further investigate the O_2 electrochemistry inside the soft mixed conducting PP-EO polymer, carbon paper composed of ~7 µm thick carbon fibers and a paper thickness ~160 µm as the substrate for electropolymerization were used instead of the flat GC. This way battery electrodes could be obtained that allow for further characterization with methods like pressure measurements, XRD, FTIR, and SEM. First, C-paper was coated with various amounts of PP-EO, the electrodes washed and used to build batteries with $LiFePO_4$ counter and reference electrodes. The cells were built with a connected pressure transducer to follow the O_2 consumption. During discharge in Li^+-containing aprotic electrolytes, molecular oxygen (O_2) is transformed to lithium peroxide (Li_2O_2) according to $O_2 + 2e^- + 2Li^+ \rightleftarrows Li_2O_2$. O_2 consumption is directly related to transferred electrons and thus the pressure change in the electrochemical cell can be used to measure the ratio of e^-/O_2. In an ideal case, two electrons

are required for the reduction of one molecule of O_2. If the ratio of transferred e^- to consumed O_2 (cum e^-/cum O_2) differs from 2, other (electro)chemical reactions may happen during cycling. As required for Li_2O_2 formation, the value from experimental data was ~2e^-/O_2. That result confirms, that the discharge reaction indeed forms Li_2O_2 inside the mixed conducting polymer in a practical electrochemical cell (Figure 4.20). Furthermore, the formation of Li_2O_2 was followed by other analysis methods. On the one hand, the formation of the colored complex of Ti^{4+} with O_2^{2-} was measured by UV-Vis and confirmed the formation of peroxide (Figure 4.21). Quantitative analysis of the amount of formed Li_2O_2 was not meaningful since the aqueous Ti^{4+} solution cannot be expected to leach out all peroxide from the hydrophobic PP-EO polymer. However, the selective reaction to the colored Ti-complex proved the formation of Li_2O_2 during electrochemical discharge. Finally, the morphological change of the surface was followed with SEM (Figure 4.22).

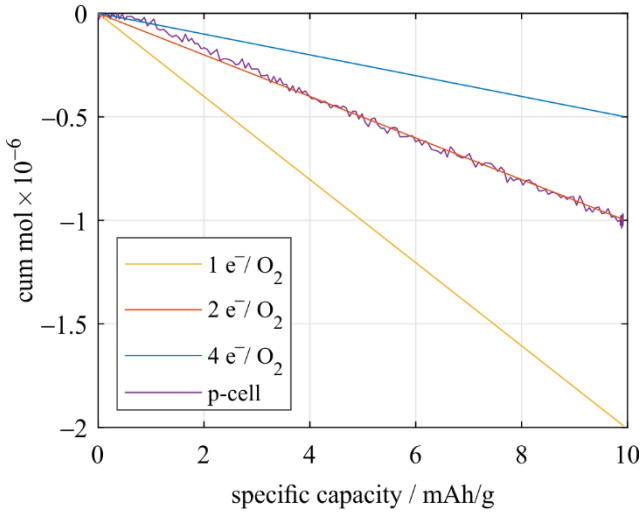

Figure 4.20: Theoretical processes for 1e^-/O_2 (yellow) 2e^-/O_2 (red), 4e^-/O_2 (blue) reactions and experimentally generated data (violet).

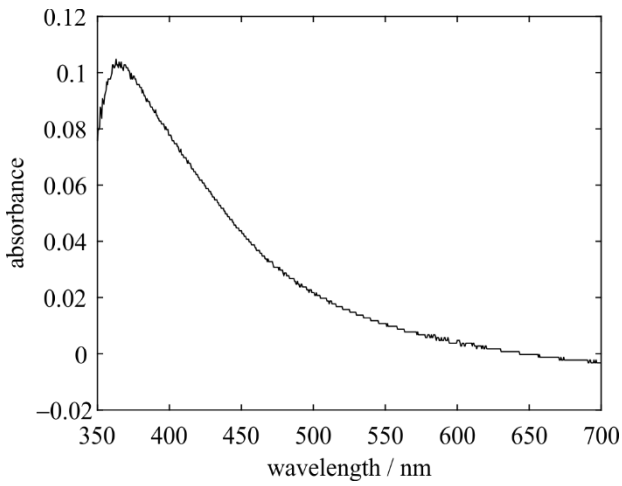

Figure 4.21: UV-Vis spectroscopy of the formed Ti-complex after reaction of titanly sulfate with Li_2O_2.

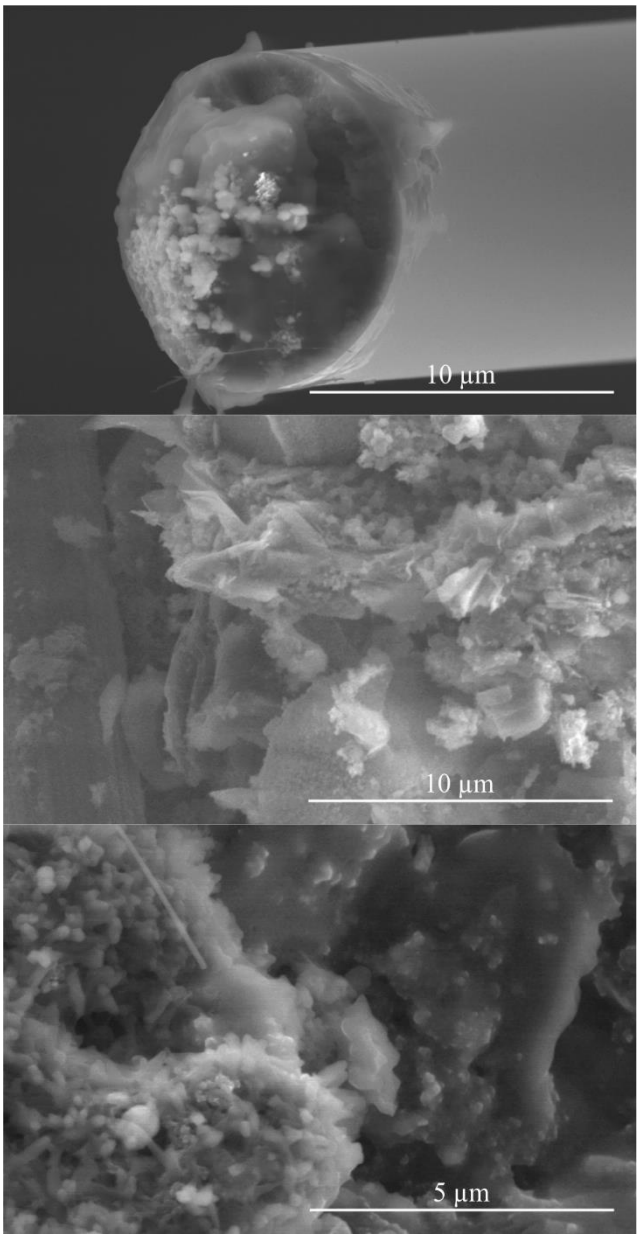

Figure 4.22: SEM image of the uncoated carbon fiber (top), fiber coated with the mixed conducting polymer (center) and Li_2O_2 formation after electrochemical discharge on the surface of the mixed conducting polymer (bottom).

In summary, we were able to form mixed conducting PP-EO polymers on conducting flat and porous electrode surfaces by electropolymerizing EO substituted phenyldiazionium salts. The mixed conductors allow for O_2 reduction to Li_2O_2 in the bulk of the polymer as evidenced by pressure measurement, peroxide-specific spectroscopic tests and SEM. Oxygen reduction reactions performed inside a polymer layer afforded a capacity of up to 50 fold compared the same surface of non-coated electrode. Li_2O_2 formation was followed by different analysis methods. Combining all results confirms, that the electrochemical reaction takes place in the volume of the polymer and not only on the surface of the supporting electron conductor.

4.4. Wet Chemical Polymerization

A different strategy to build mixed conducting polymers is by a wet chemical approach. In contrast to the electrochemical approach, the polymer consists of a classical polymer backbone with attached electronically and ionically conducting units on the side chains. The application of the polymer inside batteries demands for special chemical and physical properties. Principally, the monomers should be accessible in larger scale, furthermore the monomers should form a co-polymer. Finally, the polymer should be stable during electrochemistry and should stand the volume changes during cycling. For that reason, various strategies to synthesize such mixed conducting polymers were pursued. In detail, one way to create mixed conductors followed the polyvinyl backbone, whereas another strategy was based on ring opening metathesis polymerization. For reason of diversity and opportunity to create best working polymer for battery application, several monomers were synthesized, which are described in the following Chapter 4.4.1.

4.4.1. Polymerization of a Vinyl Group

A way to combine electronic and ionic conducting units (pyrene **1** and TEG **3**) is to attach side groups to a polymer backbone that provides ionic and electronic conduction. The chosen side groups were EO units and Pyr units, respectively. Therefore, the appropriate functional unit had to be assigned to a polymerizable functional group. A very diverse monomer that allows for various polymerization methods is the vinyl-group. It can be polymerized *via* a radical, anionic, or cationic mechanism.[54] Since the 1950s, styrene is polymerized by radical initiation.[54a] For that reason, the chosen monomers resemble styrene; 1-vinyl pyrene (**19**) has a bigger carbocyclus and 1-(2-(2-(2-methoxyethoxy)ethoxy)-ethoxy)-4-vinylbenzene (**20**) has an additional attached TEG-moiety (Figure 4.23).

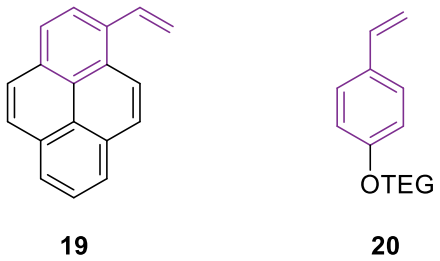

Figure 4.23: Monomers for radical, cationic and anionic polymerization: 1-vinyl pyrene (**19**), 1-(2-(2-(2-methoxyethoxy)ethoxy)ethoxy)-4-vinylbenzene (**20**).

4.4.1.1. Preparation of 1-vinyl pyrene (**19**)

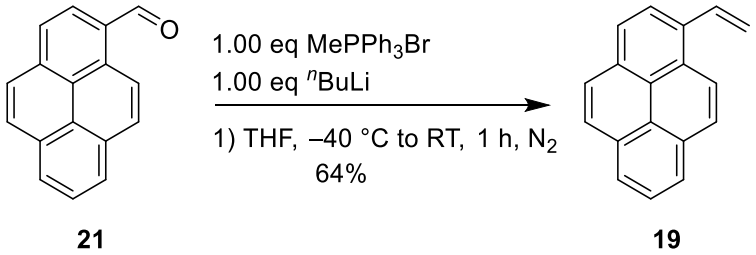

Scheme 4.13: Preparation of 1-vinyl pyrene (**19**) *via* a WITTIG reaction.

The functional group transfer reaction from a carbonyl to an olefin moiety is a well-known reaction in organic chemistry. It is frequently used and named after its inventor WITTIG. Based on literature from WANG *et al.*, 1-pyrenecarbaldehyde (**21**) reacts with 1 equivalent methyltriphenyl-phosphonium bromide ($MePPh_3Br$);[55] in this certain case, the base was exchanged by *n*-BuLi. Due to the use of *n*-BuLi, during the addition of it, reaction temperature was adapted and held at –40 °C. Afterwards, the reaction mixture was allowed to warm to RT. Purification was easy to perform, because the product was very nonpolar. Using flash chromatography, the product left the column first and all other side products remained on the stationary phase. The total obtained yield of this synthesis was 64% (Scheme 4.13).

4.4.1.2. Preparation of 1-(2-(2-(2-methoxyethoxy)ethoxy)ethoxy)-4-vinylbenzene (**20**)

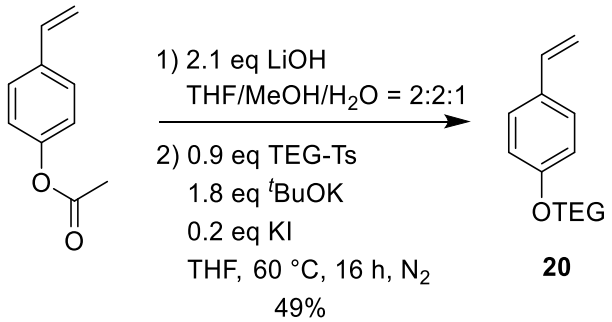

Scheme 4.14: Preparation of 1-(2-(2-(2-methoxyethoxy)ethoxy)ethoxy)-4-vinylbenzene (**20**) using a 2-step synthesis.

The second monomer for radical polymerization was generated *via* a 2-step synthesis. In the first reaction step, a saponification reaction was performed using 2.1 equivalents of lithium hydroxide in a solvent mixture of THF/MeOH/H_2O = 2:2:1 (v/v/v). This special solvent mixture ensured homogenous reaction of the base with the substrate. After full conversion, the pH was adjusted to a value of 6. After removal of the organic solvents, the product was extracted into EtOAc. If THF or MeOH were in the organic phase, no phase separation would occur. Furthermore, at high pH values, the product would be deprotonated and, due to its ionic

construction, it would not be extracted into the organic phase. Afterwards, the standard conditions of the WILLIAMSON etherification reaction were set up. Again, a little excess of alcohol was used because of separation issues. After full conversion, the product was separated from the excess of unreacted alcohol by flash chromatography. Due to 2 work ups and additional flash chromatography, the yield was affected and amounted to 49% (Scheme 4.14).

4.4.1.3. Polymerization of 1-vinyl pyrene (**19**) and 1-(2-(2-(2-methoxyethoxy)ethoxy)-ethoxy)-4-vinylbenzene (**20**)

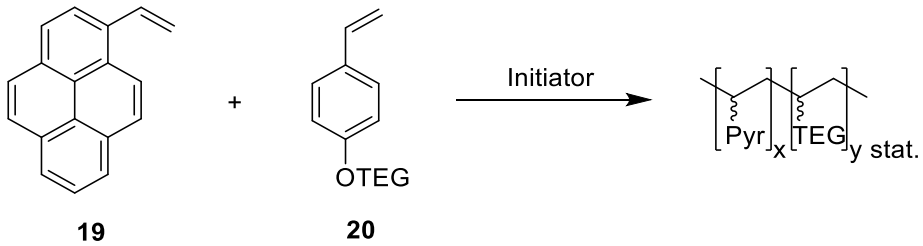

Scheme 4.15: Polymerization of 1-vinyl pyrene (**19**) and 1-(2-(2-(2-methoxyethoxy)ethoxy)ethoxy)-4-vinylbenzene (**20**) to synthesize a statistically distributed polymer with functional unit pyrene **1** and TEG **3** on the side chain.

Different types of mechanisms were screened for the co-polymerization reaction of 1-vinyl pyrene (**19**) and 1-(2-(2-(2-methoxyethoxy)ethoxy)ethoxy)-4-vinylbenzene (**20**). However, for getting a feeling how the polymerization reaction behaved, homo-polymerization reactions of both monomers were performed first. The first tested initiation system was the radical induced one. For that reason, azobisisobutyronitrile (AIBN) and benzoyl peroxide (BPO) + dimethyl-*p*-toluidine (DMT) acted as initiation systems. The AIBN system generates radicals when it is heated to a certain decomposition temperature. That mechanism generates desired radicals and nitrogen gas as side product. The mechanism, where BPO and DMT are included, is different; A chemical redox reaction generates radicals, which are required for the polymerization reaction. Homo polymerization of 1-vinyl pyrene resulted in polymer formation, though reaction took several days using both initiation systems. Unfortunately, no polymer formed using 1-(2-(2-(2-methoxyethoxy)ethoxy)ethoxy)-4-vinylbenzene in any radical initiation system. For that reason, the initiation mechanism was switched to an anionic one. By using strong bases e.g. *n*-BuLi, or *tert*-BuLi it is also possible to force compounds with attached vinyl groups to polymerize. However, 1-vinyl pyrene just formed oligomers with chain length from 10-20 and 1-(2-(2-(2-methoxyethoxy)ethoxy)ethoxy)-4-vinylbenzene again did not polymerize. Last opportunity for polymerization was by cationic initiation. The critical point of cationic polymerization reactions is that it could be stopped by several influences like humidity. For that reason, all reactions were performed inside an Ar-filled glovebox. Based on literature

of DE *et al.* the desired chain length can be generated using the initiator system BCl_3 + 1-chloroethylbenzene (CEB) in DCM.[54b] Fortunately, both monomers produced homo-polymers. However, the reaction rates of both homo-polymerization reactions differed a lot. Cationic polymerization of 1-vinyl pyrene was extremely fast and finished after 2 minutes, whereas polymerization of 1-(2-(2-(2-methoxyethoxy)ethoxy)ethoxy)-4-vinylbenzene took one day. The problem of co-polymerization was that due to fast homo polymerization of 1-vinyl pyrene the homo polymer precipitated and was not available for further polymerization with 1-(2-(2-(2-methoxyethoxy)ethoxy)ethoxy)-4-vinylbenzene as monomer. Changing to other solvents, where polyvinylpyrene is more soluble, e.g. benzene or toluene, would lead to side reaction such as the FRIEDEL-CRAFTS alkylation (Scheme 4.15, Table 4.2).

Table 4.2: Screening conditions of different polymerization reactions: used monomer: 1-vinyl pyrene (**19**) and 1-(2-(2-(2-methoxyethoxy)ethoxy)ethoxy)-4-vinylbenzene (**20**); reaction accomplished: +; oligomer formation: ~; reaction failed: –.

		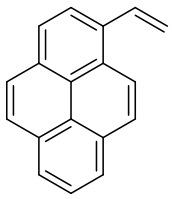 **19**	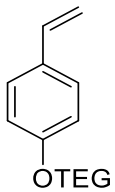 **20**
Homo-polymerization	**Radical initiation**	+	–
	Anionic initiation	~	–
	Cationic initiation	+	+
Co-polymerization	**Cationic initiation**	–	–

4.4.2. Ring Opening Metathesis Polymerization (ROMP)

Another way to generate polymers is *via* ring opening metathesis polymerization (ROMP). For ROMP, the monomer has to consist of a bicyclic structure with an included double bond such as norbornene **22**. In most cases, a ruthenium based complex is used as initiation system, due to its great properties being not sensitive against moisture and air. Many sophisticated initiation complexes can tolerate various functional groups and the chain length of the polymer depends on the structure and activity of the initiator.[56] The ruthenium based complexes are named after its inventor GRUBBS, who was awarded with the NOBEL Prize in 2013. Driving force of the

polymerization is the release of the ring strain of the bicyclic system, norbornene **22**, creating a tension free cyclopentane system **23** (Scheme 4.16).

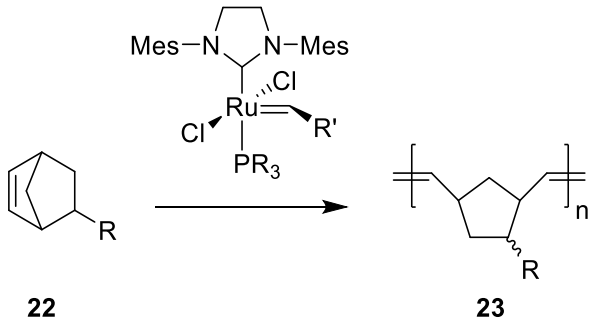

Scheme 4.16: Ring opening metathesis polymerization of norbornene (**22**) using a GRUBBS 2nd generation catalyst.

Due to the high functional group tolerance of the metathesis initiator, nearly any functional group, or structure could be attached to the norbornene unit and the initiator should still be able to create a polymer. For that reason 1-((2-((5-bicyclo[2.2.1]hept-5-en-2-yl)sulfonyl)-ethoxy)methyl)pyrene (Nbe-S-Pyr) (**24**), 1-(bicyclo[2.2.1]hept-5-en-2-yl)-2,5,8,11-tetraoxa-dodecane (Nbe-Pyr) (**25**) and 1-(bicyclo[2.2.1]hept-5-en-2-yl)-2,5,8,11-tetraoxado-decane (Nbe-OTEG) (**26**) were proper candidates for the polymerization. Additionally, they include the functional units (pyrene **1** and TEG **3**), which are necessary to synthesize a mixed conducting polymer (Figure 4.24).

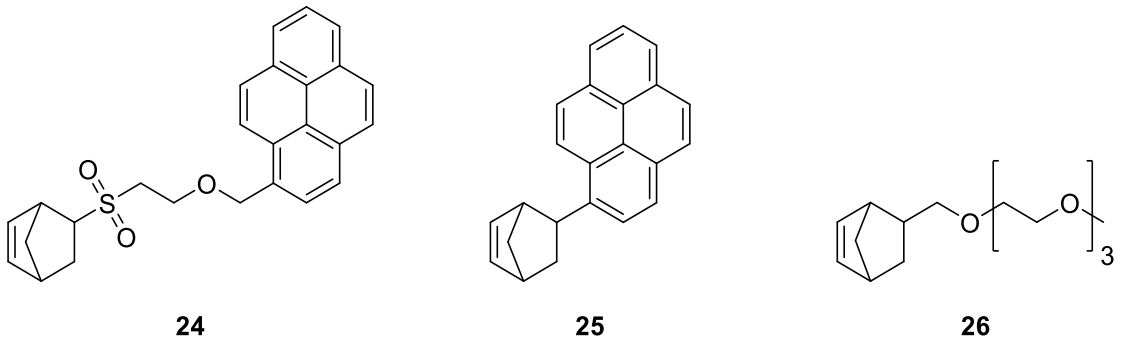

Figure 4.24: Monomers for ROMP, which should generate a mixed conductor after polymerization: 1-((2-((5-bicyclo[2.2.1]hept-5-en-2-yl)sulfonyl)ethoxy)methyl)-pyrene (Nbe-S-Pyr) (**24**), 1-((2-bicyclo[2.2.1]hept-5-en-2-yl)pyrene (Nbe-Pyr) (**25**), 1-(bicyclo[2.2.1]hept-5-en-2-yl)-2,5,8,11-tetraoxadodecane (Nbe-OTEG) (**26**).

4.4.2.1. Preparation of 1-((2-((5-bicyclo[2.2.1]hept-5-en-2-yl)sulfonyl)ethoxy)methyl)-pyrene (Nbe-S-Pyr) (**24**)

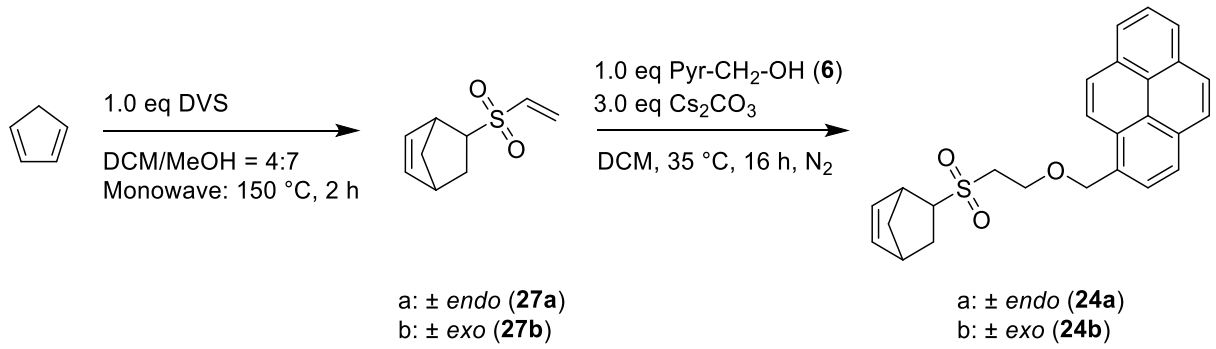

Scheme 4.17: Preparation of 1-((2-((5-bicyclo[2.2.1]hept-5-en-2-yl)sulfonyl)ethoxy)methyl)-pyrene (Nbe-S-Pyr) (**24**) using a 2-step synthesis.

The DIELS-ALDER reaction of cyclopentadiene (Cp) with divinyl sulfone (DVS) was demonstrated by DE LUCCHI.[57] However, it was tricky to selectively synthesize the cycloaddition product, in which case just one vinyl moiety reacts. Best conditions were a Cp/DVS = 1:1 (n/n) ratio in a solvent mixture of DCM/MeOH = 4:7 (v/v) using autoclavic conditions in a monowave reactor (Scheme 4.17). During the reaction a mixture consisting of educts, isomers of the mono cycloaddition product, isomers of the di cycloaddition product and dicyclopentadiene were formed. Unfortunately, the only way to purify the product was by flash chromatography. Due to almost equal retention behavior of the substances, it was hard to separate the product isomers and the yields of the pure substances were extremely low (Table 4.3). Nevertheless, we were able to get a crystal structure analysis of the *exo*-isomer (**27b**) (Figure 4.25). The product exhibited two functional groups: the norbornene **22** moiety, which is needed for ROMP and the vinyl sulfon moiety, which is a MICHAEL acceptor.

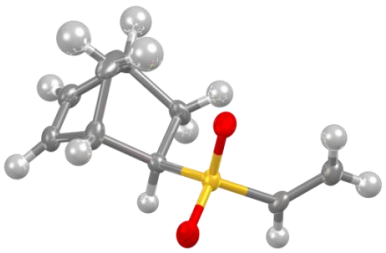

Figure 4.25: Crystal structure of (±)-exo-5-(ethenylsulfonyl)bicyclo-[2.2.1]hept-2-ene (**27b**).

Reaction conditions for the following oxa-MICHAEL addition were the same as for the 1,1'-(((sulfonylbis(ethane-2,1-diyl))bis(oxy))bis(methylene))dipyrene (**4**) preparation, except that this time one equivalent of alcohol (**6**) was used. Comparing the reaction of the *endo*- and *exo*-isomer, both of them showed full conversion, though purification using flash chromatography was harder to perform in case of the *endo*-isomer. For that reason, the difference in the yield of

the reaction was rather big (Table 4.3). However, both products had the ability to form crystals and their corresponding crystals were measured by X-ray diffractometry (Figure 4.26). The only difference of the isomers is the geometric orientation of the sulfonyl group attached to the norbornene **22** core.

Table 4.3: Isolated yield (%) of the DIELS-ALDER and oxa-MICHAEL reaction for *endo*- and *exo*-isomer respectively.

	***endo*-Isomer**	***exo*-Isomer**
Yield of DIELS-ALDER reaction (%)	6 (**27a**)	10 (**27b**)
Yield of oxa-MICHAEL addition (%)	18 (**24a**)	59 (**24b**)

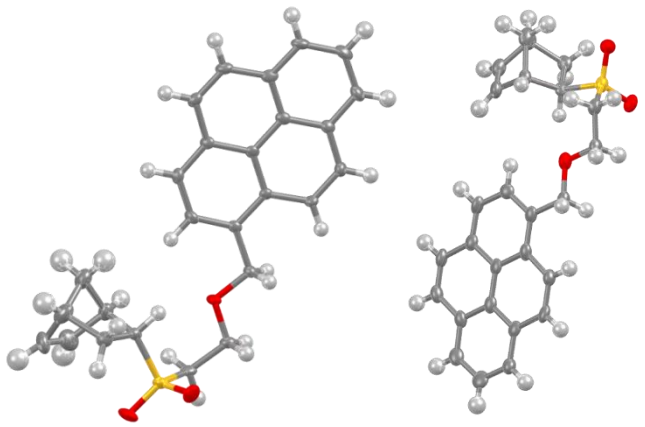

Figure 4.26: Crystal structure of (±)-1-((2-((*endo*-5-bicyclo[2.2.1]hept-5-en-2-yl)sulfonyl)ethoxy)methyl)-pyrene (**24a**, left) and (±)-1-((2-((*exo*-5-bicyclo[2.2.1]hept-5-en-2-yl)sulfonyl)-ethoxy)methyl)pyrene (**24b**, right).

Stability test of PenzOTEG (**7**) and PyrOTEG (**8**) showed that the methylene group between the pyrene core and oxygen-atom was prone for parasitic reaction during electrochemistry. Therefore, another oxa-MICHAEL addition using 1-hydroxypyrene (**9**) instead was tried. Unfortunately, no conversion was observed during reaction. The change from a primary sp^3-hybridized alcohol to a secondary sp^2 one changed the reactivity of the included reaction mechanism and was the reason for failure of the desired reaction (Scheme 4.18).

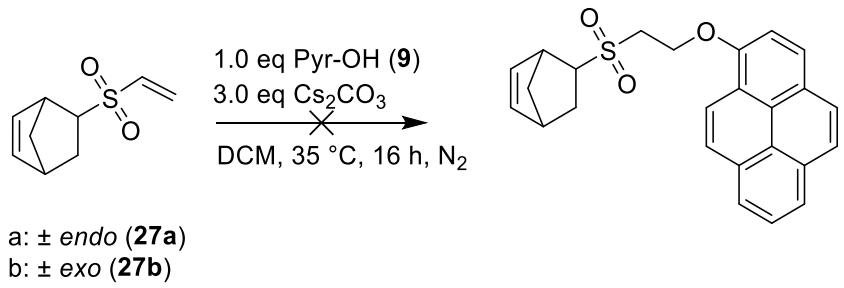

Scheme 4.18: Attempt to synthesize another monomer, which could be used for ROMP.

4.4.2.2. Preparation of 1-(bicyclo[2.2.1]hept-5-en-2-yl)-2,5,8,11-tetraoxadodecane (**25**)

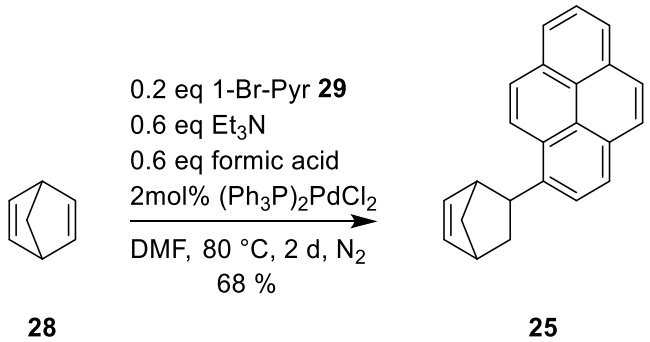

Scheme 4.19: Preparation of 1-(bicyclo[2.2.1]hept-5-en-2-yl)-2,5,8,11-tetraoxadodecane (**25**) using a cross coupling reaction.

A different way to produce a suitable monomer is by direct attachment of the pyrene core **1** to the norbornene unit **22**. One elegant way to synthesize monomer **25** is by cross coupling reaction of norbornadiene (**28**) with 1-bromopyrene (**29**).

In principle, the reaction follows the mechanism of a HECK reaction without a reductive elimination as last step in the catalytic cycle. Instead of a reductive elimination, there is a cation exchange of the palladium with a proton. Afterwards palladium is reduced to enter the catalytic cycle again. The reaction was performed according to WATANABE'S *et al.* patent.[58] Norbornadiene (**28**) was introduced in a 5-fold excess, because it would partly evaporate at 80 °C, as it has a high vapor pressure. Purification of the product was easy to perform, because the excess of norbornadiene could be removed by reduced pressure and the remaining substances were separated by flash chromatography. Due to the very nonpolar properties of the product, it eluted first, whereas all other side products stayed adsorbed on the stationary phase. Moreover, in this synthesis the *exo*-isomer was enriched formed (~7:1 = *exo*/*endo*), because of the steric demand of the palladium complex during the catalytic cycle (Scheme 4.19). Summarized, the purified *exo*-product was gained in 68% yield.

4.4.2.3. Preparation of 1-(bicyclo[2.2.1]hept-5-en-2-yl)-2,5,8,11-tetraoxadodecane (**26**)

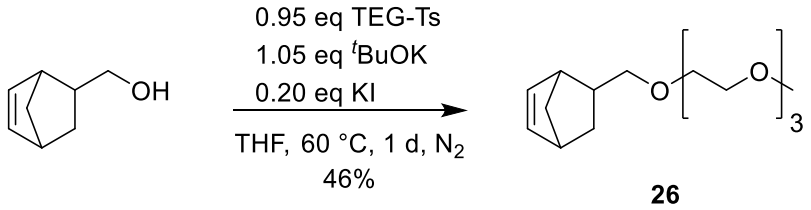

Scheme 4.20: Preparation of 1-(bicyclo[2.2.1]hept-5-en-2-yl)-2,5,8,11-tetraoxadodecane (**26**) *via* WILLIAMSON etherification.

The reaction was performed using tosylate as leaving group at the alkyl chain, *tert*-BuOK as inorganic base and KI as nucleophile catalyst according to WILLIMSON etherification reaction. Purification was performed by flash chromatography, but this time, the isomers were combined. Nevertheless, lots of fractions included the educt and therefore product yield was low (46%). According to ^{1}H-NMR spectrum the product consisted of an isomeric mixture of *endo*/*exo* = 3:1 (n/n) (Scheme 4.20).

4.4.2.4. Polymerization of ROMP Monomers

Once more, screening reactions were performed to find the best system/conditions for ROMP. In order to save resources, the screening was performed with the *exo*-isomers of Nbe-S-Pyr (**24b**), Nbe-Pyr (**25**) and Nbe-TEG (**26**). Diverse initiator systems (M2, M31 provided by UMICORE), solvents and monomer to initiator ratios were tested. Requirements for the polymers are that they are soluble in a solvent for fabrication of the working electrode, which has to be removed completely after fabrication. Furthermore, the polymer had to be insoluble in the electrolyte of the cell. Therefore, DCM and toluene were tested and DCM had better solubilization properties compared to toluene. Best conditions for polymerization were achieved using M31 as initiation system. Parts of the polymer, which were synthesized using M2 were insoluble in DCM, which made the M2 initiation system inappropriate. Perfect chain length would be 200 for *exo*-Nbe-S-Pyr and Nbe-OTEG system, whereas for polymer with included *exo*-Nbe-Pyr a chain length of 100 would be best to fulfill all requirements. If the chain length of the polymer were longer, the polymers would not be soluble in DCM anymore (Table 4.4).

Table 4.4: Screening to find best system/conditions for ROMP: good conditions: + (polymer formation, which was dissolved in the solvent); medium conditions: ~ (polymer formation, but partly precipitation occurred during reaction); bad conditions: – (polymer formation with severe precipitation).

		***exo*-Nbe-S-Pyr (24b)**	**Nbe-Pyr (25)**	**Nbe-OTEG (26)**
Solvent	**Toluene**	~	~	~
	DCM	+	+	+
Initiator	**M2**	–	–	–
	M31	+	+	+
Chain length	**500**	~	–	+
	200	+	–	+
	100		+	

After finding the best polymerization conditions, kinetic experiments of the homo-polymerization were performed using ^{1}H-NMR spectroscopy. If the kinetics do not differ much between the monomers, it is likely that the ruthenium catalyst does not favor one monomer and would create a statistically distributed polymer. Otherwise, it would prefer to react with one monomer and the polymer would have a block-co-polymer like structure. Obviously, *exo*-Nbe-S-Pyr (**24b**), *exo*-Nbe-Pyr (**25**) and Nbe-OTEG (**26**) exhibited similar kinetics, whereas *endo*-Nbe-S-Pyr (**24a**) is clearly slower. If a co-polymerization would be performed using *endo*-Nbe-S-Pyr and Nbe-OTEG as monomers, the catalyst would have converted almost all molecules of Nbe-OTEG to oligomers within 2 minutes, whereas none of the *endo*-Nbe-S-Pyr molecules reacted. Therefore, it makes a big difference which Nbe-S-Pyr isomer participates. According to the results of this kinetic screening experiment, both *exo*-Nbe-S-Pyr as well as Nbe-OTEG, and *exo*-NBE-Pyr and Nbe-OTEG should create statistically distributed co-polymers (Figure 4.27).

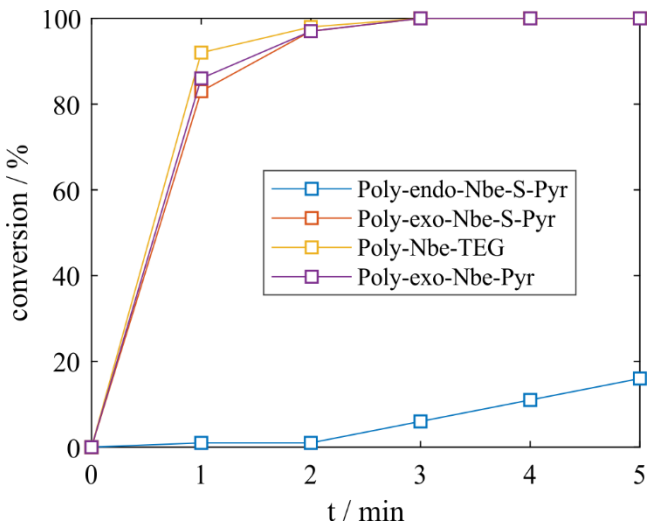

Figure 4.27: Conversion (%) over time; homo-polymerization of *endo*-Nbe-S-Pyr (blue, **24a**), *exo*-Nbe-S-Pyr (red, **24b**), Nbe-OTEG (yellow, **26**), *exo*-Nbe-Pyr (violet, **25**).

Finally, *exo*-Nbe-S-Pyr (**24b**) and Nbe-OTEG (**26**) were co-polymerized with a desired chain length of 200 to form poly(PySOTEG) (**30**). Also, *exo*-Nbe-Pyr (**25**) and Nbe-OTEG (**26**) were co-polymerized with a desired chain length of 100 to form poly(PyrOTEG) (**31**). Both contain the functional groups in a ratio of Pyr/TEG 3:1 (n/n), respectively (Figure 4.28).

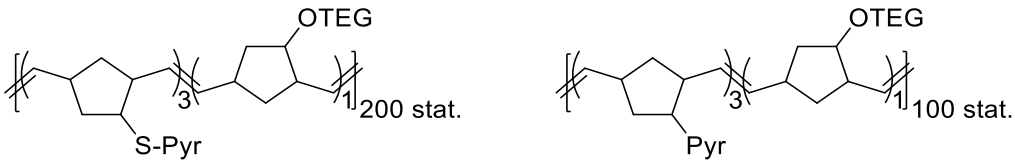

30 **31**

Figure 4.28: Statistically distributed co-polymers: poly(PySOTEG) (**30**) and poly(PyrOTEG) (**31**) with included pyrene **1** and TEG **3** units for mixed conductive properties.

The macroscopic array of the mixed conducting polymers, poly(PySOTEG) (**30**) and poly(PyrOTEG) (**31**), were examined by atomic force microscopy (AFM). Domains with higher concentration of pyrene **1** and TEG **3** units were expected, but AFM analysis showed smooth surfaces. Obviously, inside the polymers was no formation of either pyrene or TEG dominated domains. If there were some domain formation, it would be visible in the difference of surface roughness. The resolution of <1 nm was sensitive enough for detection of roughness changes (Figure 4.29).

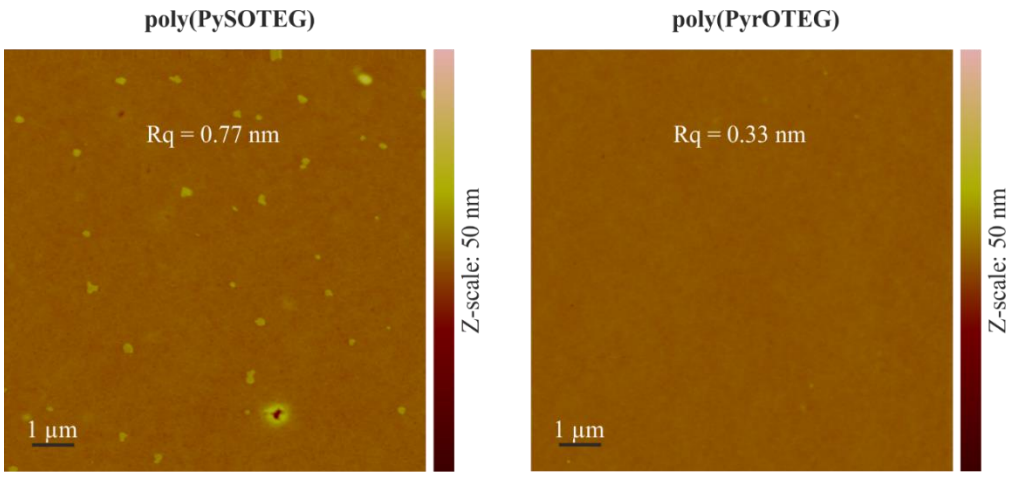

Figure 4.29: Atomic force microscopy (AFM) amplitude error images (picture size 10 × 10 µm^2) of mixed conducting polymers poly(PySOTEG) (**30**) and poly(PyrOTEG) (**31**).

Afterwards, the electronic and combined impedances were measured using impedance- and polarization experiments, as done for the liquid mixed conductors PenzOTEG (**7**)/ PyrOTEG (**8**). The ionic impedance could be calculated by subtracting the electronic from the combined impedance. The values of the electronic conductivity of poly(PySOTEG) is 10 times higher than those of poly(PyrOTEG). However, comparing the ionical impedances it is *vice versa* and the values of poly(PyrOTEG) are approximately 15 times higher than those of poly(PyrSOTEG) (Figure 4.30). The values of the impedances of the polymer do just slightly differ from those of the liquid mixed conductors PenzOTEG (**7**)/PyrOTEG (**8**).

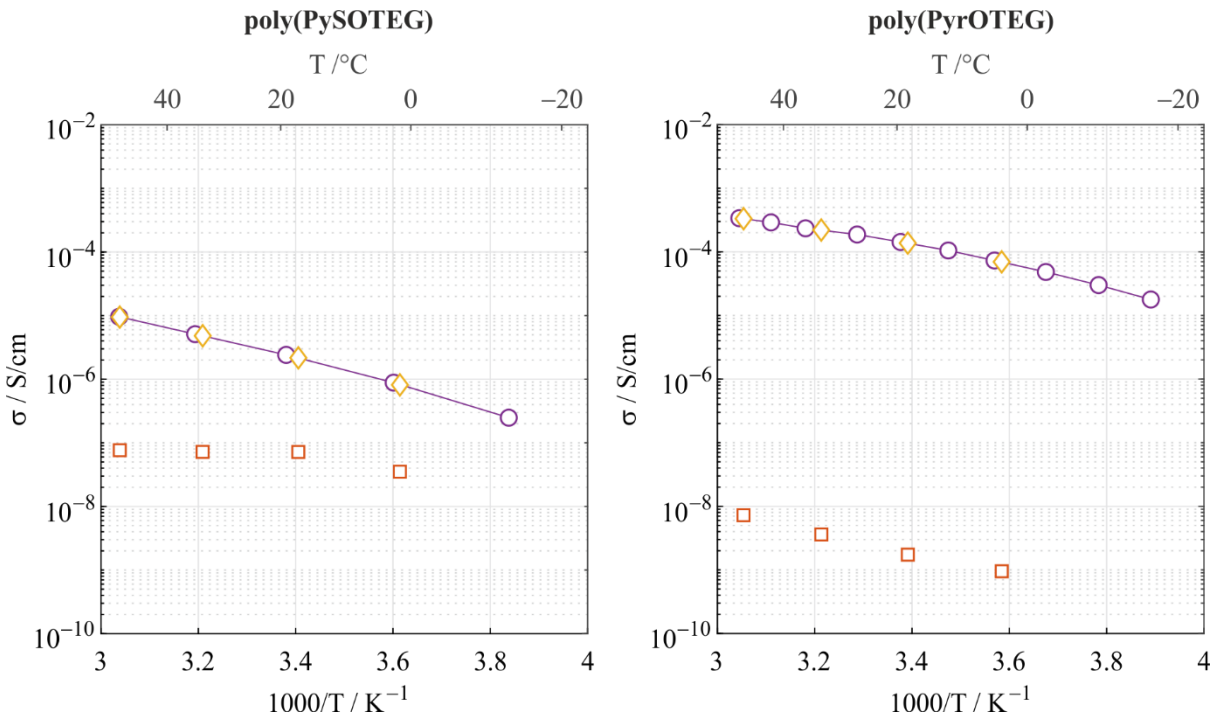

Figure 4.30: Electrochemical characterization of poly(PySOTEG (**30**, left) and poly(PyrOTEG) (**31**, right): combined impedance (violet), ionic impedance (yellow) and electronic impedance (red).

Block-co-polymerization of *exo*-Nbe-S-Pyr (**24b**) + Nbe-OTEG (**26**), as well as *exo*-Nbe-Pyr (**25**) + Nbe-OTEG (**26**) led to polymers with same impedance values compared to poly(PySOTEG) (**30**) and poly(PyrOTEG) (**31**). Unfortunately, the cycling behavior of the block-co-polymers was not sufficient. For that reason, further experiments with block-co-polymers were omitted.

4.4.2.5. Cell Cycling with Mixed Conducting Polymers poly(PySOTEG) (**30**) and poly(PyrOTEG) (**31**)

Performing electrochemical reactions in reduced states of the polymers can be helpful, because the electronic impedance would get enhanced assuming that the reaction would take place at proper potentials compared Figure 4.7. Silicon alloying with Li takes place between 0 and 1 V *vs* Li/Li^+. The mixed conducting polymers employed those circumstances to their advantage, as in that potential region the polymers exist in their reduced state. To test the electrochemical response, the polymers were dissolved in NMP with or without addition of Si nanoparticles, coated onto Cu foil current collectors, dried at elevated temperature under vaccum and assembled in 3-electrode SWAGELOK® type cells using a Li-metal counter and reference electrode and 1.2 M $LiPF_6$ in EC/DEC + FEC as the electrolyte. Galvanostatic discharge of a battery without Si particles showed that in the potential region of ~1 V there was an electrochemical reaction, which belonged to the reduction reaction of the mixed conductor (Figure 4.31). Of course, cycling experiments were performed with conversion type materials. Silicon cells were assembled and run with two different cycling programs. Cycling experiments of mixed conducting polymers inside SWAGELOK® type calls showed promising results in terms of achieved capacities. Though, over the time and with progressing cycle numbers fading issues occurred likely due to incomplete tightness of the cell body. O_2 could diffuse into the cell and could cause undesired parasitic side reaction, which decreases the capacity. Coulombic efficiencies of those cells were between 98 and 98.5% (Figure 4.32).

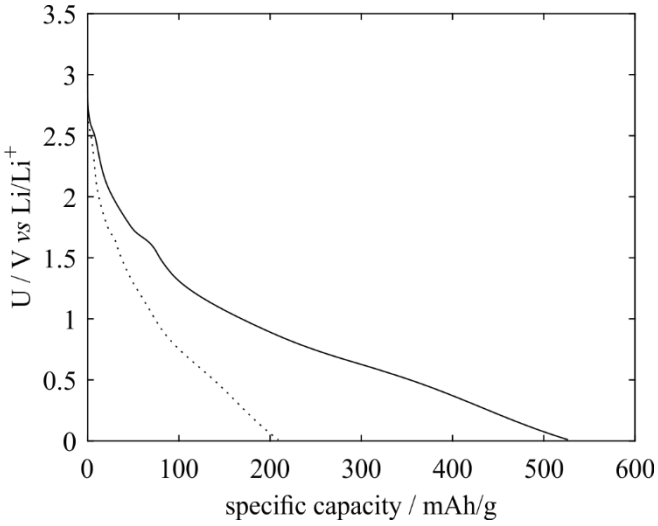

Figure 4.31: Discharge capacity of poly(PyrOTEG) (**31**, full line) and poly(PySOTEG) (**30**, dotted line).

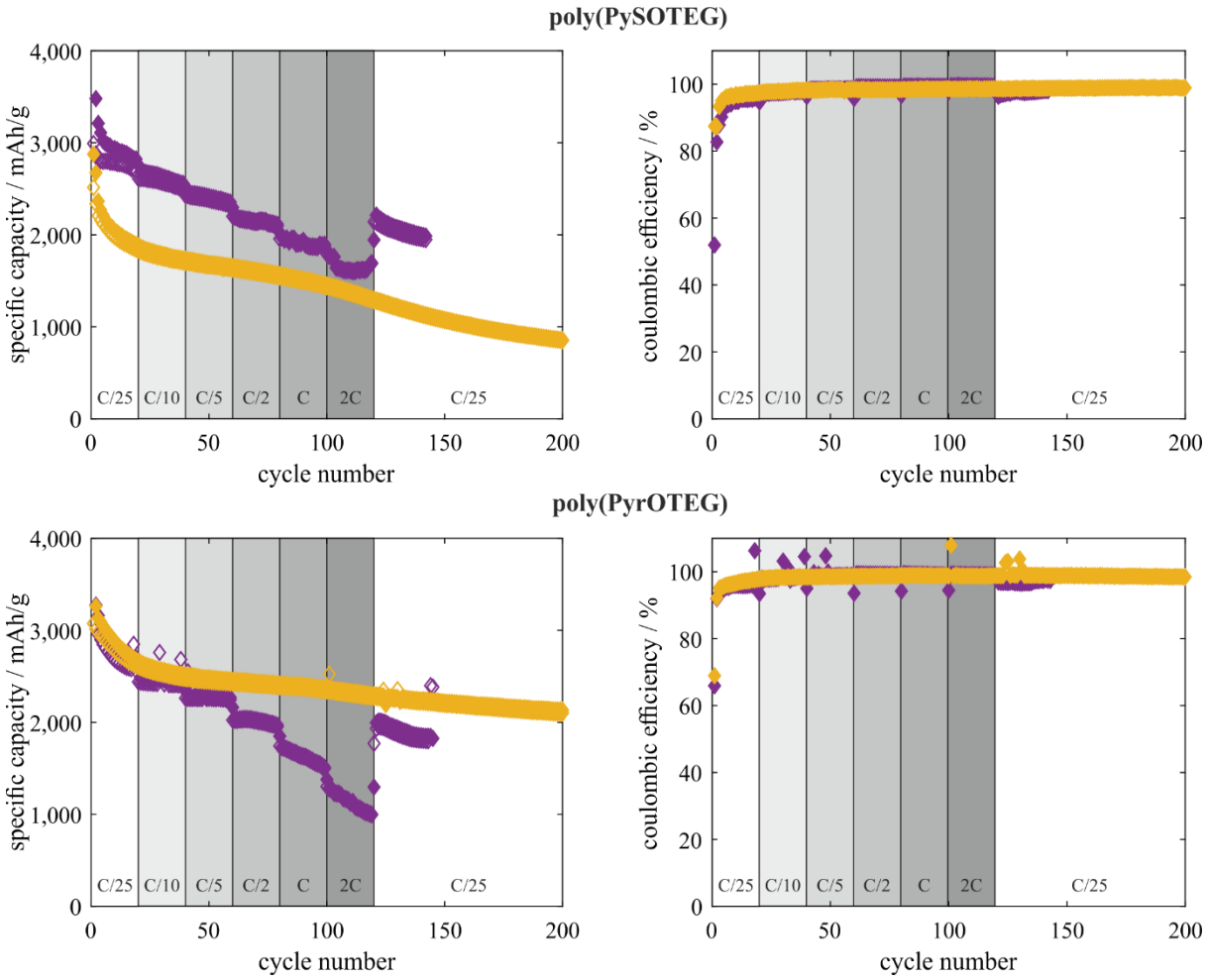

Figure 4.32: Cycling experiment of Si batteries using mixed conducting polymer (poly(PySOTEG) (**30**), top images and poly(PyrOTEG) (**31**), bottom images) inside SWAGELOK® type cells: at different cycling rate (blue markers); at C over 10 (red maker); filled marker = discharge capacity, open marker = charge capacity.

To obtain better tightness, coin cells were used for further cycling experiments over longer times which increased the coulombic efficiencies to >99.8%. The impact of increasing coulombic efficiencies could be seen in the constant cycling behavior of the cells.

Astonishingly, the capacities at fast cycling rate in coin cells were smaller compared to SWAGELOK-type cells (Figure 4.33). Using ROMP polymers for electrochemical applications is rather unusual,[59] however, results of cycling experiments could easily keep up with cycling performances of other mixed conducting polymers.[1a]

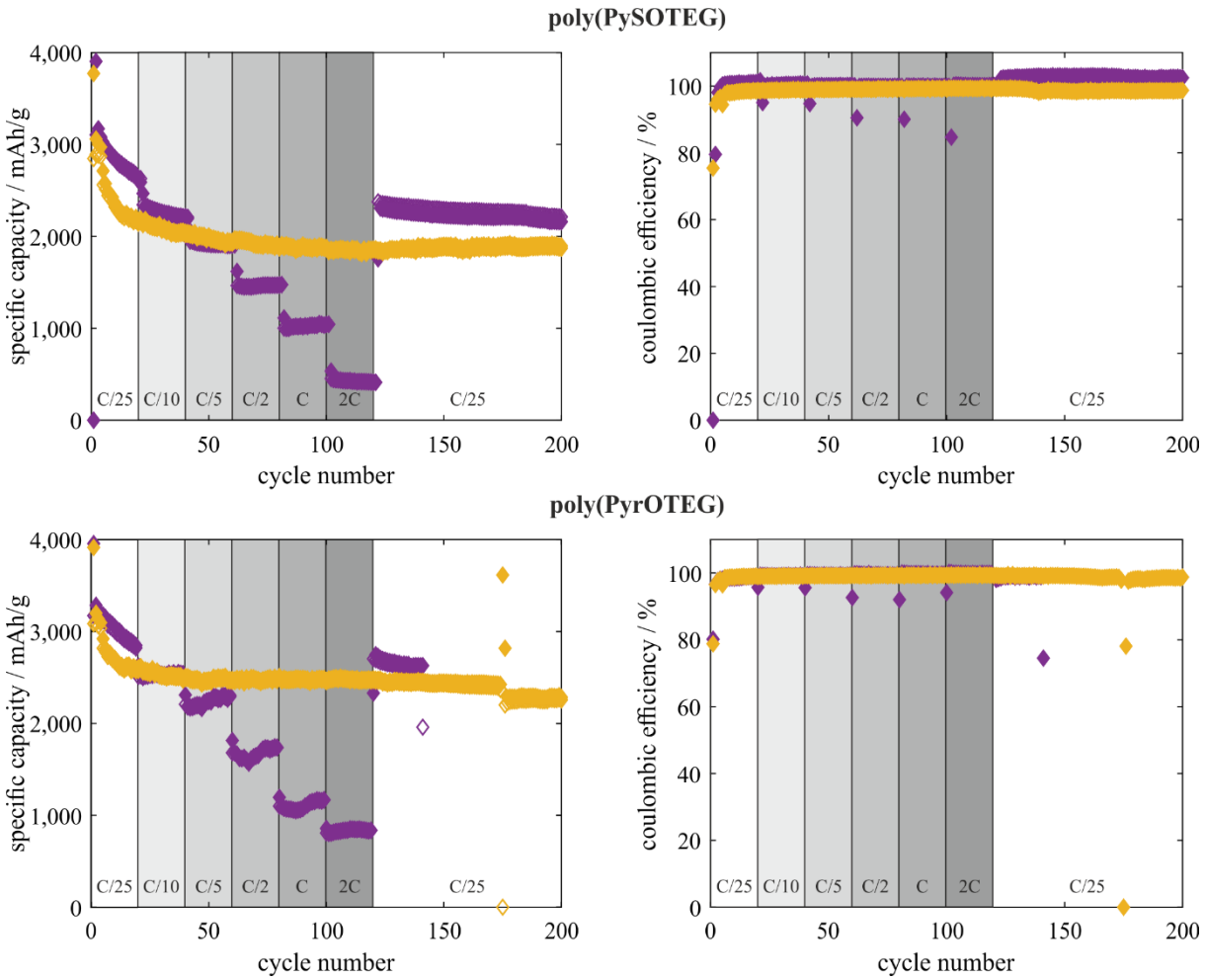

Figure 4.33: Cycling experiment of Si batteries using mixed conducting polymer (poly(PySOTEG) (**30**), top images and poly(PyrOTEG) (**31**), bottom images) inside coin cells: at different cycling rate (blue markers); at C over 10 (red maker); filled marker = discharge capacity, open marker = charge capacity.

4.4.2.6. *In situ* Displacement Measurement

Conversion type materials undergo from severe particle size changes during charge/discharge. The particle size change can result in two extreme cases with regard to the full electrode thickness. First, the inactive material host, such as carbon black, may form a rigid porous host structure and the change particle volume is accommodated by expanding into existing pores. Second, the full electrode volume expands and shrinks according to the volume of the active material. This phenomenon can be measured *in situ* by a dilatometer measurement. Inside Si-anodes the particles grew during the whole discharge and *vice versa*. Dilatometer cells were assembled with both polymers and the results are shown in Figure 4.34. The discharge curves

indicate significant solid electrolyte interphase (SEI) formation during the first discharge for both polymers. Approximately half of the volume increase disappeared in the subsequent charging process. In the case of poly(PyrOTEG) (**31**) formed/consumed volume were almost equal. Whereas, in the case of poly(PySOTEG) (**30**), result of the dilatometer measurement showed SEI formation during each discharge. Furthermore, in the case of poly(PySOTEG) relative displacement was ~10% compared to poly(PyrOTEG).

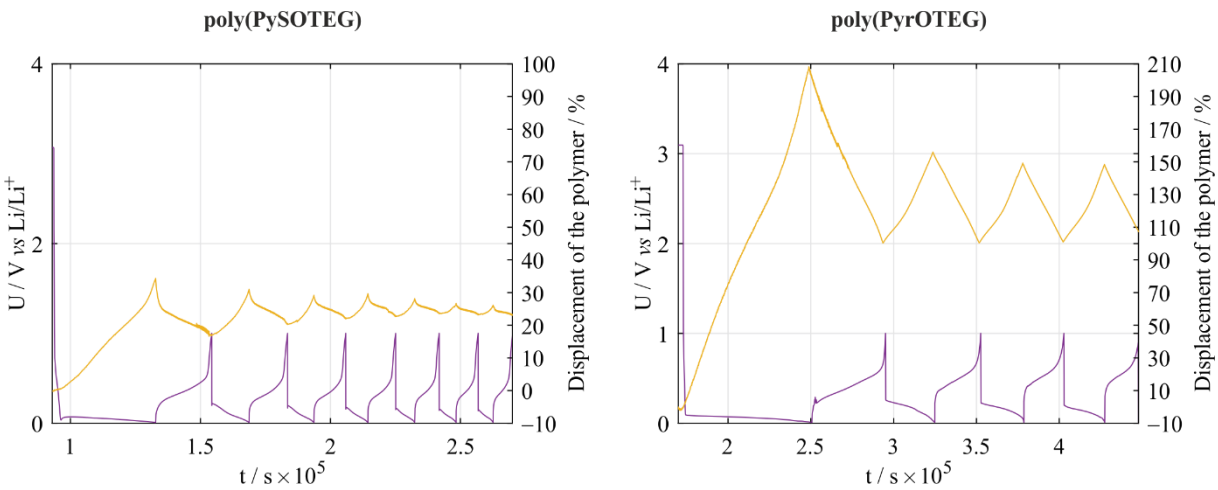

Figure 4.34: Cycling experiments of Si-anodes containing mixed conducting polymers poly(PySOTEG) (**30**) and poly(PyrOTEG) (**31**) with *in situ* dilatometer measurement: potential over the time (violet line), displacement over the time (yellow line).

4.4.2.7. Li-O_2 Cell Chemistry in ROMP Polymers

Investigations whether Li-O_2 cell chemistry can be performed with the polymers PenzOTEG/PyrOTEG were undertaken. The ideal goal is hereby that the electrolyte-swollen polymer forms a continuous mixed conducting phase rather than a porous network of electron conductor with electrolyte filled pores. Cells were constructed by coating the polymers onto Cu-foils. Afterwards, Li-O_2 cells were assembled in a sealed cell with pressure transducer using a $LiFePO_4$ counter and reference electrode and 1.2 M $LiPF_6$ in EC/DEC + FEC as the electrolyte. Cells were then discharged at a constant current of 28.6 µA/cm^2 and the results are shown in Figure 4.35.

Similar to the electrochemically polymerized material, pressure measurements were performed on the one hand to see if the mixed conducting polymer is able to reduce O_2. On the other hand, this technique gives inside into ongoing reaction mechanisms. The ratio of transferred e^- to spent O_2 (e^-/O_2) provides a basic measure for the selectivity of O_2 reduction to Li_2O_2 or side product formation. Based on stability tests of PenzOTEG/PyrOTEG, only poly(PyrOTEG) (**31**) was subjected to O_2 electrochemistry, due to the presumed high stability towards reactive

oxygen species. The pressure measurement with the mixed conductor was that it was able to perform oxygen reduction, which could be followed *in situ* by pressure change. However, the calculated e^-/O_2 value of 2.5 means, that more e^- were used than needed for O_2 reduction to Li_2O_2. Consequently, assumptions were made that the electrons beyond $2e^-/O_2$ were either used to reduce the pyrene units of the mixed conductor.

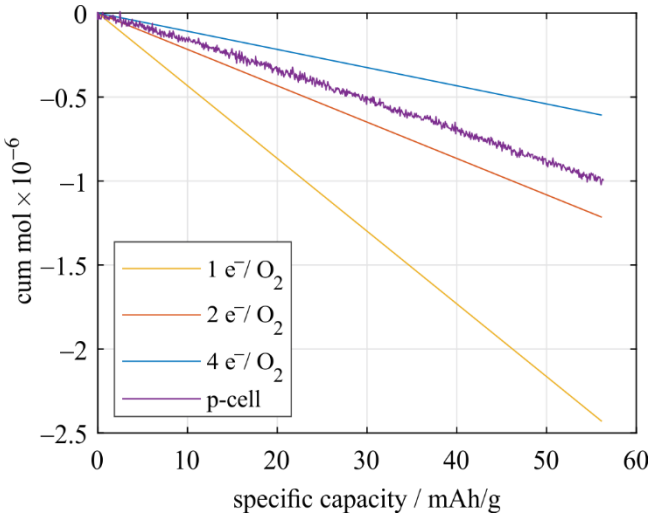

Figure 4.35: Theoretical processes for $1e^-/O_2$ (yellow) $2e^-/O_2$ (red), $4e^-/O_2$ (blue) reactions and experi-mentally generated data (violet).

In summary, mixed conducting polymers with pyrene and TEG moieties on their side chains were produced. The electrochemical properties of them were examined and they were further assembled inside Si-batteries resulting with lovely cycling performance and behavior. Furthermore, the volume change of the participating Si-particles was measured *in situ* using dilatometer assisted experiments. The mixed conducting polymers were also assembled inside Li-O_2 cells, in which Li_2O_2 formation was followed by analysis method. Combining all results, electrochemical reaction could take place inside the synthesized polymeric material, which could stand the volume changes during cycling of electrochemical active conversion materials.

5. Organic Materials in $^1O_2$ Electrochemistry

In 2011, HASSOUN et al. proposed that $^1O_2$ formation is possible during the Li_2O_2 charging process at voltages above 3.9 V.[60] The idea was picked up a few times afterwards but could not be confirmed until recently when GASTEIGER *et al.* have shown that minor amounts of $^1O_2$ are generated above ~3.5 V when Li_2O_2 is oxidized.[61] The potential of 3.5 V was rationalized based on the reversible potential of Li_2O_2 formation and the energy difference of ~1 eV between $^3O_2$ and $^1O_2$. Yet the formation of $^1O_2$ above 3.5 V cannot consistently explain the pattern of parasitic reactions during discharge and charge. Typically, there is some parasitic chemistry on discharge but substantially more from the onset of charge at ~3.5 V. The reactivity of superoxide (O_2^-), which is more abundant on discharge than on charge, and $^1O_2$ above 3.5 V cannot consistently explain the parasitic chemistry.

In this work contributions to important aspect of the FREUNBERGER-group's work to clarify the role of $^1O_2$ in non-aqueous battery chemistries were delivered. Starting point and link to the so far presented work on mixed conductors is the challenging cell chemistry in Li-O_2 cells. Li_2O_2 lends Li-O_2 cells a high formal capacity per mass and volume of active material. However, it is a poor medium to support the charge storage process of linking the redox moiety O_2 to electron and ion transport according to $O_2 + 2e^- + 2Li^+ \rightleftarrows Li_2O_2$. It would thus be desirable to bypass the poor ion and electron transport in Li_2O_2 through a medium where both are efficient. To do so requires introducing a mixed conductor. In 2012, FREUNBERGER *et al.* have introduced

oxidation redox mediators in Li-O_2 cells to form essentially a mixed conducting electrolyte to shuttle electron-holes between the solid electrode surface to the insulating Li_2O_2 to oxidize which allows recharging the cell at otherwise by far impossible rates.[62] A reduction mediator to reduce O_2 to Li_2O_2 without blocking the electrode surface would complete a mixed conductor based Li-O_2 cell system. When looking at improving oxidation mediators we had the baffling insight that the oxidation of Li_2O_2 using redox mediators does, in most cases, not yield the expected amount of O_2 according to $Li_2O_2 + 2M^+ \rightarrow O_2 + 2Li^+ + 2M$. The search for reasons triggered us to suspect $^1O_2$ to be involved. To do so, it was required to first develop a set of methods to detect $^1O_2$ in the challenging environment of non-aqueous batteries before particular questions could be addressed.

Work in thesis was concerned in general with organic materials and their interaction with $^1O_2$. In particular, the following topics were investigated:

1) An $^1O_2$ detection method based on 9,10-dimethylanthracene as $^1O_2$ trap: for non-aqueous battery chemistry confirming the identity of endoperoxides as the sole and selective product upon exposure to the Li-O_2 cell environment and excluding cross sensitivity to superoxide and peroxide.[41b]

2) Formulating likely reaction mechanisms for $^1O_2$ attack on glyme electrolytes (to be published).

3) The degradation mechanism of oxidation mediators: analyzing reaction products of oxidation mediators in contact with $^1O_2$ and superoxide (Nature Communications, submitted).

4) New efficient $^1O_2$ quenchers: synthesizing new branched amines and quarternary ammonium compounds as $^1O_2$ quenchers. The target is high quenching efficiency and an oxidation stability beyond 4.5 V to allow for the use in metal-O_2 cells and for detecting $^1O_2$ at Li-rich layered oxides (publications in preparation and at the stage of data collection, respectively).

However, $^1O_2$ is hard to detect due to its short lifetime as mentioned in Chapter 3.7.2. The special reactivity of $^1O_2$ allows it to perform reactions, which would not be possible with standard $^3O_2$. For instance, $^1O_2$ is able to react with a diene within a pericyclic reaction (Scheme 5.1). We took advantage of this selective reaction of $^1O_2$ and screened some cyclization reactions.

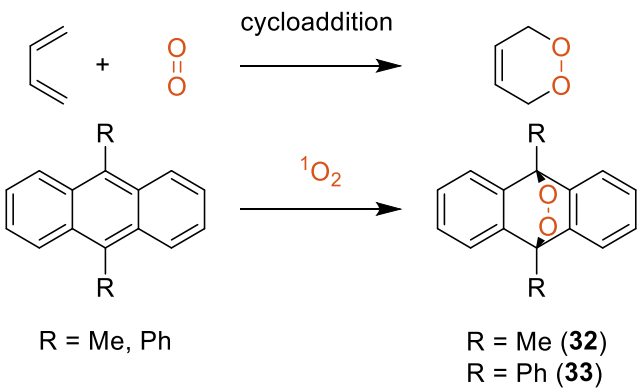

Scheme 5.1: Selective reaction of $^1O_2$ with a diene: cycloaddition reaction of $^1O_2$ with dimethylanthracene (DMA) (**32**)/diphenylanthracene (DPA) (**33**).

In cycloaddition reactions, e.g. the DIELS-ALDER reaction, the energy level of the diene and the dienophile is important.[53] Fast reaction takes place, if the energy difference of the HOMO of the diene and the LUMO of the dienophile is small. This was the reason of the different reaction rate of the used anthracene derivates. Dimethylanthracene (DMA) (**32**) reacted approximately 30 times faster compared to diphenylanthracene (DPA) (**33**). Cycloaddition reaction was followed by UV-Vis spectroscopy. After DMA succeeded the stability test against O_2^-, DMA was proposed a proper sensor with high sensitivity for $^1O_2$ detection inside an electrochemical cell.

Discharge of oxygen batteries with DMA showed that below the estimated potential of 3.5 V *vs* Li/Li^+ $^1O_2$ formation occurred. Furthermore, $^1O_2$ was detected right from the start of the charging process at ~3 V and during discharge. Those 2 observations led us to following possible $^1O_2$ formation mechanism:

On discharge, one possible $^1O_2$ source is the disproportionation of LiO_2 according to

$$2LiO_2 \rightarrow (LiO_2)_2 \rightarrow Li_2O_2 + {}^1O_2 \tag{5.1}$$

Due to the small energy difference between triplet and singlet state of a LiO_2 dimer, BRYANTSEV *et al.* reported this plausible transition.[63] Whenever proton sources are available, O_2^- will be protonated and can release $^1O_2$ according to the overall reaction.[64]

$$2O_2^- + 2H^+ \rightarrow H_2O_2 + {}^1O_2 \tag{5.2}$$

Finally, above 3.55 V the $^1O_2$ formation is thermodynamically allowed according to

$$Li_2O_2 \rightarrow {}^1O_2 + 2e^- + 2Li^+ \tag{5.3}$$

Overall, this was the first time that $^1O_2$ was detected during discharge and <3.55 V on charging inside Li-O_2 batteries.

nature energy

ARTICLES

PUBLISHED: 20 MARCH 2017 | VOLUME: 2 | ARTICLE NUMBER: 17036

Singlet oxygen generation as a major cause for parasitic reactions during cycling of aprotic lithium–oxygen batteries

Nika Mahne[1], Bettina Schafzahl[1], Christian Leypold[1], Mario Leypold[2], Sandra Grumm[1], Anita Leitgeb[1], Gernot A. Strohmeier[2,3], Martin Wilkening[1], Olivier Fontaine[4,5], Denis Kramer[6], Christian Slugovc[1], Sergey M. Borisov[7] and Stefan A. Freunberger[1]*

Non-aqueous metal–oxygen batteries depend critically on the reversible formation/decomposition of metal oxides on cycling. Irreversible parasitic reactions cause poor rechargeability, efficiency, and cycle life, and have predominantly been ascribed to the reactivity of reduced oxygen species with cell components. These species, however, cannot fully explain the side reactions. Here we show that singlet oxygen forms at the cathode of a lithium–oxygen cell during discharge and from the onset of charge, and accounts for the majority of parasitic reaction products. The amount increases during discharge, early stages of charge, and charging at higher voltages, and is enhanced by the presence of trace water. Superoxide and peroxide appear to be involved in singlet oxygen generation. Singlet oxygen traps and quenchers can reduce parasitic reactions effectively. Awareness of the highly reactive singlet oxygen in non-aqueous metal–oxygen batteries gives a rationale for future research towards achieving highly reversible cell operation.

Rechargeable non-aqueous metal–O_2 (air) batteries have attracted immense interest because of their high theoretical specific energy and potentially better sustainability and cost in comparison to current lithium-ion batteries[1–5]. Cell chemistries include Li–O_2, Na–O_2 and K–O_2, with the Li–O_2 cell being most intensely studied[6–9]. Charge is stored at the cathode by the reversible formation/decomposition of metal oxides on discharge/charge[10,11]. In the Li–O_2 cell this is typically Li_2O_2. Practical realization, however, still faces many challenges[5,8,12–14]. Perhaps the most significant obstacle arises from severe parasitic reactions during cycling[3–5,7,8,10,11,13–26]. These reactions decompose the electrolyte as well as the porous electrode (typically carbon with binder), and cause poor rechargeability, high charging voltages, low efficiency, build-up of parasitic reaction products, and early cell death within a few cycles.

Many researchers have investigated the origin of parasitic reactions and proposed strategies to mitigate them[7,8,10,16–19]. Superoxide has been most widely mentioned in causing side reactions on discharge since it forms as an intermediate in O_2 reduction and is a strong nucleophile and base[3,11,14,20,21,27]. Also, Li_2O_2 was found to react with the electrolyte and carbon on discharge[3,21–24]. These reactivities were used to explain the observation that on discharge typically close to the ideal value of two electrons per one O_2 molecule are consumed despite significant amounts of side products such as Li_2CO_3, Li formate and Li acetate being formed[17,24]. On charge, typically the e^-/O_2 ratio deviates significantly from two, and more of the side products form[5,7,15,24,25]. These parasitic reactions occur at charging potentials well within the stability window (oxidative stability) of carbon and electrolyte in the absence of Li_2O_2 (refs 21,23,25). It was therefore suggested that some sort of reactive intermediates of Li_2O_2 oxidation cause electrolyte and carbon decomposition on charge[11,23,25,28].

Chemical oxidation of alkaline peroxides in non-aqueous media is known to generate singlet oxygen ($^1\Delta_g$ or $^1O_2$), the first excited state of triplet ground state dioxygen ($^3\Sigma_g^-$)[29–32]. Based on the reversible potential of Li_2O_2 formation and the energy difference between triplet and singlet oxygen, the formation of $^1O_2$ in the Li–O_2 cell has been hypothesized to be possible at charging potentials exceeding 3.5 to 3.9 V versus Li/Li^+ (refs 11,23). Only recently $^1O_2$ was reported to form in small quantities between 3.55 and 3.75 V (ref. 28). Overall, the hitherto known processes cannot consistently explain the observed irreversibilities. Only better knowledge of parasitic reactions may allow them to be inhibited so that progress towards fully reversible cell operation can continue.

Here we show that $^1O_2$ forms in the Li–O_2 cathode during discharge and from the onset charge, and that it is responsible for a major fraction of the side products in the investigated system with ether electrolyte. The lower abundance on discharge and higher abundance on charge can consistently explain the typically observed deviations of the e^-/O_2 ratio from the ideal value of two. The origin of the $^1O_2$ on charge appears to be superoxide and peroxide. The presence of trace water enhances the formation during both

[1]Institute for Chemistry and Technology of Materials, Graz University of Technology, Stremayrgasse 9, 8010 Graz, Austria. [2]Institute of Organic Chemistry, Graz University of Technology, Stremayrgasse 9, 8010 Graz, Austria. [3]Austrian Centre of Industrial Biotechnology (acib) GmbH, Petersgasse 14, 8010 Graz, Austria. [4]Institut Charles Gerhardt Montpellier, UMR 5253, CC 1701, Université Montpellier, Place Eugène Bataillon, 34095 Montpellier Cedex 5, France. [5]Réseau sur le Stockage Électrochimique de l'Énergie (RS2E), CNRS FR3459, 33 rue Saint Leu, 80039 Amiens Cedex, France. [6]Engineering Sciences, University Road, University of Southampton, Southampton SO17 1BJ, UK. [7]Institute for Analytical Chemistry and Food Chemistry, Graz University of Technology, Stremayrgasse 9, 8010 Graz, Austria. *e-mail: freunberger@tugraz.at

© 2017 Macmillan Publishers Limited, part of Springer Nature. All rights reserved.

discharge and charge. We also show that $^1O_2$ traps and quenchers as electrolyte additives can significantly reduce the amount of side products associated with $^1O_2$.

Reactivity of the electrolyte with singlet oxygen

The discharge product formed at the Li–O_2 cathode in relatively stable electrolytes, such as the widely used glyme (oligo-ethylene glycol dimethyl ether) based ones, consists predominantly of Li_2O_2 accompanied by a typical pattern of side products, including Li_2CO_3, Li acetate and Li formate[12,15,21,23,24,26,33]. The same side products form upon oxidation of Li_2O_2 (charging), and eventually release CO_2 and other fragments at sufficiently oxidizing potentials[21,25]. A large body of work has identified the reduced O_2 species superoxide and peroxide or their lithium compounds to trigger the formation of these products[3,11,14,15,20,21,34]. To investigate whether $^1O_2$ would lead to the same products, we generated it inside a typical electrolyte, 0.1 M lithium perchlorate ($LiClO_4$) in ethylene glycol dimethyl ether (DME), and analysed the formed products (Fig. 1). $^1O_2$ was generated photochemically by illuminating the O_2-saturated electrolyte containing a small concentration of a photosensitizer inside a closed vessel (for experimental details see Methods). The head space was then purged to a mass spectrometer (MS) for analysis to detect readily evolved gases, and, after addition of acid, to detect whether Li_2CO_3 had formed (Fig. 1a). MS analysis does not show any detectable direct CO_2 evolution, but CO_2 evolving from Li_2CO_3. A second portion of equally treated electrolyte was dissolved in D_2O and subjected to ^{1}H-NMR spectroscopy (Fig. 1b). The ^{1}H-NMR spectrum confirms the presence of Li formate and Li acetate via the peaks for HCOOD and CH_3COOD that form upon contact with D_2O. The literature on the reactivity of $^1O_2$ with organic substrates most commonly states peroxides as an initial product[32]. Going along this line, we assume that $^1O_2$ produces ROOH, $R^\bullet$, and $ROO^\bullet$ as the first reactive intermediates of electrolyte degradation more efficiently than the reduced oxygen species, which were proposed to initiate electrolyte degradation via the same intermediates, albeit high activation energies have been noted[33,35,36]. Taken together, these results show that the typical pattern of parasitic reaction products formed during discharge and charge of Li–O_2 cells could to some extent originate from the presence of $^1O_2$.

Operando detection of singlet oxygen in the Li-O_2 cathode

Probing whether $^1O_2$ is involved in the cell reaction requires sensitive methods that are compatible with the cell environment. So far, described methods for detection of $^1O_2$ are based either on direct detection of characteristic light emissions upon decay into the ground state, or on the selective reactivity with probe molecules that are themselves interrogated by spectroscopic means[32]. The short lifetime of $^1O_2$ in liquid media, various competing decay routes, and low sensitivity of near-infrared (NIR) detectors make the detection of the specific emission of $^1O_2$ at 1,270 nm challenging and insensitive[31,32,37]. Therefore, the absence of a detectable signal would provide no definite proof for the absence of $^1O_2$. Nevertheless, we could detect this emission for a case with high $^1O_2$ abundance, as discussed later.

To detect $^1O_2$ at quantities which would be responsible even for small amounts of parasitic products, we devised a sensitive and selective method with a chemical probe compatible with the cell environment at any stage of cycling. Previously, highly sensitive probes for aqueous media have been described, which contain a quencher group attached to a chromophore and show fluorescence 'switch on' upon reaction of the quenching group with singlet oxygen[32,38]. However, the chromophores used so far are not electrochemically inert in the relevant potential range of ~2 to 4 V versus Li/Li^+. Typically used chromophores include fluorescein and rhodamine, which all undergo electrochemical reactions in this range (Supplementary Fig. 1). The quencher group for $^1O_2$ is typically a substituted

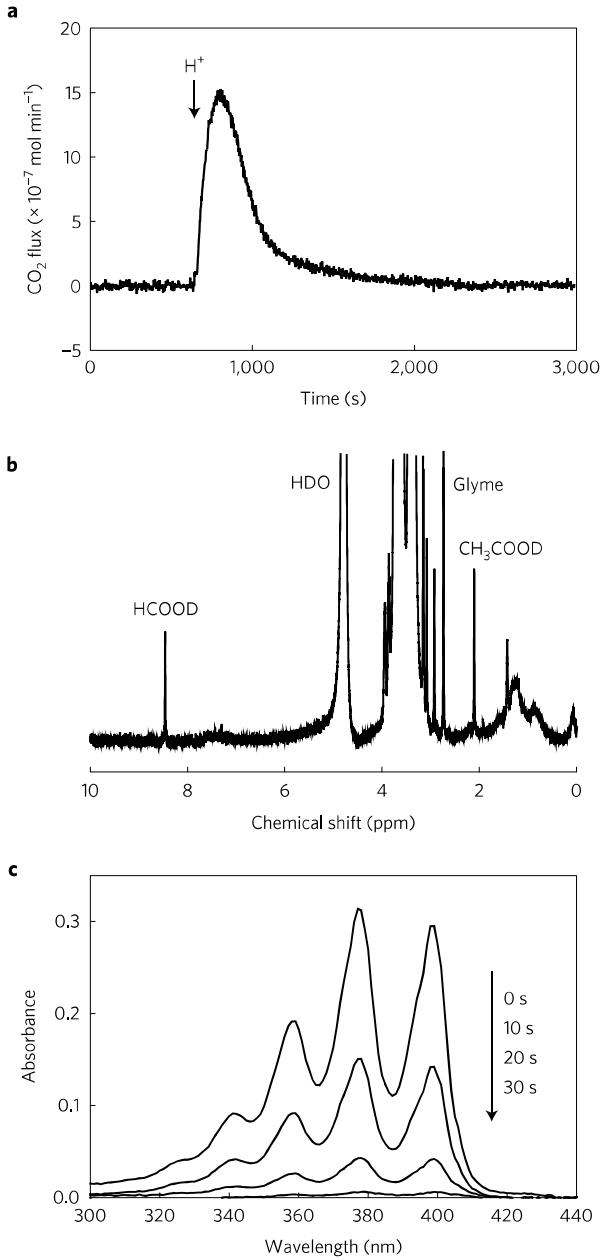

Figure 1 | Reactivity of the electrolyte with singlet oxygen. a, CO_2 evolution measured by mass spectrometry above O_2-saturated 0.1 M $LiClO_4$ in DME electrolyte that has been exposed for 30 min to $^1O_2$. The latter has been produced *in situ* by photogeneration with the sensitizer palladium(II) *meso*-tetra(4-fluorophenyl)tetrabenzoporphyrin with the head space closed. After illumination the head space was purged to the mass spectrometer and H_3PO_4 added at the time indicated to evolve CO_2 from Li_2CO_3. **b**, ^{1}H-NMR spectrum of the equally treated electrolyte when dissolved in D_2O. **c**, UV–Vis absorption spectra as a function of illumination time of the same electrolyte that additionally contained 2.6×10^{-5} M 9,10-dimethylanthracene. The absorbance in the ordinate of **c** is dimensionless, thus there is no unit.

anthracene derivative such as 9,10-dimethylanthracene (DMA) or 9,10-diphenylanthracene (DPA), which form the corresponding endoperoxide. DPA itself has been used directly as an $^1O_2$ probe based on the decrease of absorbance as a sign for the presence of $^1O_2$ (ref. 39). We have added 2.6×10^{-5} M DMA to 0.1 M $LiClO_4$ in DME and exposed the solution to *in situ* photogenerated $^1O_2$; all DMA was consumed within less than a minute, which indicates

© 2017 Macmillan Publishers Limited, part of Springer Nature. All rights reserved.

a rapid reaction with $^1O_2$ to its endoperoxide (DMA–O_2) in this environment (Fig. 1c). DPA reacted in the same experiment approximately two orders of magnitude slower (Supplementary Fig. 2). Cyclic voltammograms with 2 mM DMA and 0.1 M $LiClO_4$ in DME under Ar show electrochemical stability between 1.8 and 4.5 V (Supplementary Fig. 3). The DMA was then transformed to its endoperoxide (DMA–O_2) by means of *in situ* photogenerated $^1O_2$. Cyclic voltammograms taken thereafter show likewise stability of the DMA–O_2 between 2.5 and >4.5 V. Inertness against superoxide (O_2^-), and hence selectivity for $^1O_2$, was confirmed by stirring DMA with an excess of KO_2 in DME containing 0.1 M $LiClO_4$ and taking ^{1}H-NMR spectra and ultraviolet–visible (UV-Vis) spectra at time intervals up to 22 h. The results do not show any detectable decomposition products of the DMA (Supplementary Figs 4 to 7). Taken together, the above experiments confirm DMA to be a sensitive and selective probe for $^1O_2$ in the cell environment. We use DMA in the following first as a fluorescent probe for operando detection of $^1O_2$. Operando fluorescence requires a relatively low DMA concentration in the μM range, which slightly restricts the detection limit. Later we use DMA in the mM range to detect $^1O_2$ with maximum sensitivity and to remove it, which requires measuring the conversion of DMA to DMA–O_2 by *ex situ* high-performance liquid chromatography (HPLC).

An operando fluorescence set-up as detailed in the Methods was constructed. Briefly, the cell consisted of a porous carbon working electrode in an O_2-saturated electrolyte containing 1.6×10^{-5} M DMA and 0.1 M $LiClO_4$ in tetraethylene glycol dimethyl ether (TEGDME). As the counter electrode we used $Li_{1-x}FePO_4$ to exclude reactivity of the DMA with a Li metal anode. The cell was assembled inside a gas-tight quartz cuvette with a slightly pressurized O_2 head space. Excitation and emission wavelengths were chosen according to the respective maxima in these spectra of DMA (Supplementary Fig. 8). The electrolyte was stirred to ensure constant O_2 concentration irrespective of consumption or evolution during cycling. This is important, since O_2 is a fluorescence quencher, and changes in intensity could otherwise stem from changing O_2 concentration, as shown in Supplementary Fig. 9.

Results for charging a cathode, containing chemically produced Li_2O_2 with 0.1 M $LiClO_4$ in TEGDME as the electrolyte, by applying voltage steps are shown in Fig. 2a. At voltages up to 3.5 V the fluorescence intensity, reflecting DMA concentration, remains unchanged within the measurement accuracy. Above this voltage, the signal drops with increasing rate. The cumulatively consumed DMA corresponds to ~2% of the theoretically evolved O_2 (based on charge) being $^1O_2$. This value is the lower boundary of the actual abundance since at the low DMA concentration (~0.5% of the O_2 concentration) competing sinks for $^1O_2$ other than reaction with DMA can be expected to dominate.

To probe whether $^1O_2$ is also formed during discharge, we cycled electrodes in the fluorescence set-up. Results for galvanostatic cycling of a porous carbon cathode in dry 0.1 M $LiClO_4$ in TEGDME are shown in Fig. 2b. Upon discharge the DMA concentration remains nearly unchanged within the measurement accuracy. However, immediately after switching to charging, starting from ~3 V, the signal drops with increasing slope as charging progresses and the voltage climbs towards 4.3 V, where full recharge is reached. The cumulatively consumed DMA corresponds to ~4% of the expected O_2 being $^1O_2$. The results demonstrate that $^1O_2$ was formed from the very beginning of charge at a significant rate. However, this experiment could not tell with certainty whether $^1O_2$ was formed on discharge. A possible source of $^1O_2$ on discharge is the reaction of the superoxide intermediate, the first step of O_2 reduction, with trace water, which has been shown to result in $^1O_2$ (ref. 37). Therefore, we have run an analogous experiment with 1,000 ppm H_2O in the electrolyte (Fig. 2c). DMA consumption was seen throughout discharge at an approximately constant rate. Again,

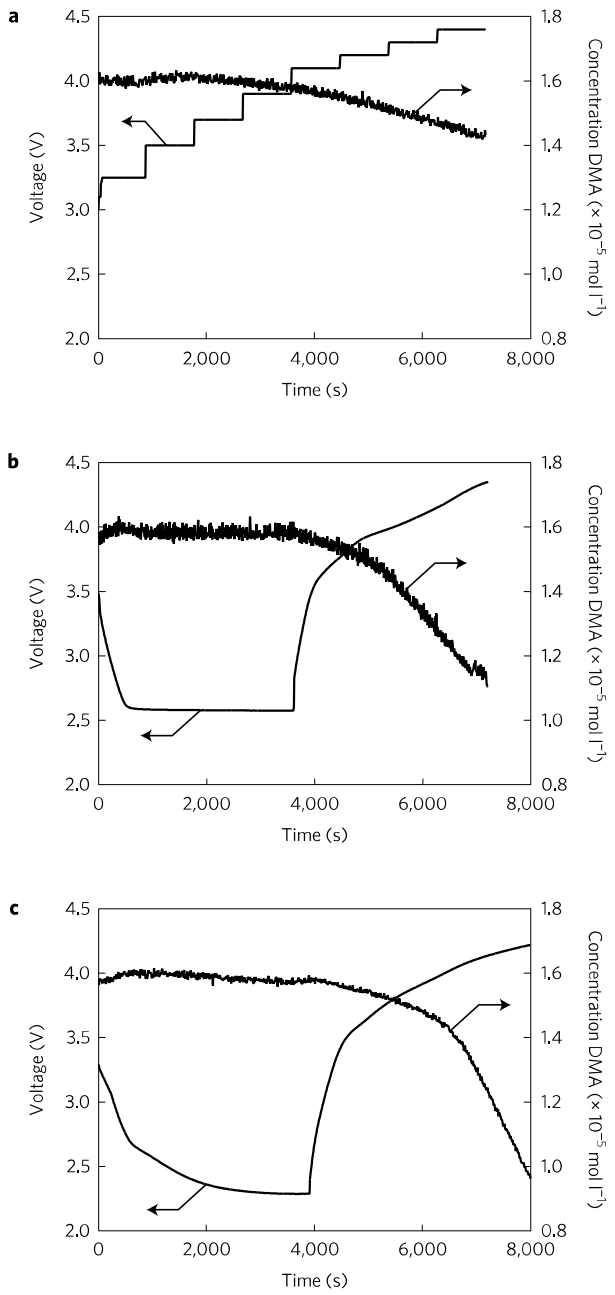

Figure 2 | Operando fluorescence spectroscopy during Li–O_2 cell operation with electrolytes containing 9,10-dimethylanthracene (DMA) as singlet oxygen trap. a, Potentiostatic oxidation of a carbon black electrode containing chemically produced Li_2O_2 in O_2-saturated 0.1 M $LiClO_4$ in TEGDME. Voltage steps and DMA concentration. **b**, Galvanostatic discharge and charge of a carbon black electrode at 25 μA cm^{-2} in dry O_2-saturated 0.1 M $LiClO_4$ in TEGDME. Voltage profile and DMA concentration. **c**, Galvanostatic discharge and charge of a carbon black electrode at 25 μA cm^{-2} in O_2-saturated 0.1 M $LiClO_4$ in TEGDME containing 1,000 ppm water. Voltage profile and DMA concentration. All electrolytes had an initial DMA concentration of 1.6×10^{-5} M.

the rate of DMA consumption increased substantially immediately after the cell was switched to charging, and increased as charge progressed to higher voltages. The consumption during charging is increased in comparison to the dry electrolyte, and reaches a value of ~6% of the expected O_2 being $^1O_2$. This suggests that trace water contributes to the formation of $^1O_2$ on discharge and charge. Since the required DMA concentration for operando fluorescence

© 2017 Macmillan Publishers Limited, part of Springer Nature. All rights reserved.

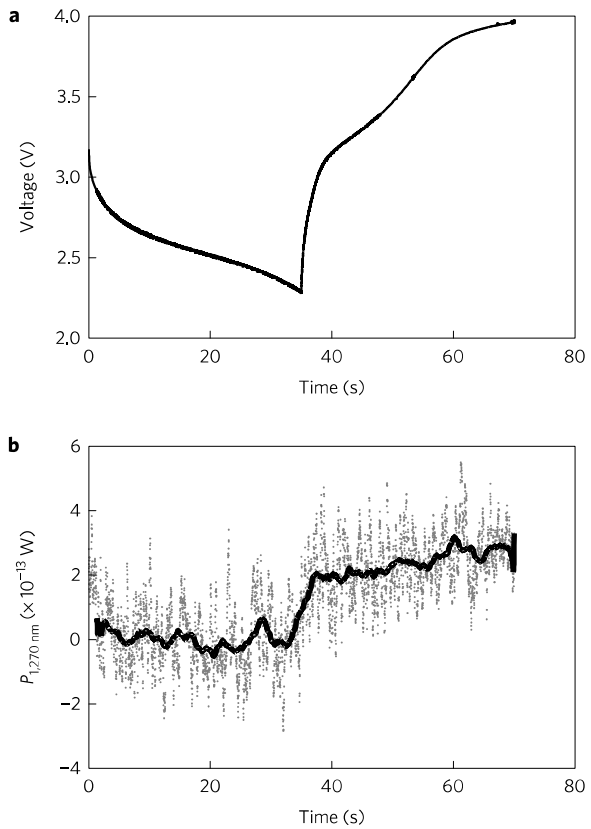

Figure 3 | Operando NIR emission measurement during cycling of a Li–O_2 cathode. a, Voltage profile during galvanostatic reduction and oxidation of an Au-grid electrode at 0.12 mA cm^{-2} in O_2-saturated 0.1 M $LiClO_4$ in deuterated acetonitrile containing 1,000 ppm D_2O. **b**, The power of the optical emission at 1,270 nm. The grey trace represents the sensor signal and the black trace the moving average to guide the eye.

is low, the abundance of $^1O_2$ on discharge appears to be close to the detection limit. Clear evidence for $^1O_2$ on discharge comes from *ex situ* measurements with ~2,000 times the DMA concentration, as discussed later.

We have shown above that DMA is very reactive with $^1O_2$ and reactive to a negligible extent with superoxide in the cell environment. To unambiguously show that there is indeed $^1O_2$ formation and that the DMA consumption does not originate from possible other reactive oxygen species, we measured the specific emission of $^1O_2$ at 1,270 nm (for experimental details see the Methods). This radiative decay to the ground state gives a very weak signal, which is further attenuated by competing sinks for $^1O_2$. One such is deactivation with the solvent with a strongly solvent-dependent lifetime[31]. Attempts to detect radiative decay in the ether electrolyte proved fruitless, which is explicable by the short lifetime in this solvent. Therefore, we have chosen deuterated acetonitrile, where the $^1O_2$ lifetime is higher than in ethers and also higher than in the non-deuterated solvents[32]. We also added 1,000 ppm D_2O, since the above experiments have shown higher $^1O_2$ generation when trace water was present, besides that the lifetime is longer in D_2O than in H_2O. Results for galvanostatic cycling are shown in Fig. 3. The signal/noise ratio does not permit a clear statement about the abundance of $^1O_2$ during discharge, which is to be expected given the low generation rate detected with operando fluorescence in Fig. 2. In accord with above results there is, however, unambiguous proof of $^1O_2$ generation from the start of charging, and increasing rate as charging progresses to higher voltages.

Trapping and quenching singlet oxygen

The above results show that $^1O_2$ forms in significant quantities from the start of charging, and suggest a smaller abundance during discharge. To estimate the fraction of the parasitic products during discharge and charge that originates from $^1O_2$ and to investigate whether removing the $^1O_2$ before it can react with cell components would effectively reduce these parasitic reactions, we examined the effect of $^1O_2$ trapping and quenching. The former removes $^1O_2$ in a chemical reaction and the latter deactivates it by physical quenching, for example, via a temporary charge transfer complex[40]. Trapping is, however, irreversible and physical quenching is therefore preferred because neither quencher nor O_2 is consumed. The literature suggests a variety of quenchers, including aliphatic amines and quinones[41]. We have chosen DMA as $^1O_2$ trap since it is effective in the cell environment, and 1,4-diazabicyclo[2.2.2]octane (DABCO) as quencher since it has been reported to be effective in a non-aqueous environment[41]. DABCO also allows access to a relevant potential range between ~2.0 and 3.6 V, and is stable with superoxide (Supplementary Figs 10 and 11).

Li–O_2 cells with porous carbon black electrodes were constructed as described in the Methods. Three electrolytes were used: 0.1 M $LiClO_4$ in TEGDME that either contained no additive, 30 mM DMA, or 10 mM DABCO. Cycling was carried out at constant current in an O_2 atmosphere. Cells were cycled to various discharge and charge capacities, then stopped and subjected to further analysis. A typical load curve is shown in Fig. 4a. As DABCO is oxidized at ~3.6 V, cells containing this additive were recharged only to 3.5 V, and then held there until the first recharge capacity was reached.

To quantify the amount of carbonaceous side products (Li_2CO_3 and Li carboxylates) formed at each stage of discharge and charge, the electrodes were analysed with a previously established procedure[25]. It involves treating the washed electrodes with acid to decompose the Li_2CO_3 present, followed by treatment with Fenton's reagent to oxidize the Li carboxylates. The evolved CO_2 was quantified by mass spectrometry, and the results are presented in Fig. 4b. DMA as a $^1O_2$ trap is consumed and forms the corresponding endoperoxide DMA–O_2. We take advantage of this feature for quantifying the $^1O_2$ present in the cell by measuring the conversion of DMA to DMA–O_2 by means of HPLC (Fig. 4c and Supplementary Fig. 12). Here we use 30 mM DMA in the electrolyte, which is close to saturation and ~2,000 times the concentration used in the fluorescence experiments. It can therefore be expected that a large fraction of any $^1O_2$ present, albeit not necessarily all, will react with the DMA instead of other cell components. At the same time, DMA becomes a significantly more sensitive probe for $^1O_2$ than as used for fluorescence.

Considering the cell without additive, there is continuous growth of the amount of side products with increasing discharge capacity. The amount further increases to the sampling point at one-third recharge, and then vanishes nearly completely towards full recharge. This is in accord with previous investigations on the build-up and removal of the side products during cycling[15,24,25]. It was shown that, on discharge, side products originate predominantly from the electrolyte. At early stages of charge, the electrolyte further decomposes to solid products, accompanied by Li_2CO_3 from the carbon electrode[24,25]. As charge continues to higher voltages, carbon decomposition becomes more significant, and carbon and electrolyte decomposition go along with CO_2 evolution from already present parasitic products. So far it was reasoned that side products during discharge stem from the reactivity of cell components with the superoxide intermediate or Li_2O_2 (refs 3,11,14,20–24,27). It is worth noting that carbon is considered stable on oxidation well beyond 4 V in the absence of Li_2O_2, and so is the ethereal electrolyte[15,21,25]. Carbon corrosion and electrolyte decomposition at lower charging voltages were therefore tentatively associated with

© 2017 Macmillan Publishers Limited, part of Springer Nature. All rights reserved.

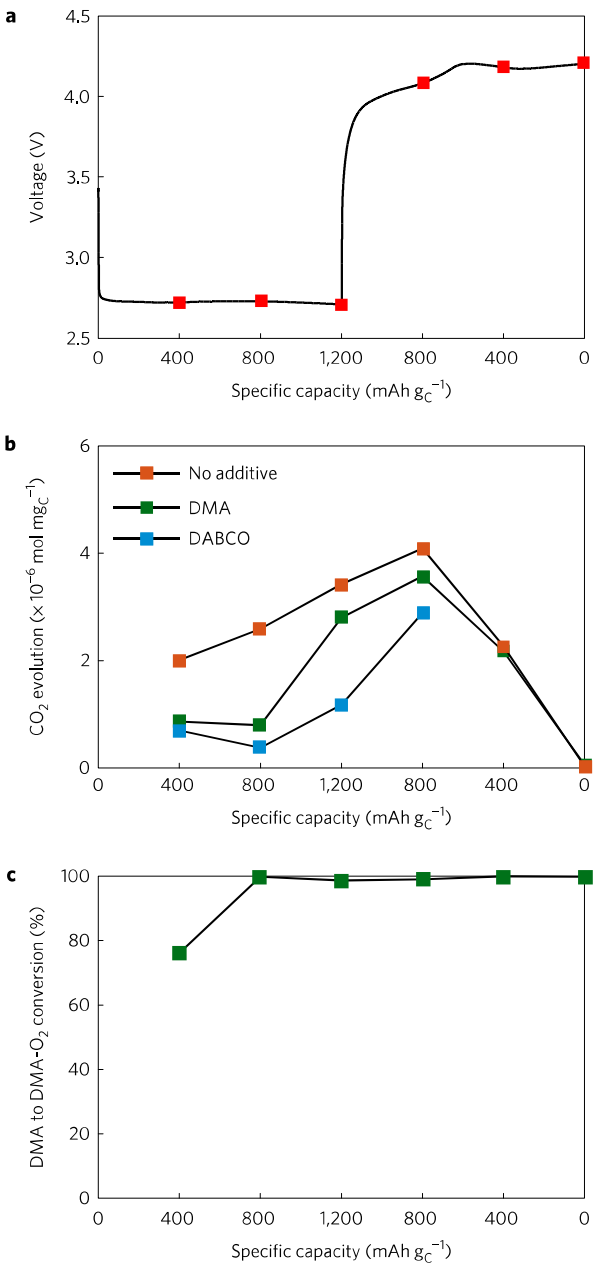

Figure 4 | *Ex situ* analysis of Li–O_2 cathodes run with electrolytes without or with $^1O_2$ trap DMA or quencher DABCO. a, Representative voltage profile during galvanostatic discharge and charge of a porous carbon black electrode at 70 mA g_C^{-1} in O_2-saturated 0.1 M $LiClO_4$ in TEGDME containing either no additive, 30 mM DMA, or 10 mM DABCO. Cells were stopped and analysed at the capacities indicated by the red squares. **b**, Amount of carbonaceous side reaction products per mg carbon. **c**, Fraction of the initial DMA that has reacted to DMA-O_2 via the reaction with $^1O_2$ in the cells that contained DMA as additive.

intermediates of Li_2O_2 oxidation[23,25]. Our operando fluorescence results show that recharging the cell forms $^1O_2$ from the very start of charging, and that it is responsible for at least part of the carbon and electrolyte decomposition from the start of charge.

Turning to the cells with $^1O_2$ trap or quencher, a significant reduction of side products during discharge is evident for both additives (Fig. 4b). Considering first the cell with DMA, the side products amount to between a half and a third of those without additive up to the second sampling point. Thereafter, the side products grow close to the level without the DMA. This can be explained considering the conversion of DMA to DMA–O_2 (Fig. 4c). At the first sampling point, 76% of the initially present DMA was consumed, and it was fully consumed at the second point. Thereafter, no effect on side product formation can be expected, as is seen in the carbonate/carboxylate data (Fig. 4b). By considering the charge passed at the first sampling point and the DMA conversion, a ratio of ~1 mol DMA consumed per 10 mol of O_2 reduced can be determined.

Turning to the cells with DABCO as quencher, side products amount to consistently less than in the case of DMA additive and to 10 to 30% of the additive-free case on discharge (Fig. 4b). From these values, we can estimate the fraction of parasitic products on discharge originating from $^1O_2$ to be at least 70%. DABCO is also effective upon charging, and significantly reduces the side products at the first sampling point on charge. We assume the reason for the lower efficiency on charging to be the much higher $^1O_2$ generation on charge than on discharge, as we have shown above with operando fluorescence. With DABCO we could, however, not recharge the cell fully due to the electrochemical stability limit of 3.5V (Supplementary Fig. 10). Quenchers need to be efficient in the cell environment, electrochemically stable and inert in contact with superoxide and Li_2O_2. These conditions are also the ones distinguishing quenchers required for the Li–O_2 cell from previous uses of quenchers[32].

To prove the effective $^1O_2$ removal by the trap over an entire cycle and to estimate the fraction of the parasitic products during charge that originates from $^1O_2$, we performed operando electrochemical mass spectrometry (OEMS) experiments with cells containing either no additive or 30 mM DMA. Figure 4c has shown that at a discharge capacity of 400 mA g_C^{-1} ~75% of the DMA had been converted to DMA–O_2. Therefore the mass spectrometry cells were discharged to only 200 mAh g_C^{-1} to ensure that most of the DMA was still present at the end of discharge and could act on charge. The results for charge are shown in Fig. 5 and the full data in Supplementary Figs 13 and 14. During discharge the e^-/O_2 ratio is close to the theoretical value of two, with the ratio being closer with DMA (2.01 e^-/O_2) than without (2.11 e^-/O_2).

With the DMA additive the recharge voltage is lower throughout than without DMA. With DMA the O_2 evolution reaches ~93% of the theoretical value at the beginning, and fades to ~2/3 towards the end of charge. Without DMA the O_2 evolution is significantly lower throughout charging, and reaches a maximum of 2/3 of the theoretical value. An even stronger difference is seen in the CO_2 evolution. Significant CO_2 evolution without DMA is contrasted by a 30-fold reduced CO_2 amount with DMA (based on the integral peak area in Supplementary Fig. 14b,f). The strong reduction of the CO_2 amount in combination with the observed O_2 evolution suggests that the majority of the parasitic products that form during charge at voltages below the oxidative stability limit of electrolyte and carbon are due to the occurrence of $^1O_2$. A more detailed discussion for this assignment is given in the Supplementary Discussion in the Supplementary Information. Taken together, the trap and quencher experiments contribute more evidence that $^1O_2$ is responsible for the majority of side products upon discharge and charge, and that suitable additives can effectively reduce side reactions. The required oxidation stability of such additives can be reduced by using redox mediators that greatly reduce the charging voltage[8,42,43].

Pathways to singlet oxygen

The results are consistent with $^1O_2$ being to a large part responsible for commonly reported observations about the O_2 balance and side products. First, on discharge the e^-/O_2 ratio is typically found within several per cent of the ideal value of two despite significant amounts of side products such as Li_2CO_3, Li formate and Li acetate with Li_2O_2 yields reported below 90% (refs 24–26). Second, on charge the

© 2017 Macmillan Publishers Limited, part of Springer Nature. All rights reserved.

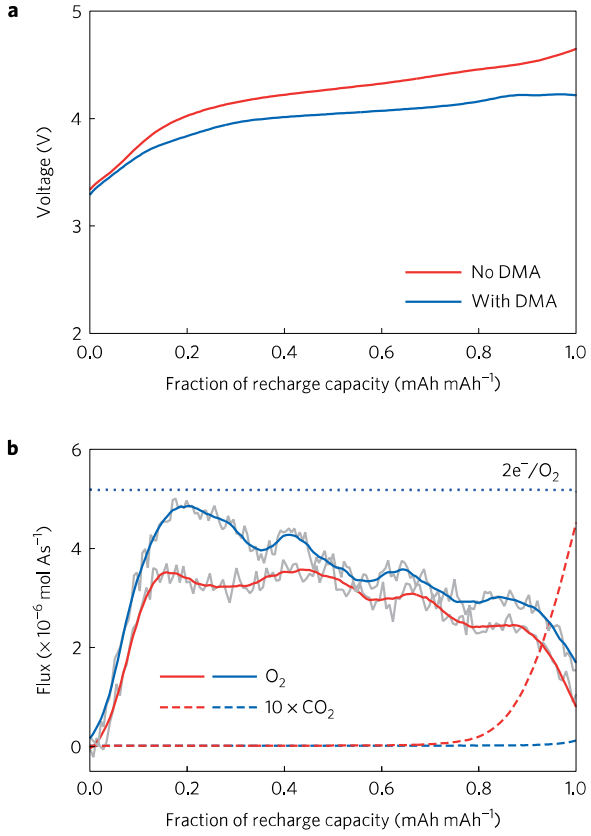

Figure 5 | Operando electrochemical mass spectrometry of Li–O_2 cathodes run with electrolytes containing either no additive or the $^1O_2$ trap DMA. a,b, Voltage profiles (**a**) and fluxes of O_2, e^- and CO_2 (**b**) during galvanostatic charge after the cells have been discharged to 200 mAh g_C^{-1}. The porous carbon black electrodes were run at 100 mA g_C^{-1} in 0.1 M $LiClO_4$ in TEGDME containing either no additive or 30 mM DMA. The grey traces in **b** represent the measurements and the blue and red traces the moving average to guide the eye.

e^-/O_2 ratio typically deviates significantly by more than 10% from the ideal value of two from the start, with the deviation increasing as charging progresses[24]. This deviation goes along with the formation of more of the mentioned solid side products until the charging voltage is sufficiently high to oxidize them to release CO_2 and other fragments[15,25,26]. So far the formation of these products could not be consistently explained by the reactivity of the known reactive species superoxide and peroxide alone[14,23–25]. The previous hypothesis that $^1O_2$ can form by charging Li_2O_2 via $Li_2O_2 \rightarrow O_2 + 2Li^+ + 2e^-$ at voltages exceeding 3.5 to 3.9 V has only recently been verified, with small quantities forming between 3.55 and 3.75 V (refs 11,23,28). The formation of $^1O_2$ on discharge and on charge below 3.5 V was, however, neither suggested on theoretical grounds nor shown experimentally before.

On discharge one possible source of $^1O_2$ is the disproportionation of LiO_2 according to

$$2LiO_2 \rightarrow (LiO_2)_2 \rightarrow Li_2O_2 + {}^1O_2 \quad (1)$$

This pathway via a $(LiO_2)_2$ dimer appears plausible when the structures and energies of some of these dimers as calculated by Bryantsev *et al.* are considered[44]. They found low lying isomers in both the triplet and singlet state. They have given reaction-free energies for the disproportionation reaction via the lowest triplet dimer to yield $^3O_2$, and it is reasonable to assume that the reaction proceeding via a singlet dimer will yield $^1O_2$. When H_2O or other proton sources are available the superoxide will be protonated to form $HOO^\bullet$, which has been reported to either undergo reduction by superoxide or disproportionate and to be able to release in either case $^1O_2$ in the overall reaction, which is more detailed in the Supplementary Discussion[37,45]:

$$2O_2^- + 2H^+ \rightarrow H_2O_2 + {}^1O_2 \quad (2)$$

Overall we propose the disproportionation of superoxide in the presence of either Li^+ or H^+ as the $^1O_2$ source on discharge. On charge we suggest three possible pathways. First, we suggest an analogous path to the one on discharge involving disproportionation of superoxide in the presence of either Li^+ or H^+. It has been suggested that the first step of charging Li_2O_2 involves a deintercalation at the surface to form LiO_2-like surface species ($Li_2O_2 \rightarrow LiO_2 + Li^+ + e^-$) that further disproportionate to evolve O_2 in an overall $2e^-/O_2$ process[46–48]. Here $^1O_2$ may form analogously to equation (1). Similarly, $^1O_2$ may form from proton sources (such as H_2O) reacting with the LiO_2-like surfaces according to equation (2). This pathway for $^1O_2$ formation can be active from the onset of charge as soon as Li^+ and e^- are extracted. Second, a further $1e^-$ oxidation of the surface LiO_2 species ($LiO_2 \rightarrow O_2 + Li^+ + e^-$) could give $^1O_2$ in an overall $2e^-/O_2$ process. Thermodynamically, $^1O_2$ formation from electrochemical oxidation of superoxide is possible above $E^0_{O_2/LiO_2} + E(^1\Delta_g \leftarrow {}^3\Sigma_g^-)$. The thermodynamic equilibrium potential $E^0_{O_2/LiO_2}$ was estimated to be between 2.29 and 2.46 V (refs 9,47,49). With an energy difference of ~1 eV between $^1O_2$ and $^3O_2$, a thermodynamic voltage for $^1O_2$ evolution of 3.26 to 3.43 V can be estimated. Finally, above ~3.55 V the known pathway sets in, as suggested before by Scrosati *et al.* and shown by Gasteiger *et al.*, with $^1O_2$ evolving from electrochemical oxidation of Li_2O_2 in a $2e^-/O_2$ process ($Li_2O_2 \rightarrow O_2 + 2Li^+ + 2e^-$). Note that superoxide is both a proficient source and efficient quencher of $^1O_2$ via equation (3)[50]:

$$O_2^- + {}^1O_2 \rightarrow {}^3O_2 + O_2^- \quad (3)$$

We therefore believe that our observation of less $^1O_2$ on discharge and more on charge in the ether electrolyte results at least in part from the differing abundance of superoxide that can reduce the $^1O_2$ lifetime by quenching, which counteracts equally superoxide-concentration-driven formation. More precisely, net formation of $^1O_2$ will depend on the relative kinetics of all superoxide sources and sinks (with $^1O_2$ being involved in both) and not solely on the superoxide concentration. These sources and sinks are both electrochemical and chemical, and change with discharge and charge, electrolyte, current and potential. We thus further suggest that the current density and electrolyte properties will influence $^1O_2$ formation in much the same way it governs the occurrence of superoxide on discharge and charge below 3.5 V (refs 5,33). Further, charge current will drive $^1O_2$ production if it causes charging voltages above 3.5 V.

Conclusions

By combining complementary methods we could give evidence that $^1O_2$ forms in the Li–O_2 battery during discharge and from the onset of charge, and that it can account for a major fraction of the side products formed. Hence, $^1O_2$ arises as perhaps the biggest obstacle for cycling of the Li–O_2 cell by reversible formation/decomposition of Li_2O_2. Presence of trace water, which was already known to increase side reactions, acts at least in part by raising the amount of $^1O_2$ generated. We show that $^1O_2$ traps and quenchers can effectively reduce the side reactions on discharge and charge. The level of $^1O_2$ abundance makes traps less likely to be effective for long-term cycling since they will be consumed rapidly. Physical quenchers are preferred since they are not consumed. Future work

© 2017 Macmillan Publishers Limited, part of Springer Nature. All rights reserved.

should therefore focus on finding quenchers that are entirely compatible with the cell environment, with the electrochemical potential window, compatibility, and stability against superoxide and peroxide being the most prominent requirements. Equally it needs to be compatible with anodes such as possibly protected Li metal. Alkaline superoxides in the cycling mechanism suggest that the Na–O_2 and K–O_2 systems would merit investigating whether $^1O_2$ is involved.

Methods

Materials. Ethylene glycol dimethyl ether (DME, >99.0%), 9,10-dimethylanthracene (DMA, >98.0%) and 9,10-diphenylanthracene (DPA, >98.0%) were purchased from TCI Europe. Tetraethylene glycol dimethyl ether (TEGDME, ≥99%), d_3-acetonitrile (≥99.8 at.%), $LiClO_4$ (battery grade, dry, 99.99%), 1,4-diazabicyclo[2.2.2]octane (DABCO, ≥99%) and H_2O (HPLC grade) were purchased from Sigma-Aldrich. APCI/APPI tuning mix was purchased from Agilent Technologies. Formic acid was bought from Fluka Analytical (puriss. p.a. ~98%). Acetonitrile (HiPerSolv Prolabo) was purchased from VWR Chemicals. High-purity oxygen (O_2 3.5, >99.95 vol%), high-purity Ar (Ar 5.0, >99.999 vol%) and a mixture of Ar 6.0 and O_2 5.5 (Ar ~5 vol%) were purchased from Messer Austria. Moisture content of the solvents and electrolytes was measured by Karl Fischer titration using a TitroLine KF trace (Schott). Solvents were purified by distillation and further dried over activated molecular sieves. $LiClO_4$ was dried under vacuum for 24 h at 160 °C. All chemicals were used without any further purification, except for DABCO, which was purified by recrystallization from absolute diethyl ether. The sensitizer palladium(II) *meso*-tetra(4-fluorophenyl)tetrabenzoporphyrin was synthesized according a previously reported procedure[51]. Li_2O_2 was synthesized according to a previously reported procedure[25].

Operando and *ex situ* electrochemical methods and analysis. Carbon cathodes were fabricated by first making a slurry of Super P carbon (TIMCAL) with polytetrafluoroethylene (PTFE) binder in the ratio 9:1 (m/m) using isopropanol. The slurry was then coated onto a stainless steel mesh current collector. The electrodes were vacuum dried at 200 °C for 24 h and then transferred to an Ar-filled glove box without exposure to air. The glass fibre separators were washed with ethanol and dried overnight at 200 °C under vacuum prior to use. The $LiFePO_4$ counter electrodes were made by mixing partially delithiated active material with Super P and PTFE in the ratio 8:1:1(m/m/m). The electrodes were vacuum dried at 200 °C for 24 h. The counter electrodes had three times the expected capacity of the positive electrode. The electrochemical cells used to investigate cycling were based on a Swagelok design. Typical working electrodes had a carbon mass loading of 1 mg and the cells were assembled with 70 μl electrolyte.

Electrochemical tests were run on either a SP-300 (BioLogic) or BT-2000 (Arbin Instruments) potentiostat/galvanostat. Cyclic voltammograms were recorded in a three-electrode arrangement with a glassy carbon disc working electrode (BAS), a Ag wire pseudo-reference and a Pt wire counter electrode inside a glass cell with a PTFE lid. The cells were run inside an Ar-filled glovebox and purged with high-purity Ar or O_2. The redox system Fc/Fc^+ was used to reference the measured data versus the Li/Li^+ scale.

UV–Vis absorption spectra were recorded on a UV–Vis spectrophotometer Cary 50 (Varian). The molar absorption coefficient of DMA was determined as an average of three independent measurements. Photochemical generation of $^1O_2$ was done by *in situ* photogeneration with the sensitizer palladium(II) *meso*-tetra(4-fluorophenyl)tetrabenzoporphyrin[51]. The sensitizer in the O_2-saturated solution was irradiated with a red light-emitting diode light source (643 nm, 7 W).

Fluorescence measurements were recorded on a Fluorolog 3 fluorescence spectrometer (Horiba) equipped with a NIR-sensitive photomultiplier R2658 (300–1,050 nm) from Hamamatsu. The operando fluorescence measurements were performed in the front face mode in kinetic acquisition mode with 0.1 s excitation every 10 s to minimize photobleaching of the DMA. The fluorophore concentration was adjusted to attain an absorbance of ~0.2 to avoid inner filter effects and to achieve good correlation between the observed fluorescence intensity (proportional to the amount of the absorbed light) and absorption (proportional to the concentration) of the $^1O_2$ trap. DMA was excited at 378 nm and the emission was detected at 425 nm. The cell for operando fluorescence was a 1 cm absorption high-precision quartz cell (Hellma Analytics) with a purpose-made gas-tight PTFE lid. The working electrode was composed of a Super P/PTFE mixture that was pasted onto a Ti grid. The electrode pre-filled with chemically synthesized Li_2O_2 was made by mixing the dried electrode material with Li_2O_2 and pressing the mixture onto the Ti grid. The reference and counter electrodes were partly delithiated $LiFePO_4$ pasted onto Al grids. The assembling was performed in an Ar-filled glovebox. The cell contained a magnetic stirrer bar, was filled with electrolyte, streamed with O_2, further connected with a pure O_2 reservoir and hermetically sealed before placing it into the spectrometer. During the measurement the electrolyte was stirred to ensure O_2 saturation and uniform DMA concentration. The DMA concentration of 1.6×10^{-5} M for the operando fluorescence was chosen to optimize the sensitivity of the method. At an absorbance of $A = 0.2$ (measurement conditions), 37% of the excitation light is absorbed by the chromophore ($=1-10^{-A}$). In a hypothetical example, reaction of 10% of DMA with $^1O_2$ will decrease absorbance by 10%—that is, from 0.2 to 0.18. Thus, after the reaction 34% of the excitation light will be absorbed by the chromophore. Since the fluorescence intensity is proportional to the amount of the absorbed light, the decrease of fluorescence intensity will be $(37 - 34)/37 \times 100 = 8\%$. Analogous calculation with ten times the DMA concentration ($A = 2$) results in 99% of excitation light absorbed before bleaching and 98.4% of the excitation light absorbed after bleaching. Thus, the decrease of fluorescence intensity would be $(99 - 98.4)/99 \times 100 = 0.6\%$, which is much lower than for the comparably low concentration of the trap. Therefore, a relatively low concentration of DMA is essential for the best sensitivity of operando fluorescence.

Operando NIR spectroscopy to detect the emission of singlet oxygen was performed using a germanium detector (model 261, UDT Instruments, Gamma Scientific Company). It was cooled to −30 °C using a Peltier cooling unit. A longpass-filter with a cut-on wavelength of 1,200 nm and a shortpass-filter with a cutoff wavelength of 1,350 nm (Edmund Optics) were placed directly in front of the sensor. The cell for operando NIR spectroscopy was a 1 mm absorption high precision quartz cell (Hellma Analytics) with a purpose-made gas-tight PTFE lid. The working electrode was an Au-grid electrode (ALS). The reference and counter electrodes were partly delithiated $LiFePO_4$ attached to an Al grid. The cell was placed directly in front of the filters followed by an Au mirror. The optical set-up containing the measurement cell was located in a blackbox to avoid ingress of stray light. The detector signal was amplified by a photodiode amplifier PDA-750 (Terahertz Technologies) and the signal recorded on the potentiostat which controlled the cell.

The operando electrochemical mass spectrometry set-up was built in-house and is similar to the one described previously[52,53]. It consisted of a commercial quadrupole mass spectrometer (Balzers) with a turbomolecular pump (Pfeiffer) that is backed by a membrane pump and leak inlet which samples from the purge gas stream. The electrochemical cell was based on a three-electrode Swagelok design. The set-up was calibrated for different gases (Ar, O_2, CO_2, H_2, N_2 and H_2O) using calibration mixtures in steps over the anticipated concentration ranges to capture nonlinearity and cross-sensitivity. During measurements either a gas mixture consisting of 95% O_2 and 5% Ar or pure Ar was used. All calibrations and quantifications were performed using in-house software. The purge gas system consisted of a digital mass flow controller (Bronkhorst) and stainless steel tubing. The procedure for the carbonate/carboxylate analysis was as described earlier[25].

High-performance liquid chromatography coupled with mass spectrometry (HPLC–MS) was used for determining the degree of the DMA to DMA–O_2 conversion. The sample handling was performed inside an Ar-filled glovebox. The electrolyte was extracted from the cell using DME that was then removed by evaporation at room temperature. The residue was dissolved in 50 μl DME and a volume of 1 μl was injected into the HPLC. The HPLC instrument was a 1200 Series (Agilent Technology) with a multiple wavelength UV–Vis detector (Agilent Technology G1365C MWD SL) coupled to a mass spectrometer using atmospheric pressure chemical ionization (APCI) as the ionization method (Agilent Technologies 6120 Quadrupole LC/MS). The samples were analysed by a reversed-phase Poroshell column (120 EC-C8, 3.0 mm × 100 mm, Ø 2.7 μm, Agilent Technology) using a gradient system of acetonitrile (solvent B) and water containing 0.01% formic acid (solvent A). A pre-column (UHPLC 3PK, Poroshell 120 EC-C8 3.0 × 5 mm 2.7 μm, Agilent Technology) was connected before the reversed-phase column. The elution started with 50% solvent B and was then increased to 100% solvent B within 5 min at a flow rate of 0.7 ml min^{-1}. The column was held at 15 °C throughout the measurements. The eluent was monitored via an UV–Vis detector at the wavelengths of 258 nm and 374 nm. The MS signal was recorded starting after 2 min in a mass range of 100–450 m/z using the APCI in the positive ion mode. The MS signal was used to identify the retention times for DMA and DMA–O_2. The extent of the transformation of 9,10-dimethylanthracene (DMA) to 9,10-dimethylanthracene-endoperoxide (DMA–O_2) was determined from the absorbance at 258 nm and the molar absorption coefficients $\varepsilon_{DMA,\,258\,nm}$ and $\varepsilon_{DMA-O_2,\,258\,nm}$. The latter was determined from DMA–O_2, which was obtained by conversion of DMA with photogenerated $^1O_2$.

Data availability. The data that support the plots within this paper and other findings of this study are available from the corresponding author upon reasonable request.

Received 29 July 2016; accepted 19 February 2017; published 20 March 2017

© 2017 Macmillan Publishers Limited, part of Springer Nature. All rights reserved.

References

1. Larcher, D. & Tarascon, J.-M. Towards greener and more sustainable batteries for electrical energy storage. *Nat. Chem.* **7**, 19–29 (2014).
2. Choi, J. W. & Aurbach, D. Promise and reality of post-lithium-ion batteries with high energy densities. *Nat. Rev. Mater.* **1**, 16013 (2016).
3. Luntz, A. C. & McCloskey, B. D. Nonaqueous Li–air batteries: a status report. *Chem. Rev.* **114**, 11721–11750 (2014).
4. Choi, N.-S. *et al.* Challenges facing lithium batteries and electrical double-layer capacitors. *Angew. Chem. Int. Ed.* **51**, 9994–10024 (2012).
5. Lu, Y.-C. *et al.* Lithium-oxygen batteries: bridging mechanistic understanding and battery performance. *Energy Environ. Sci.* **6**, 750–768 (2013).
6. Ren, X. & Wu, Y. A low-overpotential potassium–oxygen battery based on potassium superoxide. *J. Am. Chem. Soc.* **135**, 2923–2926 (2013).
7. Walker, W. *et al.* A rechargeable Li–O_2 battery using a lithium nitrate/N,N-dimethylacetamide electrolyte. *J. Am. Chem. Soc.* **135**, 2076–2079 (2013).
8. Lim, H.-D. *et al.* Rational design of redox mediators for advanced Li–O_2 batteries. *Nat. Energy* **1**, 16066 (2016).
9. Bender, C. L., Hartmann, P., Vračar, M., Adelhelm, P. & Janek, J. On the thermodynamics, the role of the carbon cathode, and the cycle life of the sodium superoxide (NaO_2) battery. *Adv. Energy Mater.* **4**, 1301863 (2014).
10. Laoire, C. O., Mukerjee, S., Plichta, E. J., Hendrickson, M. A. & Abraham, K. M. Rechargeable lithium/TEGDME-$LiPF_6$/O_2 battery. *J. Electrochem. Soc.* **158**, A302–A308 (2011).
11. Hassoun, J., Croce, F., Armand, M. & Scrosati, B. Investigation of the O_2 electrochemistry in a polymer electrolyte solid-state cell. *Angew. Chem. Int. Ed.* **50**, 2999–3002 (2011).
12. Younesi, R. *et al.* Ether based electrolyte, $LiB(CN)_4$ salt and binder degradation in the Li–O_2 battery studied by hard X-ray photoelectron spectroscopy (haxpes). *J. Phys. Chem. C* **116**, 18597–18604 (2012).
13. Amanchukwu, C. V., Harding, J. R., Shao-Horn, Y. & Hammond, P. T. Understanding the chemical stability of polymers for lithium-air batteries. *Chem. Mater.* **27**, 550–561 (2015).
14. Bryantsev, V. S. *et al.* The identification of stable solvents for nonaqueous rechargeable Li–air batteries. *J. Electrochem. Soc.* **160**, A160–A171 (2013).
15. Xu, W. *et al.* The stability of organic solvents and carbon electrode in nonaqueous Li–O_2 batteries. *J. Power Sources* **215**, 240–247 (2012).
16. Ottakam Thotiyl, M. M. *et al.* A stable cathode for the aprotic Li–O_2 battery. *Nat. Mater.* **12**, 1050–1056 (2013).
17. Adams, B. D. *et al.* Towards a stable organic electrolyte for the lithium oxygen battery. *Adv. Energy Mater.* **5**, 1400867 (2015).
18. Khetan, A., Luntz, A. & Viswanathan, V. Trade-offs in capacity and rechargeability in nonaqueous Li–O_2 batteries: solution-driven growth versus nucleophilic stability. *J. Phys. Chem. Lett.* **6**, 1254–1259 (2015).
19. Aetukuri, N. B. *et al.* Solvating additives drive solution-mediated electrochemistry and enhance toroid growth in non-aqueous Li–O_2 batteries. *Nat. Chem.* **7**, 50–56 (2015).
20. Black, R. *et al.* Screening for superoxide reactivity in Li–O_2 batteries: effect on Li_2O_2/LiOH crystallization. *J. Am. Chem. Soc.* **134**, 2902–2905 (2012).
21. McCloskey, B. D. *et al.* Twin problems of interfacial carbonate formation in nonaqueous Li–O_2 batteries. *J. Phys. Chem. Lett.* **3**, 997–1001 (2012).
22. Younesi, R., Hahlin, M., Björefors, F., Johansson, P. & Edström, K. Li–O_2 battery degradation by lithium peroxide (Li_2O_2): a model study. *Chem. Mater.* **25**, 77–84 (2012).
23. McCloskey, B. D. *et al.* Limitations in rechargeability of Li–O_2 batteries and possible origins. *J. Phys. Chem. Lett.* **3**, 3043–3047 (2012).
24. McCloskey, B. D. *et al.* Combining accurate O_2 and Li_2O_2 assays to separate discharge and charge stability limitations in nonaqueous Li–O_2 batteries. *J. Phys. Chem. Lett.* **4**, 2989–2993 (2013).
25. Ottakam Thotiyl, M. M., Freunberger, S. A., Peng, Z. & Bruce, P. G. The carbon electrode in nonaqueous Li–O_2 cells. *J. Am. Chem. Soc.* **135**, 494–500 (2013).
26. Freunberger, S. A. *et al.* The lithium–oxygen battery with ether-based electrolytes. *Angew. Chem. Int. Ed.* **50**, 8609–8613 (2011).
27. Carboni, M., Marrani, A. G., Spezia, R. & Brutti, S. 1,2-dimethoxyethane degradation thermodynamics in Li–O_2 redox environments. *Chem. Eur. J.* **22**, 17188–17203 (2016).
28. Wandt, J., Jakes, P., Granwehr, J., Gasteiger, H. A. & Eichel, R.-A. Singlet oxygen formation during the charging process of an aprotic lithium–oxygen battery. *Angew. Chem. Int. Ed.* **55**, 6892–6895 (2016).
29. Alfano, A. J. & Christe, K. O. Singlet delta oxygen production from a gas–solid reaction. *Angew. Chem. Int. Ed.* **41**, 3252–3254 (2002).
30. Li, Q. *et al.* A spectroscopic study on singlet oxygen production from different reaction paths using solid inorganic peroxides as starting materials. *Bull. Korean Chem. Soc.* **28**, 1656–1660 (2007).
31. Schweitzer, C. & Schmidt, R. Physical mechanisms of generation and deactivation of singlet oxygen. *Chem. Rev.* **103**, 1685–1758 (2003).
32. Ogilby, P. R. Singlet oxygen: there is indeed something new under the sun. *Chem. Soc. Rev.* **39**, 3181–3209 (2010).
33. Aurbach, D., McCloskey, B. D., Nazar, L. F. & Bruce, P. G. Advances in understanding mechanisms underpinning lithium–air batteries. *Nat. Energy* **1**, 16128 (2016).
34. Bryantsev, V. S. *et al.* Predicting solvent stability in aprotic electrolyte Li–air batteries: nucleophilic substitution by the superoxide anion radical ($O_2^{\cdot -}$). *J. Phys. Chem. A* **115**, 12399–12409 (2011).
35. Bryantsev, V. S. & Blanco, M. Computational study of the mechanisms of superoxide-induced decomposition of organic carbonate-based electrolytes. *J. Phys. Chem. Lett.* **2**, 379–383 (2011).
36. Bryantsev, V. S. & Faglioni, F. Predicting autoxidation stability of ether- and amide-based electrolyte solvents for Li–air batteries. *J. Phys. Chem. A* **116**, 7128–7138 (2012).
37. Khan, A. U. Direct spectral evidence of the generation of singlet molecular oxygen (1.Delta.g) in the reaction of potassium superoxide with water. *J. Am. Chem. Soc.* **103**, 6516–6517 (1981).
38. Umezawa, N. *et al.* Novel fluorescent probes for singlet oxygen. *Angew. Chem. Int. Ed.* **38**, 2899–2901 (1999).
39. Miyamoto, S., Martinez, G. R., Medeiros, M. H. G. & Di Mascio, P. Singlet molecular oxygen generated from lipid hydroperoxides by the russell mechanism: studies using ^{18}O-labeled linoleic acid hydroperoxide and monomol light emission measurements. *J. Am. Chem. Soc.* **125**, 6172–6179 (2003).
40. Young, R. H. & Brewer, D. R. in *Singlet Oxygen. Reactions with Organic Compounds Polymers* (eds Ranby, B. & Rabek, J. F.) (Wiley, 1978).
41. Enko, B. *et al.* Singlet oxygen-induced photodegradation of the polymers and dyes in optical sensing materials and the effect of stabilizers on these processes. *J. Phys. Chem. A* **117**, 8873–8882 (2013).
42. Chase, G. V. *et al.* Soluble oxygen evolving catalysts for rechargeable metal-air batteries. US patent 13/093,759 (2011).
43. Chen, Y., Freunberger, S. A., Peng, Z., Fontaine, O. & Bruce, P. G. Charging a Li–O_2 battery using a redox mediator. *Nat. Chem.* **5**, 489–494 (2013).
44. Bryantsev, V. S., Blanco, M. & Faglioni, F. Stability of lithium superoxide LiO_2 in the gas phase: computational study of dimerization and disproportionation reactions. *J. Phys. Chem. A* **114**, 8165–8169 (2010).
45. Koppenol, W. H. Reactions involving singlet oxygen and the superoxide anion. *Nature* **262**, 420–421 (1976).
46. Hummelshoj, J. S., Luntz, A. C. & Norskov, J. K. Theoretical evidence for low kinetic overpotentials in Li–O_2 electrochemistry. *J. Chem. Phys.* **138**, 034703 (2013).
47. Kang, S., Mo, Y., Ong, S. P. & Ceder, G. A facile mechanism for recharging Li_2O_2 in Li–O_2 batteries. *Chem. Mater.* **25**, 3328–3336 (2013).
48. Mo, Y., Ong, S. P. & Ceder, G. First-principles study of the oxygen evolution reaction of lithium peroxide in the lithium-air battery. *Phys. Rev. B* **84**, 205446 (2011).
49. Snow, R. H. *Thermodynamic Evaluation of the Possibility of Lithium Superoxide Production* (Aerospace Medical Research Laboratories, 1965).
50. Khan, A. U. Activated oxygen: singlet molecular oxygen and superoxide anion. *Photochem. Photobiol.* **28**, 615–626 (1978).
51. Borisov, S. M. *et al.* New NIR-emitting complexes of platinum(II) and palladium(II) with fluorinated benzoporphyrins. *J. Photochem. Photobiol. A* **201**, 128–135 (2009).
52. Chen, Y., Freunberger, S. A., Peng, Z., Bardé, F. & Bruce, P. G. Li–O_2 battery with a dimethylformamide electrolyte. *J. Am. Chem. Soc.* **134**, 7952–7957 (2012).
53. Peng, Z., Freunberger, S. A., Chen, Y. & Bruce, P. G. A reversible and higher-rate Li–O_2 battery. *Science* **337**, 563–566 (2012).

Acknowledgements

S.A.F. is indebted to the European Research Council (ERC) under the European Union's Horizon 2020 research and innovation programme (grant agreement no. 636069). We further gratefully acknowledge funding from the Austrian Federal Ministry of Economy, Family and Youth and the Austrian National Foundation for Research, Technology and Development and initial funding from the Austrian Science Fund (FWF, Project No. P26870-N19). The authors thank R. Saf for help with the MS, R. Breinbauer for discussions about the reaction mechanism, S. Landgraf for help with the NIR measurement, and J. Schlegl for manufacturing instrumentation for the methods used.

Author contributions

N.M. performed the main part of the experiments and analysed the results. B.S., S.G. and C.L. performed cell cycling, MS and NMR experiments. G.A.S. did HPLC analysis. S.A.F., D.K., C.S., O.F. and M.L. discussed the reaction mechanisms. S.M.B. supervised the optical experiments. S.A.F. conceived and directed the research, set up and performed experiments, analysed the results and wrote the manuscript with help of the other authors. All authors contributed to the discussion and interpretation of the results.

Additional information

Supplementary information is available for this paper.

© 2017 Macmillan Publishers Limited, part of Springer Nature. All rights reserved.

Reprints and permissions information is available at www.nature.com/reprints.

Correspondence and requests for materials should be addressed to S.A.F.

How to cite this article: Mahne, N. *et al.* Singlet oxygen generation as a major cause for parasitic reactions during cycling of aprotic lithium–oxygen batteries. *Nat. Energy* **2**, 17036 (2017).

Publisher's note: Springer Nature remains neutral with regard to jurisdictional claims in published maps and institutional affiliations.

Competing interests

The authors declare no competing financial interests.

© 2017 Macmillan Publishers Limited, part of Springer Nature. All rights reserved.

5.1. Novel $^1O_2$ Quenchers with High Electrochemical Oxidation Stability

The search for new quenchers was motivated by two major requirements. First, we wanted to find quenchers which are compatible with the voltage window of Li-O_2 batteries between 2 V and ~4 V *vs* Li/Li^+. Currently known quenchers such as 1,4-diazabicyclo[2.2.2]octan (DABCO) or azides are only oxidation stable to ~3.6 V and do in the most cases not allow for full recharge of the cell. Quenchers form temporary charge transfer complexes with $^1O_2$ and release $^3O_2$ and release thermal energy but leave the quencher unchanged. To be effective, electron-rich moieties are needed to interact with the electrophile $^1O_2$. This requirement creates a conflict of interest because high quenching efficiency demands high electron density which reduces the oxidation stability. Literature reports as effective physical $^1O_2$ quencher molecules containing a diethylamino moiety. DABCO (**34**) is one of the best known quenchers, but has too low oxidation stability.[42] In the course of this thesis several molecules with diethylamino moieties were synthesized. Due to the low electrochemical stability of DABCO, one attempt to enhance the electrochemical stability was by alkylation. This direction was motivated by work of FORSYTH *et al.* who reported oxidation stability up to ~5 V *vs* Li/Li^+ for alkyl-DABCOnium ionic liquid. Alkylated DABCO (**35a-c**) molecules with different chain length were synthesized within a 2-step synthesis. Also N^1,$N^{1'}$-(butane-1,4-diyl)bis(N^1-(2-(diethylamino)ethyl)-N^2,N^2-diethylethane-1,2-diamine) (BuDiBiDi) (**36a**) and N^1,$N^{1'}$-(hexane-1,6-diyl)bis(N^1-(2-(diethylamino)ethyl)-N^2,N^2-diethylethane-1,2-diamine) (HexDiBiDi) (**36b**) were proper candidates for physical $^1O_2$ quencher, because they contain 6 quenching moieties (Figure 5.1).

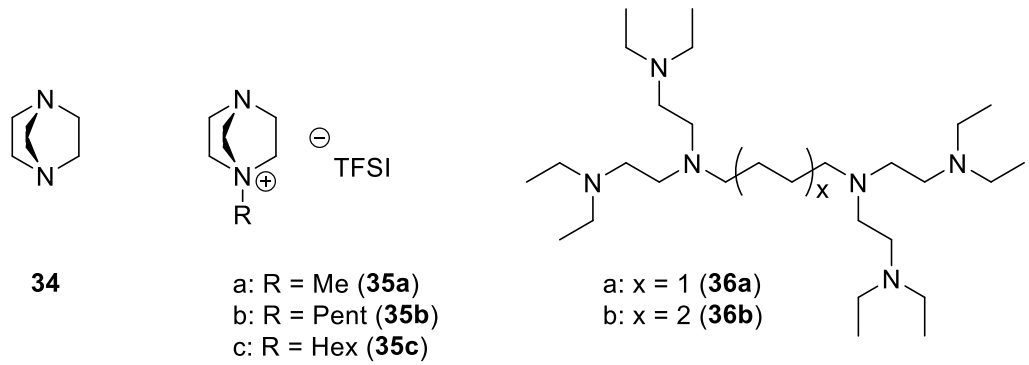

Figure 5.1: Physical $^1O_2$ quencher: DABCO (**34**), 1-methyl-1,4-diazabicyclo[2.2.2]octan-1-ium bis(trifluoromethane)sulfonimide (methyl-DABCO$^+$ TFSI$^-$) (**35a**), 1-pentyl-1,4-diazabicyclo[2.2.2]octan-1-ium bis(trifluoromethane)sulfonimide (pentyl-DABCO$^+$ TFSI$^-$) (**35b**), 1-hentyl-1,4-diazabicyclo[2.2.2]octan-1-ium bis(trifluoromethane)sulfonimide (hexyl-DABCO$^+$ TFSI$^-$(**35c**), N^1,$N^{1'}$-(butane-1,4-diyl)bis(N^1-(2-(diethylamino)-ethyl)-N^2,N^2-diethylethane-1,2-diamine) (BuDiBiDi) (**36a**) and N^1,$N^{1'}$-(hexane-1,6-diyl)bis(N^1-(2-(diethylamino)-ethyl)-N^2,N^2-diethylethane-1,2-diamine) (HexDiBiDi) (**36b**).

5.1.1. Preparation of 1-methyl-1,4-diazabicyclo[2.2.2]octan-1-ium bis(trifluoro-methane)sulfonimide (methyl-DABCO$^+$ TFSI$^-$) (**35a**), 1-pentyl-1,4-diazabicyclo[2.2.2]octan-1-ium bis(trifluoro-methane)sulfonimide (pentyl-DABCO$^+$ TFSI$^-$) (**35b**) and 1-hentyl-1,4-diazabicyclo[2.2.2]octan-1-ium bis(trifluoromethane)sulfonimide (hexyl-DABCO$^+$ TFSI$^-$) (**35c**)

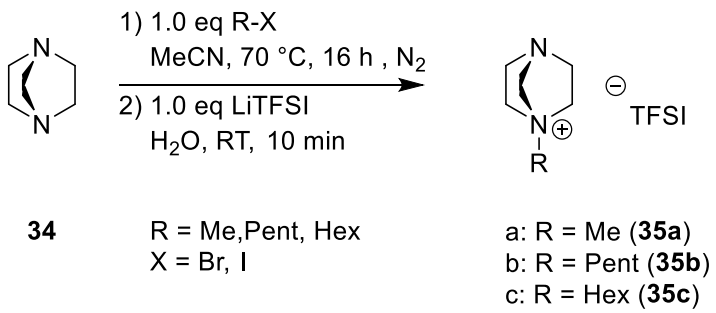

Scheme 5.2 Preparation of 1-methyl-1,4-diazabicyclo[2.2.2]octan-1-ium bis(trifluoromethane)sulfonimide (methyl-DABCO$^+$ TFSI$^-$) (**35a**), 1-pentyl-1,4-diazabicyclo[2.2.2]octan-1-ium bis(trifluoromethane)sulfonimide (pentyl-DABCO$^+$ TFSI$^-$) (**35b**) and 1-hentyl-1,4-diazabicyclo[2.2.2]octan-1-ium bis(trifluoromethane)-sulfonimide (hexyl-DABCO$^+$ TFSI$^-$) (**35c**).

According to WYKES *et al.*, reactions were performed using the halogen alkane with desired chain length. Afterwards, the anion was exchanged by bis(trifluoro-methane)sulfonimide (TFSI).[65] The first step was a S_N2 type reaction, which was performed in MeCN. 1 equivalent of alkylation agent was added and the reaction mixture was stirred for 16 h at reflux temperature. After full conversion, the solvent was removed and the intermediate product was treated with 1 equivalent of aqueous LiTFSI solution. Subsequently, the product was extracted into organic phase and dried under reduced pressure. Due to the high polarity of the molecules, it was hard to extract them into the organic phase. Product loss was the consequence of this challenging extraction. Interestingly, in the obtained ^{13}C-NMR spectra a rare phenomenon was observed. Carbon atoms in α-position next to the positive charged nitrogen atom showed a $^{13}C^{14}N$ coupling of ~5 Hz. This $^{13}C^{14}N$ coupling for alkylated DABCO molecules is already known in literature (Scheme 5.2, Table 5.1).[66]

5.1.2. Preparation of $N^1,N^{1'}$-(butane-1,4-diyl)bis(N^1-(2-(diethylamino)ethyl)-N^2,N^2-diethylethane-1,2-diamine) (BuDiBiDi) (**36a**) and $N^1,N^{1'}$-(hexane-1,6-diyl)bis(N^1-(2-(diethylamino)ethyl)-N^2,N^2-diethylethane-1,2-diamine) (HexDi-BiDi) (**36b**)

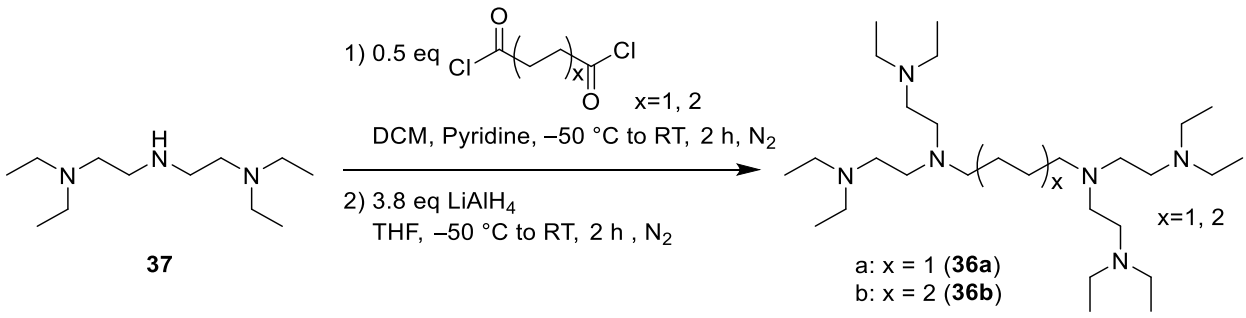

Scheme 5.3: Preparation of $N^1,N^{1'}$-(butane-1,4-diyl)bis(N^1-(2-(diethylamino)ethyl)-N^2,N^2-diethylethane-1,2-diamine) (BuDiBiDi) (**36a**) and $N^1,N^{1'}$-(hexane-1,6-diyl)bis(N^1-(2-(diethylamino)ethyl)-N^2,N^2-diethylethane-1,2-diamine) (HexDiBiDi) (**36b**).

2 molecules of *N*,*N*,*N*',*N*'-tetraethyldiethylenetriamine (**37**) had to be connected *via* an alkyl chain. Using an alkylation agent with two leaving groups (X-R-X), a macromolecular product would be generated. Due to increasing nucleophilicity of the nitrogen atom of an amine moiety with increasing number of substituents, the tertiary amine moiety would react first and generate an undesired product. For that reason, a two-step synthesis was performed to generate BuDiBiDi and HexDiBiDi (**36a**, **b**). In the first step of the synthesis, the secondary amine moiety of *N*,*N*,*N*',*N*'-tetraethyldiethylenetriamine (**37**) was selectively transformed into an amide using 0.5 equivalents of succinyl- or adipoyl chloride. After full conversion, pyridine was removed by extraction and the product was precipitated as hydro chloride adduct using ethereal HCl in Et_2O. Afterwards, the intermediate product was reduced with an excess of lithium aluminum hydride (LAH) to generate the desired $^1O_2$ quencher. Due to the high exothermic reaction of LAH, the reaction mixture was cooled to –50 °C during the addition. After full conversion, the remaining LAH was quenched and the alkaline reaction mixture was filtered. Extraction into organic phase was an easy and successful purification of the product (Scheme 5.3, Table 5.1).

Table 5.1: Over all reaction yield (%), electrochemical stability (V *vs* Li/Li$^+$) and quenching constant of synthesized $^1O_2$ quencher: 1-methyl-1,4-diazabicyclo[2.2.2]octan-1-ium bis(trifluoromethane)sulfonimide (methyl-DABCO$^+$ TFSI$^-$) (**35a**), 1-pentyl-1,4-diazabicyclo[2.2.2]octan-1-ium bis(trifluoromethane)sulfonimide (pentyl-DABCO$^+$ TFSI$^-$) (**35b**), 1-hentyl-1,4-diazabicyclo[2.2.2]octan-1-ium bis(trifluoromethane)sulfonimide (hexyl-DABCO$^+$ TFSI$^-$) (**35c**), N^1,$N^{1'}$-(butane-1,4-diyl)bis(N^1-(2-(diethylamino)ethyl)-N^2,N^2-diethylethane-1,2-diamine) (BuDiBiDi) (**36a**) and N^1,$N^{1'}$-(hexane-1,6-diyl)bis(N^1-(2-(diethylamino)ethyl)-N^2,N^2-diethylethane-1,2-diamine) (HexDiBiDi) (**36b**); the quenching constant of DABCO (**34**) is added as a reference.

	Over all yield (%)	**Electrochemical stability (V *vs* Li/Li$^+$)**	**Photooxygenation rate (s^{-1})**
DABCO	–	2.1-3.6	2.03×10^{-7}
Methyl-DABCO$^+$ TFSI$^-$	70	1.6-3.3	6.90×10^{-7}
Pentyl-DABCO$^+$ TFSI$^-$	68	1.8-4.2	4.04×10^{-7}
Hexyl-DABCO$^+$ TFSI$^-$	61	1.9-4.2	–
BuDiBiDi	45	2.5-3.5	4.94×10^{-7}
HexDiBiDi	54	2.1-3.5	4.14×10^{-7}

After synthesis, the electrochemical behavior of the new synthesized $^1O_2$ quenchers was investigated. Methyl-DABCO$^+$ TFSI$^-$ (**35a**), BuDiBiDi (**36a**) and HexDiBiDi (**36b**) had an oxidation potential of ~3.5 V *vs* Li/Li$^+$. For utilization of those structures inside Li-O_2 batteries, oxidation potential of >4.5 V *vs* Li/Li$^+$ were intended. Regarding the oxidation potentials, proper candidates were pentyl-DABCO$^+$ TFSI$^-$ (**35b**) and hexyl-DABCO$^+$ TFSI$^-$ (**35c**) (Figure 5.2).

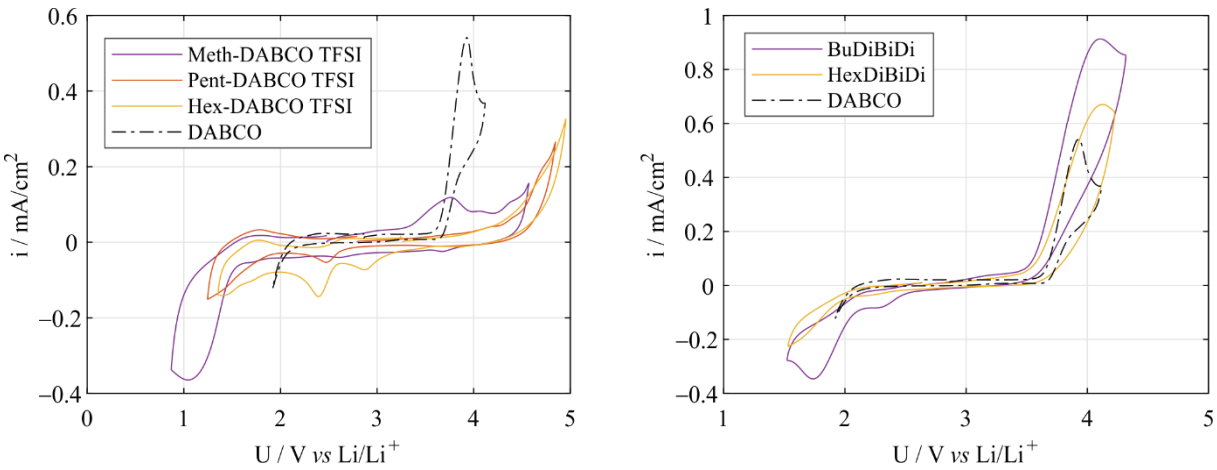

Figure 5.2: Cyclic voltammetry of 5 mM $^1O_2$ quencher in 0.1 M $LiClO_4$/TEGDME in Ar atmosphere. $^1O_2$ quencher: methyl-DABCO$^+$ TFSI$^-$ (**35a**), pentyl-DABCO$^+$ TFSI$^-$ (**35b**), hexyl-DABCO$^+$ TFSI$^-$ (**35c**), BuDiBiDi (**36a**) and HexDiBiDi (**36b**); for comparison DABCO (**34**) is plotted as a reference.

Furthermore, the physical $^1O_2$ quenching ability of the different molecules was determined. It is given by the rate constant for the quenching reaction $^1O_2 + Q \rightarrow {}^3O_2 + Q$. To measure it, a chemical trap such as DMA is exposed to a constant $^1O_2$ source in the absence and presence of the quencher. The quenching rate constant is then determined from the different decay of the trap. The determination of the quencher constant depends on 3 competitive processes: the decay of the excited $^1O_2$ to $^3O_2$ by thermal relaxation (k_d), the reaction rate of the chemical quencher with $^1O_2$ (k_r) and the quenching rate of the physical quencher (k_Q).

$^1O_2$	→	$^3O_2$	k_d, first order decay of $^1O_2$ in the solvent
$^1O_2 + A$	→	$A\text{-}O_2$	k_r, rate constant for chemical quenching (trapping) of $^1O_2$
$^1O_2 + Q$	→	$^3O_2 + Q$	k_Q, rate constant for chemical quenching of $^1O_2$

$$[A] = [A]_0 \times e^{-k \times t} \tag{5.5}$$

with $[A]_0$ as the initiation concentration, k as the rate constant and t as the time.

This is a first order, homogeneous differential equation, which has a specific solution

$$-\frac{d[A]}{dt} = k \times [A]_0 = r_{ox,0} \tag{5.6}$$

where the rate of photooxidation ($r_{ox,0}$) is proportional to the quenching constant k_Q. The coefficient of determination of the calculations (R^2) was >99%. However, further experiments had to be performed to distinguish the corresponding quencher constants k_Q. At this point the declaration could be made: the smaller the photooxygenation rate $r_{ox,0}$, the higher the quenching constant k_Q.

This methodology was applied to all quenchers with DMA as the trap and photooxygenation with the sensitizer Pd_4F as the $^1O_2$ source.

Between the values of BuDiBiDi (**36a**) and HexDiBiDi (**36b**) there is just a marginal difference. The value of hexyl-DABCO$^+$ TFSI$^-$ (**35c**) was not determined, but according to the trend between BuDiBiDi and HexDiBiDi, the value of hexyl-DABCO$^+$ TFSI$^-$ (**35c**) would be similar to pentyl-DABCO$^+$ TFSI$^-$ (**35b**). However, all values of the determined photooxygenation rate were in the range ~10^{-7} (s^{-1}). Best properties for using the $^1O_2$ quencher inside a battery show pentyl-DABCO$^+$ TFSI$^-$ (**35b**), because it is electrochemically stable up to 4.2 V and the quenching efficiency is similar to DABCO. Furthermore, pentyl-DABCO$^+$ TFSI$^-$ is soluble beyond 0.5 M in the electrolyte in comparison with DABCO which is soluble to ~30 mM in glymes. For cross checking, $r_{ox,0}$ of DMA was also determined resulting with the

value of 6.39×10^{-7} (s^{-1}). Consequently, all quenchers have a higher k_Q value except methyl-DABCO$^+$ TFSI$^-$, which had to be a requirement for this particular experiment.

Reaction mechanism inside Li-O_2 cells depends on the GUTMANN donor number (DN) of the solvent, because either a solution or a surface base mechanism takes place depending on the ability of solvents to dissolve salt.[3] Usually, the dissolution of a salt depends on the ability of the solvent to dissolve the cation. Since some of the synthesized $^1O_2$ quenchers were liquids, the idea was born to use them as solvents inside Li-O_2 cells to completely suppress $^1O_2$ formation. Therefore, the DN of TEGDME as well as physical $^1O_2$ quenchers dissolved in TEGDME and hexyl-DABCO TFSI (**33c**) was determined. An easy way for the determination of DNs was shown by JOHNSON *et al.*.[33] The shift of the sodium signal of a dissolved sodium salt was recorded in ^{23}Na-NMR for various solvents with known DN. Using a generated trend line of the known solvents with their corresponding DNs, unknown DNs of different molecules could be determined. Surprisingly, all ascertained DNs were ~12. Obviously, the cations were unaffected by the presence of the different $^1O_2$ quenchers compared to TEGDME. Also, the measurement of Na-shift in pure hexyl-DABCO TFSI showed no significant difference (Figure 5.3). Consequently, due to the low DN, inside Li-O_2 batteries the reaction mechanism is dominated by surface mechanism.

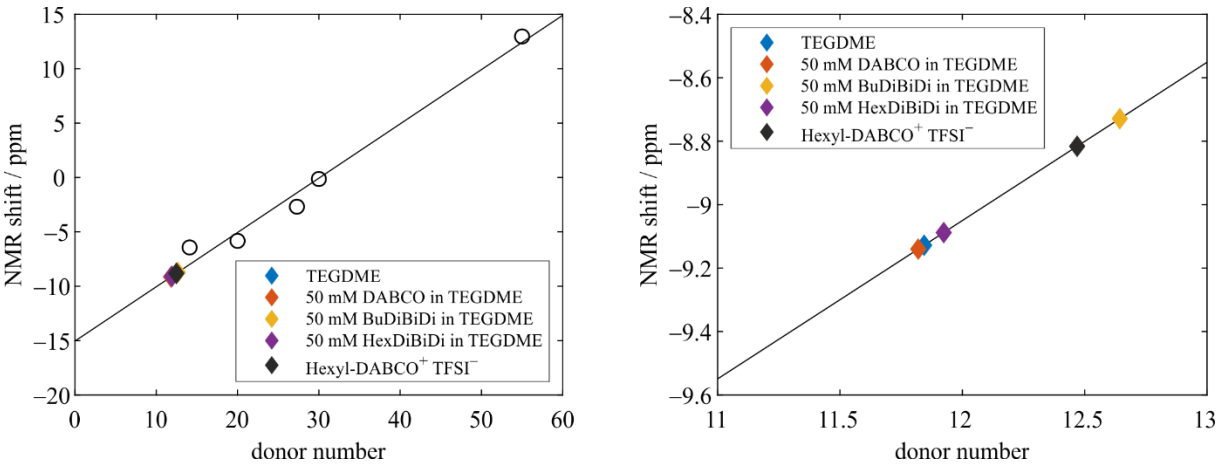

Figure 5.3: Determination of GUTMANN donor number of TEGDME (blue), 50 mM DABCO in TEGDME (red), 50 mM BuDiBiDi in TEGDME (yellow), 50 mM HexDiBiDi in TEGDME (violet) and hexyl-DABCO TFSI (black) by ^{23}Na-NMR spectroscopy according to literature of JOHNSON.[33]

In summary, the synthesis of new physical $^1O_2$ quenchers was accomplished. The molecules were tested towards their electrochemical properties and $^1O_2$ quenching ability. Furthermore, the GUTMANN DN of those molecules were determined using ^{23}Na-NMR spectroscopy. Best results showed pentyl-DABCO$^+$ TFSI$^-$.

5.2. The Mechanism of Solvent Decomposition by $^1O_2$

Given that we have revealed $^1O_2$ to form at all stages of cycling of metal-O_2 cells, the question arises how $^1O_2$ initiates solvent decomposition. Particularly, we want to establish whether there are energetically favored pathways in comparison to established reaction pathways with superoxide, which has previously been suggested as the cause for solvent decomposition albeit theoretical work has shown prohibitively high activation energies for overall strongly endergonic reactions.[67] The solvent class shall be glymes because of their predominant use in metal-O_2 cells. Reactivity of $^1O_2$ with organic substrates has been widely investigated starting in the 1970s with mainly unsaturated compounds. $^1O_2$ is known to react with organic substrates containing C=C double bonds *via* so-called "ene" or "diene" reaction which have been widely investigated experimentally and theoretically because of their interest for synthetic purposes.[68] However, we have shown that glyme electrolytes were also decomposed to compounds such as acetate, formate and Li_2CO_3 when exposed to $^1O_2$.[41b] We thus proposed the following mechanism based on chemical intuition for the activation of glyme electrolytes by $^1O_2$ *via* a group transfer reaction (Scheme 5.4).

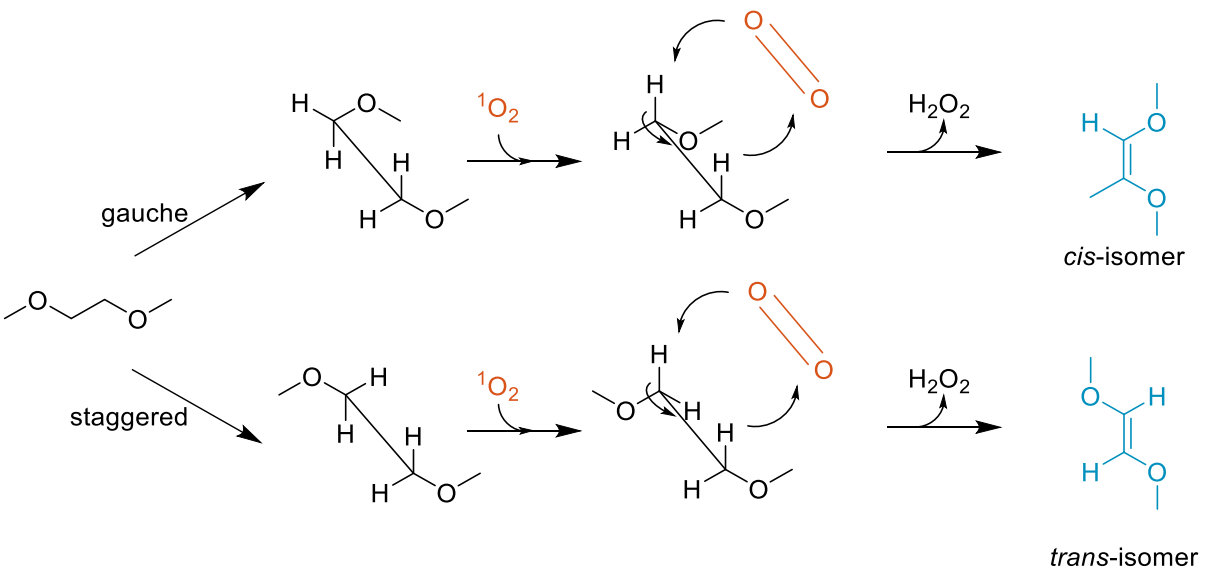

Scheme 5.4: Proposed reaction of $^1O_2$ with two conformers of ethylene glycol dimethyl ether.

During this special type of group transfer reaction, two hydrogen atom are simultaneously transferred to the oxygen molecule. Additionally, a C=C double bond is generated between the carbon atoms of the glyme. The reaction proceeds by forming two σ bonds and one π bond whilst breaking one π bond in a concerted process. The mechanism allows for two possible configurations of the in substrate before $^1O_2$ attack and thus the formation of either a *cis* or a *trans*-isomer product. In the era of computational chemistry, the energetics of reaction pathways

and thus their likelihood to occur in reality can be judged based on first principles calculations. Calculations for the proposed path were performed by M. LEYPOLD using MP2/6-311++G** basis set. The mechanistic calculations showed that the group transfer reaction of both conformers were exothermic and ~120 kJ/mol energy was generated during the reaction. The path with the staggered conformer appears somewhat more favorable with a 15 kJ/mol lower activation energy compared to the gauche conformer (Figure 5.4).

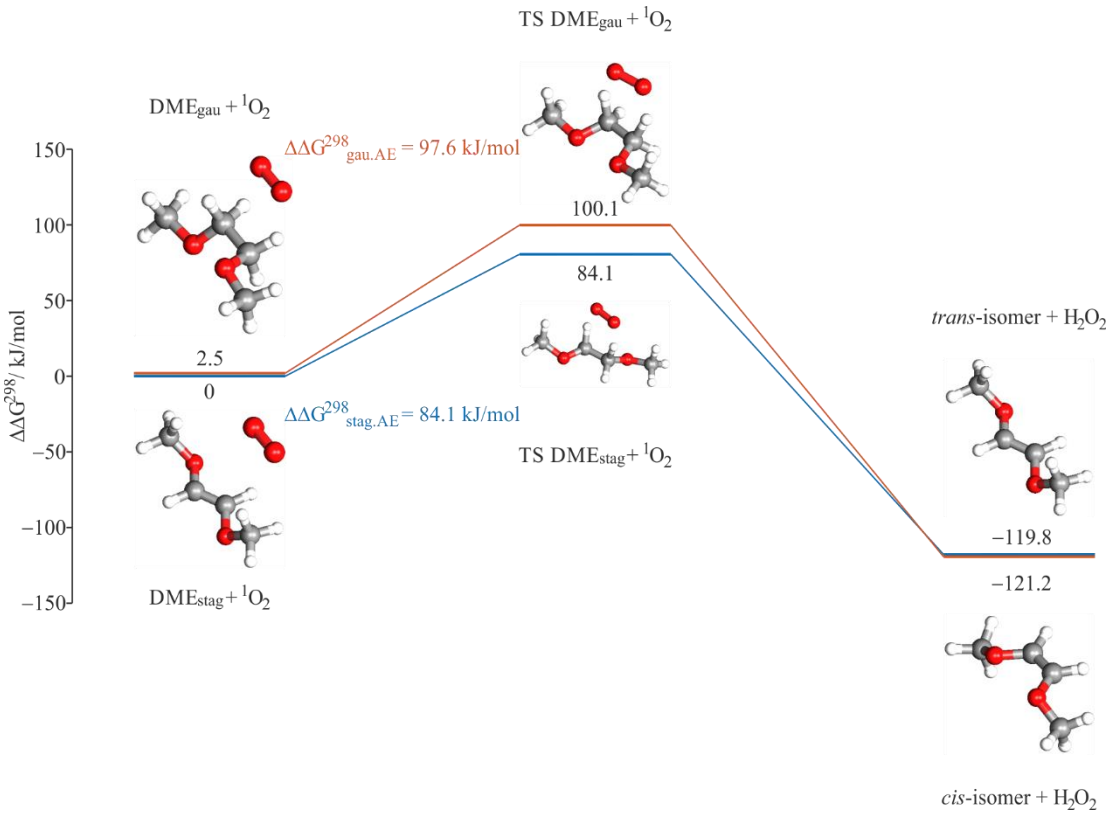

Figure 5.4: DFT calculation of the reaction of DME isomers with $^1O_2$ using MP2/6-311++G** basis set: red reaction = gauche conformer generating *cis*-isomer; blue reaction = staggered conformer yielding in *trans*-isomer.

The plausible reaction of $^1O_2$ with ethylene glycol dimethyl ether leads to an olefin, which afterwards would further react with $^1O_2$ *via* different types of mechanisms (Scheme 5.5).

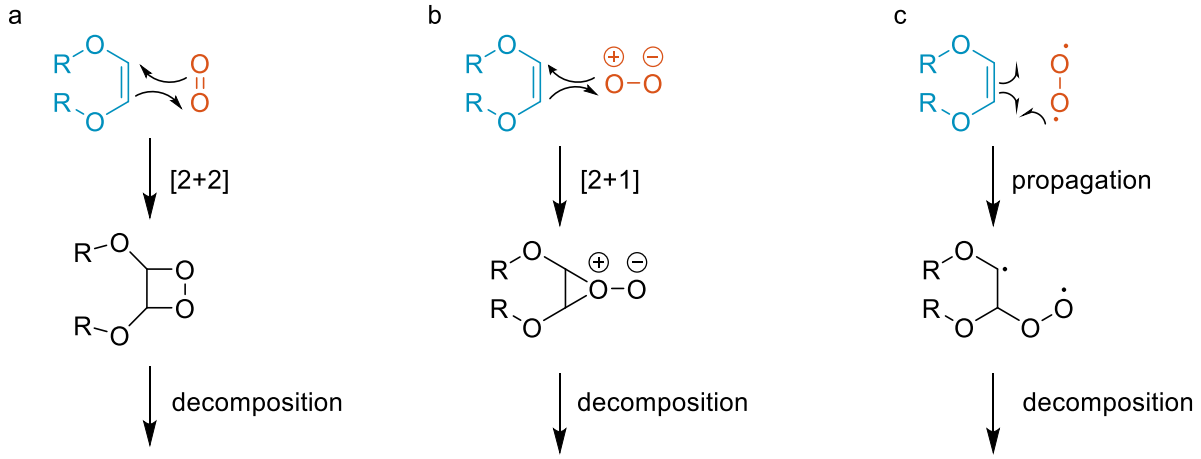

Scheme 5.5: Decomposition reaction mechanisms with $^1O_2$: [2+2]-cycloaddition (a), [2+1]-cycloaddition (b), propagation (c).

5.3 Deactivation of Redox Mediators by $^1O_2$

Inside Li-O_2 batteries, redox mediators are used to overcome the problem that the formed Li_2O_2 is a poor e^- and Li^+ conductor. To bypass the poor charge carrier transport inside Li_2O_2, mediators are widely investigated (Scheme 3.1).[3] Oxidation mediators shuttle electron-holes between the porous electron conducting electrode and the Li_2O_2 particle. The mediator gets oxidized at the surface to its oxidized form M^+, from where it diffuses to the Li_2O_2 which gets oxidized to O_2 and Li^+ by reforming the reduced form M of the mediator However, the mediators are also potential reaction partners with $^1O_2$. Therefore, the reactivity of two representative mediators, tetrathiafulvalene (TTF) and dimethylphenazine (DMPZ) toward $^1O_2$ was investigated. The choice fell on those molecules, because TTF was amongst the first mediators reported and DMPZ had lowest charging potential, which is required for Li_2O_2 oxidation. We also investigated the reaction of the mediators with the other reactive oxygen species $^3O_2$, O_2^- and O_2^{2-}. For the first case, the mediators were exposed to saturated O_2 electrolyte solution. For reaction with superoxide and peroxide, the mediators were dissolved in the electrolyte and stirred with an excess of KO_2 or Li_2O_2. In the case of KO_2 an excess 18-crown-6 was additionally added to dissolve KO_2 and enhance the reactivity. $^1O_2$ was generated photochemically by illuminating O_2 saturated electrolyte solution in the presence of palladium(II) *meso*-tetra(4-fluorophenyl)-tetrabenzoporphyrin (Pd_4F).[69] The consumption of the mediator was recorded by UV-Vis spectroscopy as well as ^{1}H-NMR spectroscopy.

Furthermore, oxidized mediators were subjected to the same stability test against with $^1O_2$, because during the catalytic cycle oxidized mediators are created and the potential point of attack for $^1O_2$. According to our results, TTF decomposed ~4,000 times faster with $^1O_2$ than DMPZ and the oxidized mediator reacted ~2 orders of magnitudes slower than their corresponding neutral species. The reactivity of $^1O_2$ with electron rich olefins *via* a so-called "ene" or "diene" reaction is known in literature.[70] The electrophilic nature of $^1O_2$ makes the molecule attractive for diverse substituted C=C double bonds. The higher the nucleophilicity of a double bond of an olefin, the higher the reaction rate of the product formation compared Scheme 5.1. This corresponds to the obtained results of the stability tests. Moreover, DFT calculations of the mediators with $^1O_2$ were performed using B3LYP/6-31G* basis set. Calculation of the reaction of DMPZ with $^1O_2$ showed, that the reaction free enthalpy was positive with an activation energy >100 kJ/mol. However, further decomposition reaction could force the overall reaction to spontaneous reaction with energy gain. The reaction of TTF with $^1O_2$ required lower activation energy. Furthermore, lot of energy was released, which indicated to spontaneous reaction. Overall, we do not rule out the reactivity of the mediators with $^3O_2$, KO_2 and Li_2O_2, but our results exhibited the higher reaction towards $^1O_2$.

6. Summary and Outlook

One goal of this PhD thesis was to synthesize organic mixed conductors, which could be used in novel battery types. In detail, pyrene **1** as well as poly(paraphenylene) **2** units were used for introduction of electronic conduction into the material. Tetraethylene glycol methyl ether **3** units were used to supply ionic conductivity (Scheme 6.1).

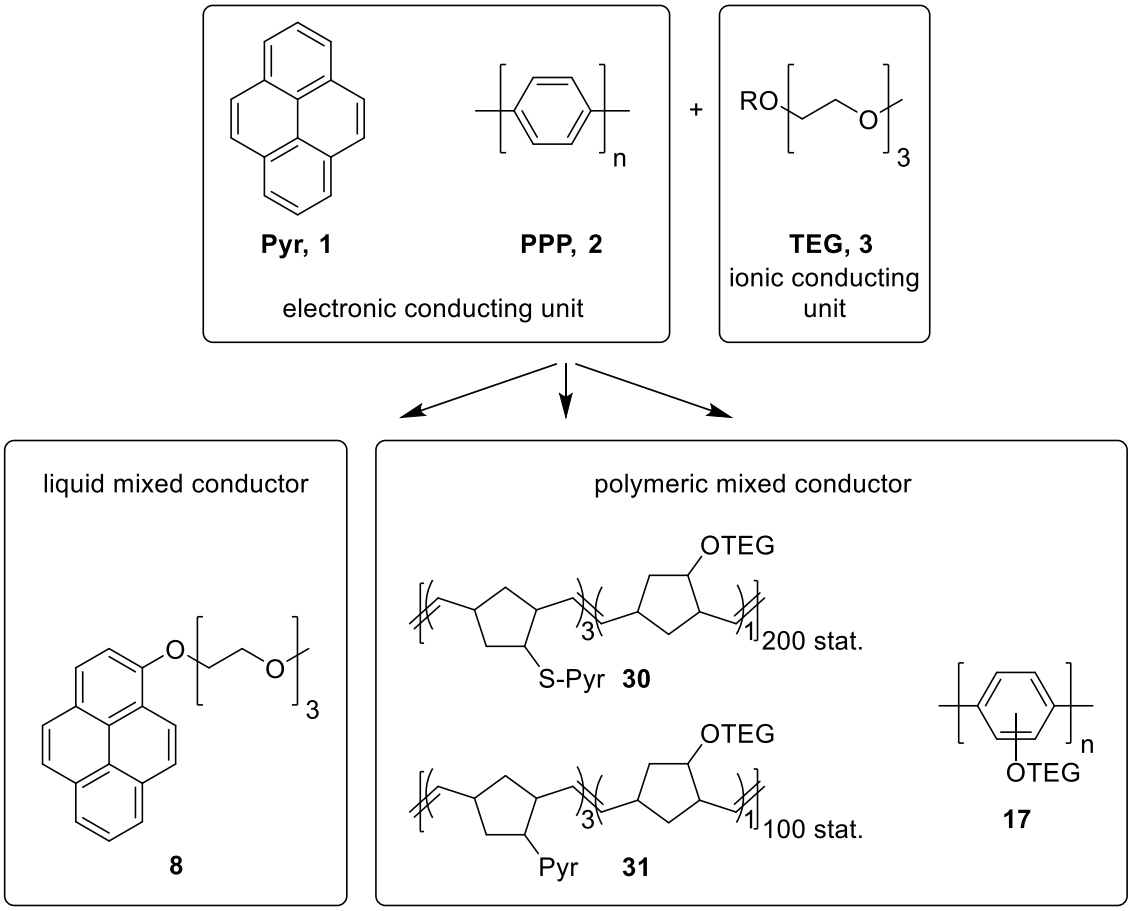

Scheme 6.1: Synthesized mixed conducting substances consisting of Pyr **1**, PPP **2** and TEG **3** units.

1-(2-(2-(2-Methoxyethoxy)ethoxy)ethoxy)pyrene (PyrOTEG) (**8**) was the easiest combination of pyrene and TEG unit. Due to the molecule's unique liquid physical property regarding mixed conducting substances, PyrOTEG could be used as electrolyte inside batteries. Furthermore, the molecule exhibited an increased electrochemical potential window, good electronic and ionic impedance, and resistivity against high reactive oxygen species. These properties lead to PyrOTEG becoming an efficient candidate for the use inside oxygen batteries. Poly(PySOTEG) (**30**) and poly(PyrOTEG) (**31**) are polymeric mixed conducting compounds, which were produced *via* ROMP. ROMP-polymers are hardly used in battery systems, however, those two materials showed good behavior during cycling of silicon anodes. The impedances are in the region of other mixed conducting polymers, and the specific capacities of the cycling experiment could keep up with their competitors. Moreover, poly(PyrOTEG) showed good results during oxygen cycling experiments. Poly((2-(2-(2-methoxyethoxy)-ethoxy)ethoxy)phenylene) (**17**) instead was electrochemically generated. Cycling experiments of oxygen cells showed the polymer is able to deliver electrons and ions. Furthermore, the capacities increased compared to experiments without the mixed conducting polymer.

The second part of the thesis focused on organic materials in singlet oxygen ($^1O_2$) (electro)chemistry. We were first to demonstrate that singlet oxygen forms at all stages of cycling of non-aqueous metal-O_2 cells and is predominantly responsible for parasitic chemistry which degrades the cell. Singlet oxygen causes severe problems and parasitic side reactions during cycling of an oxygen battery and is hard to detect. During this thesis, aspects of organic material interactions were investigated, including:

1) The qualification of cyclic aromatic hydrocarbons as a selective and sensitive $^1O_2$ trap that allows for its detection in the battery environment. With the aid of these traps, the unexpected formation of $^1O_2$ <3.5 V *vs* Li/Li^+ was detected during discharge and formation occurred from the beginning of the charging process at ~3 V *vs* Li/Li^+ $^1O_2$. Those two phenomena led to new reaction mechanisms of the formation of $^1O_2$ in electrochemical reactions.

2) Formulation of possible reaction mechanisms for $^1O_2$ attack on glyme electrolytes.

3) The degradation mechanism of oxidation mediators in the presence of reactive oxygen species. In detail, singlet oxygen reacts preferentially within pericyclic reactions. High reaction energy is produced if singlet oxygen reacts with heteroatoms. These studies showed that $^1O_2$ owns high enough energy to react with almost any organic molecule.

4) The synthesis of novel physical $^1O_2$ quenchers with an increased electrochemical stability window. Modified DABCOnium-molecules **35a-c**, as well as substances with several diethylamino moieties **36a,b**, showed higher electrochemical stability and good quenching ability compared to literature known molecules. These chemical properties made them proper candidates for application inside oxygen batteries (Figure 6.1).

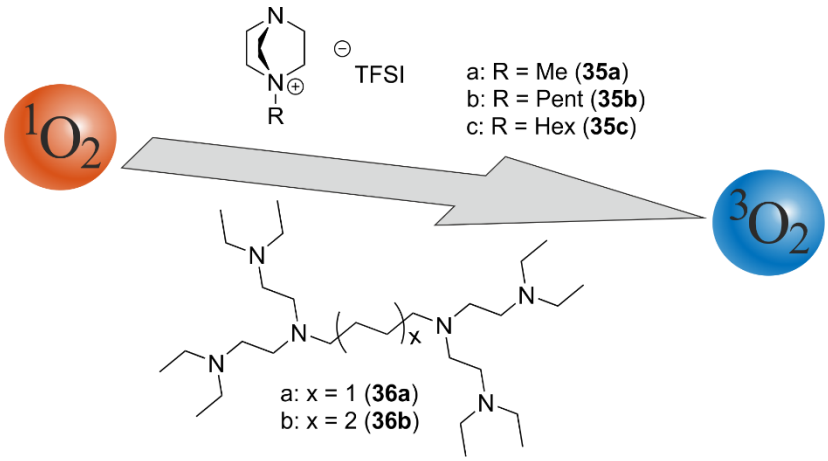

Figure 6.1: Physical singlet oxygen quenching using synthesized compounds.

Future experiments will need to be performed to complete these started projects. Electrochemical experiments with the liquid mixed conductor should be performed in which 1-(2-(2-(2-methoxyethoxy)ethoxy)ethoxy)pyrene (PyrOTEG) (**8**) is used as electrolyte to confirm the expected mixed conductivity. Moreover, the efficiency of the physical $^1O_2$ quencher molecules should be examined in electrochemical cells. Other molecules with potentially higher electrochemical stability and quenching ability will be determined and evaluated in electrochemical cells.

7. Experimental Part

7.1. General Aspects

All chemicals were purchased from ABCR CHEMICALS, ACROS ORGANICS, ALFA AESAR, CARL ROTH, FISHER SCIENTIFIC, FLUKA, MERCK, SIGMA ALDRICH, SOLVIONIC and VWR CHEMICALS. Every chemical was used without further purification, unless it is explicitly noted in the experimental section. For synthesis, standard SCHLENK technique was used, if it is not elsewise noted. Therefore, all of the glassware was evacuated and heated with a heat gun. After cooling to room temperature, the glassware was flushed with inert gas (nitrogen). Absolute solvents were received by different methods, which are described in Chapter 7.2. Reaction control was either performed with TLC, or NMR-spectroscopy. Cyclomatic voltammetry-, impedance- and polarization experiments as well as assembling of all batteries were executed in an argon filled glovebox by MBRAUN® (UNILAB Plus; Ar 5.0).

Molecular sieves (MS, SIGMA ALDRICH, 3 Å, beads with 8-12 mesh) were activated in a SCHLENK flask, which was heated to 300 °C under high vacuum until complete dryness was reached. These activated molecular sieves were stored at RT in an argon filled glove box.

Generally, all reaction took place at RT if not further noted. All temperatures were measured externally. An ice-water bath was used to cool the reaction flasks to 0 °C. If temperatures below 0 °C were required, a cooling bath consisting of acetone/dry ice was used. A silicon oil bath on a heating plate equipped with an external temperature controller (HEIDOLPH® MR Hei-Tec) was used, if reaction temperatures higher than RT were required.

A monowave 50 reactor from ANTON PAAR was used for special synthesis. During operation temperature and pressure was measured internally. If not further noted all reactions used the heating sequence ‘as fast as possible’ and held a temperature of 150 °C for 2 h.

Electrochemical tests were performed on either a SP-150, SP-300, MPG-2 from BIOLOGIC SA or BT-2000 from ARBIN INSTRUMENTS potentiostat/galvanostat. The electrochemical cells used to investigate cycling were based on a SWAGELOK® design or CR2032 coin cells.

7.2. Solvents

Reactions, which took place under inert atmosphere, and electrolytes for battery assembling required anhydrous solvents. Anhydrous acetonitrile (MeCN) was purchased from SIGMA ALDRICH and transferred into a 1 L SCHLENK bottle. Dry diethyl carbonate (DEC) ethylene carbonate (EC) were purchased from TCI and transferred into a 1 L SCHLENK flask. Dry dichloromethane (DCM) was produced by heating it under reflux over P_4O_{10} for 12 h under inert atmosphere. Afterwards it was distilled in a 1 L SCHLENK bottle. Anhydrous dimethoxyethane (DME) and tetraethylene glycol dimethyl ether (TEGDME) were produced heating them to 80 °C over sodium metal for 12 h under inert atmosphere. Afterwards they were distilled (TEGDME under reduced pressure) in a 1 L SCHLENK bottle. Anhydrous *N*,*N*-dimethylformamide (DMF) was purchased from SIGMA ALDRICH and transferred into a 1 L SCHLENK bottle. Dry tetrahydrofuran (THF) and toluene were generated *via* a drying aluminum oxide column apparatus. All anhydrous solvents were store over 3 Å molecular sieves under inert atmosphere.

The following list of solvents was used for reactions, which took place without an inert atmosphere, work-ups, or purifications of products. They were used as purchased from CARL ROTH, FISHER SCIENTIFIC, SIGMA ALDRICH, TCI and VWR CHEMICALS without further purification of the respective solvent: Acetone, acetic acid, cyclohexane, dichloromethane (DCM), diethylether (Et_2O), ethyl acetate (EtOAc), nitrobenzene, *n*-hexane, methanol (MeOH), *N*-methyl-2-pyrrolidone (NMP), tetrahydrofuran (THF) and toluene.

Saturated aqueous sodium chloride solution (brine) and saturated aqueous sodium bicarbonate solution were prepared by adding the corresponding salt into distilled water under stirring until precipitation occurred.

7.3. Reagents

n-Butyllithium was purchased as a 2.5 M solution in hexanes from SIGMA ALDRICH. The concentration was determined by titration according to the method by W. G. KOFRON *et. al.*.[71] Hence an oven dried 25 mL SCHLENK flask equipped with a TEFLON®-coated magnetic stir bar was charged with 100.0 mg diphenylacetic acid and 4 mL dry THF. The reaction mixture was stirred vigorously, while the *n*-BuLi solution was added *via* a 1 mL syringe until the color of the reaction mixture changed to yellow. The added amount of *n*-BuLi corresponds to the weighted amount of diphenylacetic acid. The concentration of *n*-BuLi was determined as the average value of at least three assays.

7.4. Experimental Procedures

7.4.1. General ROMP-Polymerization Process

An oven dried 25 mL SCHLENK flask equipped with a TEFLON®-coated magnetic stirring bar was charged with 0.08 mmol (1.0 eq) TEG containing monomer, 0.24 mmol (3.0 eq) pyrene containing monomer and 3 mL of absolute, degassed DCM under nitrogen atmosphere. Afterwards a solution of dichloro[1,3-bis(2,4,6-trimethylphenyl)-2-imidazolidinylidene](3-phenyl-1*H*-inden-1-ylidene)(pyridyl)ruthenium(II) (**M31** from UMICORE) and 0.2 mL of absolute, degassed DCM was added to the reaction mixture. In the case of synthesizing poly(PySOTEG) (**30**), the amount of ROMP catalyst was 1.6 µmol (2 mol%), in the case of poly(PyrOEG) (**31**) the amount of 4.4 µmol (4 mol%) was used. The reaction mixture was stirred for 2 h at RT. Afterwards the polymerization reaction was stopped by the addition of 150 µL of ethyl vinyl ether. The reaction mixture was further stirred for 2 h. Afterwards the polymer was precipitated in 100 mL of cold MeOH twice. Finally, the off white polymer was dried in oil pump vacuum at 10^{-2} mbar for 5 h.

7.4.2. General Procedure for NMR-Screening Reaction with KO_2

A 2 mL glass vial was charged with 20 mg (0.28 mmol) potassium superoxide, 10 mg synthesized product and 1 mL absolute deuterated DMSO. After a certain reaction time, the product mixture was pushed through a small patch of basic activated Al_2O_3. The entire procedure was done in glove box with argon atmosphere.

7.4.3. Electrode Preparation for Si-Anodes

6.0 mg of polymer were dissolved in 140 µL of NMP. Afterwards 12.0 mg of Si-nanoparticles (50-100 nm) were added. The mixture was homogenized for 1 h and the slurry was coated on a copper foil. The coated electrode dried overnight at RT and was further dried in vacuum at 90 °C for 12 h to remove the NMP completely. The electrodes had a Si loading of 0.2-0.3 mg/cm^2.

7.4.4. General Procedure for Si-Anode Assembling

Cell assembling was done in an Ar-filled glovebox. Glass fiber separators (WHATMAN) and polypropylene separators (CELGARD PP2068) were washed with EtOH and acetone and dried in vacuum at 100 °C for 24 h before use. Lithium was used as counter electrode and reference material in SWAGELOK® cell and as counter electrode in coin cells. The used electrolyte consisted of 1.2 M lithium hexafluorophosphate ($LiPF_6$) in ethylene carbonate (EC), diethyl carbonate (DEC) (ED/DEC = 3:7 (m/m)) and 30 m% of fluoroethylene carbonate (FEC). 40 µL electrolyte and polypropylene separators were used in coin cells. SWAGELOK® cells were assembled with 100 µL electrolyte and glass fiber separators.

7.4.5. General Procedure for Cyclomatic Voltammetry (CV) Measurement

A solution consisting of 0.1 M supporting electrolyte salt (tetrabutylammonium bis(trifluoromethan)sulfonimide (TBATFSI)) and 2 mM substance which should be examined in acetonitrile is put into a homemade CV-cell. The working electrode was made of gold with a diameter of 1.6 mm, the counter electrode material was made of platinum and a silber wire was used as a pseudo reference electrode. Ferrocene was used as standard reference material to convert the resulting potentials to Li/Li^+ scale. If not further described all measurements were performed with a scan rate of 100 mV/s and in conditions, which are described above.

7.4.6. General Procedure for Impedance Measurements

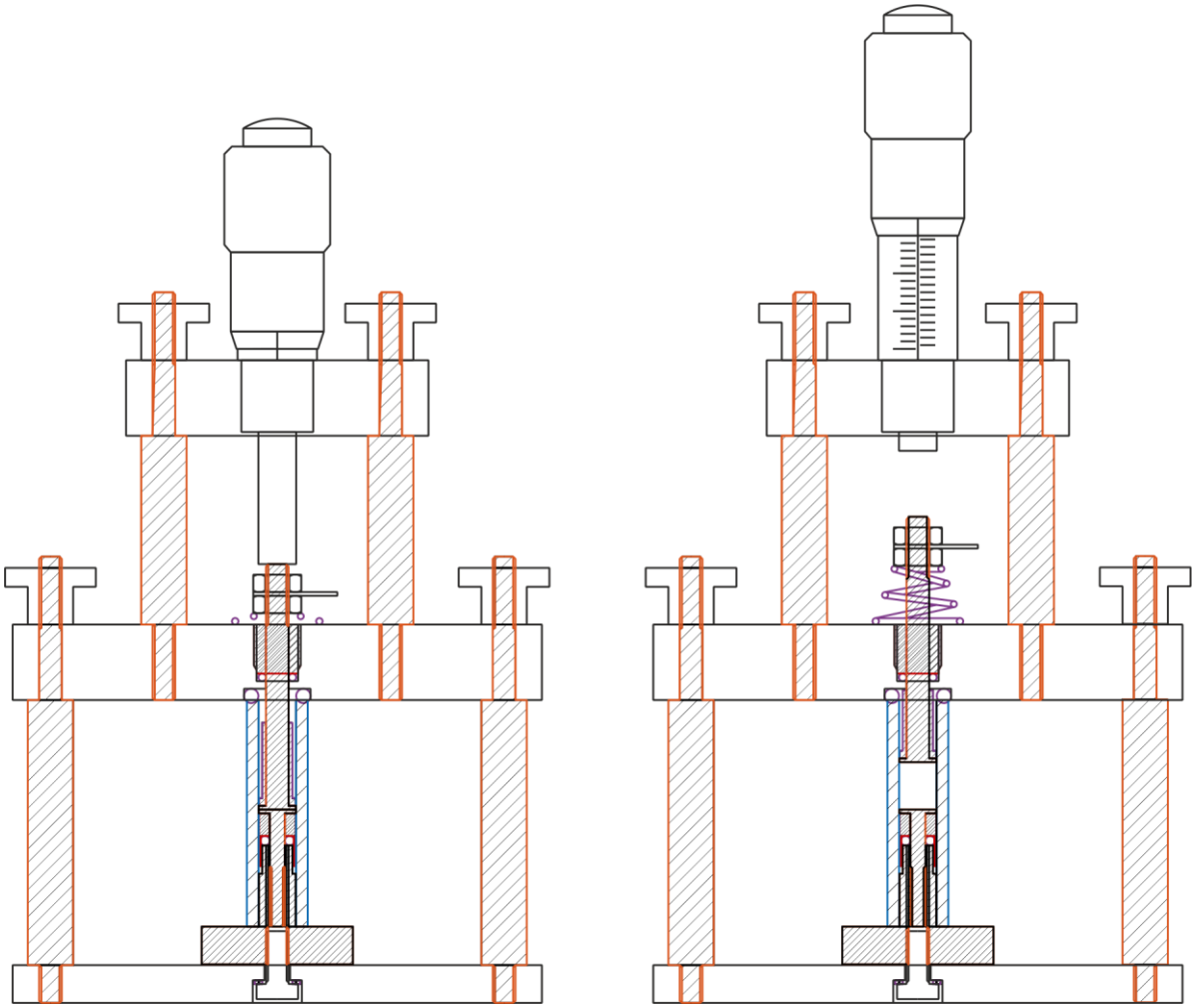

Figure 7.1: Construction image of the self-made electrochemical cell, which was used for impedance and polarization experiments of either solid or liquid samples.

The sample was filled into a self-made electrochemical cell (Figure 7.1), which was prepared for low volume measurements, to a certain high (usually 300 µm). The experiment was performed from 7 MHz to 50 mHz at different temperatures. The surfaces of the electrodes were covered with gold.

7.4.7. General Procedure for Polarization Measurements

The sample was filled into a self-made electrochemical cell (Figure 7.1), which was prepared for low volume measurements, to a certain high (usually 300 µm). The experiment was performed at different temperatures. The electrodes were polarized from 0 V to 500 mV in 100 mV-steps and the potential was held for 1 h before switching to the next potential. The surface of the electrodes was covered with gold.

7.4.8. General Procedure for Pressure Measurements

Cell assembly was performed inside an Ar-filled glovebox with a PAT-Cell-Press from EL-CELL®. Glass fiber separators (WHATMAN) were washed with EtOH and acetone and dried in vacuum at 100 °C for 24 h before use. Delithiated LFP with a capacity of 2 mAh was used as counter electrode and partly delithiated LFP was used as reference material. 250 µL electrolyte, which consisted of 0.1 M lithium bis(trifluoromethane)sulfonimide (LiTFSI) in TEGDME were used. Finally, the cell was flushed with O_2 with an overpressure of 1.3 mbar.

7.4.9. General Procedure for Dilatometer Measurements

Cell assembly was performed inside an Ar-filled glovebox with an ECD-3 Electrochemical Dilatometer from EL-CELL®. Ceramic separators were washed with H_2O and EtOH using ultrasonication and dried in vacuum at 100 °C for 24 h before use. Lithium was used as counter electrode as well as reference material. ~500 µL electrolyte, which consisted of 1.2 M lithium hexafluorophosphate ($LiPF_6$) in ethylene carbonate (EC), diethyl carbonate (DEC) (ED/DEC = 3:7 (m/m)) and 30 m% of fluoroethylene carbonate (FEC) were used. YANN PETIT performed dilatometer assembling and measurements.

7.5. Analytical Methods

7.5.1. Thin Layer Chromatography (TLC)

Reaction control was performed using thin layer chromatography silica gel on aluminum foil (60 F_{254}). Detections were carried out with UV-light (254; 366 nm) or TLC-stains.

7.5.2. Flash Chromatography

60 Å silica gel with a particle size between 35-70 µm (ACROS ORGANICS) was used for column chromatography. Amount of silica gel (20-100 fold) and applied pressure depended on the separation problem.

7.5.3. High Resolution Mass Spectrometry (HR-MS)

A WATERS GCT premier micromass spectrometer was used for high resolution mass spectrometry measurements. The substances were ionized by an electron impact ionization (EI)-source with 70 eV. Samples were either injected *via* direct inlet or *via* an AGILENT TECHNOLOGIES GC 7890A with capillary column (DB-5MS, 30 m × 0.25 mm × 0.25 µm film). For analysis of heavier molecules, a micromass Tofspec 3E spectrometer with matrix assisted laser desorption ionization (MALDI) was used. *trans*-2-[3-(4-*tert*-Butylphenyl)-2-methyl-2-

propenylidene] malononitrile was taken as matrix, sodium trifluoroacetate as sodium source and a time of flight mass analyzer (TOF) as mass analyzer.

7.5.4. Nuclear Magnetic Resonance Spectroscopy (NMR)

NMR-spectra were either recorded on a BRUKER Avance III 300 MHz FT NMR spectrometer with autosampler (300.36 MHz (^{1}H-NMR), 75.53 MHz (^{13}C-NMR)) or on a VARIAN Inova 500 MHz spectrometer (499.88 MHz (^{1}H-NMR), 125.70 MHz (^{13}C-NMR), 470.39 MHz (^{19}F-NMR), 132.22 MHz (^{23}Na-NMR)). Chemical shifts δ are referenced to the residual protonated solvent signals as internal standard. APT and ^{13}C spectra were proton decoupled. Signal multiplicities J are abbreviated as s (singlet), d (doublet), dd (doublet of doublet), ddd (doublet of doublet of doublet), t (triplet), and m (multiplet). For the correct assignment of the signals HH-COSY, HMBC, HSQC and NOE experiments were recorded if necessary. Moreover, the deuterated solvent, the chemical shifts δ in ppm (parts per million), the coupling constant J in Hertz (Hz) and the integral and assignment of the respective signals are given. All measurements on the 500 MHz spectrometer were performed by PETRA KASCHNITZ.

7.5.5. Infrared Spectroscopy (FTIR)

A BRUKER ALPHA-P FT-IR spectrometer with a Standard Pike ATR cell was used to perform FT-IR-spectroscopy. It is equipped with a room temperature detector, mid IR source (4000-400 cm^{-1}). Before every measurement of a product background spectra were performed. 16 scans were executed per analytical measurement in a range of 4000-400 cm^{-1}.

7.5.6. Differential Scanning Calorimetry (DSC)

A PERKIN ELMER DCS 8500 instrument with a nitrogen purge gas flow of 20 mL/min was used for differential scanning calorimetry measurements. If not further described a heating/cooling rate of 10 °C/min was used. All measurements were performed by JOSEFINE HOBISCH.

7.5.7. Scanning Electron Microscopy (SEM)

An ESEM Quanta 600 FEG from FEI Company was used for scanning electron microscopy. The images were produced in low vacuum mode. All measurements were performed by MANFRED NACHTNEBEL or ARMIN ZANKEL.

7.5.8. Gel Permeation Chromatography (GPC)

All GPC measurements were performed on a WGE DR. BURES SEC-3010 instrument with a capillary column (MZ-Gel SD plus, linear 5 µm, 300 × 80 mm) in tetrahydrofuran (THF) with

a purge flow of 1 mL/min. For calibration Polystyrene Standards purchased from POLYMER STANDARD SERVICE were used. All measurements were performed by JOSEFINE HOBISCH.

7.5.9. Contact Angle (CA)

A drop shape analyzer DSA 100 from KRÜSS was used for contact angle measurements. The contact angle (Θ) was measured on several surfaces (Au, C, Si) and was calculated *via* circle-fitting evaluation mode.

7.5.10. Atomic Force Microscopy (AFM)

A single side polished silicon wafer (SIEGERT WAFERS, thickness 675 ± 25 µm) was coated with a polymer film. Therefore, 20 µL per square centimeter wafer of 1 w% polymer solution in $CHCl_3$ were deposited on the wafer surface and subjected to spin coating (a = 2500 rpm/s, v = 4000 rpm/s, t = 60 s). A Veeco Multimode Quadrax MM AFM from BRUKER in tapping mode was used for taking atomic force microscopy images. A NCH-VS1-W silicon cantilever with a resonance frequency of 297 kHz from NANOWORLD AG was used. All measurements were performed by MATHIAS HOBISCH.

7.5.11. X-Ray Diffraction

The crystal suitable for single crystal X-ray diffraction was mounted on a glass rod on a copper pin. XRD data collection was performed on a BRUKER APEX II diffractometer with use of Mo Kα radiation (λ = 0.71073 Å) and a CCD area detector. Empirical absorption corrections were applied using SADABS.[72] The structure was solved with use of direct methods option in SHELXS and refined by the full-matrix least-squares procedures in SHELXL.[73] The space group assignment and structural solution was evaluated using PLATON.[74] Non-hydrogen atoms were refined anisotropically. Hydrogen atoms were located in calculated positions corresponding to standard bond lengths and angles. All measurements and data evaluations were performed by ANA TORVISCO GOMEZ.

7.5.12. Ultraviolet-Visible Spectroscopy (UV-Vis)

UV-Vis spectra were recorded on a UV-1800 spectrometer from SHIMADZU. Therefore, a quartz-cuvette was filled with a 1.6×10^{-4} M solution and scanned from 200-800 nm.

7.5.13. Rheological Measurements

A MCR 502 Modular Compart Rheometer from ANTON PAAR was used for all rheological measurements. All measurements were done with a cone-plate system (CP50-1 (50 mm)) with

a gap of 1.0 mm at temperatures from 15-35 °C. For viscosity measurements a shear rate of 50 s^{-1} was applied.

7.5.14. Melting Point

Melting points were determined in open capillary tubes using a Mel Temp melting point apparatus with integrated microscopical support from ELECTROTHERMAL. Melting points were not corrected and the temperature was measured using a mercury thermometer.

7.5.15. Thickness Measurement

Thickness measurements were performed with a MITUTOYO Absolute. Every measurement was done 3 times and the average value is calculated.

7.5.16. General Procedure for Determination of the Quenching Constant for Physical $^1O_2$ Quenchers

$^1O_2$ was produced photochemically by illuminating O_2-saturated solution containing 1 µM of the photosensitizer palladium(II) *meso*-tetra(4-fluorophenyl)-tetrabenzoporphyrin (Pd_4F) according to the literature of BORISOV.[69] Additionally, the solution contained 50 µM of DMA and 50 µM of the physical quencher. The solution was illuminated with a red light-emitting diode light source (OSRAM®, 643 nm, 7 W) for 10 min. Every 30 s a UV-Vis spectrum was recorded. NIKA MAHNE performed every measurement and YANN PETIT the corresponding calculation.

7.5.17. Experimental Prescription for Synthesis

7.5.17.1. 1,1'-(((Sulfonylbis(ethane-2,1-diyl))bis(oxy))bis(methylene)) dipyrene (**4**)

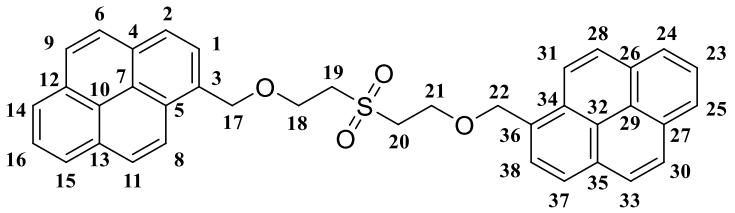

A 25 mL round bottom flask equipped with a TEFLON®-coated magnetic stirring bar was charged with 242 mg (1.04 mmol, 3.0 eq) pyren-1-ylmethanol. It was dissolved in 10 mL DCM and the yellow solution was stirred for 5 min at RT. Afterwards 570 mg (1.75 mmol, 5.0 eq) Cs_2CO_3 were added and the yellow suspension was stirred for further 5 min at RT. Then 34.9 µL (0.35 mmol, 1.0 eq) divinyl sulfone were added and the yellow suspension was stirred over the weekend at RT. The reaction control was performed by TLC. Afterwards the reaction

mixture was diluted with 25 mL EtOAc and transferred into a separatory funnel. The organic phase was washed with H_2O (1 × 10 mL) and sat. $NaHCO_3$ (2 × 15 mL). The aqueous phase was reextracted with EtOAc (3 × 20 mL). Then the combined organic phases were washed with brine (1 × 20 mL). Subsequently the organic phase was dried over Na_2SO_4, filtered and the solvent was removed under reduced pressure. The product was purified by recrystallization from 5 mL EtOAc.

Yield: 150 mg (0.59 mmol, 75 % o. th.), bright yellow solid

$C_{38}H_{30}O_4S$ [582.71 g/mol]

HR-MS (EI: [M]) [*m/z*]: calculated: 582.1865, found: 582.1851

mp: 147-151 °C

R_f = 0.10 (cyclohexane/EtOAc = 3:1 (v/v)), (366 nm)

^{1}H-NMR (300.36 MHz, $CDCl_3$): δ = 8.11-8.20 (m, 4H, H-9, H-14, H-25, H-30), 8.08 (d, 2H, $^3J_{HH}$ = 7.4 Hz, H-15, H-24), 8.01 (d, 2H, $^3J_{HH}$ = 8.9 Hz, H-1, H-38), 7.90-7.99 (m, 8H, H-2, H-6, H-11, H-16, H-23, H-28, H-33, H-37), 7.76 (d, 2H, H-8, H-31), 5.05 (s, 4H, H-17, H-22), 3.98 (t, 4H, $^3J_{HH}$ = 5.5 Hz, H-18, H-21), 3.38 (t, 4H, $^3J_{HH}$ = 5.5 Hz, H-19, H-20).

^{13}C{H}-NMR (75.53 MHz, $CDCl_3$): δ = 131.6 (C-13, C-26), 131.3 (C-4, C-35), 130.8 (C-3, C-36), 130,3 (C-12, C-27), 129.4 (C-5, C-34), 128.0 (C-16, C-23), 127.7 (C-6, C-33), 127.4 (C-1, C-38), 127.1 (C-8, C-31), 126.1 (C-11, C-28), 125.4 (C-14, C-15, C-24, C-25), 125.0 (C-7, C-32), 124.7 (C-10, C-29), 124.6 (C-2, C-37), 123.3 (C-9, C-30), 71.9 (C-17, C-22), 64.2 (C-18, C-21), 55.2 (C-19, C-20).

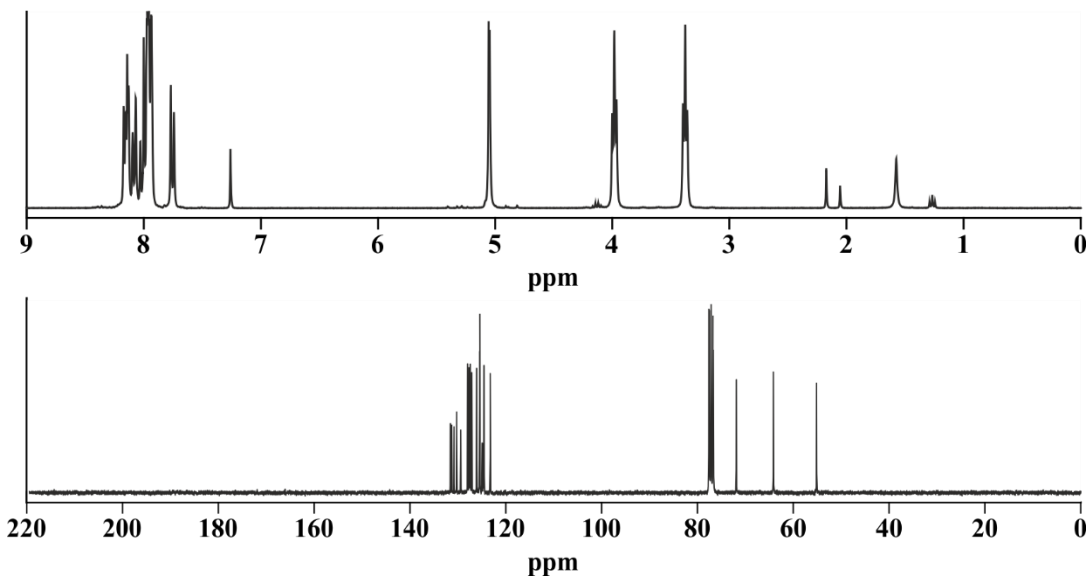

7.5.17.2. 1-Methoxy-2-(2-((2-(2-methoxyethoxy)ethyl)sulfonyl)ethoxy)ethane (**5**)

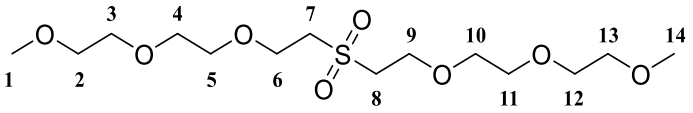

A 25 mL round bottom flask equipped with a TEFLON®-coated magnetic stirring bar was charged with 357 µL (3.00 mmol, 3.0 eq) 2-(2-methoxyethoxy)ethanol, 1.66 g (5.09 mmol, 5.0 eq) Cs_2CO_3 and 10 mL DCM. The colorless suspension was stirred for 5 min at RT. Then 100 µL (1.00 mmol, 1.0 eq) divinyl sulfone were added and the colorless solution was stirred over the weekend at RT. The reaction control was performed by TLC. Afterwards the reaction mixture was diluted with 25 mL EtOAc and transferred into a separatory funnel. The organic phase was washed with H_2O (1 × 10 mL) and sat. $NaHCO_3$ (2 × 15 mL). The aqueous phase was reextracted with EtOAc (3 × 20 mL). Then the combined organic phases were washed with brine (1 × 20 mL). Subsequently the organic phase was dried over Na_2SO_4, filtered and the solvent was removed under reduced pressure. The product was purified *via* flash column chromatography (35 g SiO_2 100 × 25 mm, eluent: EtOAc/MeOH = 150:1 (v/v), fraction size: 20 mL, detection: $KMnO_4$).

Yield: 100 mg (0.28 mmol, 28 % o. th.), bright yellow oil

$C_{14}H_{30}O_8S$ [358.45 g/mol]

HR-MS (MALDI: [M+Na]) [*m/z*]: calculated: 381.1559, found: 381.1526

R_f = 0.41 (EtOAc/MeOH = 10:1 (v/v)), ($KMnO_4$)

^{1}H-NMR (300.36 MHz, $CDCl_3$): δ = 3.91 (t, 4H, $^3J_{HH}$ = 5.7 Hz, H-6, H-9), 3.64 (s, 8H, H-4, H-5, H-10, H-11), 3.60-3.64 (m, 4H, H-3, H-12), 3.53 (m, 4H, H-2, H-13), 3.36 (s, 6H, H-1, H-14), 3.35 (t, 4H, $^3J_{HH}$ = 5.7 Hz, H-7, H-8).

^{13}C{H}-NMR (75.53 MHz, $CDCl_3$): δ = 72.1 (C-2, C-13), 70.6 (C-5, C-10), 70.6 (C-4, C-11), 70.5 (C-3, C-12), 64.8 (C-6, C-9), 59.1 (C-1, C-14), 55.0 (C-7, C-8).

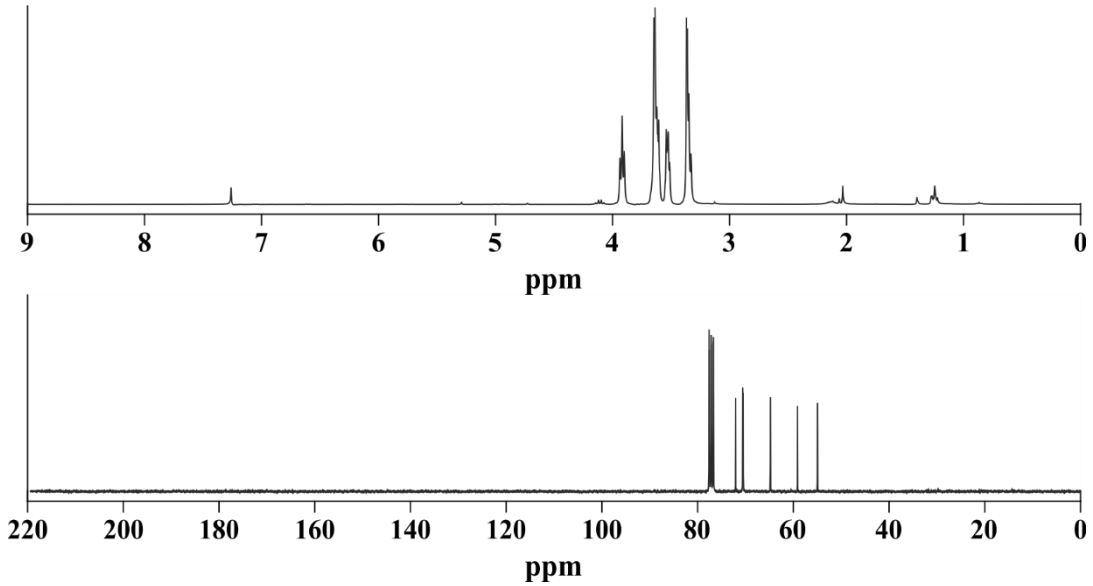

7.5.17.3. Pyren-1-ylmethanol (**6**)

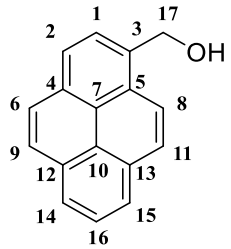

An oven dried 25 mL SCHLENK flask equipped with a TEFLON®-coated magnetic stirring bar was charged with 1.00 mL (8.10 mmol, 1.0 eq) *N*-methylformanilide. Then 760 µL (8.32 mmol, 1.1 eq) phosphoroxychloride were added and the reaction mixture was stirred for 15 min at RT under nitrogen atmosphere. In the meanwhile, the reaction mixture turned yellowish. Afterwards 1.62 g (8.00 mmol, 1.0 eq) pyrene were added in small portions. The reaction mixture turned orange immediately. Subsequently the orange suspension was heated to 100 °C for 6 h under nitrogen. During the heating process the solid dissolved and the color of the solution turned brownish. After 1.5 h a brown solid precipitated. When the heating process of 6 h was finished, 5 mL of ice-water were poured onto the brown solid. Thereby the solid changed the color into yellow. The yellow solid was filtered, washed with 10 mL of ice-water and dried. Afterwards a 100 mL round bottom flask equipped with a TEFLON®-coated magnetic stirring bar was charged with 1.60 g crude product and 50 mL THF. 320 mg (8.32 mmol, 1.1 eq) $NaBH_4$ were dissolved in 40 mL MeOH and the $NaBH_4$-solution was added to the reaction mixture. The yellow reaction mixture was stirred for 16 h at RT and the reaction control was performed by TLC. Then the reaction mixture was diluted with 25 mL of EtOAc and transferred into a separatory funnel. The organic phase was washed with 1 M HCl

(1 × 20 mL) and sat. $NaHCO_3$ (3 × 15 mL). The aqueous phase was reextracted with EtOAc (3 × 20 mL). Then the combined organic phases were washed with brine (1 × 20 mL). Subsequently the organic phase was dried over Na_2SO_4, filtered and the solvent was removed under reduced pressure. The product was purified *via* flash column chromatography (40 g SiO_2 100 × 25 mm, eluent: cyclohexane then DCM, fraction size: 20 mL, detection: 366 nm).

Yield: 1.16 g (4.97 mmol, 62 % o. th.), yellow solid

$C_{17}H_{12}O$ [232.28 g/mol]

mp: 125-130 °C

R_f = 0.25 (cyclohexane/EtOAc = 3:1 (v/v)), (366 nm)

^{1}H-NMR (300.36 MHz, $CDCl_3$): δ = 8.38 (d, 1H, $^3J_{HH}$ = 9.3 Hz, H-9), 8.13-8.24 (m, 4H, H-2, H-6, H-14, H-15), 7.99-8.10 (m, 4H, H-1, H-8, H-11, H-16), 5.41 (d, 2H, $^3J_{HH}$ = 5.4 Hz, H-17), 1.87 (t, 1H, $^3J_{HH}$ = 5.4 Hz, OH).

^{13}C{H}-NMR (75.53 MHz, $CDCl_3$): δ = 133.9 (C-3), 131.4 (C-4), 131.4 (C-13), 130.9 (C-12), 129.0 (C-5), 128.1 (C-8), 127.6 (C-16), 127.5 (C-11), 126.2 (C-2), 126.2 (C-1), 125.5 (C-14), 125.4 (C-15), 125.1 (C-7), 124.9 (C-10), 124.9 (C-6), 123.2 (C-9), 64.0 (C-17).

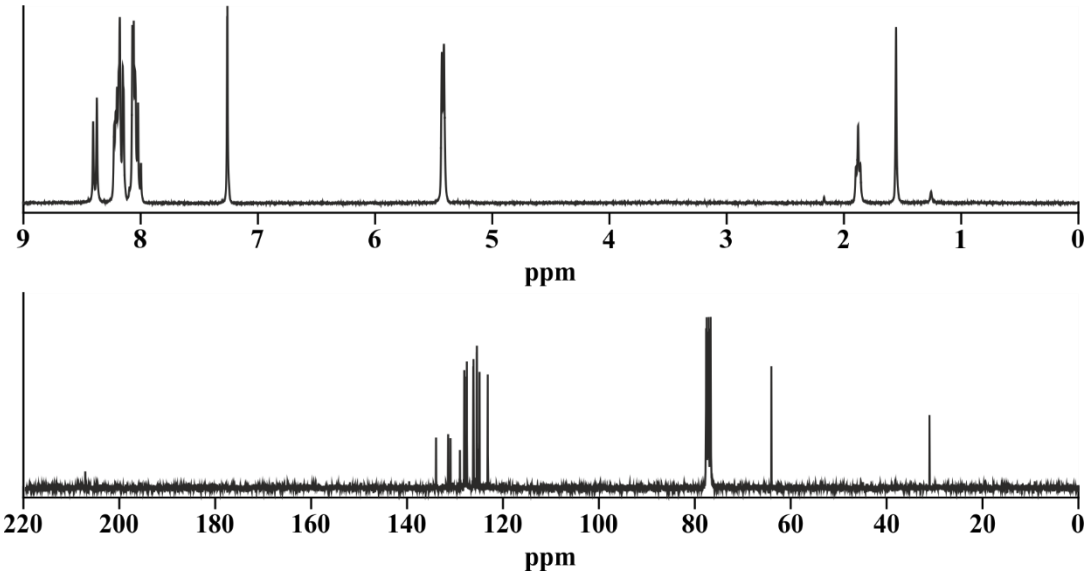

7.5.17.4. 1-(Pyren-1-yl)-2,5,8,11-tetraoxadodecane (**7**)

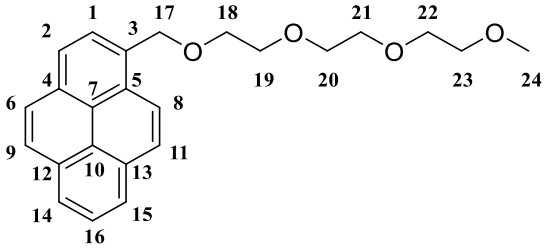

An oven dried 25 mL SCHLENK flask equipped with a TEFLON®-coated magnetic stirring bar was charged with 131 mg (0.56 mmol, 1.5 eq) pyren-1-ylmethanol, 63 mg (0.56 mmol, 1.5 eq) potassium *tert*-butoxide and 50 mg (0.30 mmol, 0.7 eq) potassium iodide under nitrogen atmosphere. The reagents were dried in oil pump vacuum at 10^{-2} mbar for 10 min. Afterwards 15 mL of absolute THF were added and the yellow suspension was stirred for further 5 min. Then 124 mg (0.39 mmol, 1.0 eq) 2-(2-(2-methoxyethoxy)ethoxy)ethyl 4-methylbenzene-sulfonate were slowly added to the yellow suspension and the reaction mixture was heated to reflux for 20 h under nitrogen. The reaction control was performed by NMR-spectroscopy. After cooling to RT, the reaction mixture was diluted with 25 mL of EtOAc and transferred into a separatory funnel. The organic phase was washed with 1 M HCl (3 × 15 mL). Subsequently the aqueous phase was reextracted with EtOAc (3 × 15 mL). The combined organic phases were washed with brine (1 × 20 mL), dried over Na_2SO_4, filtered and the solvent was removed under reduced pressure. The product was purified *via* flash column chromatography (30 g SiO_2 150 × 20 mm, eluent: EtOAc/toluene = 1:1 (v/v), fraction size: 15 mL, detection: 366 nm; $KMnO_4$).

Yield: 94 mg (0.25 mmol, 66 % o. th.), brown oil

$C_{24}H_{26}O_4$ [378.47 g/mol]

HR-MS (EI: [M]) [*m/z*]: calculated: 378.1831, found: 378.1798

Mp: 39 °C

R_f = 0.18 (EtOAc/toluene = 1:1 (v/v)), (366 nm; $KMnO_4$)

^{1}H-NMR (300.36 MHz, $CDCl_3$): δ = 8.41 (d, 1H, $^3J_{HH}$ = 9.2 Hz, H-9), 8.11-8.23 (m, 4H, H-2, H-6, H-14, H-15), 7.97-8.07 (m, 4H, H-1, H-8, H-11, H-16), 5.29 (s, 2H, H-17), 3.72-3.76 (m, 2H, H-18), 3.70-3.72 (m, 2H, H-19), 3.67 (s, 4H, H-20, H-21), 3.60-3.64 (m, 2H, H-22), 3.49-3.52 (m, 2H, H-23), 3.35 (s, 3H, H-24).

^{13}C{H}-NMR (75.53 MHz, $CDCl_3$): δ = 131.6 (C-4), 131.4 (C-3), 131.4 (C-13), 131.0 (C-12), 129.5 (C-5), 127.8 (C-6), 127.5 (C-8), 127.4 (C-11), 127.2 (C-1), 126.0 (C-16), 125.4 (C-14, C-15), 125.1 (C-10), 124.9 (C-7), 124.6 (C-2), 123.7 (C-9), 72.1 (C-23), 72.0 (C-17), 71.9 (C-19), 70.8 (C-21), 70.8 (C-20), 70.7 (C-22), 69.7 (C-18), 59.1 (C-24).

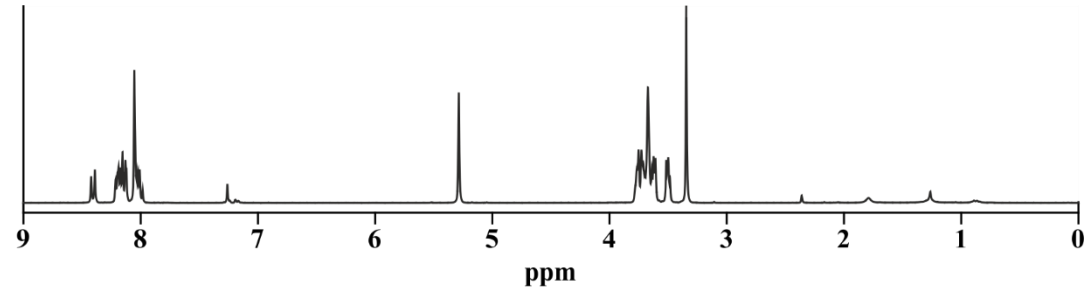

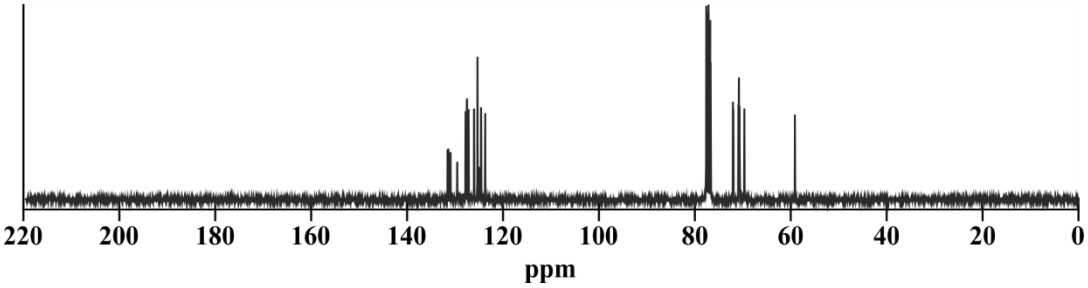

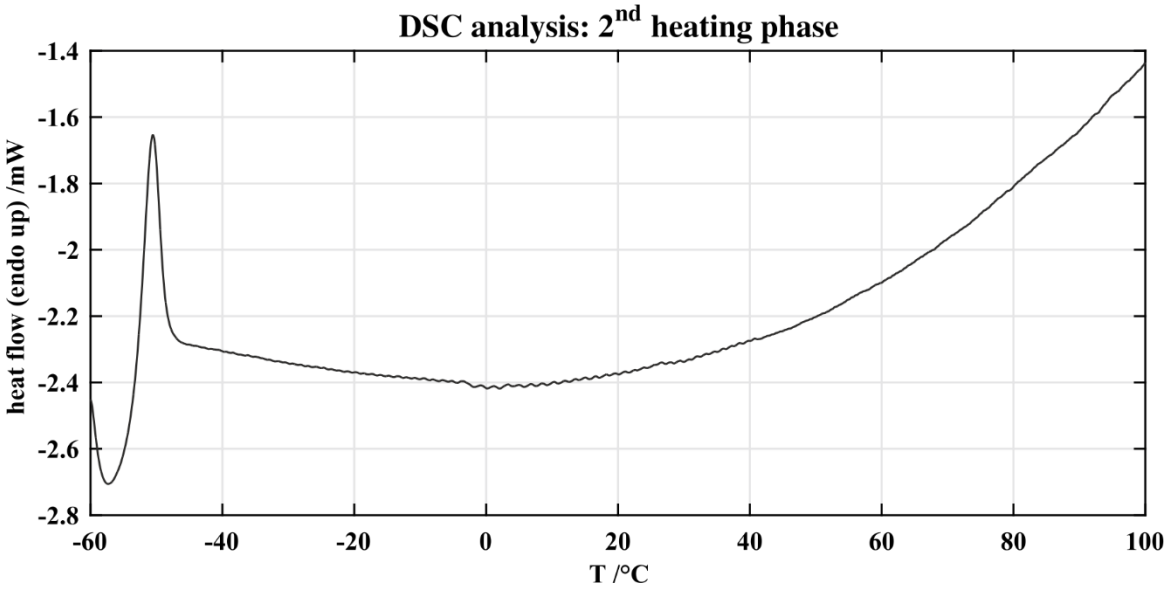

7.5.17.5. 1-(2-(2-(2-Methoxyethoxy)ethoxy)ethoxy)pyrene (**8**)

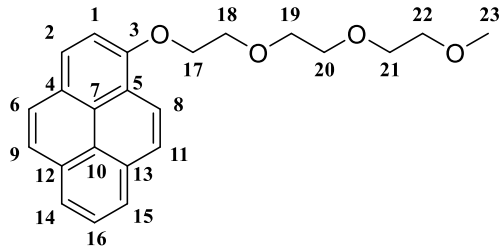

An oven dried 100 mL SCHLENK flask equipped with a TEFLON®-coated magnetic stirring bar was charged with 134 mg (0.61 mmol, 1.5 eq) 1-hydroxypyrene, 78 mg (0.70 mmol, 1.7 eq) potassium *tert*-butoxide and 51 mg (0.30 mmol, 0.8 eq) potassium iodide under nitrogen atmosphere. The reagents were dried in oil pump vacuum at 10^{-2} mbar for 10 min. Afterwards 15 mL of absolute THF were added and the orange suspension was stirred for further 5 min. Then 129 mg (0.41 mmol, 1.0 eq) 2-(2-(2-methoxyethoxy)ethoxy)ethyl 4-methylbenzene-sulfonate were slowly added to the orange suspension and the reaction mixture was heated to reflux for 20 h under nitrogen. The reaction control was performed by NMR-spectroscopy. After cooling to RT, the reaction mixture was diluted with 25 mL of EtOAc and transferred into a separatory funnel. The organic phase was washed with 1 M HCl (3 × 20 mL). Subsequently the aqueous phase was reextracted with EtOAc (3 × 15 mL). The combined organic phases were washed with brine (1 × 20 mL), dried over Na_2SO_4, filtered and the solvent was removed under reduced pressure. The product was purified *via* flash column chromatography (30 g SiO_2 150 × 20 mm, eluent: EtOAc/toluene = 1:2 (v/v), fraction size: 15 mL, detection: 366 nm; $KMnO_4$).

Yield: 142 mg (0.39 mmol, 96 % o. th.), brown oil

$C_{23}H_{24}O_4$ [364.44 g/mol]

HR-MS (EI: [M]) [*m/z*]: calculated: 364.1674, found: 364.1669

ρ (20 °C) = 1.19 g/mL

R_f = 0.36 (EtOAc/toluene = 1:1 (v/v)), (366 nm; $KMnO_4$)

Θ_{Carbon} = 18.6 ± 0.65 °

$\Theta_{Silicon}$ = 40.5 ± 4.15 °

Θ_{Gold} = 50.5 ± 2.43 °

^{1}H-NMR (300.36 MHz, $CDCl_3$): δ = 8.48 (d, 1H, $^{3}J_{HH}$ = 9.3 Hz, H-6), 8.06-8.14 (m, 3H, H-2, H-14, H-15), 8.04 (d, 1H, $^{3}J_{HH}$ = 9.3 Hz, H-9), 7.92-8.00 (m, 2H, H-11, H-16), 7.89 (d, 1H, $^{3}J_{HH}$ = 9.1 Hz, H-8), 7.56 (d, 1H, H-1), 4.50 (t, 2H, $^{3}J_{HH}$ = 4.9 Hz, H-17), 4.07 (t, 2H, $^{3}J_{HH}$ = 4.9 Hz, H-18), 3.86 (t, 2H, $^{3}J_{HH}$ = 5.1 Hz, H-19), 3.74 (t, 2H, $^{3}J_{HH}$ = 5.1 Hz, H-20), 3.67 (t, 2H, $^{3}J_{HH}$ = 4.8 Hz, H-21), 3.54 (t, 2H, $^{3}J_{HH}$ = 4.8 Hz, H-21), 3.37 (s, 3H, H-23).

^{13}C{H}-NMR (75.53 MHz, $CDCl_3$): δ = 153.0 (C-3), 131.9 (C-13), 131.8 (C-12), 127.4 (C-11), 126.5 (C-9), 126.2 (C-16), 126.0 (C-10), 125.6 (C-7), 125.6 (C-2), 125.3 (C-8), 125.0 (C-4), 124.4 (C-15), 124.3 (C-14), 121.5 (C-6), 120.8 (C-5), 109.7 (C-1), 72.1 (C-22), 71.2 (C-19), 70.9 (C-20), 70.8 (C-21), 70.2 (C-18), 68.9 (C-17), 59.2 (C-23).

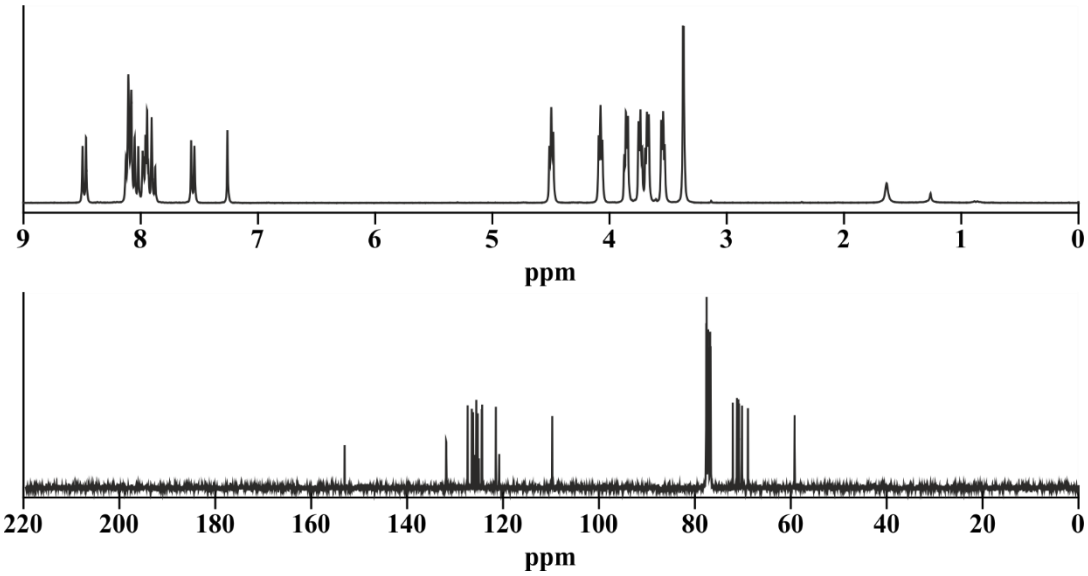

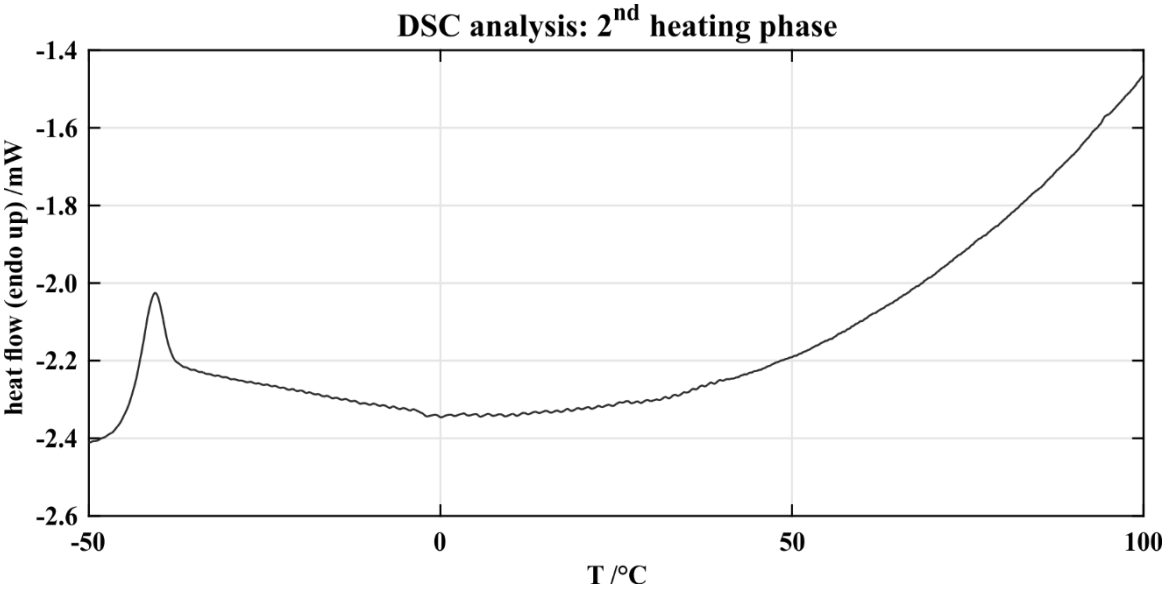

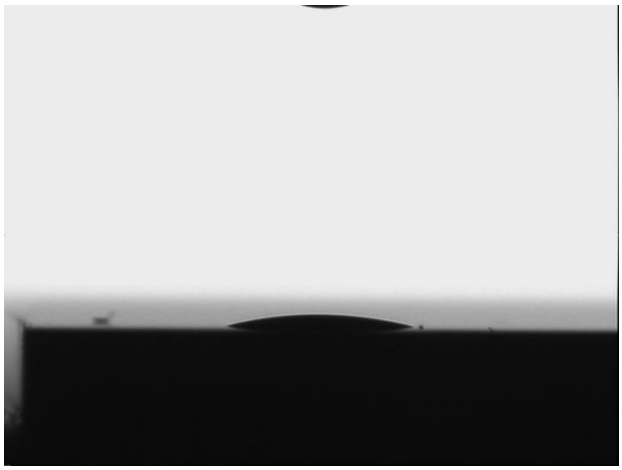

7.5.17.6. 1-(Pyren-1-yl)ethan-1-one

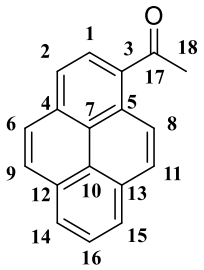

An oven dried 100 mL SCHLENK flask equipped with a TEFLON®-coated magnetic stirring bar was charged with 3.00 g (14.8 mmol, 1.0 eq) pyrene, 1.12 mL (15.6 mmol, 1.1 eq) acetyl chloride and 40 mL of absolute DCM under nitrogen atmosphere. The yellow solution was cooled in an ice-water bath and stirred at 0 °C for 10 min. Then 2.37 g (17.8 mmol, 1.2 eq) aluminum chloride were added in small portions to the cooled reaction mixture. During the addition of aluminum chloride, the reaction mixture turned brown. After 10 min of stirring at 0 °C the reaction mixture was allowed to warm to RT and was further stirred for 16 h under nitrogen. The reaction control was performed by NMR spectroscopy. Then 100 mL of saturated $NaHCO_3$ were added to the reaction mixture. The generated precipitate was filtered off and the filter cake was washed with 50 mL of DCM. Afterwards the phases were separated and the aqueous phase was washed with DCM (4 × 20 mL). The combined organic phases were washed with brine (1 × 20 mL). Subsequently the organic phase was dried over Na_2SO_4, filtered and the solvent was removed under reduced pressure. The product was purified *via* flash column chromatography (150 g SiO_2 400 × 50 mm, eluent: cyclohexane then DCM, fraction size: 70 mL, detection: 366 nm; $KMnO_4$).

Yield: 2.61 g (10.7 mmol, 72 % o. th.), yellow solid

$C_{18}H_{12}O$ [244.29 g/mol]

mp: 83-85 °C

R_f = 0.28 (cyclohexane/DCM = 1:1 (v/v)), (366 nm; $KMnO_4$)

^{1}H-NMR (300.36 MHz, $CDCl_3$): δ = 9.08 (d, 1H, $^3J_{HH}$ = 9.4 Hz, H-6), 8.38 (d, 1H, $^3J_{HH}$ = 8.1 Hz, H-11), 8.19-8.29 (m, 3H, H-9, H-14, H-15), 8.17 (d, 2H, H-2, H-8), 8.02-8.09 (m, 2H, H-1, H-16), 2.91 (s, 3H, H-18).

^{13}C{H}-NMR (75.53 MHz, $CDCl_3$): δ = 202.3 (C-17), 134.2 (C-4), 132.1 (C-3), 131.2 (C-13), 130.7 (C-5), 129.9 (C-9), 129.8 (C-8), 129.6 (C-12), 127.3 (C-11), 127.2 (C-1), 126.5 (C-16), 126.5 (C-14), 126.2 (C-15), 125.1 (C-6, C-7), 124.4 (C-10), 124.1 (C-2), 30.6 (C-18).

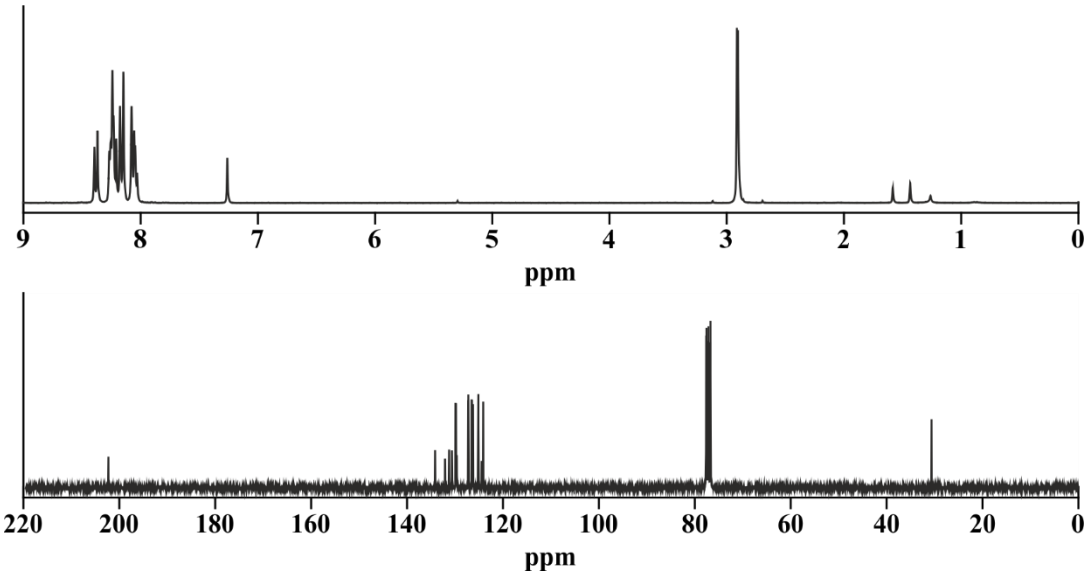

7.5.17.7. 1-Hydroxypyrene (**9**)

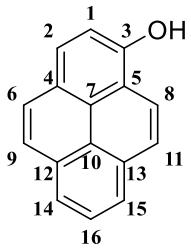

A 100 mL round bottom flask equipped with a TEFLON®-coated magnetic stirring bar was charged with 2.05 g (13.3 mmol, 3.3 eq) sodium perborate tetrahydrate and 25 mL of glacial acetic acid. The colorless suspension was for 10 min at RT. Then 1.00 g (4.09 mmol, 1.0 eq) 1-(pyren-1-yl)ethan-1-one were added in small portions to the reaction mixture. The reaction mixture was stirred for 2 d at RT. During the reaction the color of the suspension turned orange. The reaction control was performed by NMR spectroscopy. Afterwards the reaction mixture was diluted with 50 mL of EtOAc and transferred into a separatory funnel. The organic phase

was washed with sat. $NaHCO_3$ (3 × 100 mL). The aqueous phase was reextracted with EtOAc (4 × 30 mL). Then the combined organic phases were washed with brine (1 × 20 mL). Subsequently the organic phase was dried over Na_2SO_4, filtered and the solvent was removed under reduced pressure. Afterwards a 250 mL round bottom flask equipped with a TEFLON®-coated magnetic stirring bar was charged with the isolated crude product, 50 mL THF and 40 mL MeOH. To the brown reaction mixture 10 mL (20.9 mmol, 5.1 eq) 2.1 M NaOH-solution were slowly added. During the addition of the NaOH-solution the color of the reaction mixture became darker. The reaction mixture was stirred overnight at RT. Afterwards most of the solvent was removed under reduced pressure. The residual was dissolved with 100 mL DCM and afterwards the reaction mixture was washed with 1 M HCl (3 × 30 mL). The aqueous phase was reextracted with DCM (3 × 20 mL) and the combined organic phases were washed with brine (1 × 25 mL). Then the organic phase was dried over Na_2SO_4, filtered and the solvent was removed under reduced pressure. Finally, the dark violet solid was dried in oil pump vacuum at 10^{-2} mbar.

Yield: 831 mg (3.80 mmol, 93 % o. th.), dark violet solid

$C_{16}H_{10}O$ [218.26 g/mol]

mp: 171-173 °C

R_f = 0.35 (cyclohexane/EtOAc = 3:1 (v/v)), (366 nm; $KMnO_4$)

^{1}H-NMR (499.88 MHz, $CDCl_3$): δ = 8.34 (d, 1H, $^3J_{HH}$ = 9.5 Hz, H-6), 8.11 (d, 2H, H-14, H-15), 8.05 (d, 1H, $^3J_{HH}$ = 9.5 Hz, H-9), 8.03 (m, 1H, $^3J_{HH}$ = 8.4 Hz, H-2), 7.94-8.00 (m, 2H, H-11, H-16), 7.90 (d, 1H, $^3J_{HH}$ = 9.2 Hz, H-8), 7.47 (d, 1H, $^3J_{HH}$ = 8.5 Hz, H-1), 5.51 (bs, 1H, OH).

^{13}C{H}-NMR (125.70 MHz, $CDCl_3$): δ = 149.8 (C-3), 131.9 (C-12), 131.8 (C-13), 127.4 (C-11), 126.7 (C-9), 126.3 (C-16), 126.2 (C-7), 125.8 (C-10), 125.7 (C-2), 125.1 (C-8), 124.6 (C-4), 124.4 (C-14, C-15), 120.6 (C-6), 118.8 (C-5), 113.2 (C-1).

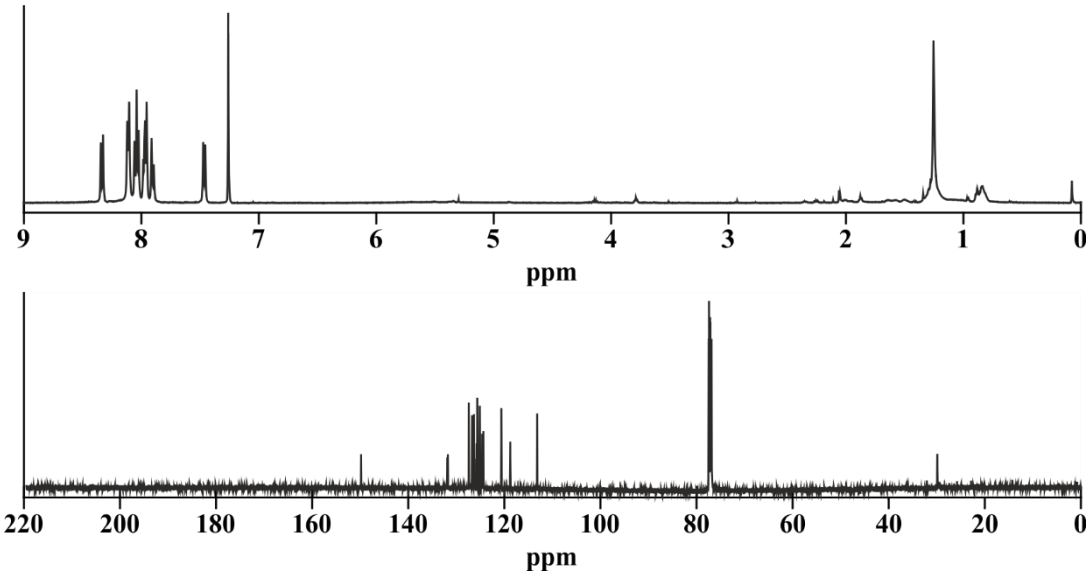

7.5.17.8. 1-(2-(2-(2-Methoxyethoxy)ethoxy)ethoxy)-3-nitrobenzene (**15a**)

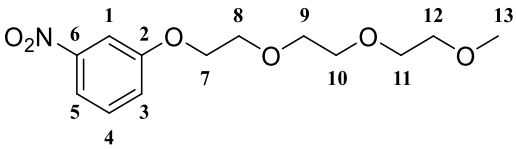

An oven dried 100 mL SCHLENK flask equipped with a TEFLON®-coated magnetic stirring bar was charged with 324 mg (2.33 mmol, 1.5 eq) 3-nitrophenol, 300 mg (2.67 mmol, 1.7 eq) potassium *tert*-butoxide, 240 mg (1.44 mmol, 0.9 eq) potassium iodide and 20 mL of absolute THF under nitrogen atmosphere. The orange suspension was stirred for 10 min at RT. Afterwards 500 mg (1.57 mmol, 1.0 eq) 2-(2-(2-methoxyethoxy)ethoxy)ethyl 4-methyl-benzenesulfonate were added and the orange suspension was heated to reflux for 20 h under nitrogen. During the heating process the suspension turned reddish. The reaction control was performed by NMR-spectroscopy. After cooling to RT the reaction mixture was diluted with 20 mL of EtOAc and transferred into a separatory funnel. The organic phase was washed with 1 M HCl (3 × 10 mL). Subsequently the aqueous phase was reextracted with EtOAc (3 × 15 mL). The combined organic phases were washed with brine (1 × 20 mL), dried over Na_2SO_4, filtered and the solvent was removed under reduced pressure. The product was purified *via* flash column chromatography (35 g SiO_2 300 × 25 mm, eluent: EtOAc/cyclohexane = 1:1 (v/v), fraction size: 25 mL, detection: 254 nm; $KMnO_4$).

Yield: 422 mg (1.48 mmol, 94 % o. th.), yellow oil

$C_{13}H_{19}NO_6$ [285.30 g/mol]

HR-MS (EI: [M]) [*m/z*]: calculated: 285.1212, found: 285.1221

R_f = 0.39 (EtOAc/cyclohexane = 2:1 (v/v)), (254 nm; $KMnO_4$)

^{1}H-NMR (300.36 MHz, $CDCl_3$): δ = 7.82 (dd, 1H, $^3J_{HH}$ = 8.1 Hz, H-5), 7.75 (t, 1H, $^4J_{HH}$ = 2.3 Hz, H-1), 7.41 (t, 1H, $^3J_{HH}$ = 8.1 Hz, H-4), 7.25 (dd, 1H, $^3J_{HH}$ = 8.1 Hz, $^4J_{HH}$ = 2.3 Hz, H-3), 4.20 (t, 2H, $^3J_{HH}$ = 4.8 Hz, H-7), 3.89 (t, 2H, $^3J_{HH}$ = 4.8 Hz, H-8), 3.73-3.75 (m, 2H, H-10), 3.67-3.69 (m, 2H, H-9), 3.63-3.66 (m, 2H, H-11), 3.53-3.55 (m, 2H, H-12), 3.37 (s, 3H, H-13).

^{13}C{H}-NMR (75.53 MHz, $CDCl_3$): δ = 159.4 (C-2), 149.2 (C-6), 129.9 (C-4), 121.8 (C-3), 115.9 (C-5), 109.0 (C-1), 72.0 (C-12), 70.9 (C-10), 70.7 (C-9), 70.6 (C-11), 69.5 (C-8), 68.2 (C-7), 59.1 (C-13).

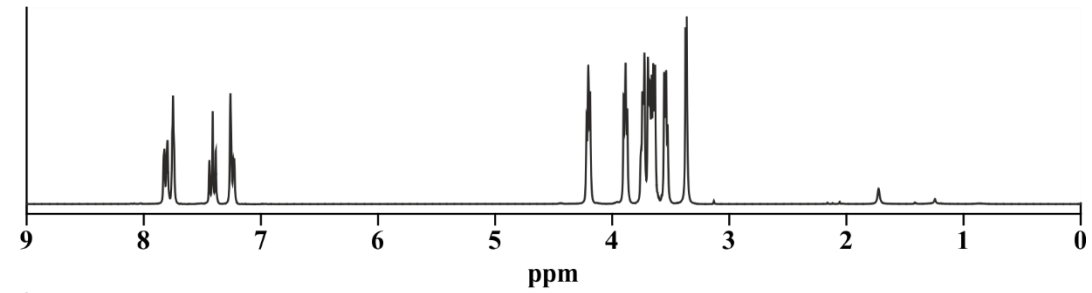

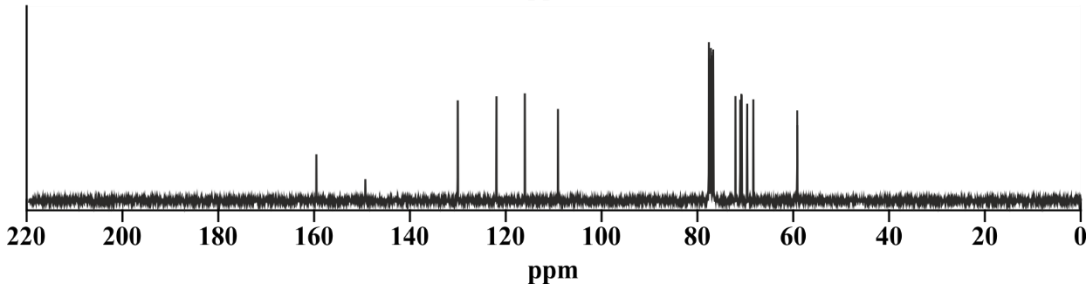

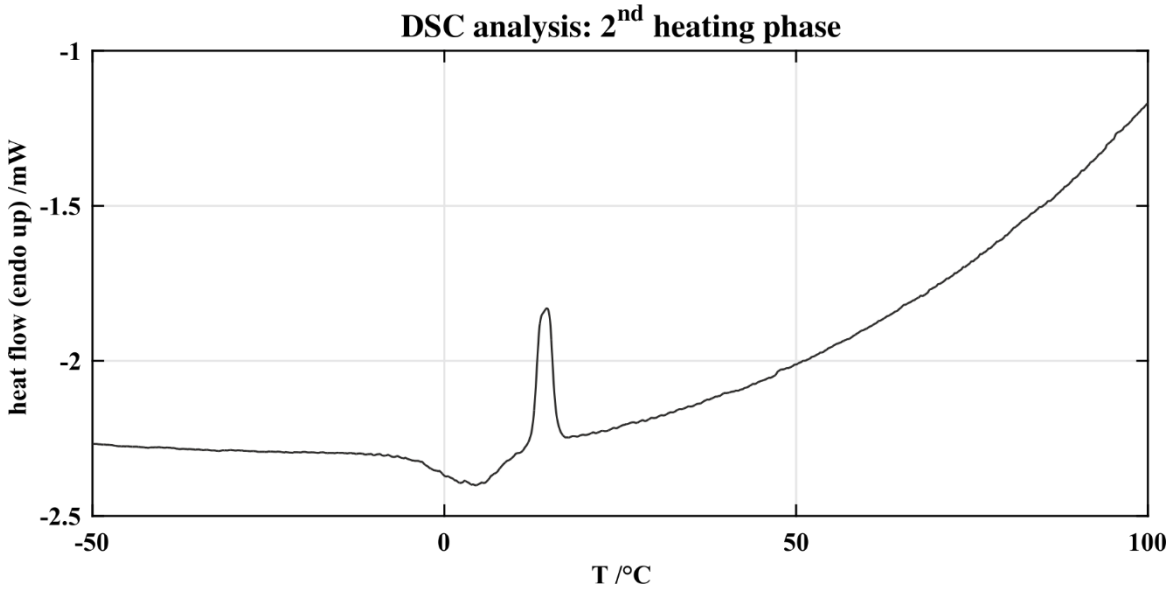

7.5.17.9. 1-(2-(2-(2-Methoxyethoxy)ethoxy)ethoxy)-4-nitrobenzene (**15b**)

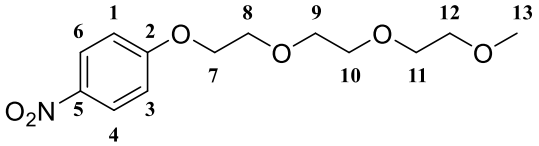

An oven dried 100 mL SCHLENK flask equipped with a TEFLON®-coated magnetic stirring bar was charged with 648 mg (4.66 mmol, 1.5 eq) 4-nitrophenol, 600 mg (5.35 mmol, 1.7 eq) potassium *tert*-butoxide, 400 mg (2.41 mmol, 0.7 eq) potassium iodide and 40 mL of absolute THF under nitrogen atmosphere. The orange suspension was stirred for 10 min at RT. Afterwards 1.00 g (3.14 mmol, 1.0 eq) 2-(2-(2-methoxyethoxy)ethoxy)ethyl 4-methylbenzene-sulfonate were added and the orange suspension was heated to reflux for 2 d under nitrogen. During the heating process, the suspension turned yellowish. The reaction control was performed by NMR-spectroscopy. After cooling to RT, the reaction mixture was diluted with 50 mL of EtOAc and transferred into a separatory funnel. The organic phase was washed with 1 M HCl (3 × 20 mL). Subsequently the aqueous phase was reextracted with EtOAc (3 × 15 mL). The combined organic phases were washed with brine (1 × 20 mL), dried over Na_2SO_4, filtered and the solvent was removed under reduced pressure. The product was purified *via* flash column chromatography (70 g SiO_2 300 × 25 mm, eluent: EtOAc/cyclohexane = 2:1 (v/v), fraction size: 25 mL, detection: 254 nm; $KMnO_4$).

Yield: 496 mg (1.73 mmol, 55 % o. th.), yellow oil

$C_{13}H_{19}NO_6$ [285.30 g/mol]

R_f = 0.22 (EtOAc/cyclohexane = 2:1 (v/v)), (254 nm; $KMnO_4$)

^{1}H-NMR (300.36 MHz, $CDCl_3$): δ = 8.19 (d, 2H, $^3J_{HH}$ = 9.4 Hz, H-5), 6.97 (d, 2H, $^3J_{HH}$ = 9.4 Hz, H-1), 4.22 (t, 2H, $^3J_{HH}$ = 4.8 Hz, H-7), 3.89 (t, 2H, $^3J_{HH}$ = 4.8 Hz, H-8), 3.72-3.75 (m, 2H, H-9), 3.67-3.69 (m, 2H, H-10), 3.63-3.66 (m, 2H, H-11), 3.53-3.55 (m, 2H, H-12), 3.37 (s, 3H, H-13).

^{13}C{H}-NMR (75.53 MHz, $CDCl_3$): δ = 164.0 (C-2), 141.8 (C-5), 126.0 (C-4, C-6), 114.7 (C-3, C-1), 72.1 (C-12), 71.1 (C-9), 70.8 (C-10), 70.7 (C-11), 69.5 (C-8), 68.4 (C-7), 59.2 (C-13).

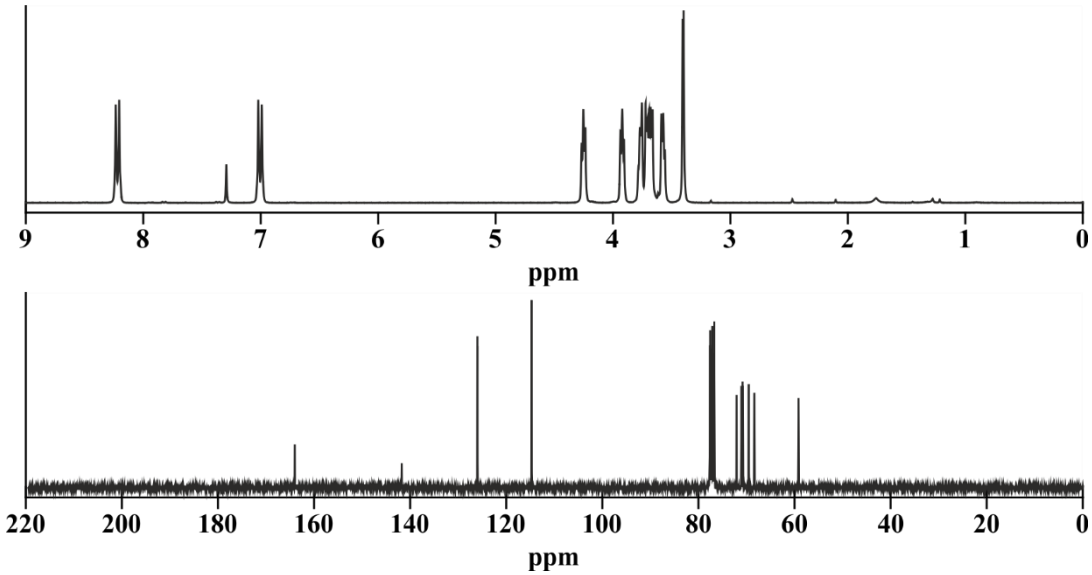

7.5.17.10. 1-(2-(2-(2-Methoxyethoxy)ethoxy)ethoxy)-3-aniline (**16a)**

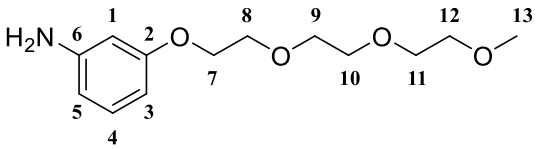

A 100 mL round bottom flask equipped with a TEFLON®-coated magnetic stirring bar was charged with 298 mg (1.04 mmol, 1.0 eq) 1-(2-(2-(2-methoxyethoxy)ethoxy)ethoxy)-3-nitrobenzene, 9.6 mL (57.2 mmol, 55 eq) 6 M HCl and 4.8 mL of methanol. The orange solution was cooled in an ice-water bath and stirred at 0 °C for 10 min. Afterwards 4.76 g (71.5 mmol, 69 eq) zinc were added in small portions at 0 °C. During the addition of zinc, evolution of gas could be observed. After complete addition of zinc, the reaction mixture was stirred at 0 °C for further 10 min. Subsequently the reaction was allowed to warm to RT and stirring was continued for 4 h. The reaction control was performed by NMR-spectroscopy. After cooling to 0 °C saturated $NaHCO_3$-solution was added until pH 9 was reached. Generated precipitates were filtered and washed with 50 mL of DCM. Afterwards the phases were separated and the aqueous phase was washed with DCM (4 × 15 mL). The combined organic phases were washed with brine (1 × 20 mL), dried over Na_2SO_4, filtered and the solvent was removed under reduced pressure. Finally, the orange-brown oil was dried in oil pump vacuum at 10^{-2} mbar.

Yield: 264 mg (1.03 mmol, 99 % o. th.), orange-brown oil

$C_{13}H_{21}NO_4$ [255.31 g/mol]

HR-MS (EI: [M]) [*m/z*]: calculated: 255.1471, found: 255.1462

R_f = 0.18 (EtOAc/cyclohexane = 2:1 (v/v)), (254 nm; $KMnO_4$)

^{1}H-NMR (499.88 MHz, $CDCl_3$): δ = 7.03 (t, 1H, $^3J_{HH}$ = 8.0 Hz, H-4), 6.32 (dd, 1H, $^3J_{HH}$ = 8.0 Hz, $^4J_{HH}$ = 2.0 Hz, H-3), 6.29 (dd, 1H, $^3J_{HH}$ = 8.0 Hz, $^4J_{HH}$ = 1.2 Hz, H-5), 6.27 (t, 1H, $^4J_{HH}$ = 2.1 Hz, H-1), 4.07 (t, 2H, $^3J_{HH}$ = 5.1 Hz, H-7), 3.82 (t, 2H, $^3J_{HH}$ = 5.1 Hz, H-8), 3.71-3.74 (m, 4H, H-9, NH_2), 3.66-3.68 (m, 2H, H-10), 3.63-3.66 (m, 2H, H-11), 3.53-3.56 (m, 2H, H-12), 3.37 (s, 3H, H-13).

^{13}C{H}-NMR (75.53 MHz, $CDCl_3$): δ = 160.0 (C-2), 147.6 (C-6), 130.2 (C-4), 108.3 (C-1), 104.9 (C-3), 102.1 (C-5), 72.1 (C-12), 70.9 (C-9), 70.8 (C-10), 70.7 (C-11), 69.9 (C-8), 67.4 (C-7), 59.1 (C-13).

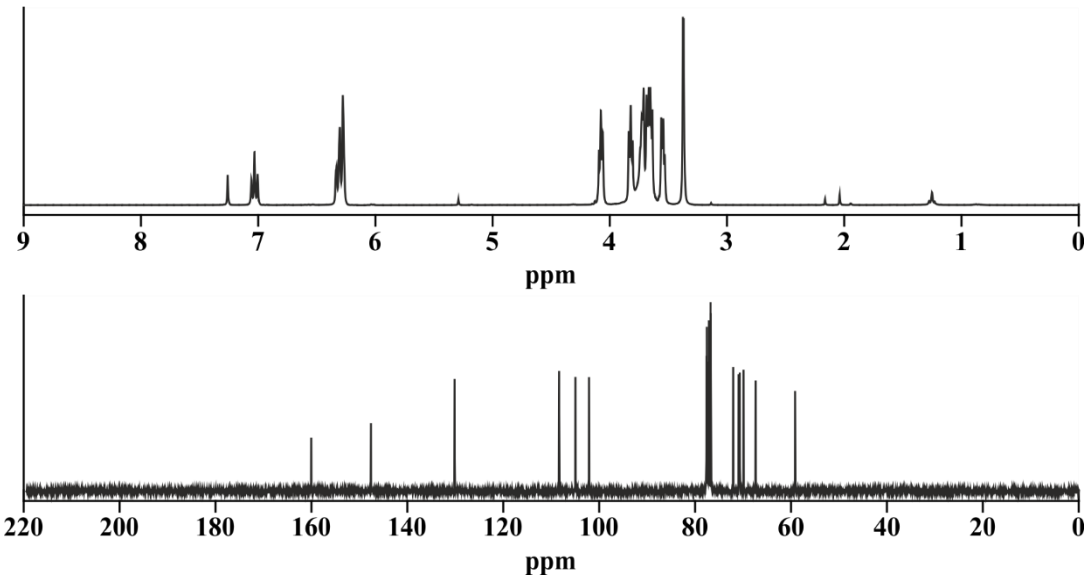

7.5.17.11. 1-(2-(2-(2-Methoxyethoxy)ethoxy)ethoxy)-4-aniline (**16b**)

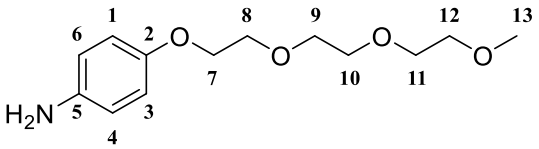

A 100 mL round bottom flask equipped with a TEFLON®-coated magnetic stirring bar was charged with 295 mg (1.03 mmol, 1.0 eq) 1-(2-(2-(2-methoxyethoxy)ethoxy)ethoxy)-3-nitrobenzene, 9.6 mL (57.2 mmol, 55 eq) 6 M HCl and 4.8 mL of methanol. The orange solution was cooled in an ice-water bath and stirred at 0 °C for 10 min. Afterwards 4.76 g (71.5 mmol, 69 eq) zinc were added in small portions at 0 °C . During the addition of zinc, evolution of gas could be observed. After complete addition of zinc, the reaction mixture was stirred at 0 °C for further 10 min. Subsequently the reaction was allowed to warm to RT and stirring was continued for 4 h. The reaction control was performed by NMR-spectroscopy.

After cooling to 0 °C saturated $NaHCO_3$-solution was added until pH 9 was reached. Generated precipitates were filtered and washed with 50 mL of DCM. Afterwards the phases were separated and the aqueous phase was washed with DCM (4 × 15 mL). The combined organic phases were washed with brine (1 × 20 mL), dried over Na_2SO_4, filtered and the solvent was removed under reduced pressure. Finally, the orange-brown oil was dried in oil pump vacuum at 10^{-2} mbar.

Yield: 243 mg (0.95 mmol, 94 % o. th.), orange-brown oil

$C_{13}H_{21}NO_4$ [255.31 g/mol]

R_f = 0.46 (EtOAc/MeOH = 9:1 (v/v)), (254 nm; $KMnO_4$)

^{1}H-NMR (300.36 MHz, $CDCl_3$): δ = 6.76 (d, 2H, $^3J_{HH}$ = 8.7 Hz, H-4, H-6), 6.63 (d, 2H, $^3J_{HH}$ = 8.7 Hz, H-1, H-3), 4.05 (t, 2H, $^3J_{HH}$ = 5.0 Hz, H-7), 3.81 (t, 2H, $^3J_{HH}$ = 5.0 Hz, H-8), 3.71-3.74 (m, 4H, H-9), 3.67-3.69 (m, 2H, H-10), 3.63-3.65 (m, 2H, H-11), 3.53-3.56 (m, 2H, H-12), 3.38-3.55 (bs, NH_2), 3.38 (s, 3H, H-13).

^{13}C{H}-NMR (75.53 MHz, $CDCl_3$): δ = 152.2 (C-2), 140.1 (C-5), 116.5 (C-1, C-3), 116.0 (C-4, C-6), 72.1 (C-12), 70.9 (C-10), 70.8 (C-11), 70.7 (C-9), 70.1 (C-8), 68.3 (C-7), 59.2 (C-13).

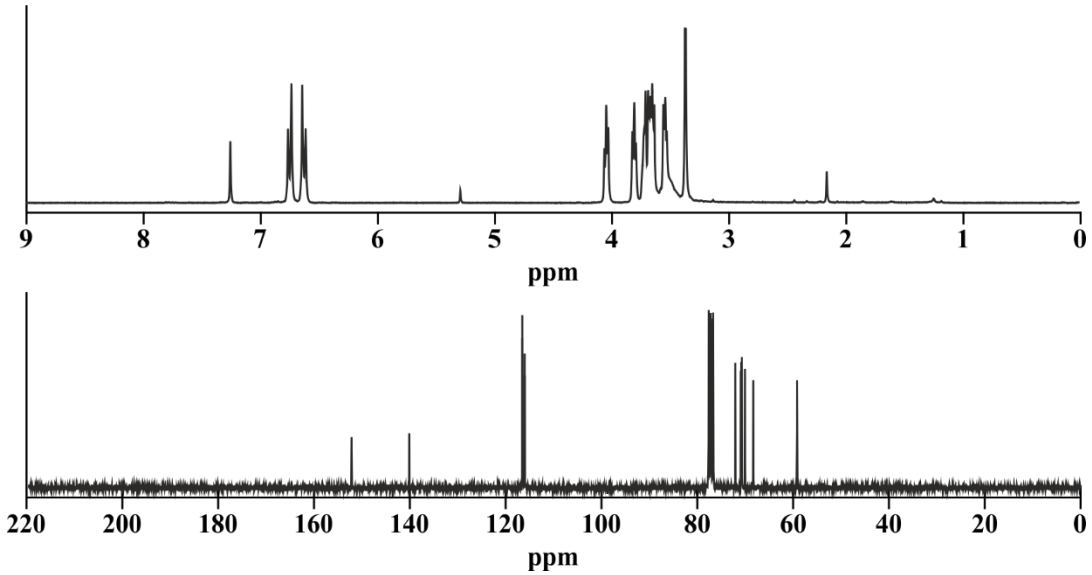

7.5.17.12. Electrochemical polymerization: Preparation of the Monomer

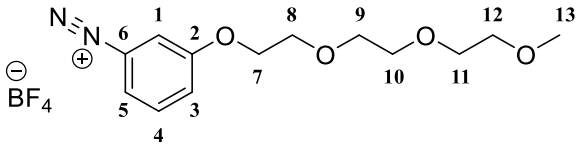

An oven dried 25 mL SCHLENK flask equipped with a TEFLON®-coated magnetic stirring bar was charged with 30.1 mg (0.12 mmol, 1.0 eq) 1-(2-(2-(2-methoxyethoxy)ethoxy)ethoxy)-3-aniline and 1.0 mL of absolute acetonitrile. The brown solution was cooled to –30 °C for 15 min. Afterwards another oven dried 25 mL SCHLENK flask was charged with 13.7 mg (0.12 mmol, 1.0 eq) nitrosyl tetrafluoroborate and 3 mL of absolute acetonitrile. Afterwards the nitrosyl tetrafluoroborate solution was added to the reaction flask over a period of 30 min at –30 °C under nitrogen. During the addition, the color of the reaction mixture turned from brown to red. Afterwards the reaction mixture was further stirred for 1 h at –30 °C under nitrogen. The reaction control was performed by NMR-spectroscopy. After warming to RT the reaction mixture was transferred into an argon filled glovebox and stored over 3 Å for 1 d.

^{1}H-NMR (499.88 MHz, CD_3CN): δ = 7.25 (s, 1H, H-1), 7.19 (t, 1H, $^3J_{HH}$ = 7.8 Hz, H-4), 7.05 (d, 1H, $^3J_{HH}$ = 7.8 Hz, H-5), 6.62 (t, 1H, $^3J_{HH}$ = 7.8 Hz, H-3), 4.07 (t, 2H, $^3J_{HH}$ = 4.7 Hz, H-7), 3.76 (t, 2H, $^3J_{HH}$ = 4.7 Hz, H-8), 3.54-3.59 (m, 6H, H-9, H-10, H-11), 3.45-3.48 (m, 2H, H-12), 3.29 (s, 3H, H-13).

^{13}C{H}-NMR (75.53 MHz, CD_3CN): δ = 160.2 (C-2), 141.4 (C-6), 130.6 (C-4), 112.6 (C-1), 110.3 (C-3), 106.7 (C-5), 72.6 (C-12), 71.4 (C-9), 71.1 (C-10), 71.0 (C-11), 70.3 (C-8), 68.4 (C-7), 58.9 (C-13).

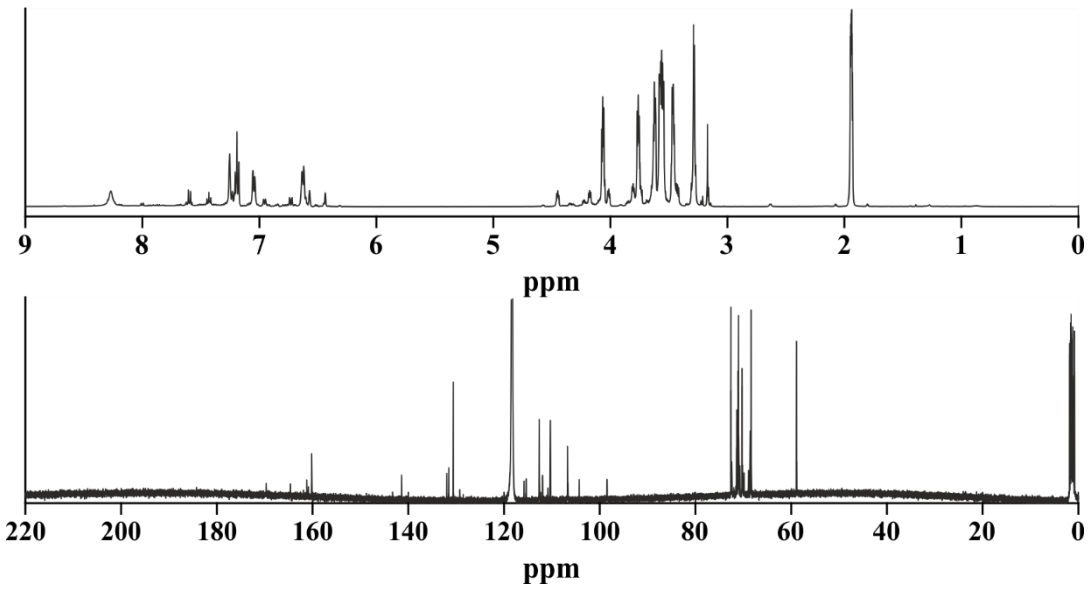

7.5.17.12.1. Polymerization on Flat Electrode: Poly-(2-(2-(2-methoxyethoxy)ethoxy)-ethoxy)phenylene (**17**)

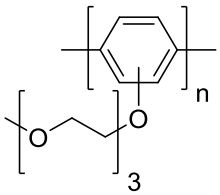

A solution consisting of 0.5 M supporting electrolyte salt (lithium tetrafluoroborate (LiTFSI)) and 30 mM monomer in acetonitrile was filled into a homemade CV-cell. Glassy carbon was used as working electrode material, the counter electrode material was made of platinum and a silber wire was used as a pseudo reference electrode. Ferrocene was used as standard reference material to convert the resulting potentials to Li/Li^+ scale. A scan rate of 10 mV/s was applied.

7.5.17.12.2. Polymerization on Carbon Paper: Poly-(2-(2-(2-methoxyethoxy)ethoxy)-ethoxy)phenylene (**17**)

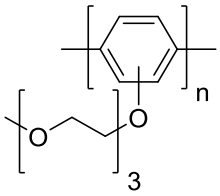

A solution consisting of 0.5 M supporting electrolyte salt (lithium tetrafluoroborate (LiTFSI)) and 30 mM monomer in acetonitrile was filled into an oven dried 50 mL five-necked pear flask. AV-Carbon paper was used as working electrode material, the counter electrode material was made of lithiated lithium iron phosphate (LFP) and a partly delithiated LFP was used as a reference electrode. 10 mV/s was applied.

7.5.17.13. 1-Vinylpyrene (**19**)

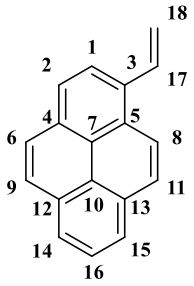

A 500 mL SCHLENK flask equipped with a TEFLON®-coated magnetic stirring bar was charged with 3.17 g (8.69 mmol, 1.0 eq) methyltriphenylphosphonium bromide and 60 mL deoxygenated absolute THF. Afterwards the reaction flask was cooled to –80 °C and 5.90 mL (8.69 mmol, 1.0 eq) 1.47 M *n*-BuLi solution in hexane were added *via* syringe over 10 min. During the addition of *n*-BuLi the color of the reaction mixture changed from colorless to yellowish. The reaction mixture was stirred for 1 h at –40 °C and afterwards a solution of 2.00 g (8.68 mmol, 1.0 eq) 1-pyrenecarbaldehyde in 15 mL deoxygenated absolute THF was added. During the addition of 1pyrenecarbaldehyde, the color of the reaction mixture changed from yellow to orange. The reaction mixture was stirred for 1 h at –40 °C and afterwards the reaction mixture was allowed to warm up to RT and was stirred for 16 h under inert atmosphere. Reaction control was performed by NMR-spectroscopy. The reaction mixture was diluted with 50 mL EtOAc, transferred into a separatory funnel and washed with 1 M HCl (3 × 30 mL). The aqueous phase was reextracted with DCM (3 × 20 mL). The combined organic phases were washed brine (1 × 40 mL), dried over Na_2SO_4, filtered and the solvent was removed under reduced pressure. The product was purified *via* flash column chromatography (60 g SiO_2 300 × 40 mm, eluent: cyclohexane, fraction size: 50 mL, detection: 254 nm).

Yield: 1.27 g (36.9 mmol, 64 % o. th.), yellow solid

$C_{18}H_{12}$ [228.29 g/mol]

R_f = 0.45 (cyclohexane), (254 nm)

mp: 78-87 °C

^{1}H-NMR (300.36 MHz, $CDCl_3$): δ = 8.38 (d, 1H, $^3J_{HH}$ = 9.1 Hz, H-9), 8.14-8.25 (m, 4H, H-1, H-11, H-14, H-15), 7.97-8.14 (m, 4H, H-2, H-6, H-8, H-16), 7.80 (dd, 1H, $^3J_{HH\ trans}$ = 17.0 Hz, $^3J_{HH\ cis}$ = 10.3 Hz, H-17), 6.02 (d, 1H, $^3J_{HH\ trans}$ = 17.0 Hz, H-18), 5.64 (d, 1H, $^3J_{HH\ cis}$ = 10.3 Hz, H-18).

^{13}C{H}-NMR (75.53 MHz, $CDCl_3$): δ = 134.4 (C-17), 132.5 (C-4), 131.6 (C-3), 131.1 (C-12), 131.0 (C-13), 128.2 (C-5), 127.7 (C-2), 127.5 (C-6), 127.4 (C-8), 126.0 (C-16), 125.4 (C-11), 125.1 (C-14, C-15), 125.0 (C-7, C-10), 123.8 (C-1), 123.1 (C-9), 117.3 (C-18).

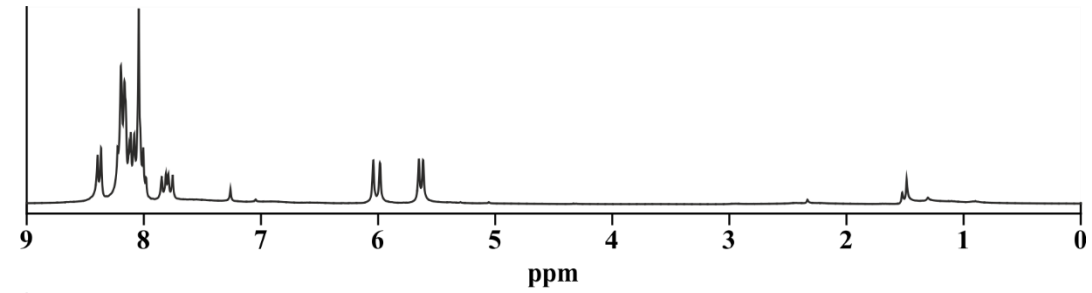

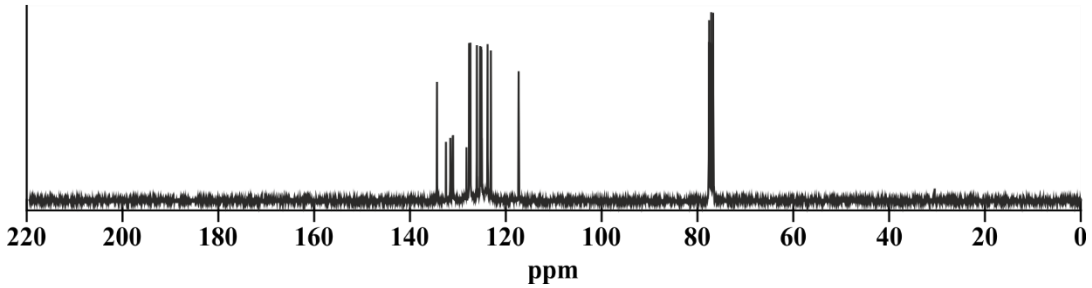

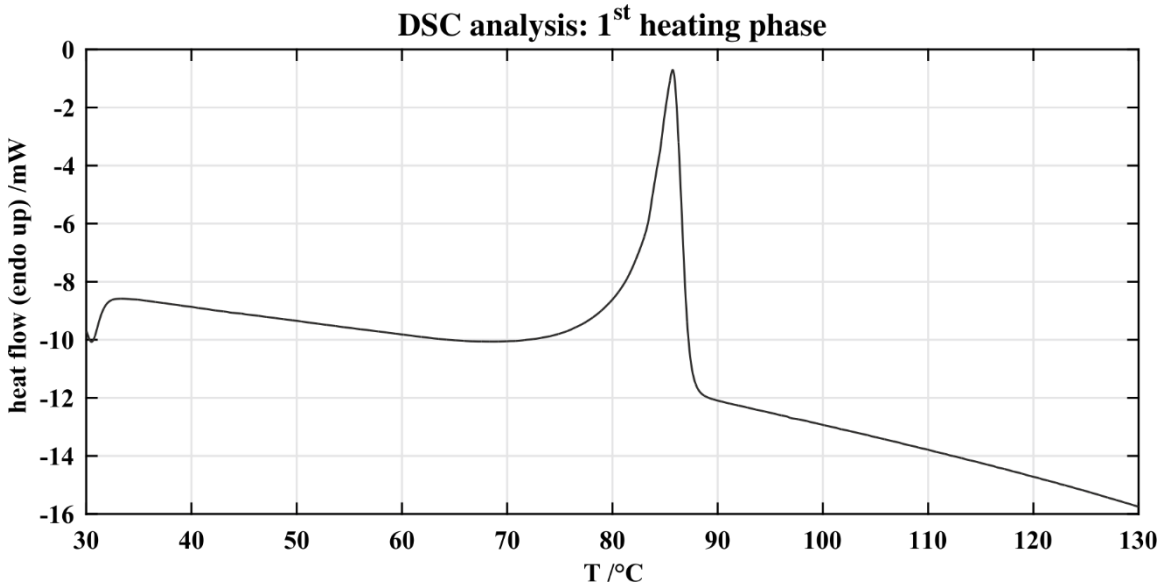

7.5.17.14. 1-(2-(2-(2-Methoxyethoxy)ethoxy)ethoxy)-4-vinylbenzene (**20**)

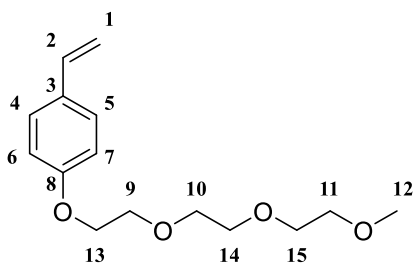

An oven dried 4 mL glas vial equipped with a TEFLON®-coated magnetic stirring bar was charged with 103 mg (0.61 mmol, 1.0 eq) acetoxystyrene, 500 µL THF, 500 µL MeOH and

250 µL H_2O. Afterwards 54.4 mg (1.30 mmol, 2.1 eq) lithium hydroxide monohydride was added to the reaction mixture at RT. The reaction mixture was stirred for 4 h at RT under protection from light. The reaction control was performed by TLC. Afterwards 1 M HCl solution was added until a pH 6 was reached. The reaction mixture was transferred into a separatory funnel and was extracted with EtOAc (3 × 5 mL). Afterwards the organic phase was washed with brine (1 × 5 mL), dried over Na_2SO_4, filtered and the solvent was removed under reduced pressure. An oven dried 25 mL SCHLENK flask equipped with a TEFLON®-coated magnetic stirring bar was charged with the colorless crude product. The crude product was further dried in oil pump vacuum at 10^{-2} mbar for 30 min. Afterwards 129 mg (1.10 mmol, 1.8 eq) potassium *tert*-butoxide, 85.8 mg (0.51 mmol, 0.8 eq) potassium iodide and 7 mL of absolute THF were added under nitrogen atmosphere. The reaction mixture was stirred for 10 min at RT. Afterwards 180 mg (0.57 mmol, 0.9 eq) 2-(2-(2-methoxyethoxy)ethoxy)ethyl 4-methylbenzenesulfonate were added and the reaction mixture was heated to reflux for 20 h under nitrogen and under protection from light. The reaction control was performed by TLC. The reaction mixture was transferred into a separatory funnel, 25 mL EtOAc were added and the reaction mixture was washed with 1 M HCl (3 × 15 mL). Subsequently the aqueous phase was reextracted with EtOAc (3 × 10 mL). The combined organic phases were washed with brine (1 × 20 mL), dried over Na_2SO_4, filtered and the solvent was removed under reduced pressure. Finally, the product was purified *via* flash column chromatography (20 g SiO_2 150 × 15 mm, eluent: cyclohexane/EtOAc = 3:2 (v/v), fraction size: 10 mL, detection: 254 nm; $KMnO_4$).

Yield: 74 mg (0.28 mmol, 49 % o. th.), colorless oil

$C_{15}H_{22}O_4$ [266.34 g/mol]

HR-MS (EI: [M]) [*m/z*]: calculated: 266.1518, found: 266.1532

R_f = 0.45 (cyclohexane/EtOAc = 1:2 (v/v)), (254 nm; $KMnO_4$)

^{1}H-NMR (300.36 MHz, $CDCl_3$): δ = 7.33 (d, 2H, $^3J_{HH}$ = 8.5 Hz, H-4, H-5), 6.87 (d, 2H, $^3J_{HH}$ = 8.5 Hz, H-6, H-7), 6.65 (dd, 1H, $^3J_{HH\,trans}$ = 17.9 Hz, $^3J_{HH\,cis}$ = 11.1 Hz, H-2), 5.60 (d, 1H, $^3J_{HH\,trans}$ = 17.9 Hz, H-1$_{trans}$), 5.12 (d, 1H, $^3J_{HH\,cis}$ = 11.1 Hz, H-1$_{cis}$), 4.13 (t, 2H, $^3J_{HH}$ = 5.2 Hz, H-13), 3.85 (t, 2H, $^3J_{HH}$ = 5.2 Hz, H-9), 3.73 (t, 2H, H-10), 3.67-3.69 (m, 2H, H-15), 3.64-3.67 (m, 2H, H-14), 3.55 (t, 2H, H-11), 3.38 (s, 3H, H-12).

^{13}C{H}-NMR (75.53 MHz, $CDCl_3$): δ = 158.7 (C-8), 136.3 (C-2), 130.7 (C-3), 127.5 (C-4, C-5), 114.8 (C-6, C-7), 111.7 (C-1), 72.1 (C-11), 71.0 (C-10), 70.8 (C-15), 70.7 (C-14), 69.9 (C-9), 67,6 (C-13), 59.2 (C-12).

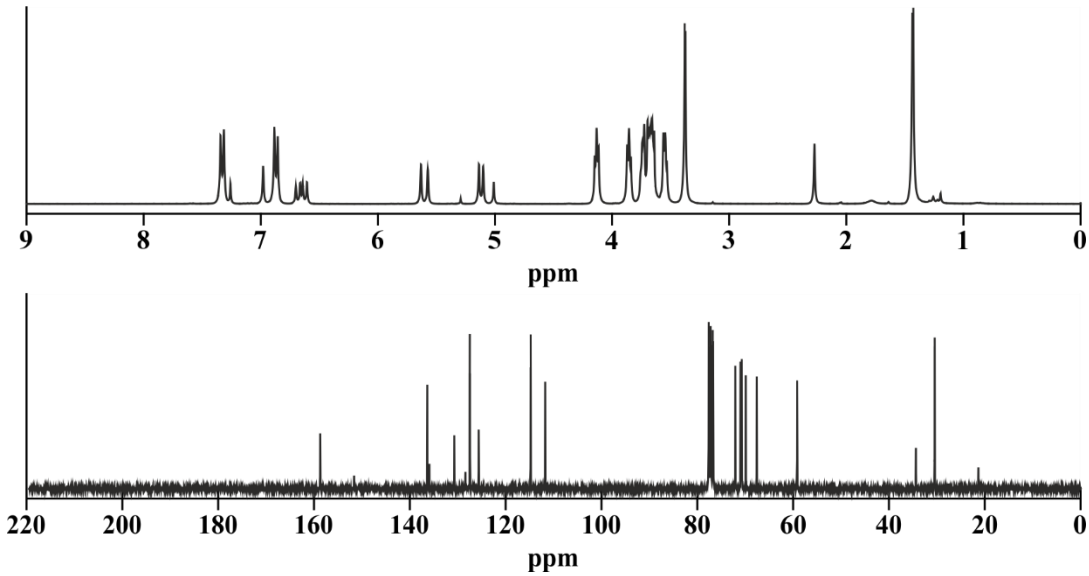

7.5.17.15. 1-Pyrenecarbaldehyde (**21**)

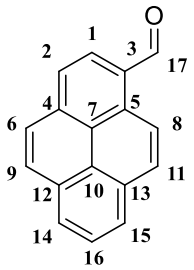

A 500 mL two necked round bottom flask equipped with a TEFLON®-coated magnetic stirring bar was charged with 12.5 g (44.4 mmol, 1.0 eq) 1-bromopyrene and 180 mL deoxygenated absolute THF. Afterwards the reaction flask was cooled to –80 °C and 36.2 mL (57.9 mmol, 1.3 eq) 1.6 M *n*-BuLi solution in hexane were added *via* dropping funnel over 10 min. During the addition of *n*-BuLi, the color of the reaction mixture got slightly darker. The reaction mixture was stirred for 1 h at –78 °C and afterwards 4.9 mL (63.0 mmol, 1.4 eq) absolute DMF were added. During the addition of DMF, the color of the reaction mixture changed from yellow to brown. The reaction mixture was allowed to warm up to RT and was stirred for 16 h under inert atmosphere. Afterward the reaction mixture was carefully poured into 250 mL of a 6 M HCl solution, which was rapidly stirred, transferred into a separatory funnel and extracted with Et_2O (3 × 150 mL). The combined organic phases were washed with H_2O (3 × 150 mL), dried over Na_2SO_4, filtered and the solvent was removed under reduced pressure. Finally the crude product was purified by recrystallization from 250 mL EtOH.

Yield: 8.49 g (36.9 mmol, 83 % o. th.), yellow solid

$C_{17}H_{10}O$ [230.27 g/mol]

R_f = 0.77 (cyclohexane/EtOAc = 1:1 (v/v)), (254 nm)

mp: 123-130 °C

^{1}H-NMR (300.36 MHz, $CDCl_3$): δ = 10.72 (s, 1H, H-17), 9.33 (d, 1H, $^3J_{HH}$ = 9.3 Hz, H-6), 8.35 (d, 1H, $^3J_{HH}$ = 7.9 Hz, H-5), 8.20-8.28 (m, 3H, H-9, H-14, H-15), 8.16 (d, 2H, H-2, H-11), 8.04 (t, 3H, H-1, H-16), 8.01 (d, 1H, $^3J_{HH}$ = 8.4 Hz, H-8).

^{13}C{H}-NMR (75.53 MHz, $CDCl_3$): δ = 193.1 (C-17), 135.5 (C-3), 131.4 (C-1), 131.1 (C-12), 131.0 (C-5), 130.8 (C-9), 130.7 (C-11), 130.5 (C-13), 127.4 (C-4), 124.2 (C-14), 127.1 (C-8), 126.9 (C-15), 126.6 (C-16), 124.6 (C-7), 124.6 (C-2), 124.1 (C-10), 123.0 (C-6).

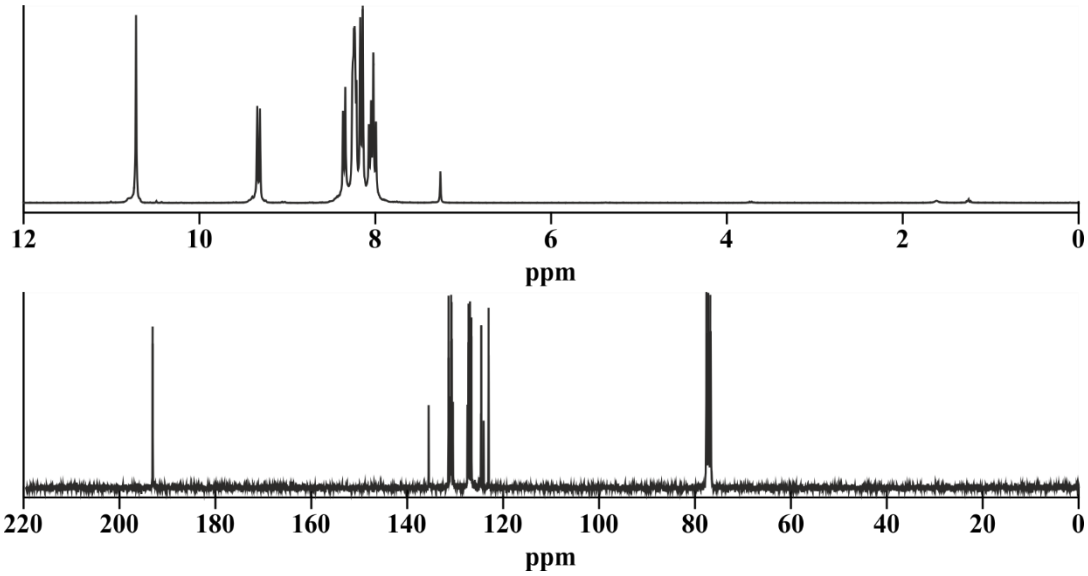

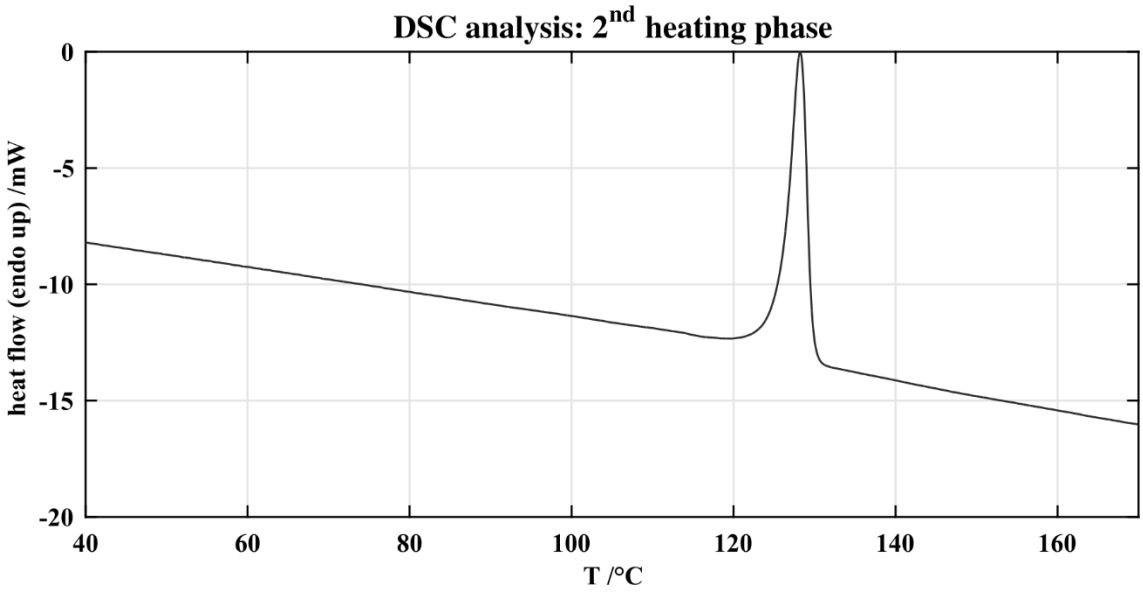

7.5.17.16. (±)-1-((2-((*endo*-5-Bicyclo[2.2.1]hept-5-en-2-yl)sulfonyl)ethoxy)-methyl)pyrene (**24a**)

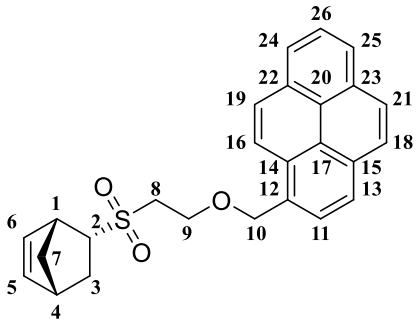

An oven dried 25 mL SCHLENK flask equipped with a TEFLON®-coated magnetic stirring bar was charged with 96.7 mg (0.42 mmol, 1.0 eq) pyren-1-ylmethanol, 408 mg (1.25 mmol, 3.0 eq) Cs_2CO_3 and 2 mL of absolute DCM under nitrogen atmosphere. Afterwards 77.2 mg (0.42 mmol, 1.0 eq) of (±)-*endo*-5-(ethenylsulfonyl)bicyclo[2.2.1]hept-2-ene were dissolved in another 2 mL of absolute DCM and added to the reaction mixture. The yellow solution was stirred overnight at 40 °C. The reaction control was performed by NMR-spectroscopy. Afterwards the reaction mixture was transferred into a separatory funnel and was washed with 1 M HCl (3 × 15 mL). Subsequently the aqueous phase was reextracted with DCM (3 × 15 mL). The combined organic phases were washed with brine (1 × 15 mL), dried over Na_2SO_4 and filtered. The solvent was removed under reduced pressure and the crude product was purified *via* flash column chromatography (13 g SiO_2, 300 × 15 mm, eluent: cyclohexane/EtOAc = 4:1 (v/v), fraction size: 10 mL, detection: $KMnO_4$).

Yield: 34.6 mg (0.08 mmol, 18 % o.th.), yellow solid

$C_{26}H_{24}O_3S$ [416.61 g/mol]

HR-MS (EI: [M]) [*m/z*]: calculated: 416.1446, found: 416.1457

R_f = 0.28 (cyclohexane/EtOAc = 2:1 (v/v)), ($KMnO_4$)

mp: 114-124 °C

^{1}H-NMR (499.88 MHz, $CDCl_3$): δ = 8.35 (d, 1H, $^3J_{HH}$ = 9.1 Hz, H-21), 8.19-8.26 (m, 2H, H-24, H-25), 8.15-8.19 (m, 2H, H-13, H-18), 8.09 (d, 1H, $^3J_{HH}$ = 8.9 Hz, H-19), 8.07 (d, 1H, $^3J_{HH}$ = 8.9 Hz, H-16), 8.03 (t, 1H, $^3J_{HH}$ = 7.6 Hz, H-26), 8.00 (d, 1H, $^3J_{HH}$ = 7.6 Hz, H-11), 6.20 (dd, 1H, $^3J_{HH}$ = 5.3 Hz, $^3J_{HH}$ = 2.9 Hz, H-5), 6.07 (dd, 1H, $^3J_{HH}$ = 5.3 Hz, $^3J_{HH}$ = 2.9 Hz, H-6), 5.22-5.29 (m, 2H, H-10), 4.03-4.12 (m, 2H, H-9), 3.69-3.79 (m, 1H, H-2), 3.29 (s, 1H, H-1),

3.17 (t, 2H, $^3J_{HH}$ = 5.5 Hz, H-8), 2.84 (s, 1H, H-4), 1.92 (ddd, 1H, $^3J_{HH}$ = 12.7 Hz, $^3J_{HH}$ = 9.3 Hz, $^3J_{HH}$ = 3.7 Hz, H-3$_{eq}$), 1.45 (ddd, 1H, $^3J_{HH}$ = 12.0 Hz, $^3J_{HH}$ = 4.9 Hz, $^3J_{HH}$ = 2.7 Hz, H-3$_{ax}$), 1.28-1.36 (m, 1H, H-7$_{dou}$), 0.90 (d, 1H, $^3J_{HH}$ = 8.7 Hz, H-7$_{sulf}$).

^{13}C{H}-NMR (75.53 MHz, $CDCl_3$): δ = 137.5 (C-5), 131.8 (C-12), 131.5 (C-22), 131.4 (C-6), 130.9 (C-23), 130.4 (C-15), 129.6 (C-14), 128.2 (C-18), 127.9 (C-19), 127.5 (C-16), 127.3 (C-11), 126.3 (C-26), 125.7 (C-25), 125.6 (C-24), 125.1 (C-17), 124.8 (C-20), 124.7 (C-13), 123.3 (C-21), 72.4 (C-10), 64.3 (C-9), 63.2 (C-2), 54.6 (C-8), 49.8 (C-7), 44.9 (C-1), 42.7 (C-4), 29.0 (C-3).

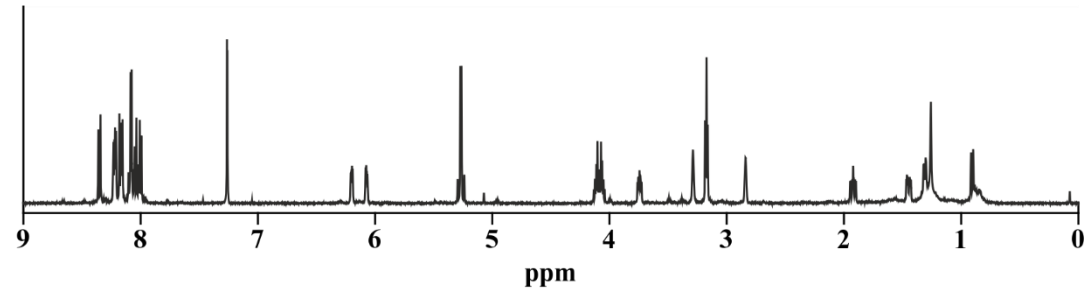

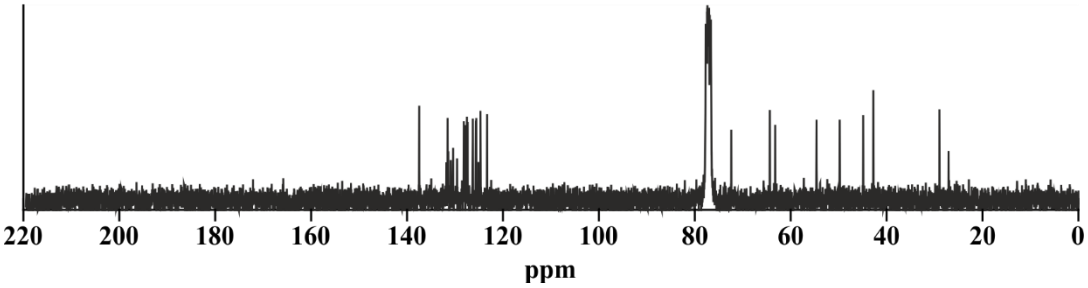

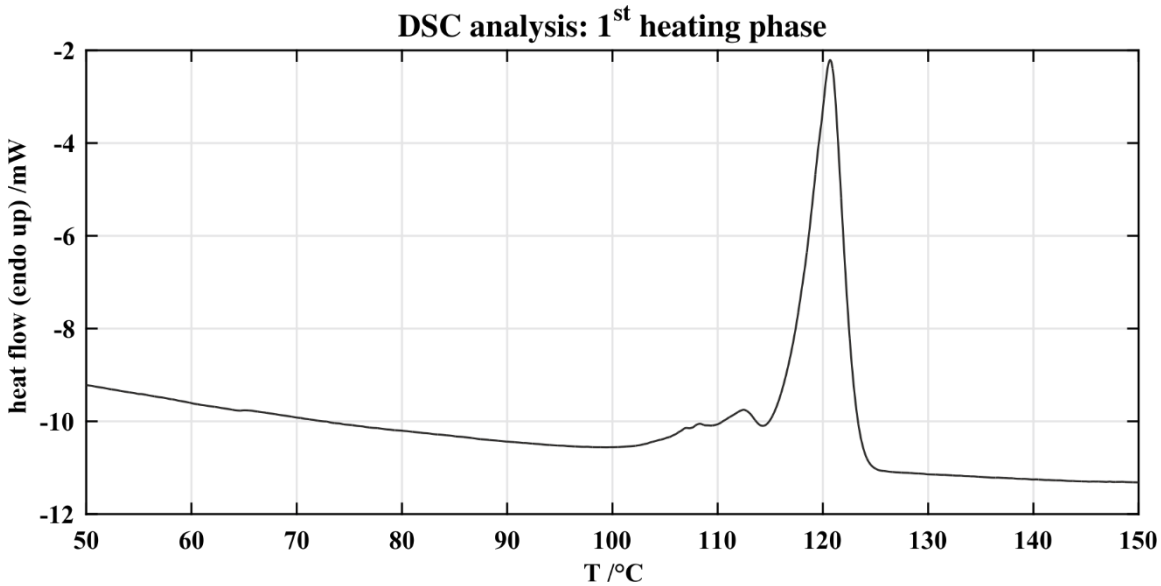

7.5.17.17. (±)-1-((2-((*exo*-5-Bicyclo[2.2.1]hept-5-en-2-yl)sulfonyl)ethoxy)methyl)-pyrene (**24b**)

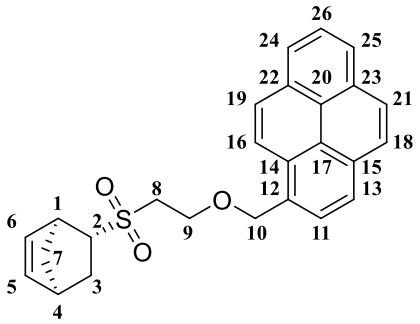

An oven dried 25 mL SCHLENK flask equipped with a TEFLON®-coated magnetic stirring bar was charged with 498.9 mg (2.14 mmol, 1.0 eq) pyren-1-ylmethanol, 1.21 g (6.44 mmol, 3.0 eq) Cs_2CO_3 and 7 mL of absolute DCM under nitrogen atmosphere. Afterwards 395.4 mg (2.15 mmol, 1.0 eq) of (±)-*exo*-5-(ethenylsulfonyl)bicyclo[2.2.1]hept-2-ene were dissolved in another 7 mL of absolute DCM and added to the reaction mixture. The yellow solution was stirred overnight at 40 °C. The reaction control was performed by NMR-spectroscopy. Afterwards the reaction mixture was transferred into a separatory funnel and was washed with 1 M HCl (3 × 15 mL). Subsequently the aqueous phase was reextracted with DCM (3 × 15 mL). The combined organic phases were washed with brine (1 × 15 mL), dried over Na_2SO_4 and filtered. The solvent was removed under reduced pressure and the crude product was purified *via* flash column chromatography (100 g SiO_2, 300 × 15 mm, eluent: cyclohexane/EtOAc = 6:1 (v/v), fraction size: 70 mL, detection: $KMnO_4$).

Yield: 562.4 mg (1.26 mmol, 59 % o.th.), yellow solid

$C_{26}H_{24}O_3S$ [416.61 g/mol]

HR-MS (EI: [M]) [*m/z*]: calculated: 416.1446, found: 416.1459

R_f = 0.29 (cyclohexane/EtOAc = 2:1 (v/v)), ($KMnO_4$)

mp: 113-127 °C

^{1}H-NMR (499.88 MHz, $CDCl_3$): δ = 8.29 (d, 1H, $^3J_{HH}$ = 9.2 Hz, H-21), 8.20-8.24 (m, 2H, H-24, H-25), 8.12-8.17 (m, 2H, H-13, H-18), 8.09 (d, 1H, $^3J_{HH}$ = 8.9 Hz, H-19), 8.06 (d, 1H, $^3J_{HH}$ = 9.0 Hz, H-16), 8.03 (t, 1H, $^3J_{HH}$ = 7.6 Hz, H-26), 7.96 (d, 1H, $^3J_{HH}$ = 7.7 Hz, H-11), 5.91 (dd, 1H, $^3J_{HH}$ = 5.5 Hz, $^3J_{HH}$ = 2.9 Hz, H-5), 5.63 (dd, 1H, $^3J_{HH}$ = 5.5 Hz, $^3J_{HH}$ = 2.9 Hz, H-6), 5.22 (s, 2H, H-10), 4.02-4.13 (m, 2H, H-9), 3.23-3.29 (m, 3H, H-1, H-8), 2.92-2.98 (m, 1H, H-

2), 2.88 (s, 1H, H-4), 2.01 (ddd, 1H, $^3J_{HH}$ = 12.7 Hz, $^3J_{HH}$ = 4.8 Hz, $^3J_{HH}$ = 3.6 Hz, H-3$_{eq}$), 1.84 (dd, 1H, $^3J_{HH}$ = 8.7 Hz, H-7$_{sulf}$), 1.87-1.81 (m, 2H, H-3$_{ax}$, H-7$_{dou}$).

^{13}C{H}-NMR (75.53 MHz, $CDCl_3$): δ = 139.7 (C-5), 135.3 (C-6), 131.7 (C-12), 131.4 (C-22), 130.9 (C-23), 130.3 (C-15), 129.6 (C-14), 128.2 (C-18), 127.9 (C-19), 127.5 (C-16), 127.3 (C-11), 126.2 (C-26), 125.6 (C-25), 125.5 (C-24), 125.1 (C-17), 124.8 (C-20), 124.6 (C-13), 123.3 (C-21), 72.3 (C-10), 64.2 (C-9), 62.5 (C-2), 53.9 (C-8), 46.0 (C-7), 44.1 (C-1), 41.5 (C-4), 28.3 (C-3).

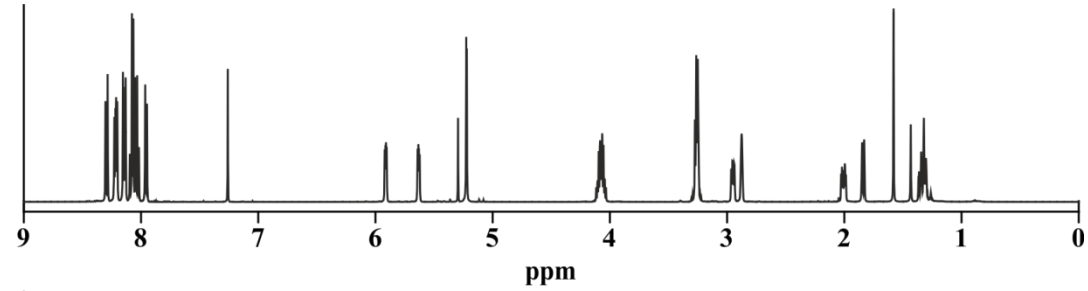

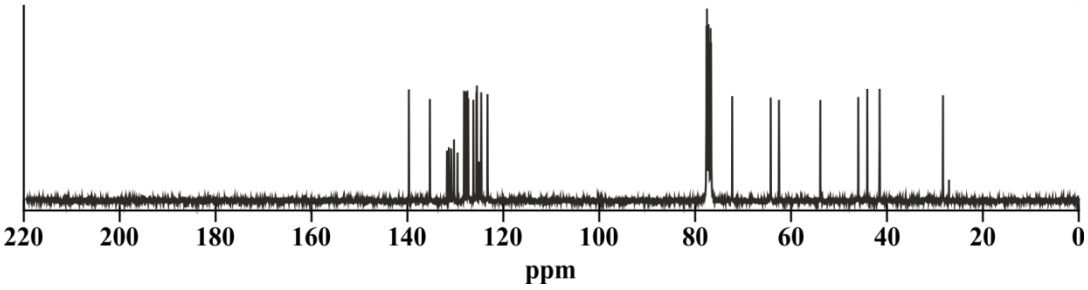

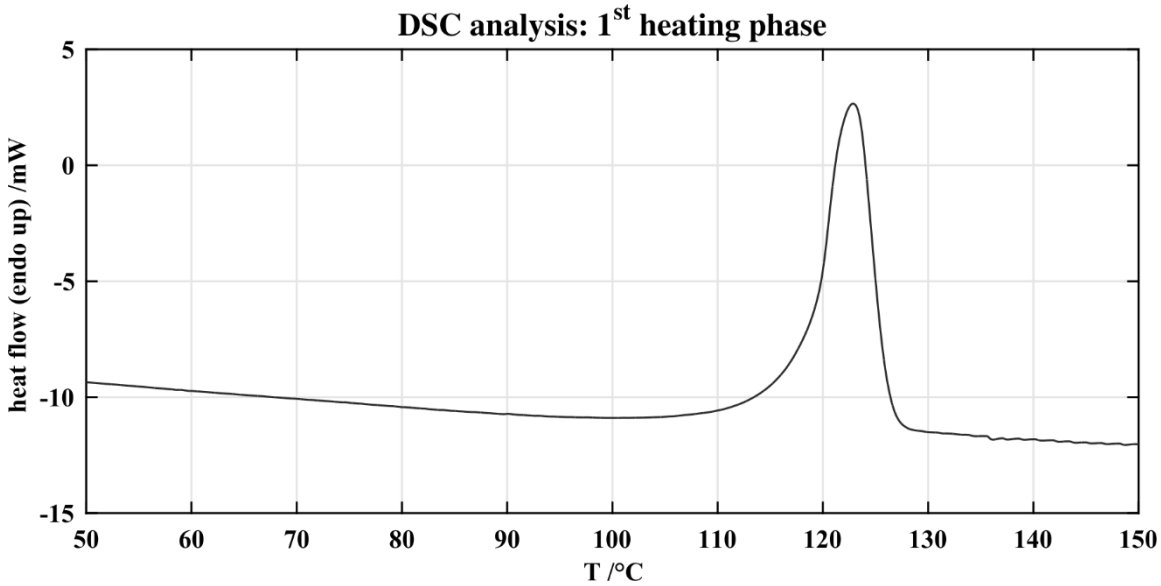

7.5.17.18. (±)-1-((2-*exo*-Bicyclo[2.2.1]hept-5-en-2-yl)pyrene (**25**)

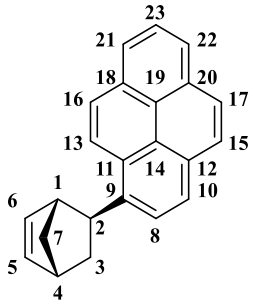

An oven dried 100 mL SCHLENK flask equipped with a TEFLON®-coated magnetic stirring bar was charged with 1.08 g (3.83 mmol, 1.0 eq) 1-bromopyrene, 2.00 mL (19.2 mmol, 5.0 eq) 2,5-norbornadiene, 1.8 ml (12.8 mmol, 3.3 eq) triethylamine, 400 µL (10.6 mmol, 2.8 eq) formic acid and 1.8 mL of absolute DMF. Afterwards 31.2 mg (0.04 mmol, 10 mol%) bis(triphenylphosphine)palladium dichloride were added under nitrogen atmosphere. The yellow reaction mixture was heated to 80 °C for 2 d under nitrogen. During heating the color of the reaction mixture turned from yellow to brown. The reaction control was performed by NMR-spectroscopy. After cooling to RT, the reaction mixture was diluted with 50 mL of EtOAc and transferred into a separatory funnel. The organic phase was washed with H_2O (3 × 30 mL). Subsequently the aqueous phase was reextracted with DCM (3 × 20 mL). The combined organic phases were washed with brine (1 × 25 mL), dried over Na_2SO_4, filtered and the solvent was removed under reduced pressure. The product was purified *via* flash column chromatography (150 g SiO_2 500 × 30 mm, eluent: cyclohexane, fraction size: 80 mL, detection: 366 nm).

Yield: 770 mg (2.62 mmol, 68 % o.th.), bright yellow oil

$C_{23}H_{18}$ [294.40 g/mol]

HR-MS (EI: [M]) [*m/z*]: calculated: 294.1408, found: 294.1406

R_f = 0.31 (cyclohexane), (366 nm)

T_g: 4 °C

^{1}H-NMR (499.88 MHz, $CDCl_3$): δ = 8.31 (d, 1H, $^3J_{HH}$ = 9.2 Hz, H-17), 8.13-8.19 (m, 3H, H-13, H-21, H-22), 8.10 (d, 1H, $^3J_{HH}$ = 9.2 Hz, H-15), 7.95-8.05 (m, 4H, H-8, H-10, H-16, H-23), 6.46 (dd, 1H, $^3J_{HH}$ = 5.5 Hz, $^3J_{HH}$ = 3.1 Hz, H-6), 6.35 (dd, 1H, $^3J_{HH}$ = 5.5 Hz, $^3J_{HH}$ = 3.1 Hz, H-5), 3.64 (dd, 1H, $^3J_{HH}$ = 8.8 Hz, $^3J_{HH}$ = 4.8 Hz, H-2), 3.33 (s, 1H, H-1), 3.08 (s, 1H, H-4),

2.09 (ddd, 1H, $^3J_{HH}$ = 11.4 Hz, $^3J_{HH}$ = 9.2 Hz, $^3J_{HH}$ = 2.2 Hz, H-3_{ax}), 1.87 (d, 1H, $^3J_{HH}$ = 8.4 Hz, H-7_{Pyr}), 1.80 (m, 1H, H-3_{eq}), 1.67 (d, 1H, $^3J_{HH}$ = 8.4 Hz, H-7_{dou}).

^{13}C{H}-NMR (75.53 MHz, $CDCl_3$): δ = 140.7 (C-9), 138. (C-5), 137.4 (C-6), 131.7 (C-18), 131.0 (C-20), 129.6 (C-11), 129.5 (C-12), 127.6 (C-10), 127.2 (C-15), 126.7 (C-23), 125.9 (C-16), 125.2 (C-14), 125.1 (C-19), 125.0 (C-21, C-22), 124.9 (C-13), 124.0 (C-17), 123.0 (C-8), 47.1 (C-1), 46.9 (C-7), 42.9 (C-4), 40.4 (C-2), 35.7 (C-3).

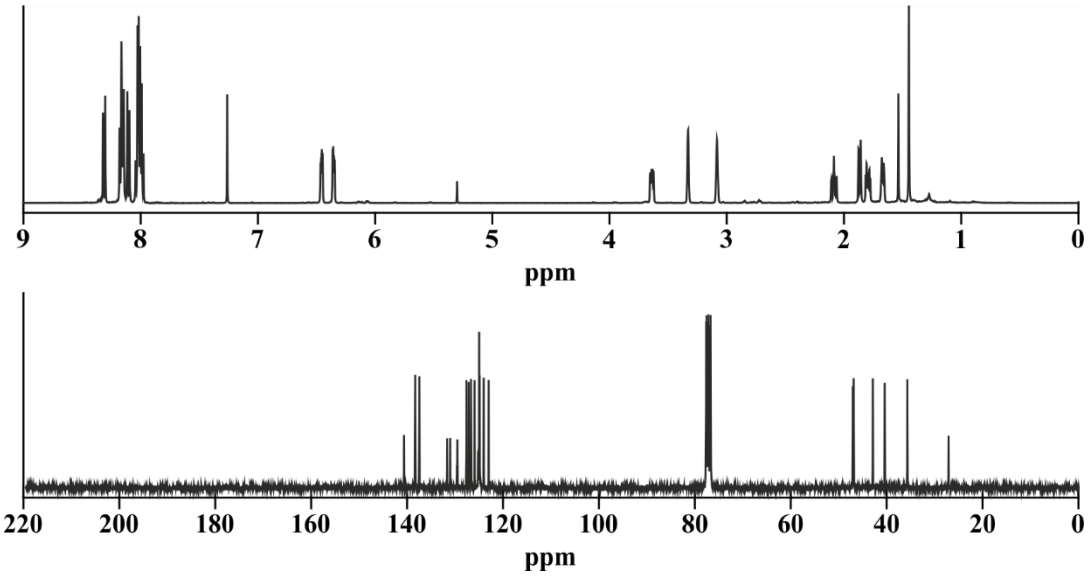

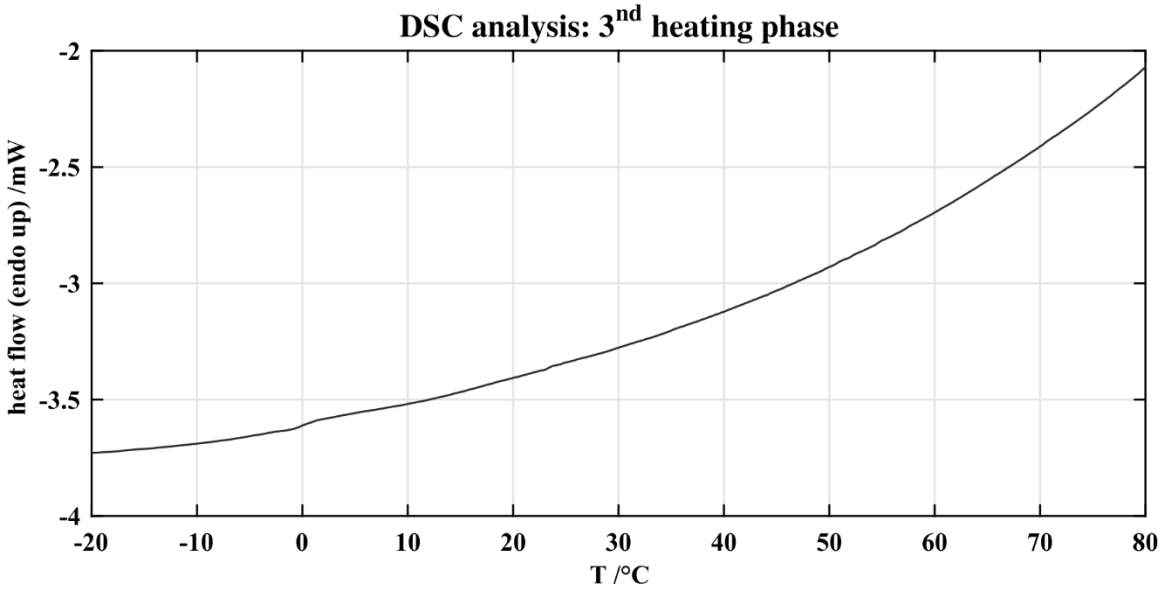

7.5.17.19. 1-(Bicyclo[2.2.1]hept-5-en-2-yl)-2,5,8,11-tetraoxadodecane (**26**)

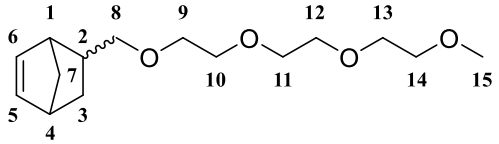

An oven dried 100 mL SCHLENK flask equipped with a TEFLON®-coated magnetic stirring bar was charged with 423 mg (3.41 mmol, 1.05 eq) bicyclo[2.2.1]hept-5-en-2-ylmethanol, 1.00 g (3.14 mmol, 1.0 eq) 2-(2-(2-methoxyethoxy)ethoxy)ethyl 4-methylbenzenesulfonate and 30 mL of absolute THF. Afterwards 372 mg (2.24 mmol, 0.7 eq) potassium iodide and 645 mg (5.75 mmol, 1.8 eq) potassium *tert*-butoxide were added under nitrogen atmosphere. The yellow reaction mixture was heated to reflux for 20 h under nitrogen. During heating, the color of the reaction mixture turned from yellow to light orange. The reaction control was performed by NMR-spectroscopy. After cooling to RT the reaction mixture was diluted with 50 mL of EtOAc and transferred into a separatory funnel. The organic phase was washed with 1 M HCl (3 × 20 mL). Subsequently the aqueous phase was reextracted with DCM (3 × 15 mL). The combined organic phases were washed with brine (1 × 20 mL), dried over Na_2SO_4, filtered and the solvent was removed under reduced pressure. The product was purified *via* flash column chromatography (150 g SiO_2 300 × 30 mm, eluent: EtOAc/cyclohexane = 1:4 (v/v), fraction size: 80 mL, detection: $KMnO_4$).

Yield: 381 mg (1.41 mmol, 46 % o. th.), yellow oil, *exo*/*endo* = 1/3

$C_{15}H_{26}O_4$ [270.37 g/mol]

R_f = 0.24 (cyclohexane/EtOAc = 2:1 (v/v)), ($KMnO_4$)

^{1}H-NMR (*endo*-isomer 300.36 MHz, $CDCl_3$): δ = 6.11 (dd, 1H, $^3J_{HH}$ = 5.3 Hz, $^3J_{HH}$ = 2.7 Hz, H-5), 5.92 (dd, 1H, $^3J_{HH}$ = 5.3 Hz, $^3J_{HH}$ = 2.7 Hz, H-6), 3.59-3.71 (m, 8H, H-9, H-10, H-11, H-12), 3.49-3.59 (m, 4H, H-13, H-14), 3.38 (s, 3H, H-15), 3.14-3.22 (m, 1H, H-8_a), 3.07 (t, 1H, $^3J_{HH}$ = 9.2 Hz, H-1, H-8_b), 2.90 (s, 1H, H-1), 2.78 (s, 1H, H-4), 2.28-2.42 (m, 1H, H-2), 1.75-1.86 (m, 1H, H-3_{eq}), 1.41 (d, 1H, $^3J_{HH}$ = 7.2 Hz, H-7_{ox}), 1.23 (d, 1H, $^3J_{HH}$ = 7.7 Hz, H-7_{dou}), 0.48 (ddd, 1H, $^3J_{HH}$ = 11.4 Hz, $^3J_{HH}$ = 3.9 Hz, $^3J_{HH}$ = 2.5 Hz, H-3_{ax}).

^{13}C{H}-NMR (*endo*-isomer 75.53 MHz, $CDCl_3$): δ = 137.2 (C-5), 132.6 (C-6), 75.2 (C-8), 72.1 (C-14), 70.8 (C-10, C-12), 70.7 (C-9, C-11), 70.4 (C-13), 59.2 (C-15), 49.5 (C-7), 44.1 (C-1), 42.3 (C-4), 38.8 (C-2), 29.3 (C-3).

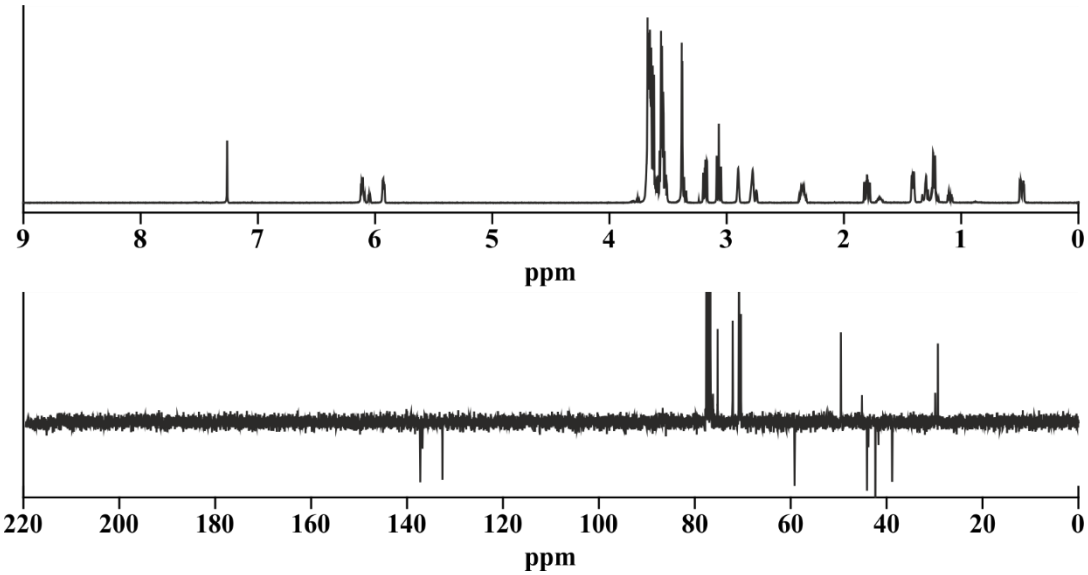

7.5.17.20. (±)-*endo*-5-(Ethenylsulfonyl)bicyclo[2.2.1]hept-2-ene (**27a**)

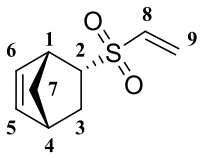

An oven dried 10 mL monowave reaction vessel was charged with 1 mL distilled cyclopentadiene (12.0 mmol, 1.0 eq), 1.22 mL divinyl sulfone (12.0 mmol, 1.0 eq), 1 mL DCM and 1.78 mL MeOH. Afterwards the reaction vial was placed into the monowave reactor and was heated to 150 °C for 2 h. The reaction control was performed by TLC. The solvent was removed under reduced pressure and the crude product was purified *via* flash column chromatography (220 g SiO_2 250 × 30 mm, eluent: 1100 mL cyclohexane/EtOAc = 10:1 (v/v), 800 mL cyclohexane/EtOAc = 7:1 (v/v), 3000 mL cyclohexane/EtOAc = 5:1 (v/v), fraction size: 80 mL, detection: $KMnO_4$).

Yield: 140 mg (0.76 mmol, 6 % o. th.), colorless solid

$C_9H_{12}O_2S$ [184.25 g/mol]

R_f = 0.31 (cyclohexane/EtOAc = 2:1 (v/v)), ($KMnO_4$)

mp: 34-38 °C

^{1}H-NMR (499.88 MHz, $CDCl_3$): δ = 6.55 (dd, 1H, $^3J_{HH\,trans}$ = 16.7 Hz, $^3J_{HH\,cis}$ = 9.9 Hz, H-8), 6.34 (d, 1H, $^3J_{HH\,trans}$ = 16.7 Hz, H-9), 6.27 (dd, 1H, $^3J_{HH}$ = 5.6 Hz, $^3J_{HH}$ = 3.1 Hz, H-5), 6.06-6.11 (m, 2H, H-6, H-9), 3.54 (ddd, 1H, $^3J_{HH}$ = 9.2 Hz, $^3J_{HH}$ = 4.9 Hz, $^3J_{HH}$ = 3.2 Hz, H-2), 3.33 (s, 1H, H-1), 3.03 (s, 1H, H-4), 2.12 (ddd, 1H, $^3J_{HH}$ = 12.8 Hz, $^3J_{HH}$ = 9.3 Hz, $^3J_{HH}$ = 3.7 Hz, H-

3_{eq}), 1.55 (ddd, 1H, $^3J_{HH}$ = 8.7 Hz, $^3J_{HH}$ = 4.3 Hz, $^3J_{HH}$ = 1.9 Hz, H-7_{dou}), 1.47 (ddd, 1H, $^3J_{HH}$ = 12.4 Hz, $^3J_{HH}$ = 4.9 Hz, $^3J_{HH}$ = 3.7 Hz, H-3_{ax}), 1.32 (d, 1H, $^3J_{HH}$ = 8.8 Hz, H-7_{sulf}).

^{13}C{H}-NMR (75.53 MHz, $CDCl_3$): δ = 137.7 (C-5), 136.9 (C-8), 131.7 (C-6), 129.6 (C-9), 63.3 (C-2), 50.1 (C-7), 44.9 (C-1), 42.8 (C-4), 28.8 (C-3).

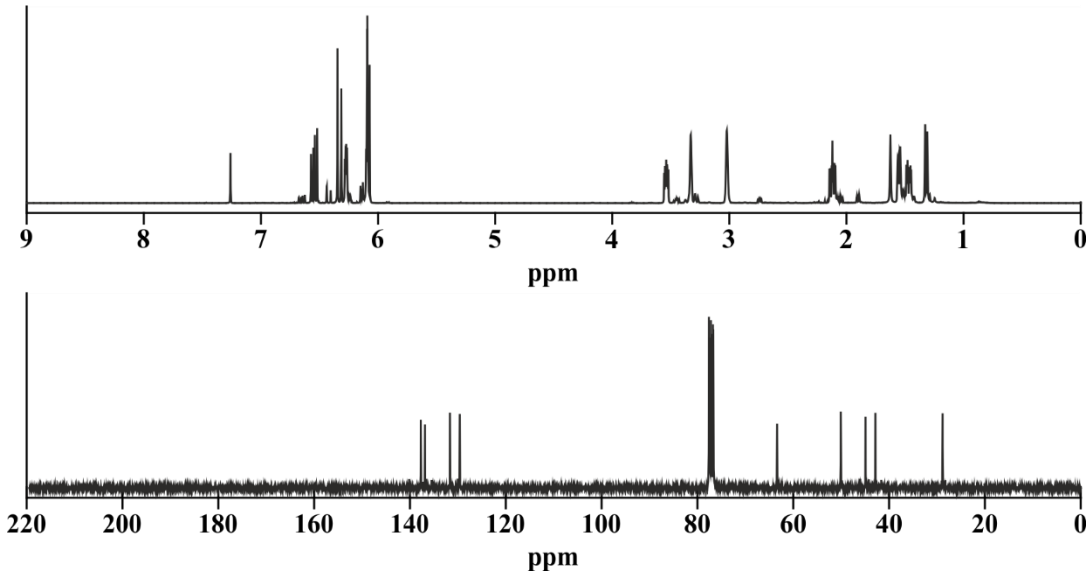

7.5.17.21. (±)-*exo*-5-(Ethenylsulfonyl)bicyclo[2.2.1]hept-2-ene (**27b**)

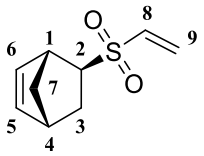

An oven dried 10 mL monowave reaction vessel was charged with 1 mL distilled cyclopentadiene (12.0 mmol, 1.0 eq), 1.22 mL divinyl sulfone (12.0 mmol, 1.0 eq), 1 mL DCM and 1.78 mL MeOH. Afterwards the reaction vial was placed into the monowave reactor and was heated to 150 °C for 2 h. The reaction control was performed by TLC. The solvent was removed under reduced pressure and the crude product was purified *via* flash column chromatography (220 g SiO_2 250 × 30 mm, eluent: 1100 mL cyclohexane/EtOAc = 10:1 (v/v), 800 mL cyclohexane/EtOAc = 7:1 (v/v), 3000 mL cyclohexane/EtOAc = 5:1 (v/v), fraction size: 80 mL, detection: $KMnO_4$).

Yield: 237 mg (1.29 mmol, 10 % o. th.), yellow solid

$C_9H_{12}O_2S$ [184.25 g/mol]

R_f = 0.43 (cyclohexane/EtOAc = 2:1 (v/v)), ($KMnO_4$)

mp: 39-52 °C

^{1}H-NMR (499.88 MHz, $CDCl_3$): δ = 6.65 (dd, 1H, $^{3}J_{HH\ trans}$ = 16.7 Hz, $^{3}J_{HH\ cis}$ = 9.8 Hz, H-8), 6.42 (d, 1H, $^{3}J_{HH\ trans}$ = 16.7 Hz, H-9), 6.27 (dd, 1H, $^{3}J_{HH}$ = 5.5 Hz, $^{3}J_{HH}$ = 3.0 Hz, H-5), 6.11-6.16 (m, 2H, H-6, H-9), 3.30 (s, 1H, H-1), 3.03 (s, 1H, H-4), 2.75 (ddd, 1H, $^{3}J_{HH}$ = 8.5 Hz, $^{3}J_{HH}$ = 4.9 Hz, $^{3}J_{HH}$ = 0.8 Hz, H-2), 2.05 (ddd, 1H, $^{3}J_{HH}$ = 12.3 Hz, $^{3}J_{HH}$ = 4.8 Hz, $^{3}J_{HH}$ = 3.7 Hz, H-3_{eq}), 1.90 (d, 1H, $^{3}J_{HH}$ = 9.0 Hz, H-7_{sulf}), 1.53-1.47 (m, 1H, H-3_{ax}), 1.44 (d, 1H, $^{3}J_{HH}$ = 8.8 Hz, H-7_{dou}).

^{13}C{H}-NMR (75.53 MHz, $CDCl_3$): δ = 140.2 (C-5), 136.6 (C-8), 135.5 (C-6), 130.0 (C-9), 62.4 (C-2), 46.1 (C-7), 44.2 (C-1), 41.6 (C-4), 28.2 (C-3).

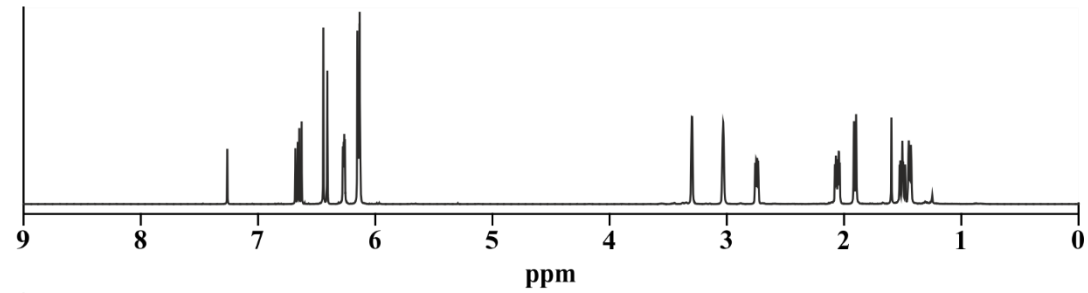

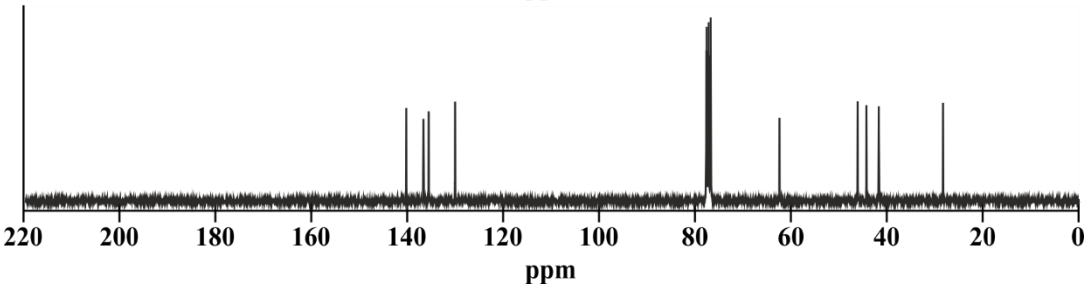

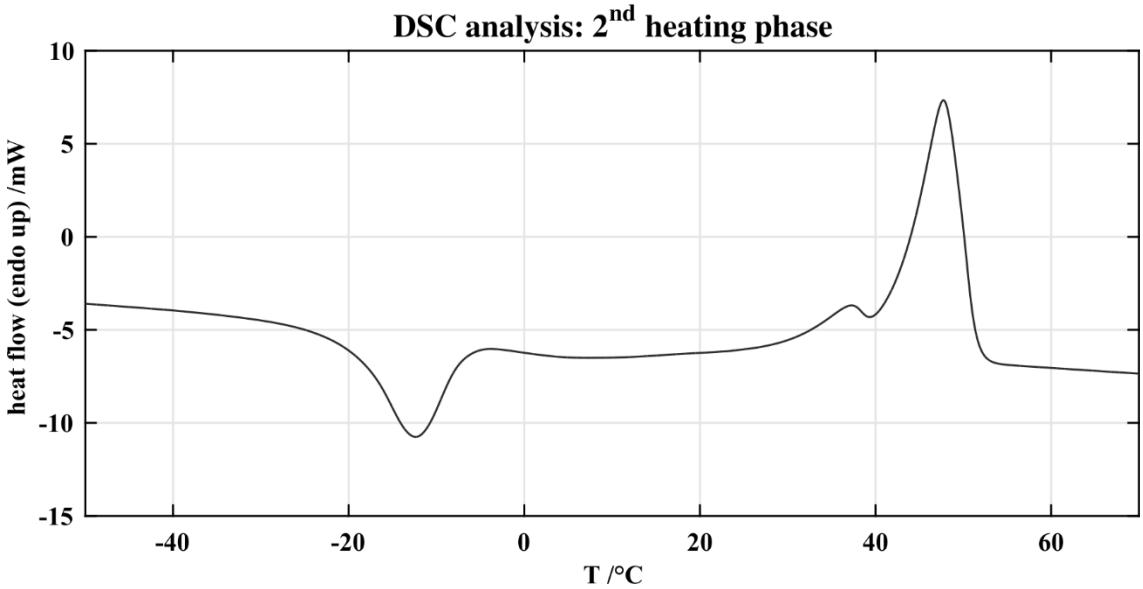

7.5.17.22. 1-Bromopyrene (**29**)

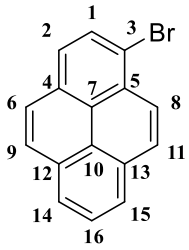

A 250 mL one necked round bottom flask equipped with a TEFLON®-coated magnetic stirring bar was charged with 10.0 g (49.4 mmol, 1.0 eq) pyrene, 62.5 mL MeOH, 62.5 mL Et_2O and 6.15 mL (54.5 mmol, 1.1 eq, 48 % (w/w) aq.) HBr. Afterwards the reaction flask was cooled to 15 °C and 5.2 mL (52.0 mmol, 1.1 eq, 30 % (w/w) aq.) H_2O_2 were added *via* dropping funnel over 15 min. During the addition of H_2O_2, the color of the reaction mixture changed from yellow to orange and a yellowish precipitate was formed. The reaction mixture was stirred overnight at RT. Reaction control was performed by NMR-spectroscopy. Afterwards the reaction mixture was diluted with 75 mL H_2O, transferred into a separatory funnel and the reaction mixture was extracted with DCM (2 × 125 mL). The combined organic phases were washed with 1 M NaOH (1 × 75 mL) and brine (2 × 75 mL). Afterwards the organic phase was dried over Na_2SO_4, filtered and the solvent was removed under reduced pressure. The crude material was placed in a SOXHLET extractor and was extracted with 350 mL *n*-pentane for 4 d. After cooling to room temperature the *n*-pentane fraction was concentrated to 180 mL by rotary evaporation and placed in a refrigerator overnight. The formed precipitate was collected by filtration, dried in oil pump vacuum at 10^{-2} mbar for 2 h and afterwards the crude product was purified by recrystallization from 500 mL *n*-hexane.

Yield: 12.8 g (45.5 mmol, 92 % o. th.), bright yellow solid

$C_{16}H_9Br$ [281.15 g/mol]

R_f = 0.88 (cyclohexane/EtOAc = 1:1 (v/v)), (254 nm)

mp: 91-97 °C

^{1}H-NMR (300.36 MHz, $CDCl_3$): δ = 8.43 (d, 1H, $^3J_{HH}$ = 9.1 Hz, H-9), 8.22-8.24 (m, 3H, H-11, H-14, H-15), 8.17 (d, 1H, $^3J_{HH}$ = 9.1 Hz, H-6), 7.98-8.12 (m, 4H, H-1, H-2, H-8, H-16).

^{13}C{H}-NMR (75.53 MHz, $CDCl_3$): δ = 131.3 (C-13), 131.1 (C-12), 130.7 (C-4), 130.2 (C-14), 129.8 (C-5), 129.1 (C-6), 127.9 (C-2), 127.2 (C-1), 126.6 (C-8), 126.1 (C-9), 126.0 (C-10), 125.9 (C-15), 125.7 (C-11), 125.6 (C-16), 124.2 (C-7), 120.0 (C-3).

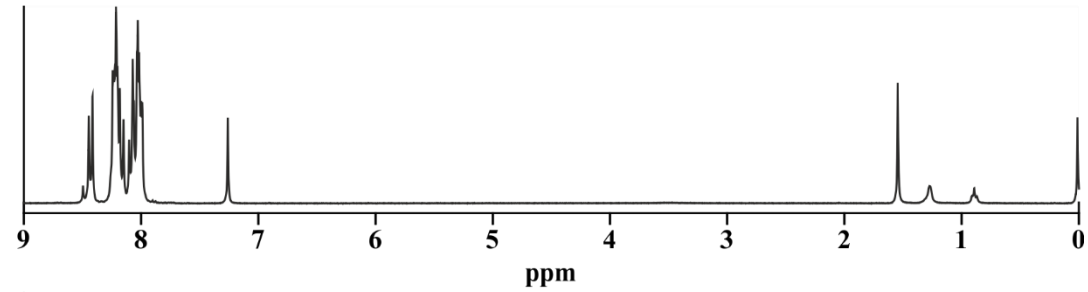

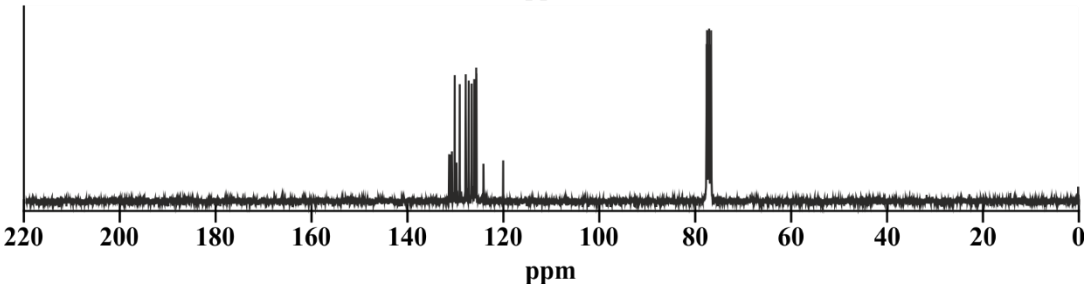

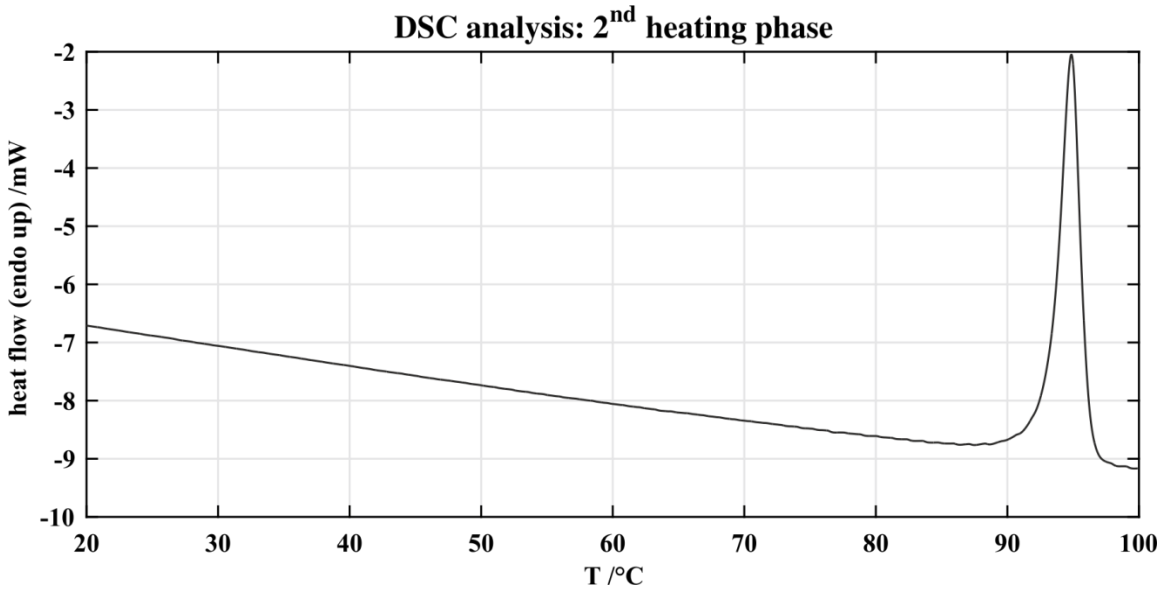

7.5.17.23. $[(\text{Nbe-S-Pyr})_3(\text{Nbe-TEG})_1]_{200\ \text{stat.}}$ (**30**)

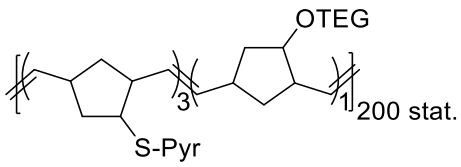

An oven dried 25 mL SCHLENK flask equipped with a TEFLON®-coated magnetic stirring bar was charged with 98.2 mg (0.24 mmol, 3.0 eq) (±)-1-((2-((*exo*-5-bicyclo[2.2.1]hept-5-en-2-yl)sulfonyl)ethoxy)methyl)pyrene, 22.6 mg (0.08 mmol, 1.0 eq) 1-(bicyclo[2.2.1]hept-5-en-2-yl)-2,5,8,11-tetraoxadodecane and 3 mL of absolute, degassed DCM under nitrogen atmosphere. The reaction mixture was stirred for 5 min. Afterwards another oven dried 25 mL SCHLENK flask equipped with a TEFLON®-coated magnetic stirring bar was charged with 1.3 mg (1.6 µmol, 2 mol%) of dichloro[1,3-bis(2,4,6-trimethylphenyl)-2-imidazolidinylidene](3-

phenyl-1*H*-inden-1-ylidene)(pyridyl)ruthenium(II) and 0.2 mL of absolute, degassed DCM and added to the reaction mixture. During the addition of the catalyst, the color of the reaction mixture changed from yellow to orange. The reaction mixture was stirred for 2 h at RT and reaction control was performed by NMR-spectroscopy. Afterwards the polymerization reaction was stopped by the addiction of 50 µL of ethyl vinyl ether. The reaction mixture was further stirred for 2 h. Afterwards the polymer was precipitated in 100 mL of cold MeOH twice. Finally, the off white polymer was dried in oil pump vacuum at 10^{-2} mbar for 5 h.

Yield: 98.2 mg (96 % o. th.), off-white solid

M_n: 51,000 g/mol

PDI: 1.37

T_g: 90 °C

^{1}H-NMR (300.36 MHz, $CDCl_3$): δ = 7.77-8.27 (bs), 4.34-5.27 (bs), 2.49-4.06 (bs), 0.30-2.34 (bs).

^{13}C{H}-NMR (75.53 MHz, $CDCl_3$): δ = 131.3-131.7 (C_{Ar}), 130.4-130.8 (C_{Ar}), 129.3-129.5 (C_{Ar}), 127.3-128.1 (C_{Ar}), 126.1-126.3 (C_{Ar}), 125.4-125.8 (C_{Ar}), 124.3-125.0 (C_{Ar}), 123.3-123.5 (C_{Ar}), 71.8-72.1 (C_{Al}), 70.4-70.6 (C_{Al}), 64.1-64.2 (C_{Al}), 59.1 (C_{Al}), 52.5-52.8 (C_{Al}), 40.9-43.0 (C_{Al}), 39.2-39.3 (C_{Al}).

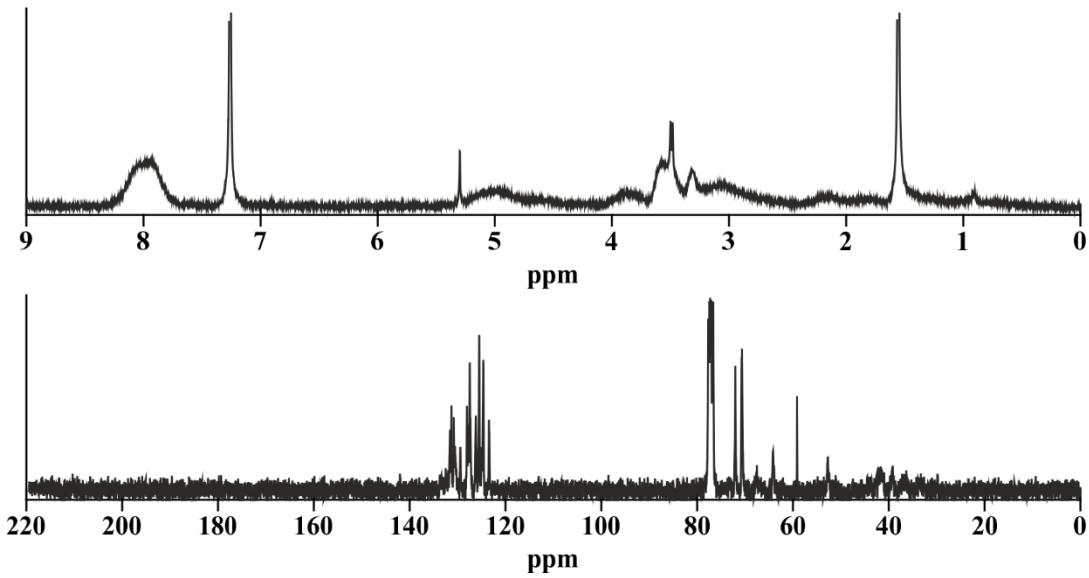

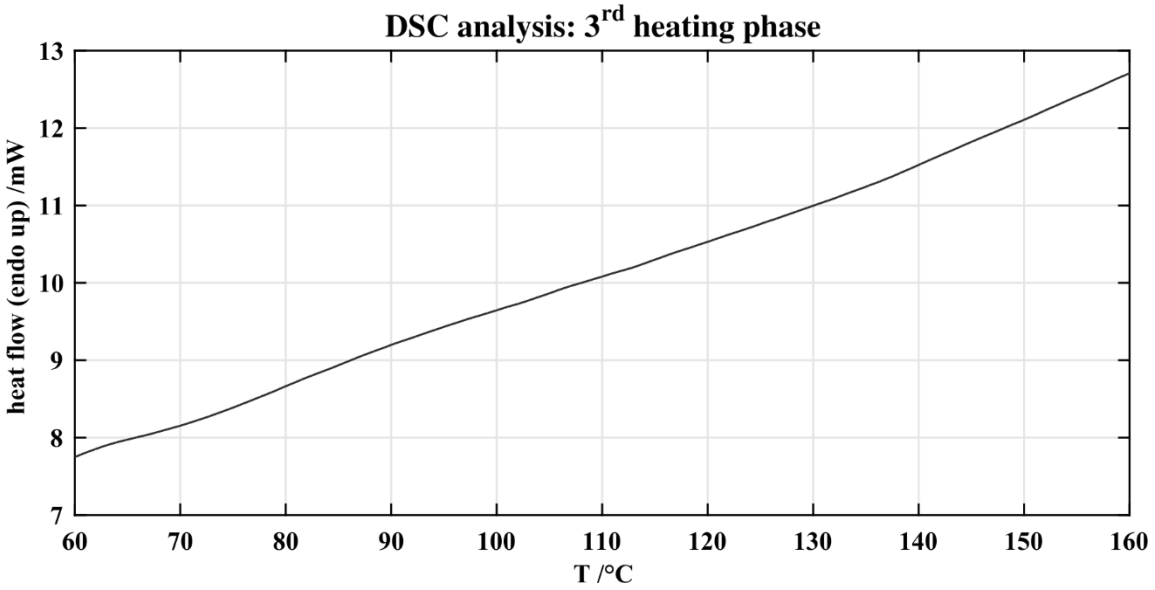

7.5.17.24. $[(\text{Nbe-Pyr})_3(\text{Nbe-TEG})_1]_{100\ \text{stat.}}$ (**31**)

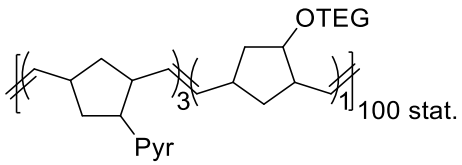

An oven dried 25 mL SCHLENK flask equipped with a TEFLON®-coated magnetic stirring bar was charged with 98.7 mg (0.34 mmol, 3.0 eq) (±)-1-((2-*exo*-bicyclo[2.2.1]hept-5-en-2-yl)pyrene, 30.2 mg (0.11 mmol, 1.0 eq) 1-(bicyclo[2.2.1]hept-5-en-2-yl)-2,5,8,11-tetraoxadodecane and 3 mL of absolute, degassed DCM under nitrogen atmosphere. The reaction mixture was stirred for 5 min. Afterwards another oven dried 25 mL SCHLENK flask equipped with a TEFLON®-coated magnetic stirring bar was charged with 3.4 mg (4.5 µmol, 4 mol%) of dichloro[1,3-bis(2,4,6-trimethylphenyl)-2-imidazolidinylidene](3-phenyl-1*H*-inden-1-ylidene)(pyridyl)ruthenium(II) and 0.2 mL of absolute, degassed DCM and added to the reaction mixture. During the addition of the catalyst, the color of the reaction mixture changed from yellow to orange. The reaction mixture was stirred for 2 h at RT and reaction control was performed by NMR-spectroscopy. Afterwards the polymerization reaction was stopped by the addition of 150 µL of ethyl vinyl ether. The reaction mixture was further stirred for 2 h. Afterwards the polymer was precipitated in 100 mL of cold MeOH twice. Finally, the off white polymer was dried in oil pump vacuum at 10^{-2} mbar for 5 h.

Yield: 92.1 mg (71 % o. th.), off-white solid

M_n: 30,000 g/mol

PDI: 1.94

T_g: 111 °C

^{1}H-NMR (300.36 MHz, $CDCl_3$): δ = 6.88-8.44 (bs), 4.87-5.66 (bs), 2.45-4.03 (bs), 0.74-2.42 (bs).

^{13}C{H}-NMR (75.53 MHz, $CDCl_3$): δ = 138.7-140.7 (C_{Ar}), 132.9-135.5 (C_{Ar}), 130.6-131.8 (C_{Ar}), 128.5-129.6 (C_{Ar}), 127.2-127.7 (C_{Ar}), 126.0-127.0 (C_{Ar}), 125.5-125.9 (C_{Ar}), 124.1-125.4 (C_{Ar}), 122.8-123.9 (C_{Ar}), 71.8-72.1 (C_{Al}), 70.2-70.9 (C_{Al}), 59.1 (C_{Al}), 46.0-47.6 (C_{Al}), 43.5-44.2 (C_{Al}), 36.4-38.2 (C_{Al}).

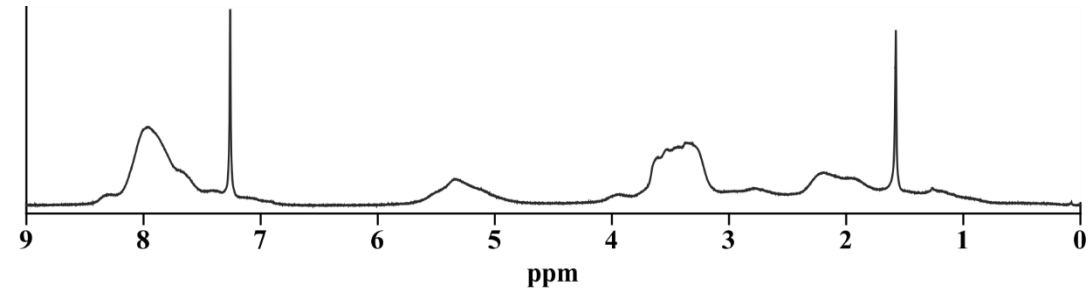

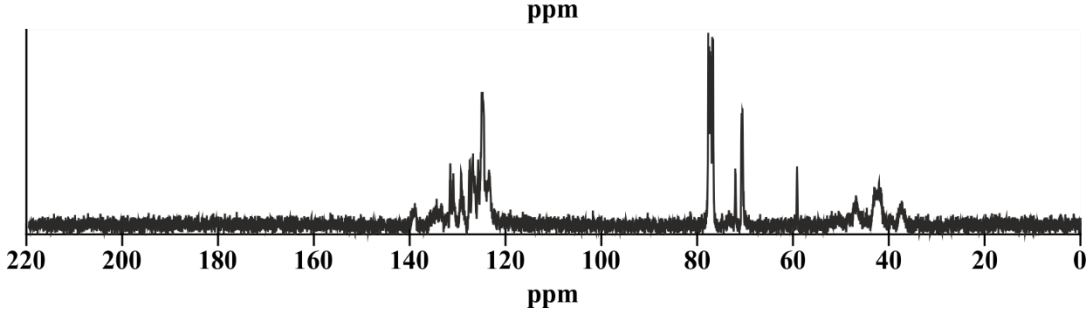

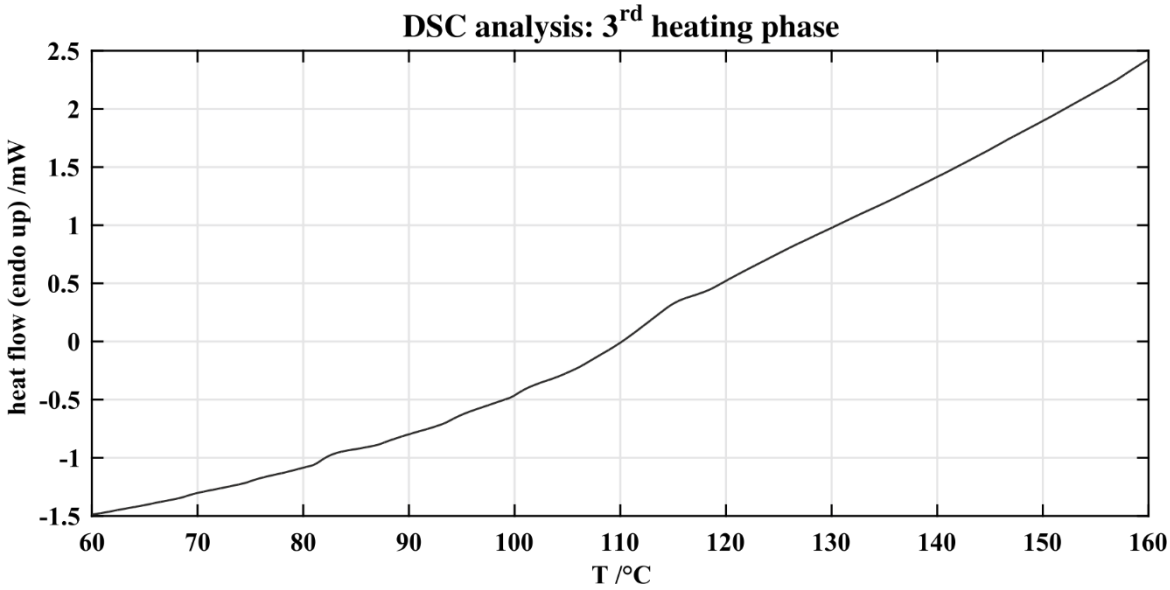

7.5.17.25. 1-Methyl-1,4-diazabicyclo[2.2.2]octan-1-ium bis(trifluoromethane)sulfonimide (**35a**)

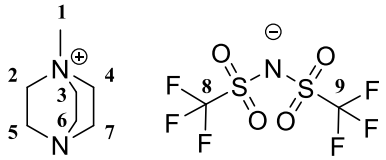

An oven dried 100 mL round-bottom flask equipped with a TEFLON®-coated magnetic stirring bar was charged with 2.00 g (17.8 mmol, 1.0 eq) diazabicyclo[2.2.2]octan and 70 mL of EtOAc. The colorless solution was stirred for 5 min at RT. Afterwards 1.08 mL (17.4 mmol, 1.0 eq) methyl iodide were added. During the addition of methyl iodide a colorless solid was formed. The reaction mixture was stirred for 2 h at RT and the reaction control was performed by NMR-spectroscopy. Afterwards the colorless precipitate was collected by filtration and was dried in vacuum. Finally, the product was recrystallized from 20 mL isopropanol. Afterwards the crude product was dissolved in 5 mL of H_2O and 30 mL of a 0.5 M (15.0 mmol, 0.9 eq) lithium bis(trifluoromethane)sulfonimide solution in H_2O were added at RT. The reaction mixture was stirred for 5 min and transferred into a separatory funnel. The aqueous phase was extracted with DCM (3 × 20 mL). Subsequently the organic phase was washed with H_2O (3 × 10 mL). The solvent of the organic phases was removed and to the residue 40 mL acetone and activated charcoal were added. The suspension was stirred for 3 h and filtered through a small plug of activated alumina. Finally, the solvent was removed and the product was dried in oil pump vacuum at 10^{-2} mbar for 3 h.

Yield: 120 mg (12.2 mmol, 70 % o. th.), bright yellow solid

$C_9H_{15}F_6N_2O_4S_2$ [407.35 g/mol]

mp: 77-84 °C

^{1}H-NMR (300.36 MHz, DMSO d_6): δ = 3.26 (t, 6H, $^3J_{HH}$ = 7.5 Hz, H-1, H-2, H-3), 3.03 (t, 6H, $^3J_{HH}$ = 7.5 Hz, H-4, H-5, H-6), 2.95 (s, 3H, H-1).

^{13}C{H}-NMR (75.53 MHz, DMSO d_6): δ = 119.5 (J_{CF} = 320.7 Hz, C-8, C-9), 53.3 (J_{CN} = 3.3 Hz, C-2, C-3, C-4), 50.8 (J_{CN} = 4.4 Hz, C-1), 44.7 (C-5, C-6, C-7).

^{19}F-NMR (470.39 MHz, DMSO-d_6): δ = –78.8.

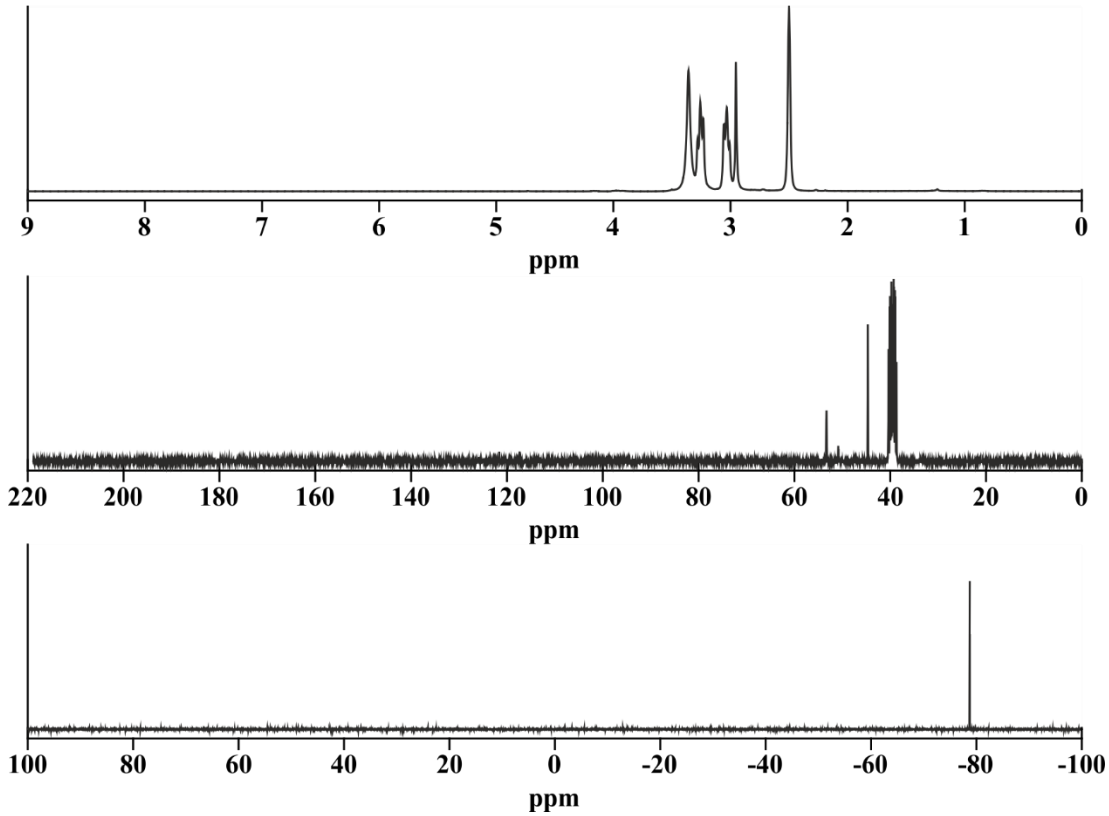

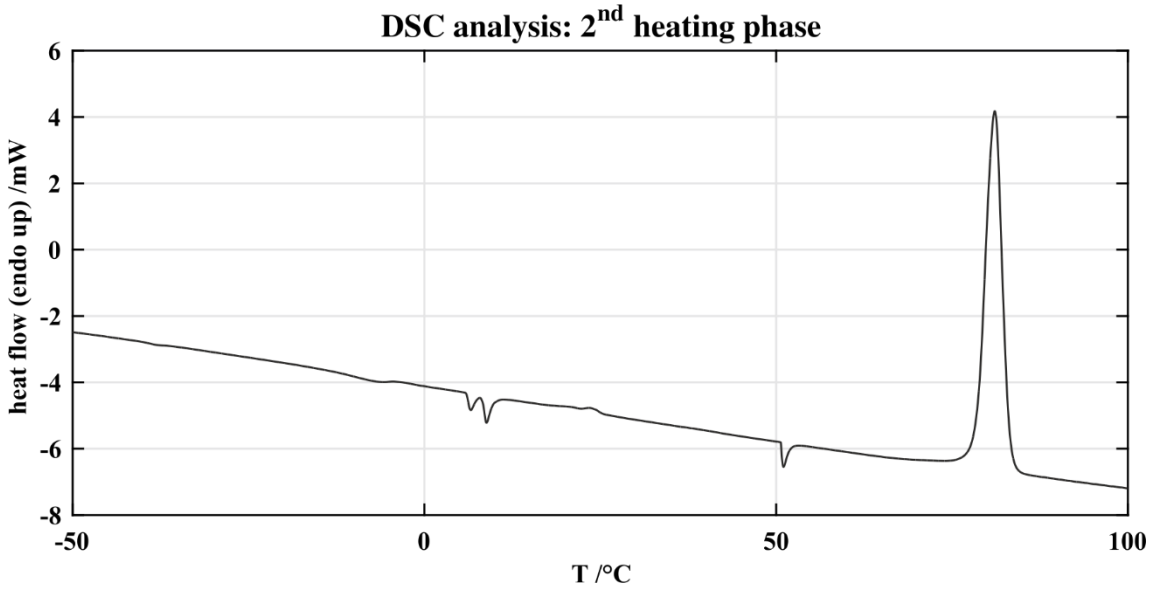

7.5.17.26. 1-Pentyl-1,4-diazabicyclo[2.2.2]octan-1-ium bis(trifluoromethane)sulfonimide (**35b**)

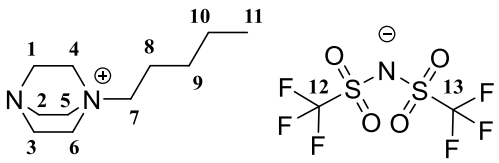

An oven dried 100 mL round-bottom flask equipped with a TEFLON®-coated magnetic stirring bar was charged with 1.00 g (8.92 mmol, 2.0 eq) diazabicyclo[2.2.2]octan and 10 mL of

MeCN. The colorless solution was stirred for 5 min at RT. Afterwards 552 µL (4.37 mmol, 1.0 eq) 1-bromopentane were added. The reaction mixture was stirred for 16 h at 70 °C and the reaction control was performed by NMR-spectroscopy. Afterwards the reaction mixture was diluted with 30 mL Et_2O. 2 Phases were formed and the denser layer was washed with Et_2O (3 × 5 mL). The crude product was dried in oil pump vacuum at 10^{-2} mbar for 5 h. Afterwards the crude product was dissolved in 5 mL of H_2O and 6.66 mL of a 0.5 M (3.33 mmol, 0.8 eq) lithium bis(trifluoromethane)sulfonimide solution in H_2O were added at RT. The reaction mixture was stirred for 5 min and transferred into a separatory funnel. The aqueous phase was extracted with DCM (3 × 20 mL). Subsequently the organic phase was washed with H_2O (3 × 10 mL). The solvent of the organic phases was removed and to the residue 40 mL acetone and activated charcoal were added. The suspension was stirred for 3 h and filtered through a small plug of activated alumina. Finally, the solvent was removed and the product was dried in oil pump vacuum at 10^{-2} mbar for 3 h.

Yield: 1.83 g (2.97 mmol, 68 % o. th.), colorless oil

$C_{13}H_{23}F_6N_3O_4S_2$ [463.45 g/mol]

mp: 43-49 °C

^{1}H-NMR (300.36 MHz, $CDCl_3$): δ = 3.32 (t, 6H, $^3J_{HH}$ = 6.6 Hz, H-4, H-5, H-6), 3.13-3.27 (m, 8H, $^3J_{HH}$ = 6.6 Hz, H-1, H-2, H-3, H-7), 1.61-1.79 (m, 2H, H-8), 1.26-1.44 (m, 4H, H-9, H-10), 0.91 (t, 3H, $^3J_{HH}$ = 6.8 Hz, H-11).

^{13}C{H}-NMR (75.53 MHz, $CDCl_3$): δ = 120.0 (J_{CF} = 322.0 Hz, C-12, C-13), 65.3 (J_{CN} = 2.4 Hz, C-7), 52.8 (J_{CN} = 3.1 Hz, C-4, C-5, C-6), 45.3 (C-1, C-2, C-3), 28.3 (C-10), 22.2 (C-9), 21.6 (C-8), 13.8 (C-11).

^{19}F-NMR (470.39 MHz, DMSO-d_6): δ = –78.9.

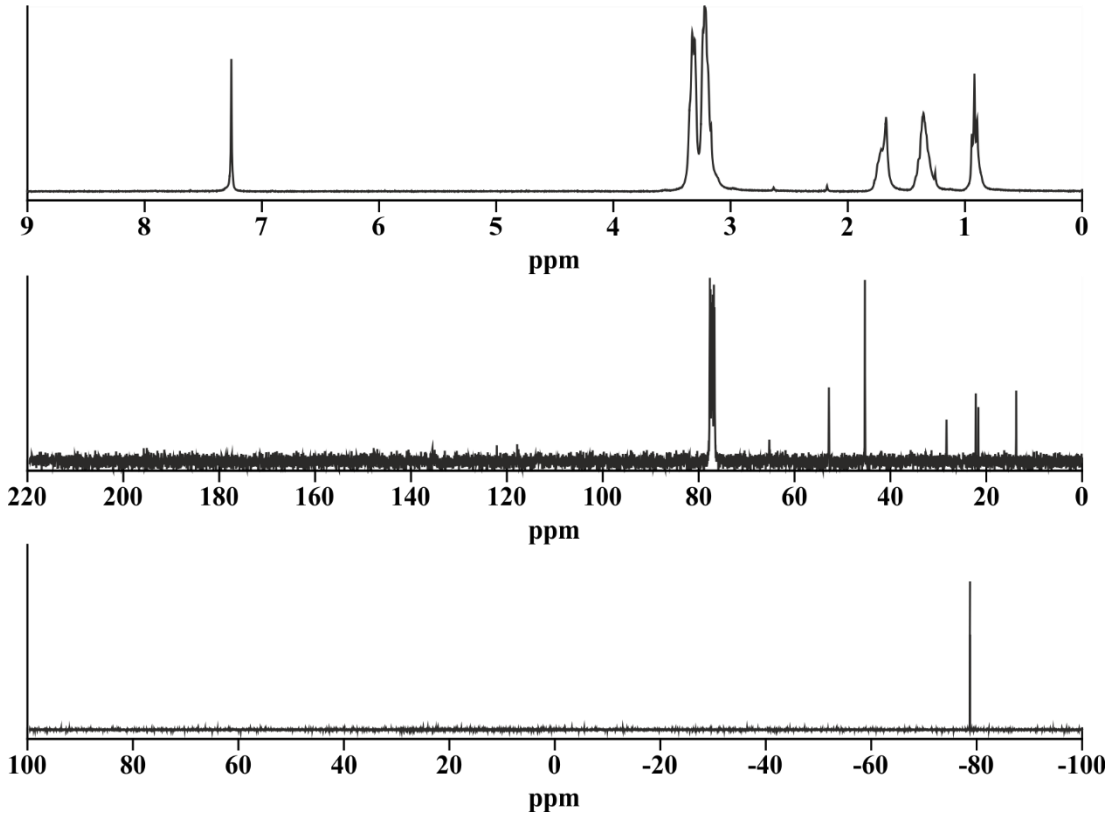
9
8
7
6
5
4
3
2
1
0
ppm
220
200
180
160
140
120
100
80
60
40
20
0
ppm
100
80
60
40
20
0
-20
-40
-60
-80
-100
ppm

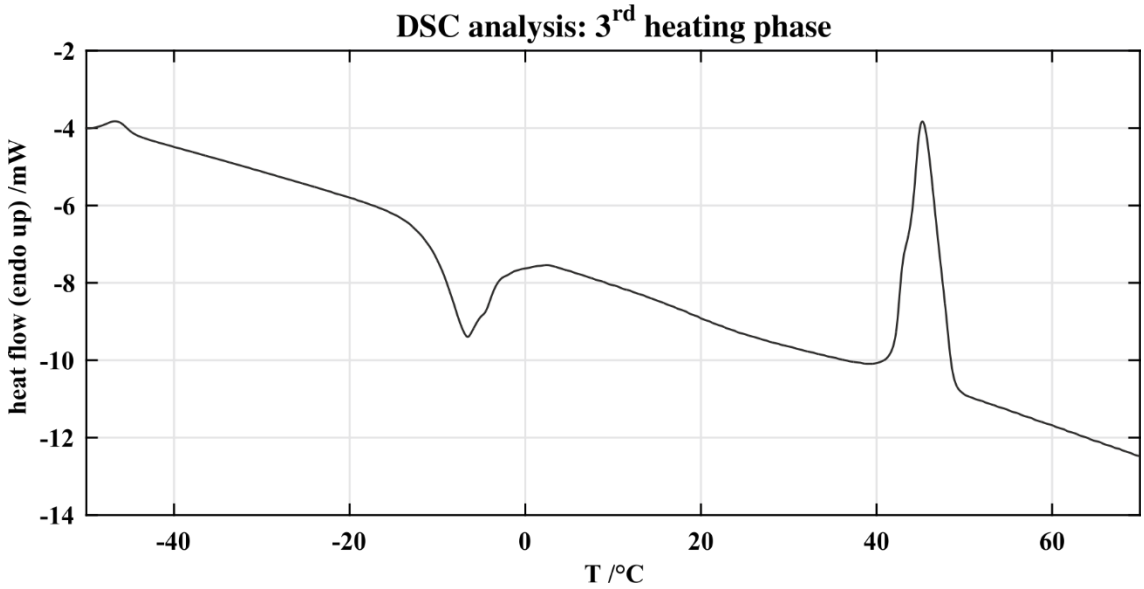
DSC analysis: 3rd heating phase
heat flow (endo up) /mW
-2
-4
-6
-8
-10
-12
-14
-40
-20
0
20
40
60
T /°C

7.5.17.27. 1-Hexyl-1,4-diazabicyclo[2.2.2]octan-1-ium bis(trifluoromethane)sulfonimide (**35c**)

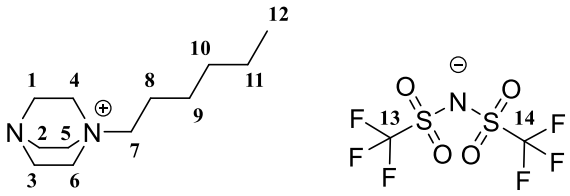

An oven dried 100 mL round-bottom flask equipped with a TEFLON®-coated magnetic stirring bar was charged with 1.00 g (8.92 mmol, 2.0 eq) diazabicyclo[2.2.2]octan and 10 mL of MeCN. The colorless solution was stirred for 5 min at RT. Afterwards 682 µL (4.36 mmol, 1.0 eq) 1-iodohexane were added. The reaction mixture was stirred for 16 h at 70 °C and the reaction control was performed by NMR-spectroscopy. Afterwards the reaction mixture was diluted with 30 mL Et_2O. 2 Phases were formed and the denser layer was washed with Et_2O (3 × 5 mL). During washing with Et_2O a colorless solid precipitated. The crude product was dried in oil pump vacuum at 10^{-2} mbar for 5 h. Afterwards the crude product was dissolved in 10 mL of H_2O and 6.60 mL of a 0.5 M (3.30 mmol, 0.8 eq) lithium bis(trifluoromethane)-sulfonimide solution in H_2O were added at RT. The reaction mixture was stirred for 5 min and transferred into a separatory funnel. The aqueous phase was extracted with DCM (3 × 20 mL). Subsequently the organic phase was washed with H_2O (3 × 10 mL). The solvent of the organic phases was removed and to the residue 40 mL acetone and activated charcoal were added. The suspension was stirred for 3 h and filtered through a small plug of activated alumina. Finally, the solvent was removed and the product was dried in oil pump vacuum at 10^{-2} mbar for 3 h.

Yield: 1.27 g (2.67 mmol, 61 % o. th.), colorless oil

$C_{14}H_{25}F_6N_3O_4S_2$ [477.48 g/mol]

mp: 30-36 °C

^{1}H-NMR (300.36 MHz, $CDCl_3$): δ = 3.29 (t, 6H, $^3J_{HH}$ = 6.6 Hz, H-4, H-5, H-6), 3.12-3.24 (m, 8H, $^3J_{HH}$ = 6.6 Hz, H-1, H-2, H-3, H-7), 1.63-1.76 (m, 2H, H-8), 1.24-1.40 (m, 6H, H-9, H-10, H-11), 0.89 (t, 3H, $^3J_{HH}$ = 6.7 Hz, H-12).

^{13}C{H}-NMR (75.53 MHz, $CDCl_3$): δ = 120.0 (J_{CF} = 322.0 Hz, C-13, C-14), 65.2 (J_{CN} = 2.9 Hz, C-7), 52.8 (J_{CN} = 3.3 Hz, C-4, C-5, C-6), 45.3 (C-1, C-2, C-3), 31.1 (C-11), 25.9 (C-9), 22.4 (C-10), 21.8 (C-8), 13.9 (C-12).

^{19}F-NMR (470.39 MHz, $CDCl_3$): δ = –78.9.

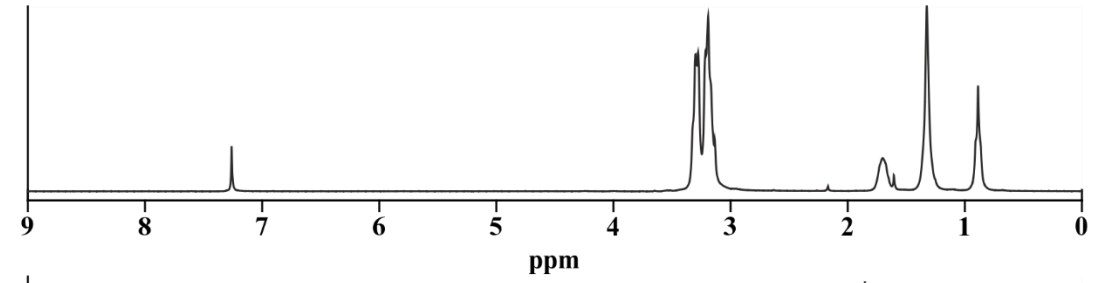
9
8
7
6
5
4
3
2
1
0
ppm

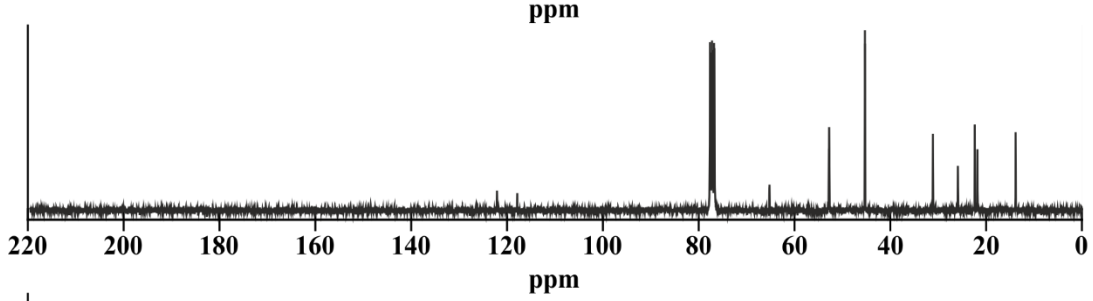
220
200
180
160
140
120
100
80
60
40
20
0
ppm

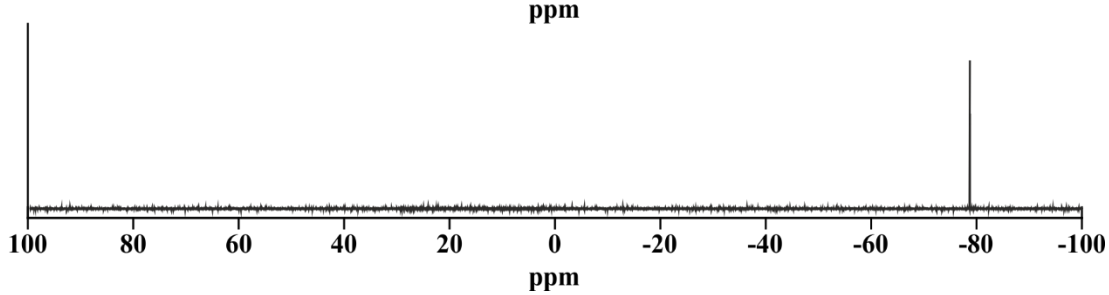
100
80
60
40
20
0
-20
-40
-60
-80
-100
ppm

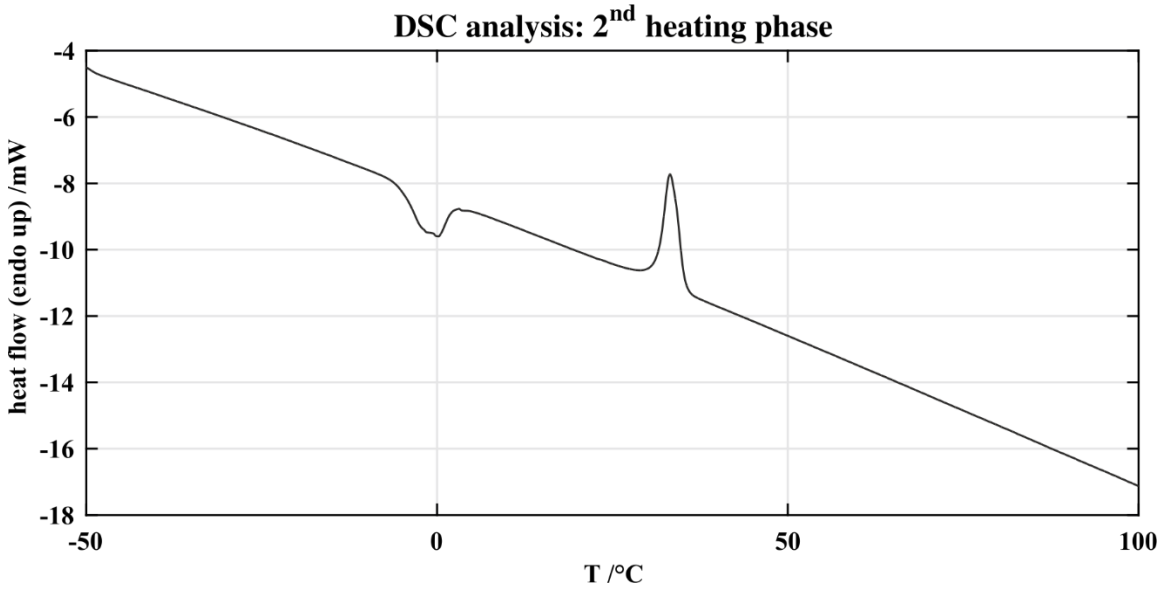
DSC analysis: 2nd heating phase
heat flow (endo up) /mW
-4
-6
-8
-10
-12
-14
-16
-18
-50
0
50
100
T /°C

7.5.17.28. $N^1,N^{1'}$-(Butane-1,4-diyl)bis(N^1-(2-(diethylamino)ethyl)-N^2,N^2-diethylethane-1,2-diamine) (**36a**)

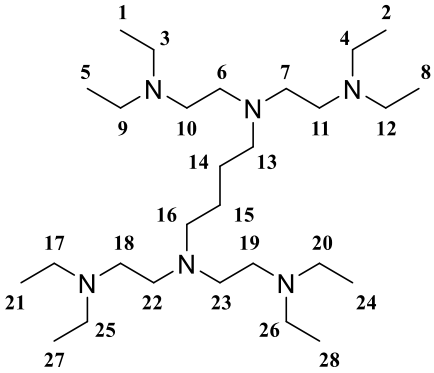

An oven dried 250 mL SCHLENK flask equipped with a TEFLON®-coated magnetic stirring bar was charged with 1.00 mL (3.50 mmol, 2.0 eq) *N*,*N*,*N*',*N*'-tetraethyldiethylenetriamine, 325 µL (3.99 mmol, 2.2 eq) pyridine and 25 mL of absolute DCM under nitrogen atmosphere. The yellow solution was stirred for 10 min and cooled to –50 °C. A further oven dried 25 mL SCHLENK flask equipped with a TEFLON®-coated magnetic stirring bar was charged with 204 µL (1.75 mmol, 1.0 eq) succinyl chloride and 5 mL of absolute DCM under nitrogen atmosphere. Afterwards the acid chloride-solution was added slowly to the cold reaction solution over a period of 30 min. During the addition the color of the solution changed from yellow to dark brown. After 2 h of stirring at –50 °C, the reaction flask was allowed to warm up to RT and stirring was continued overnight. The reaction control was performed by NMR-spectroscopy. The reaction mixture was transferred into a separatory funnel and was washed with sat. $NaHCO_3$ (3 × 15 mL). Subsequently the aqueous phase was reextracted with DCM (3 × 10 mL). The combined organic phases were washed with brine (1 × 20 mL), dried over Na_2SO_4, filtered and the solvent was removed under reduced pressure. The residue was dissolved in 60 mL of Et_2O and an excess of HCl dissolved in Et_2O (9 mL of a 1.5 M solution) was added. The formed precipitate was collected, dissolved in 5 mL of MeOH and dried in oil pump vacuum at 10^{-2} mbar for 3 h. Afterwards an oven dried 100 mL SCHLENK flask equipped with a TEFLON®-coated magnetic stirring bar was charged with the crude-product and 20 mL of absolute THF under nitrogen atmosphere. The yellow reaction mixture was stirred for 10 min and cooled to –50 °C. 249 mg (6.55 mmol, 3.8 eq) lithium aluminum hydride were added slowly to the cold reaction flask over a period of 5 min. During the addition gas evolution was observed. After 2 h of stirring at –50 °C the reaction flask was allowed to warm up to RT and stirring was continued overnight. The reaction control was performed by NMR-spectroscopy. 3 mL H_2O, followed by 3 mL of 15% NaOH-solution and 9 mL H_2O were slowly added to the

reaction mixture. Afterwards the organic phase was transferred into a separatory funnel and was washed with sat. $NaHCO_3$ (3 × 10 mL). Subsequently the aqueous phase was reextracted with DCM (3 × 10 mL). The combined organic phases were washed with brine (1 × 15 mL), dried over Na_2SO_4, filtered and the solvent was removed under reduced pressure. Finally, the product was dried in oil pump vacuum at 10^{-2} mbar for 5 h.

Yield: 381 mg (0.79 mmol, 45 % o. th.), brown oil

$C_{28}H_{64}N_6$ [484.86 g/mol]

HR-MS (MALDI: [M+1]) [*m/z*]: calculated: 485.5271, found: 485.5286

R_f = too polar for SiO_2-TLC plates

^{1}H-NMR (300.36 MHz, $CDCl_3$): δ = 2.42-2.60 (m, 36H, H-3, H-4, H-6, H-7, H-9, H-10, H-11, H-12, H-13, H-16, H-17, H-18, H-19, H-20, H-22, H-23, H-25, H-26), 1.42 (bs, 4H, H-14, H-15), 1.02 (t, 24H, $^3J_{HH}$ = 7.1 Hz, H-1, H-2, H-5, H-8, H-21, H-24, H-27, H-28).

^{13}C{H}-NMR (75.53 MHz, $CDCl_3$): δ = 55.4 (C-13, C-16), 52.9 (C-6, C-7, C-22, C-23), 51.3 (C-10, C-11, C-18, C-19), 47.6 (C-3, C-4, C-9, C-12, C-17, C-20, C-25, C-26), 25.3 (C-14, C-15), 11.8 (C-1, C-2, C-5, C-8, C-21, C-24, C-27, C-28).

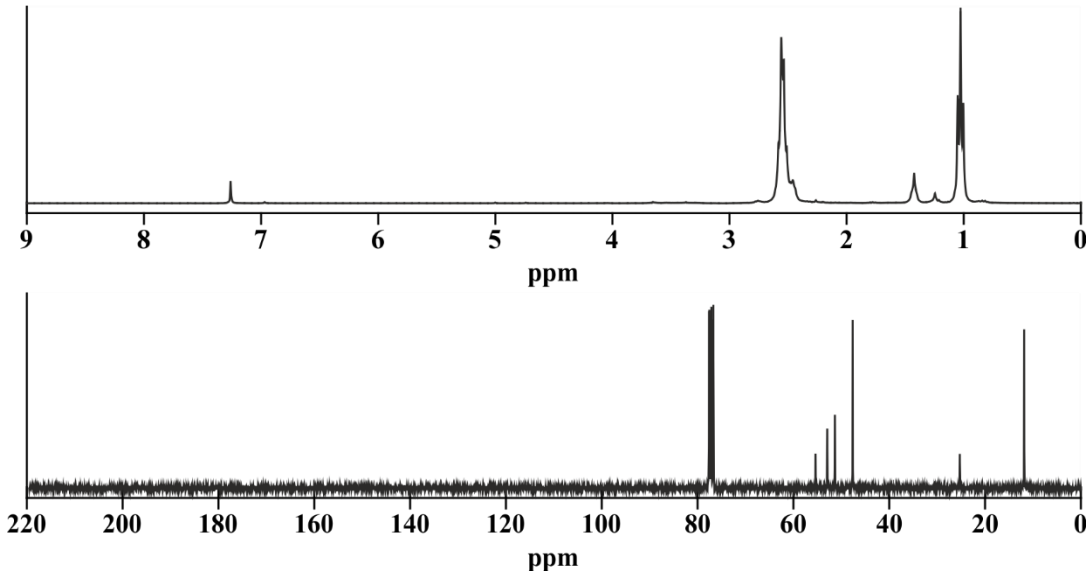

7.5.17.29. N^1,$N^{1'}$-(Hexane-1,6-diyl)bis(N^1-(2-(diethylamino)ethyl)-N^2,N^2-diethylethane-1,2-diamine) (**36b**)

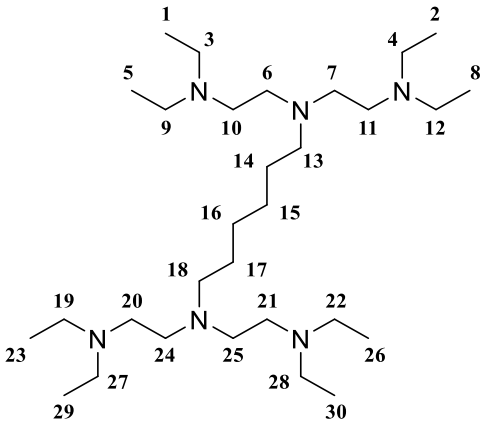

An oven dried 100 mL SCHLENK flask equipped with a TEFLON®-coated magnetic stirring bar was charged with 1.00 mL (3.50 mmol, 2.0 eq) *N*,*N*,*N*',*N*'-tetraethyldiethylenetriamine, 325 µL (3.99 mmol, 2.2 eq) pyridine and 25 mL of absolute DCM under nitrogen atmosphere. The yellow solution was stirred for 10 min and cooled to –50 °C. A further oven dried 25 mL SCHLENK flask equipped with a TEFLON®-coated magnetic stirring bar was charged with 262 µL (1.75 mmol, 1.0 eq) adipoyl chloride and 5 mL of absolute DCM under nitrogen atmosphere. Afterwards the acid chloride-solution was added slowly to the cold reaction solution over a period of 30 min. During the addition the color of the solution changed from yellow to brown. After 2 h of stirring at –50 °C, the reaction flask was allowed to warm up to RT and stirring was continued overnight. The reaction control was performed by NMR-spectroscopy. The reaction mixture was transferred into a separatory funnel and was washed with sat. $NaHCO_3$ (3 × 15 mL). Subsequently the aqueous phase was reextracted with DCM (3 × 10 mL). The combined organic phases were washed with brine (1 × 20 mL), dried over Na_2SO_4, filtered and the solvent was removed under reduced pressure. The residue was dissolved in 60 mL of Et_2O and an excess of HCl dissolved in Et_2O (9 mL of a 1.5 M solution) was added. The formed precipitate was collected, dissolved in 5 mL of MeOH and dried in oil pump vacuum at 10^{-2} mbar for 3 h. Afterwards an oven dried 100 mL SCHLENK flask equipped with a TEFLON®-coated magnetic stirring bar was charged with the crude-product and 20 mL of absolute THF under nitrogen atmosphere. The yellow reaction mixture was stirred for 10 min and cooled to –50 °C. 251 mg (6.55 mmol, 3.8 eq) lithium aluminum hydride were added slowly to the cold reaction flask over a period of 5 min. During the addition gas evolution was observed. After 2 h of stirring at –50 °C the reaction flask was allowed to warm up to RT and stirring was continued overnight. The reaction control was performed by NMR-spectroscopy. 3 mL H_2O, followed by

3 mL of 15% NaOH-solution and 9 mL H_2O were slowly added to the reaction mixture. Afterwards the organic phase was transferred into a separatory funnel and was washed with sat. $NaHCO_3$ (3 × 10 mL). Subsequently the aqueous phase was reextracted with DCM (3 × 10 mL). The combined organic phases were washed with brine (1 × 15 mL), dried over Na_2SO_4, filtered and the solvent was removed under reduced pressure. Finally, the product was dried in oil pump vacuum at 10^{-2} mbar for 5 h.

Yield: 491 mg (0.96 mmol, 54 % o. th.), brown oil

$C_{28}H_{64}N_6$ [512.92 g/mol]

HR-MS (MALDI: [M+1]) [*m/z*]: calculated: 513.5583, found: 513.5523

R_f = too polar for SiO_2-TLC plates

^{1}H-NMR (300.36 MHz, $CDCl_3$): δ = 2.46-2.59 (m, 32H, H-3, H-4, H-6, H-7, H-9, H-10, H-11, H-12, H-19, H-20, H-21, H-22, H-24, H-25, H-27, H-28), 2.39-2.65 (m, 4H, H-13, H-18), 1.36-1.47 (m, 4H, H-14, H-17), 1.20-1.29 (m, 4H, H-15, H-16), 1.01 (t, 24H, $^3J_{HH}$ = 7.1 Hz, H-1, H-2, H-5, H-8, H-23, H-26, H-29, H-30).

^{13}C{H}-NMR (75.53 MHz, $CDCl_3$): δ = 55.5 (C-13, C-18), 53.0 (C-6, C-7, C-24, C-25), 51.3 (C-10, C-11, C-20, C-21), 47.6 (C-3, C-4, C-9, C-12, C-19, C-22, C-27, C-28), 27.7 (C-15, C-16), 27.4 (C-14, C-17), 11.9 (C-1, C-2, C-5, C-8, C-23, C-26, C-29, C-30).

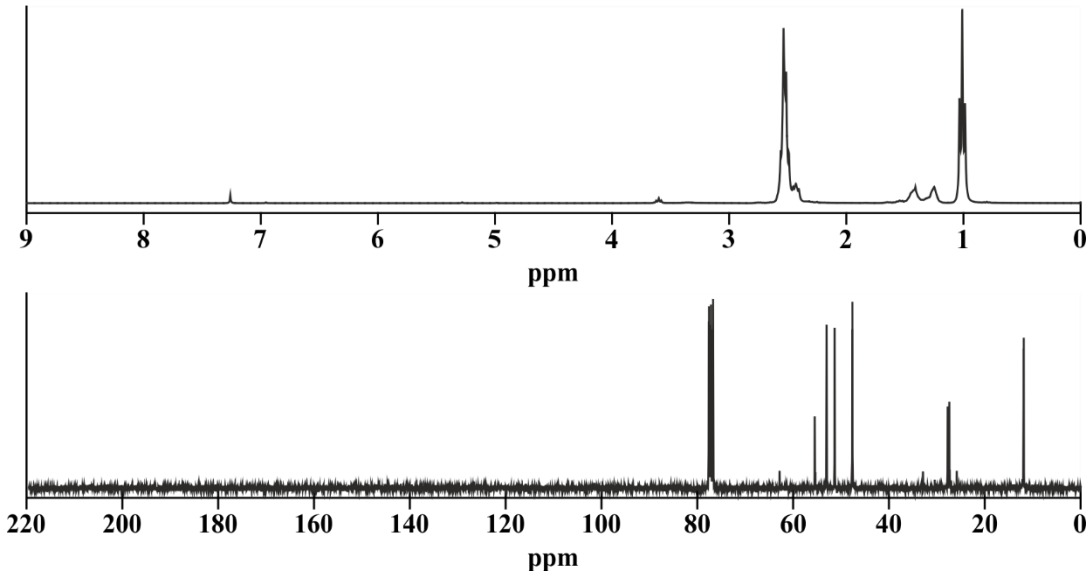

7.5.17.30. 2-(2-(2-Methoxyethoxy)ethoxy)ethyl 4-methylbenzenesulfonate (**38**)

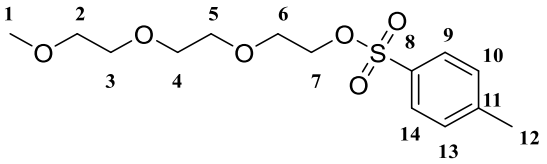

A 250 mL round bottom flask equipped with a TEFLON®-coated magnetic stirring bar was charged with 8.20 g (50 mmol, 1.0 eq) 2-(2-(2-methoxyethoxy)ethoxy)ethanol, 15 mL (185 mmol, 3.7 eq) pyridine and 100 mL DCM. The bright yellow solution was stirred for 5 min at RT. Then 15.3 g (80 mmol, 1.6 eq) *p*-toluenesulfonyl chloride were added over a period of 5 min and the yellow solution was stirred overnight at RT. The reaction control was performed by TLC. Afterwards the reaction mixture was diluted with 80 mL DCM and 20 mL H_2O and stirred for further 30 min at RT. The reaction mixture was transferred into a separatory funnel. The organic phase was washed with 1 M HCl (3 × 80 mL). The aqueous phase was reextracted with DCM (3 × 50 mL). Then the combined organic phases were washed with brine (1 × 40 mL), dried over Na_2SO_4, filtered and the solvent was removed under reduced pressure. Finally, the yellow oil was dried in oil pump vacuum at 10^{-2} mbar for 1 d.

Yield: 15.9 g (50 mmol, 99 % o. th.), bright yellow oil

$C_{14}H_{22}O_6S$ [318.38 g/mol]

R_f = 0.20 (EtOAc/cyclohexane = 1:1 (v/v)), ($KMnO_4$)

^{1}H-NMR (300.36 MHz, $CDCl_3$): δ = 7.79 (d, 2H, $^3J_{HH}$ = 8.3 Hz, H-9, H-14), 7.33 (d, 2H, $^3J_{HH}$ = 8.3 Hz, H-10, H-13), 4.17 (t, 2H, $^3J_{HH}$ = 5.0 Hz, H-7), 3.68 (t, 2H, $^3J_{HH}$ = 5.0 Hz, H-6), 3.56-3.62 (m, 6H, H-3, H-4, H-5), 3.50-3.55 (m, 2H, H-2), 3.36 (s, 3H, H-1), 2.43 (s, 3H, H-12).

^{13}C{H}-NMR (75.53 MHz, $CDCl_3$): δ = 144.9 (C-8), 133.2 (C-11), 129.9 (C-10, C-13), 128.1 (C-9, C-14), 72.0 (C-2), 70.9 (C-3), 70.8 (C-4, C-5), 69.4 (C-7), 68.8 (C-6), 59.1 (C-1), 21.8 (C-12).

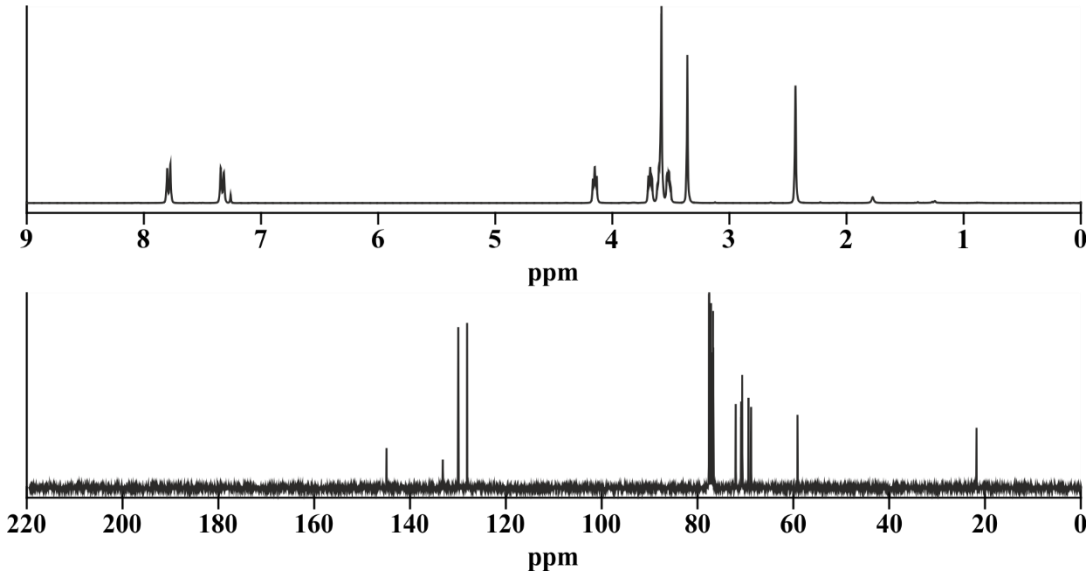
9
8
7
6
5
4
3
2
1
0
ppm
220
200
180
160
140
120
100
80
60
40
20
0
ppm

8. Appendix

8.1. Synthesis of Literature Known Molecules

For reasons of saving money, diverse substrates for synthesis were produced by ourselves, because buying larger amounts were too expensive (Figure 8.1).

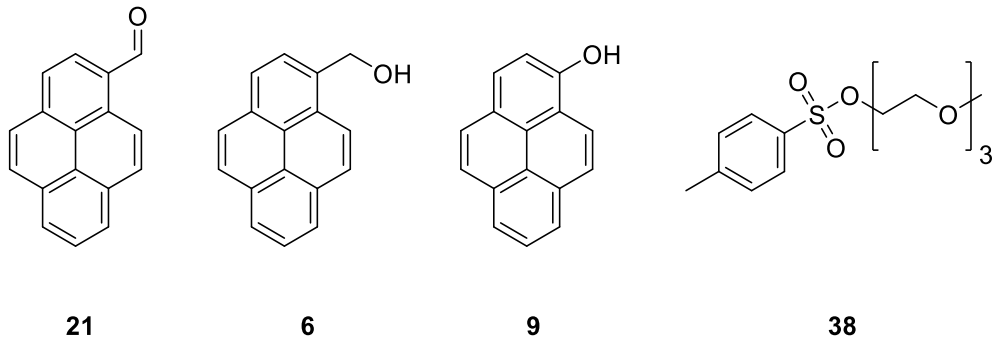

Figure 8.1: Substrates, which were prepared in the laboratory, because they are expensive.

8.1.1. Preparation of pyren-1-ylmethanol (**6**)[75]

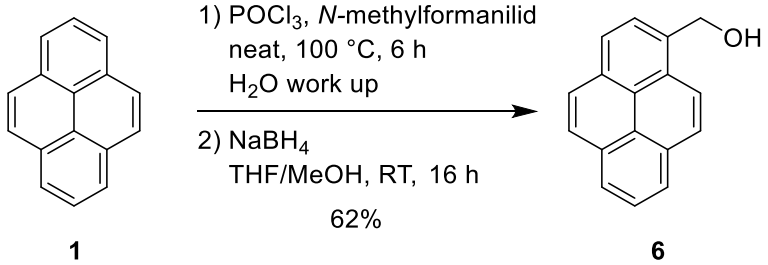

Scheme 8.1: 2-Step reaction of pyrene (**1**) to of pyren-1-ylmethanol (**6**).

Based on the literature of ZENG *et al.*, pyren-1-ylmethanol was produced the same way.[75] In the first step of the reaction, 1.0 equivalents of *N*-methylformanilide were treated with

1.1 equivalents of $POCl_3$ to create a chloriminium ion. After the addition of 1.0 equivalent of pyrene **1**, a further intermediate was generated, which produced desired product after aqueous work up according to VILSMEIER-HAACK reaction. The reaction mixture was no purified. The intermediate product was dissolved in THF and $NaBH_4$ dissolved in MeOH was added to reduce the carbonyl moiety. After work up, the product was purified by flash chromatography from unreacted remaining pyrene. Purification itself was easy to perform, because the difference in polarity of the substrate and the product was huge. The reaction was performed in 1 g scale and compared to literature we lost 1% of product yield (Scheme 8.1).

8.1.2. Preparation of 1-hydroxypyrene (**9**)[76]

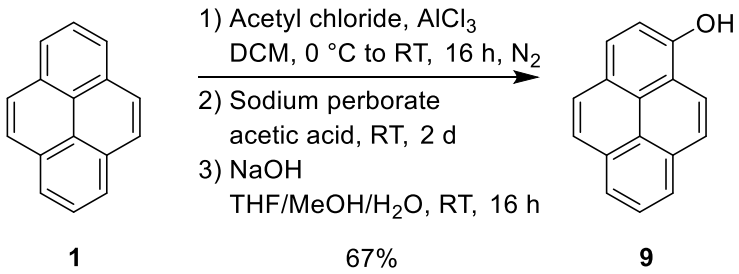

Scheme 8.2: 3-Step reaction of pyrene (**1**) to of 1-hydroxypyrene (**9**).

Preparation of 1-hydroxypyrene was performed according to the literature of GEORGE *et al.* and HARVEY *et al.*.[76] In the first step of this multistep synthesis, 1.1 equivalents of acetyl chloride reacted with 1.0 equivalent pyrene **1** *via* catalysis of $AlCl_3$ according to FRIEDEL-CRAFTS acylation reaction. After purification by flash chromatography, the purified intermediate product was oxidized with 3.3 equivalents of sodium perborate according to DAKIN reaction. During the reaction, 1-acetoxypyrene was oxidized to the corresponding ester. Due to the higher reactivity of the aryl moiety, arylesters were generated selectively. Finally, the arylester was saponificated and after acidic work up, the product was purified by extraction. The reaction was performed in 1 g scale and compared to literature we obtained 26% higher product yield (Scheme 8.2).

8.1.3. Preparation of 1-pyrenecarbaldehyde (**21**)[77]

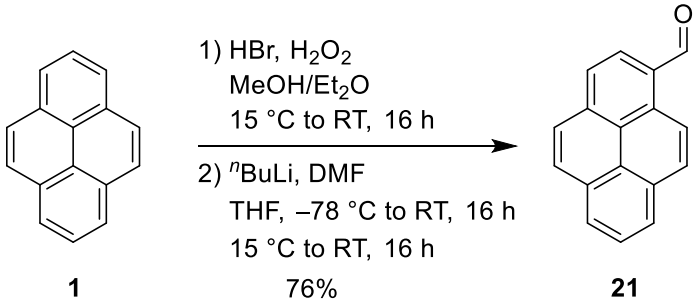

Scheme 8.3: 2-Step reaction of pyrene (**1**) to of 1-pyrencarbaldehyde (**21**).

Based on the literature of SCHULZE *et al.*, 1-pyrenecarbaldehyde was produced the same way.[77] In the first step of the reaction, pyrene **1** was treated with 1.1 equivalents hydrobromic acid and H_2O_2. The *in situ* generated bromine reacted according to an electrophilic substitution of an aromatic compound reaction. Purification of the intermediate product was done by a SOXHLET extraction and further recrystallization. Afterwards, the purified intermediate product was treated with 1.3 equivalents of ^{n}BuLi to perform a metal halogen exchange reaction at –78 °C. Afterwards, the functional group exchange reaction was performed by the addition of DMF. Again, the purification was done by recrystallization of the crude product. Compared to literature, the reaction was downscaled to 50%. However, we increased the overall yield from 57% to 76% and ended up with 8.5 g product in total mass (Scheme 8.3).

8.1.4. Preparation of 2-(2-(2-methoxyethoxy)ethoxy)ethyl 4-methylbenzenesulfonate (**37**)[78]

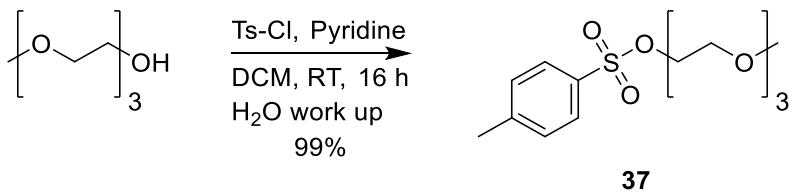

Scheme 8.4: Preparation of 2-(2-(2-methoxyethoxy)ethoxy)ethyl 4-methylbenzenesulfonate (**37**).

The simple group transformation reaction was performed according to literature of ZHU *et al.*.[78] The reaction used pyridine as nucleophilic catalyst as well as base. Furthermore, an excess of 1.6 equivalents of tosyl chloride was used from this reaction. After full conversion, the excess of tosyl chloride was quenched with H_2O over a period of 30 min. The product was purified by extraction ending up with quantitative yield. The reaction was performed in a 30 g scale (Scheme 8.4).

8.2. Crystallographic Parameters of Synthesized Compounds

Table 8.1: Crystallographic data and details of measurements for 1,1'-(((sulfonylbis(ethane-2,1-diyl))bis(oxy)bis(methylene)dipyrene (**4**), 1-(pyren-1-yl)-2,5,8,11-tetraoxadodecane (**7**), (±)-exo-5-(ethenyl-sulfonyl)bicyclo-[2.2.1]hept-2-ene (**27b**), (±)-1-((2-((*endo*-5-bicyclo[2.2.1]hept-5-en-2-yl)sulfonyl)ethoxy)-methyl)pyrene (**24a**) and (±)-1-((2-((*exo*-5-bicyclo[2.2.1]hept-5-en-2-yl)sulfonyl)ethoxy)methyl)pyrene (**24b**) Mo Kα (λ=0.71073Å). $R_1 = \Sigma/ |F_o|- |F_c|/|\Sigma|F_d$; $wR2 = [\Sigma_w(F_o^2-F_2^2)^2/\Sigma_w(F_o^2)^2]^{1/2}$.

Compound	**4**	**7**	**27b**	**24a**	**24b**
Formula	$C_{38}H_{30}O_4S$	$C_{24}H_{26}O_6$	$C_9H_{12}O_2S$	$C_{26}H_{24}O_3S$	$C_{26}H_{24}O_3S$
Fw (g/mol)	582.68	378.45	184.25	416.51	416.51
***a* (Å)**	20.7413 (10)	8.9168 (13)	5.5052(2)	11.4616(6)	12.7368(19)
***b* (Å)**	12.0102 (6)	11.7881 (18)	10.0320(4)	14.8509(8)	12.6508(14)
***c* (Å)**	11.2816 (6)	16.457 (2)	15.9491(7)	12.0866(6)	12.794(2)
***α* (°)**	90	84.819 (7)	880.84(6)	2052.17(18)	2034.4(5)
***β* (°)**	91.340 (2)	87.969 (6)	90	90	90
***γ* (°)**	90	73.991 (7)	90	94.054(2)	99.299(8)
***V* (Å³)**	2809.6 (2)	1957.7 (5)	90	90	90
Z	4	4	4	4	4
Crystal size (mm)	0.07 × 0.07 × 0.02	0.20 × 0.19 × 0.15	0.12 × 0.09 × 0.07	0.09 × 0.07 × 0.01	0.20 × 0.16 × 0.14
Crystal habit	Plate, yellow	Block, colorless	Block, colorless	Plate, colorless	Block, yellow
Crystal system	Monoclinic	Triclinic	Orthorhombic	Monoclinic	Monoclinic
Space group	$P2_1/c$	$P\bar{1}$	$P2_12_12_1$	$P2_1/c$	$P2_1/c$
d_{calc} (mg/m³)	1.378	1.284	1.389	1.348	1.360
μ (mm⁻¹)	0.16	0.09	0.32	0.18	0.19
***T* (K)**	100(2)	100(2)	100(2)	100(2)	100(2)
2*θ* range (°)	2.5-33.1	2.4-33.3	2.4-33.2	2.2–33.1	2.3–33.3
***F*(000)**	1224	808	392	880	880
R_{int}	0.078	0.212	0.111	0.118	0.077
independent reflections	10730	6859	1544	3610	3563
No. of parameters	388	507	109	271	271
R1, wR2 (all data)	R1 = 0.0760 wR2 = 0.1459	R1 = 0.1826 wR2 = 0.0649	R1 = 0.0347 wR2 = 0.0643	R1 = 0.1142 wR2 = 0.1665	R1 = 0.0554 wR2 = 0.1295
R1, wR2 (>2*σ*)	R1 = 0.0490 wR2 = 0.1293	R1 = 0.1714 wR2 = 0.1312	R1 = 0.0297 wR2 = 0.0621	R1 = 0.0640 wR2 = 0.1386	R1 = 0.0477 wR2 = 0.1219

9. Bibliography

[1] a) S. J. Park, H. Zhao, G. Ai, C. Wang, X. Song, N. Yuca, V. S. Battaglia, W. Yang, G. Liu, *J Am Chem Soc* **2015**, *137*, 2565-2571; b) T. M. Higgins, S. H. Park, P. J. King, C. J. Zhang, N. McEvoy, N. C. Berner, D. Daly, A. Shmeliov, U. Khan, G. Duesberg, V. Nicolosi, J. N. Coleman, *ACS Nano* **2016**, *10*, 3702-3713; c) S. D. Xun, X. Y. Song, V. Battaglia, G. Liu, *J. Electrochem. Soc.* **2013**, *160*, A849-A855; d) S. D. Xun, B. Xiang, A. Minor, V. Battaglia, G. Liu, *J. Electrochem. Soc.* **2013**, *160*, A1380-A1383; e) H. Zhao, Y. Wei, R. Qiao, C. Zhu, Z. Zheng, M. Ling, Z. Jia, Y. Bai, Y. Fu, J. Lei, X. Song, V. S. Battaglia, W. Yang, P. B. Messersmith, G. Liu, *Nano Lett* **2015**, *15*, 7927-7932; f) K. L. Wang, T. H. Kuo, C. F. Yao, S. W. Chang, Y. S. Yang, H. K. Huang, C. J. Tsai, M. Horie, *Chem Commun (Camb)* **2017**, *53*, 1856-1859.

[2] a) M. N. Obrovac, L. Christensen, D. B. Le, J. R. Dahn, *J. Electrochem. Soc.* **2007**, *154*, A849; b) M. Winter, J. O. Besenhard, *Electrochim. Acta* **1999**, *45*, 31-50; c) D. Mazouzi, B. Lestriez, L. Roué, D. Guyomard, *Electrochemical and Solid-State Letters* **2009**, *12*, A215; d) J. Cabana, L. Monconduit, D. Larcher, M. R. Palacin, *Adv Mater* **2010**, *22*, E170-192; e) J. Christensen, P. Albertus, R. S. Sanchez-Carrera, T. Lohmann, B. Kozinsky, R. Liedtke, J. Ahmed, A. Kojic, *J. Electrochem. Soc.* **2011**, *159*, R1-R30; f) P. G. Bruce, S. A. Freunberger, L. J. Hardwick, J. M. Tarascon, *Nat Mater* **2011**, *11*, 19-29; g) X. Ji, K. T. Lee, L. F. Nazar, *Nat Mater* **2009**, *8*, 500-506; h) S. A. Freunberger, *Nature Energy* **2017**, *2*, 17091.

[3] N. Mahne, O. Fontaine, M. O. Thotiyl, M. Wilkening, S. A. Freunberger, *Chemical science* **2017**, *8*, 6716-6729.

[4] R. M. Dell, D. A. J. Rand, **2001**, 1-8.

[5] A. Volta, *Philosophical Transactions of the Royal Society of London* **1800**, *90*, 403-431.

[6] a) C. Julien, A. Mauger, A. Vijh, K. Zaghib, **2016**, 29-68; b) J. Światowska, P. Barboux, **2015**, 125-166.

[7] M. B. Armand, M. S. Whittingham, R. A. Huggins, *Mater. Res. Bull.* **1972**, *7*, 101-+.

[8] a) G. E. Blomgren, *J. Electrochem. Soc.* **2017**, *164*, A5019-A5025; b) K. Mizushima, P. C. Jones, P. J. Wiseman, J. B. Goodenough, *Mater. Res. Bull.* **1980**, *15*, 783-789.

[9] a) S. Basu, *Vol. US4423125*, USA, **1982**; b) R. Yazami, P. Touzain, *J. Power Sources* **1983**, *9*, 365-371.

[10] A. Yoshino, K. Sanechika, T. Nakajima, *Vol. US4668595*, Japan, **1987**.

[11] Y. Nishi, in *Lithium Ion Batteries*, Wiley-VCH Verlag GmbH, **2007**, pp. 181-198.

[12] a) S.-W. Kim, D.-H. Seo, X. Ma, G. Ceder, K. Kang, *Advanced Energy Materials* **2012**, *2*, 710-721; b) P. Hartmann, C. L. Bender, M. Vracar, A. K. Durr, A. Garsuch, J. Janek, P. Adelhelm, *Nat Mater* **2013**, *12*, 228-232; c) B. L. Ellis, L. F. Nazar, *Current Opinion in Solid State and Materials Science* **2012**, *16*, 168-177.

[13] a) M. M. Thackeray, C. Wolverton, E. D. Isaacs, *Energy & Environmental Science* **2012**, *5*, 7854; b) B. Scrosati, J. Hassoun, Y.-K. Sun, *Energy & Environmental Science* **2011**, *4*, 3287.

[14] L. Dai, in *Intelligent Macromolecules for Smart Devices*, Springer-Verlag London, **2004**, pp. 41-80.

[15] P. V. Wright, *Polymer International* **1975**, *7*, 319-327.

[16] K. Xu, *Chemical Reviews* **2004**, *104*, 4303-4418.

[17] a) I. Riess, *Solid State Ionics* **2000**, *136*, 1119-1130; b) N. Gondaliya, D. K. Kanchan, P. Sharma, P. Joge, *Materials Sciences and Applications* **2011**, *02*, 1639-1643.

[18] H. Shirakawa, S. Ikeda, *Polymer Journal* **1971**, *2*, 231.

[19] a) C. K. Chiang, Y. W. Park, A. J. Heeger, H. Shirakawa, E. J. Louis, A. G. MacDiarmid, *The Journal of Chemical Physics* **1978**, *69*, 5098-5104; b) M. Levi, D. Aurbach, in *Solid State Electrochemistry I*, Wiley-VCH Verlag GmbH & Co. KGaA, **2009**, pp. 365-396.

[20] a) T.-H. Le, Y. Kim, H. Yoon, *Polymers* **2017**, *9*, 150; b) W.-S. Huang, B. D. Humphrey, A. G. MacDiarmid, *Journal of the Chemical Society, Faraday Transactions 1: Physical Chemistry in Condensed Phases* **1986**, *82*, 2385-2400; c) R. D. McCullough, R. D. Lowe, M. Jayaraman, D. L. Anderson, *The Journal of Organic Chemistry* **1993**, *58*, 904-912.

[21] a) A. Opik, I. Golovtsov, A. Lobanov, K. Kerm, *Synthetic Metals* **1993**, *57*, 4924-4929; b) N. Puanglek, A. Sittattrakul, W. Lerdwijitjarud, *Sci. J. UBU* **2010**, *1*, 35-42; c) K. Kaneto, K. Yoshino, Y. Inuishi, *Solid State Communications* **1983**, *46*, 389-391; d) S. Islam, G. B. V. S. Lakshmi, A. M. Siddiqui, M. Husain, M. Zulfequar, *International Journal of Polymer Science* **2013**, *2013*, 1-7.

[22] H. S. Nalwa, in *Handbook of organic conductive molecules and polymers, Vol. 2*, Wiley, **1997**, pp. 1-60.

[23] a) M. Wan, in *Conducting Polymers with Micro or Nanometer Structure*, Springer Berlin Heidelberg, Berlin, Heidelberg, **2008**, pp. 1-15; b) Y. Li, in *Organic Optoelectronic Materials* (Ed.: Y. Li), Springer International Publishing, Cham, **2015**, pp. 23-50.

[24] B. Philip, J. Xie, J. K. Abraham, V. K. Varadan, *Smart Materials and Structures* **2004**, *13*, N105-N108.

[25] a) Y. Zhang, B. de Boer, P. W. M. Blom, *Advanced Functional Materials* **2009**, *19*, 1901-1905; b) Y. Zhang, P. W. M. Blom, *Applied Physics Letters* **2011**, *98*, 143504; c) A. Nollau, M. Pfeiffer, T. Fritz, K. Leo, *Journal of Applied Physics* **2000**, *87*, 4340-4343; d) M. Bajpai, R. Srivastava, R. Dhar, R. S. Tiwari, *Indian Journal of Materials Science* **2016**, *2016*, 1-8.

[26] H. Borchert, in *Solar Cells Based on Colloidal Nanocrystals*, Springer International Publishing, Cham, **2014**, pp. 39-60.

[27] C. Michot, D. Baril, M. Armand, *Solar energy materials and solar cells* **1995**, *39*, 289-299.

[28] a) F. Tran-Van, T. Henri, C. Chevrot, *Electrochim. Acta* **2002**, *47*, 2927-2936; b) D. Witker, M. D. Curtis, *J. Power Sources* **2006**, *156*, 525-532; c) A. E. Javier, S. N. Patel, D. T. Hallinan, Jr., V. Srinivasan, N. P. Balsara, *Angew Chem Int Ed Engl* **2011**, *50*, 9848-9851; d) N. Costantini, G. Wegner, M. Mierzwa, T. Pakula, *Macromolecular Chemistry and Physics* **2005**, *206*, 1345-1354; e) X. M. Ren, P. G. Pickup, *J. Electrochem. Soc.* **1992**, *139*, 2097-2105; f) A. Giovannitti, D. T. Sbircea, S. Inal, C. B. Nielsen, E. Bandiello, D. A. Hanifi, M. Sessolo, G. G. Malliaras, I. McCulloch, J. Rivnay, *Proc Natl Acad Sci U S A* **2016**, *113*, 12017-12022.

[29] M. P. Bhatt, J. L. Thelen, N. P. Balsara, *Chemistry of Materials* **2015**, *27*, 5141-5148.

[30] a) S. N. Patel, A. E. Javier, K. M. Beers, J. A. Pople, V. Ho, R. A. Segalman, N. P. Balsara, *Nano Lett* **2012**, *12*, 4901-4906; b) S. N. Patel, A. E. Javier, G. M. Stone, S. A. Mullin, N. P. Balsara, *Acs Nano* **2012**, *6*, 1589-1600.

[31] C. O. Laoire, S. Mukerjee, K. Abraham, E. J. Plichta, M. A. Hendrickson, *The Journal of Physical Chemistry C* **2010**, *114*, 9178-9186.

[32] a) B. D. McCloskey, R. Scheffler, A. Speidel, G. Girishkumar, A. C. Luntz, *The Journal of Physical Chemistry C* **2012**, *116*, 23897-23905; b) V. Viswanathan, K. S. Thygesen, J. Hummelshøj, J. K. Nørskov, G. Girishkumar, B. McCloskey, A. Luntz, *The Journal of chemical physics* **2011**, *135*, 214704.

[33] L. Johnson, C. Li, Z. Liu, Y. Chen, S. A. Freunberger, P. C. Ashok, B. B. Praveen, K. Dholakia, J.-M. Tarascon, P. G. Bruce, *Nature Chemistry* **2014**, *6*, 1091.

[34] S. Kang, Y. Mo, S. P. Ong, G. Ceder, *Chemistry of Materials* **2013**, *25*, 3328-3336.

[35] a) Y. Mo, S. P. Ong, G. Ceder, *Physical Review B* **2011**, *84*, 205446; b) J. Hummelshøj, A. Luntz, J. Nørskov, *The Journal of chemical physics* **2013**, *138*, 034703.

[36] a) M. J. Lacey, J. T. Frith, J. R. Owen, *Electrochemistry Communications* **2013**, *26*, 74-76; b) L. Yang, J. Frith, N. Garcia-Araez, J. R. Owen, *Chemical Communications* **2015**, *51*, 1705-1708; c) D. Sun, Y. Shen, W. Zhang, L. Yu, Z. Yi, W. Yin, D. Wang, Y. Huang, J. Wang, D. Wang, *Journal of the American Chemical Society* **2014**, *136*, 8941-8946.

[37] X. Gao, Y. Chen, L. Johnson, P. G. Bruce, *Nature materials* **2016**, *15*, 882.

[38] a) A. F. Holleman, E. und Nils Wiberg, G. Fischer, in *Lehrbuch der Anorganischen Chemie*, **2007**; b) M. Derosa, R. J Crutchley, *Photosensitized Singlet Oxygen and Its Applications, Vol. 233–234*, **2002**.

[39] P. B. Merkel, D. R. Kearns, *Journal of the American Chemical Society* **1972**, *94*, 7244-7253.

[40] a) L. F. Agnez-Lima, J. T. Melo, A. E. Silva, A. H. S. Oliveira, A. R. S. Timoteo, K. M. Lima-Bessa, G. R. Martinez, M. H. Medeiros, P. Di Mascio, R. S. Galhardo, *Mutation Research/Reviews in Mutation Research* **2012**, *751*, 15-28; b) C. S. Foote, Y. C. Chang, R. W. Denny, *Journal of the American Chemical Society* **1970**, *92*, 5216-5218.

[41] a) L. Schafzahl, N. Mahne, B. Schafzahl, M. Wilkening, C. Slugovc, S. M. Borisov, S. A. Freunberger, *Angewandte Chemie* **2017**, *129*, 15934-15938; b) N. Mahne, B. Schafzahl, C. Leypold, M. Leypold, S. Grumm, A. Leitgeb, Gernot A. Strohmeier, M. Wilkening, O. Fontaine, D. Kramer, C. Slugovc, Sergey M. Borisov, Stefan A. Freunberger, *Nature Energy* **2017**, *2*, 17036.

[42] F. Wilkinson, W. P. Helman, A. B. Ross, *Journal of Physical and Chemical Reference Data* **1995**, *24*, 663-677.

[43] S. Strasser, C. Slugovc, *Catalysis Science & Technology* **2015**, *5*, 5091-5094.

[44] A. W. Williamson, *Quarterly Journal of the Chemical Society of London* **1852**, *4*, 229-239.

[45] A. Bard, L. Faulkner, *Electrochemical Methods: Fundamentals and Applications*, John Wiley & Sons, Inc, **2001**.

[46] P. Seiler, J. D. Dunitz, *Acta Crystallographica Section B* **1979**, *35*, 1068-1074.

[47] P. Kovacic, A. Kyriakis, *Tetrahedron Letters* **1962**, *3*, 467-469.

[48] W. H. Meyer, *Advanced materials* **1998**, *10*, 439-448.

[49] L. Guo, Y. Zhang, J. Wang, L. Ma, S. Ma, Y. Zhang, E. Wang, Y. Bi, D. Wang, W. C. McKee, Y. Xu, J. Chen, Q. Zhang, C. Nan, L. Gu, P. G. Bruce, Z. Peng, *Nature Communications* **2015**, *6*, 7898.

[50] S. Mahouche-Chergui, S. Gam-Derouich, C. Mangeney, M. M. Chehimi, *Chemical Society Reviews* **2011**, *40*, 4143-4166.

[51] J. L. Bahr, J. Yang, D. V. Kosynkin, M. J. Bronikowski, R. E. Smalley, J. M. Tour, *Journal of the American Chemical Society* **2001**, *123*, 6536-6542.

[52] P. Béchamp, *Annales de chimie et de physique* **1854**, *42*, 186-196.

[53] L. Kurti, B. Czakó, *Strategic applications of named reactions in organic synthesis*, Elsevier, **2005**.

[54] a) S. Fritz, G. Rudolf, BASF SE, **1954**; b) P. De, R. Faust, *Macromolecules* **2004**, *37*, 7930-7937; c) I. Natori, S. Natori, N. Hanawa, K. Ogino, *Polymer* **2016**, *91*, 194-202.

[55] J. Wang, L. M. Leung, *European Polymer Journal* **2013**, *49*, 3722-3733.

[56] C. W. Bielawski, R. H. Grubbs, *Angewandte Chemie International Edition* **2000**, *39*, 2903-2906.

[57] O. De Lucchi, L. Pasquato, *Tetrahedron* **1988**, *44*, 6755-6794.

[58] S. Watanabe, Y. Nozoe, S. Sakurai, K. Takeuchi, FUJIFILM Corporation, **2009**.

[59] a) Y. Gao, Y. Zhao, Y. C. Li, Q. Huang, T. E. Mallouk, D. Wang, *Journal of the American Chemical Society* **2017**, *139*, 15288-15291; b) A. Mishra, M. Ulaganathan, E. Edison, P. Borah, A. Mishra, S. Sreejith, S. Madhavi, M. C. Stuparu, *ACS Macro Letters* **2017**, *6*, 1212-1216.

[60] J. Hassoun, F. Croce, M. Armand, B. Scrosati, *Angewandte Chemie* **2011**, *123*, 3055-3058.

[61] J. Wandt, P. Jakes, J. Granwehr, H. A. Gasteiger, R.-A. Eichel, *Angewandte Chemie* **2016**, *128*, 7006-7009.

[62] Y. Chen, S. A. Freunberger, Z. Peng, O. Fontaine, P. G. Bruce, *Nature Chemistry* **2013**, *5*, 489.

[63] V. S. Bryantsev, M. Blanco, F. Faglioni, *The Journal of Physical Chemistry A* **2010**, *114*, 8165-8169.

[64] W. Koppenol, *Nature* **1976**, *262*, 420.

[65] A. Wykes, S. L. MacNeil, *Synlett* **2007**, *2007*, 0107-0110.

[66] L. A. Valckx, F. A. M. Borremans, C. E. Becu, R. H. K. De Mar, M. J. O. Anteunis, *Organic Magnetic Resonance* **1979**, *12*, 302-305.

[67] a) M. Carboni, A. G. Marrani, R. Spezia, S. Brutti, *Chemistry – A European Journal* **2016**, *22*, 17188-17203; b) V. S. Bryantsev, F. Faglioni, *The Journal of Physical Chemistry A* **2012**, *116*, 7128-7138; c) V. S. Bryantsev, V. Giordani, W. Walker, M. Blanco, S. Zecevic, K. Sasaki, J. Uddin, D. Addison, G. V. Chase, *The Journal of Physical Chemistry A* **2011**, *115*, 12399-12409; d) B. Liu, W. Xu, P. Yan, X. Sun, M. E. Bowden, J. Read, J. Qian, D. Mei, C.-M. Wang, J.-G. Zhang, *Advanced Functional Materials* **2016**, *26*, 605-613; e) B. Genorio, J. Staszak-Jirkovský, R. S. Assary, J. G. Connell, D. Strmcnik, C. E. Diesendruck, P. P. Lopes, V. R. Stamenkovic, J. S. Moore, L. A. Curtiss, N. M. Markovic, *The Journal of Physical Chemistry C* **2016**, *120*, 15909-15914.

[68] N. Hoffmann, *Chemical Reviews* **2008**, *108*, 1052-1103.

[69] S. Borisov, G. Nuss, W. Haas, R. Saf, M. Schmuck, I. Klimant, *Journal of Photochemistry and Photobiology A: Chemistry* **2009**, *201*, 128-135.

[70] D. A. Singleton, C. Hang, M. J. Szymanski, M. P. Meyer, A. G. Leach, K. T. Kuwata, J. S. Chen, A. Greer, C. S. Foote, K. Houk, *Journal of the American Chemical Society* **2003**, *125*, 1319-1328.

[71] W. G. Kofron, L. M. Baclawski, *The Journal of Organic Chemistry* **1976**, *41*, 1879-1880.

[72] R. H. Blessing, *Acta Crystallographica Section A* **1995**, *51*, 33-38.

[73] a) G. Sheldrick, *Acta Crystallographica Section A* **1990**, *46*, 467-473; b) G. M. Sheldrick, *Acta Crystallographica Section A: Foundations of Crystallography* **2008**, *64*, 112-122.

[74] a) A. L. Spek, *Journal of Applied Crystallography* **2003**, *36*, 7-13; b) A. L. Spek, *Acta Crystallographica Section D: Biological Crystallography* **2009**, *65*, 148-155.

[75] Z. Zeng, A. A. Torriero, A. M. Bond, L. Spiccia, *Chemistry–A European Journal* **2010**, *16*, 9154-9163.

[76] a) S. R. George, T. D. Frith, D. S. Thomas, J. B. Harper, *Organic & biomolecular chemistry* **2015**, *13*, 9035-9041; b) R. G. Harvey, J. T. Hahn, M. Bukowska, H. Jackson, *The Journal of Organic Chemistry* **1990**, *55*, 6161-6166.

[77] M. Schulze, A. Scherer, C. Diner, R. R. Tykwinski*, *Organic Syntheses* **2003**, *93*, 100-114.

[78] J. Zhu, T. Chen, G. Jin, J. Xu, K. Zhong, B. Yin, L. Y. Jin, *Polymer International* **2014**, *63*, 1070-1075.

10. Abbreviation List

10.1. Chemical Abbreviations

AIBN	azobisisobutyronitrile
Al_2O_3	aluminum oxide
AsF_5	arsenic pentafluoride
BCl_3	boron trichloride
BPO	benzoyl peroxide
CEB	1-chloroethylbenzene
DABCO	1,4-diazabicyclo[2.2.2]octane
DCM	dichloomethane
DMA	dimethylanthracene
DMPZ	dimethylphenazine
DMT	dimethyl-*p*-toluidine
DPA	diphenylanthracene
C	carbon
Cl^-	chloride
Cd	cadmium
Cs_2CO_3	cesium carbonate
CuO	copper oxide
DMSO	dimethylsulfoxide
DME	dimethoxyethane

e^-	electron
EtOAc	ethyl acetate
Fc	ferrocene
GC	glassy carbon
H^+	protons
H_2	hydrogen
HCl	hydrochloric acid
KI	potassium iodide
KO_2	potassium superoxide
Li	lithium
LiC_6	lithiated coke
$LiCoO_2$	lithium cobaldate
$LiFeO_2$	lithium iron oxide
$LiFePO_4$	lithium iron phosphate
LFP	lithium iron phosphate
LiM	lithium mediator complex
$LiMO_2$	lithium mediator oxygen complex
$Li\text{-}O_2$	lithium-oxygen
LiO_2	lithium superoxide
Li_2O_2	lithium peroxide
$Li_{2-x}O_2$	partly oxidized lithium peroxide
$LiPF_6$	lithium hexafluorophosphate
Li_2S	lithium sulfide
Li_xSi	lithiated silicon
M	mediator
MeCN	acetonitrile
MeOH	methanol
MgH_2	magnesium hydride
MnO_2	manganese dioxide
n-BuLi	*n*-butyllithium
Na^+	sodium-ion

$NaMnO_2$	sodium manganese oxide
NaO_2	sodium superoxide
Nbe	norbornene
Ni	nickel
O_2	oxygen
$^1O_2$	singlet oxygen
$^3O_2$	triplet oxygen
O_2^-	superoxide
O_2^{2-}	peroxide
O_3	ozone
O_4	tetraoxygen
P	phosphorous
PA	polyacetylene
PANI	polyaniline
Pb	lead
PEI	poly(ethylene imine)
PEO	poly(ethylene oxide)
PPO	poly(propylene oxide)
PPP	poly(paraphenylene)
PPy	polypyrrole
PT	polythiophene
Pyr	pyrene
S	sulfur
Si	silicon
Sn	tin
SO_2	sulfur dioxide
tert-BuLi	*tert*-butyllithium
TEG	tetraethylene glycol monomethyl ether
TEGDME	tetraethylene glycol dimethyl ether
TFSI	bis(trifluoromethanesulfonyl)imide
THF	tetrahydrofuran

TTF	tetrathiofulvalene
WE	working electrode
Zn	zinc

10.2. Others

°C	degree Celsius
Å	Angstrom
AFM	atomic force microscopy
aq.	aqueous
ASPB	anionic spherical polyelectrolyte brushes
CA	contact angle
cm	centimeter
d	day
d.c.	direct current
DSC	differential scanning calorimetry
e.g.	for example
eq	equivalents
et al.	et alii
eV	electronvolt
ECP	electronically conducting polymer
g	gram
GPC	gel permeation chromatography
h	hour
HOMO	highest occupied molecular orbital
HR-MS	high resolution mass spectrometry
ICP	ionically conduction polymer
in situ	local
IR	infrared
j	current density
K	Kelvin
LIB	lithium ion battery

LUMO	lowest unoccupied molecular orbital
μ	electrochemical potential
µA	microampere
µL	microliter
µm	micrometer
m	*meta*
mA	milliampere
mAh	milliampere hour
M	mols per liter (mol/L)
MIECP	mixed ionic and electronic conducting polymers
min	minute
mL	milliliter
mm	millimeter
mM	millimols per liter (mmol/L)
m/m	mass/mass
mmol	millimol
mol%	mole fraction
mPa	millipascal
m%	mass fraction
η	viscosity
nm	nanometer
NMR	nuclear magnetic resonance spectroscopy
n/n	mol/mol
%	percent
p	*para*
pH	pondus Hydrogenii
ppm	parts per million
q	elementary charge
ROMP	ring opening metathesis polymerization
rpm	revolutions per minute
RT	room temperature

SEM	scanning electron microscopy
Θ	contact angle in °
s	second
SHE	standard hydrogen electrode
σ	conductivity
$^3\Sigma_g^-$	molecular term symbol for triplet oxygen
$^1\Delta_g$ and $^1\Sigma_g^+$	molecular term symbols for singlet oxygen
T	temperature
t	time
^{t}BuOK	potassium *tert*-butoxide
TLC	thin layer chromatography
UV-Vis	ultraviolet-visible
vice versa	the other way around
V	volt
v/v	volume/volume
vs	*versus*

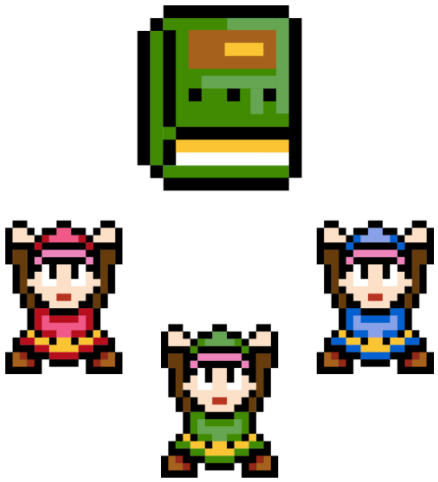

© by Nintendo®